LUND UNIVERSITY

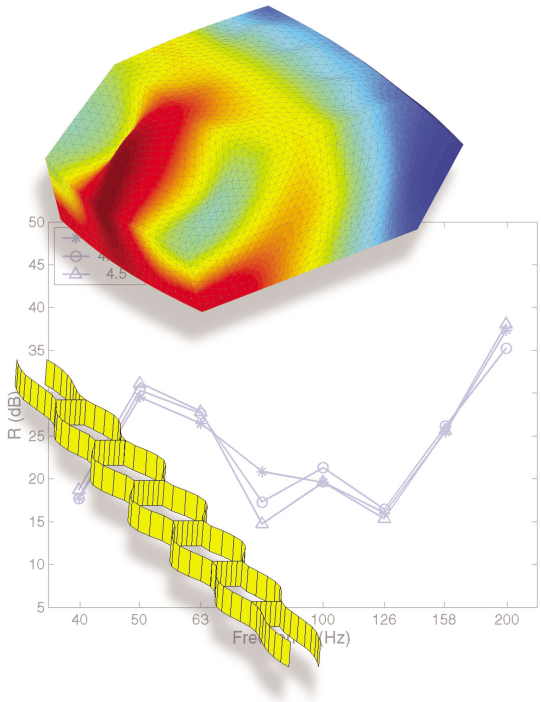

STRUCTURE-ACOUSTIC ANALYSIS; FINITE ELEMENT MODELLING AND REDUCTION METHODS

PETER DAVIDSSON

Structural Mechanics

Doctoral Thesis

Structural Mechanics

ISRN LUTVDG/TVSM--04/1018--SE (1-180)
ISBN 91-628-6176-X ISSN 0281-6679

STRUCTURE-ACOUSTIC ANALYSIS; FINITE ELEMENT MODELLING AND REDUCTION METHODS

Doctoral Thesis by

PETER DAVIDSSON

Printed by KFS i Lund AB, Lund, Sweden, August 2004.

For information, address:
Division of Structural Mechanics, LTH, Lund University, Box 118, SE-221 00 Lund, Sweden.
Homepage: http://www.byggmek.lth.se

Preface

The work presented in this thesis has been carried out at the Division of Structural Mechanics at Lund University. I would like to express my gratitude to my supervisor Professor Göran Sandberg, both for the opportunity to conduct my research studies at this division and for the support provided. The friendship and support of all colleagues at the division are very appreciated. I also would like to thank my colleagues at the Division of Engineering Acoustics, especially Dr. Jonas Brunskog, for the invaluable discussions and help during the course of this work. A special thanks to Mr. Bo Zadig for the help on creating a variety of the figures.

The work was initiated by and conducted as a part of the national research programme Integral Vehicle Structures (IVS), which concerns the development of future generations of vehicles. IVS is financed by the Swedish Foundation for Strategic Research (SSF). This financial support as well as the courses and other events within the programme have been very appreciated.

Paper 5 presents work carried out in cooperation with Dr. Gunnar Björkman and Johan Svenningstorp at Volvo Technological Development in Göteborg. I very much appreciate their efforts on introducing me to the modelling environment described in the paper.

The work conducted in Papers 6 and 7 was partly financed by Lindab Profile AB, which is gratefully acknowledged.

I would also like to thank my friends and family. Especially, thank you Åsa for your love and support.

Lund, August 2004,

Peter Davidsson

Overview of the thesis

This thesis investigates structure-acoustic problems, which involves a flexible structure coupled to an enclosed acoustic fluid. In the literature, this type of problems are usually referred to as vibroacoustic problems or structural-acoustic problems with fluid interaction. The thesis consists of two parts. The first part provides an introduction into the field of structure-acoustic analysis within the finite element framework, including the description of porous materials. The second part of the thesis comprises seven papers in which analysis procedures for modal reduction of structure-acoustic systems are developed. Two of the included papers also investigate the sound transmission loss of double walls.

Included papers

Paper 1 Göran Sandberg and Peter Davidsson, A strategy for modal reduction of structure-acoustic systems, 2002.

Paper 2 Peter Davidsson and Göran Sandberg, Reduction of structure-acoustic problems that include hysteretic damping, 2002.

Paper 3 Peter Davidsson and Göran Sandberg, Substructuring and modal reduction of finite element formulated poroelastic systems, Submitted to *Computer methods in applied mechanics and engineering*, 2004.

Paper 4 Peter Davidsson and Göran Sandberg, A reduction procedure for structure-acoustic and poroelastic–acoustic problems using interface-dependent Lanczos vectors, Submitted to *Computer methods in applied mechanics and engineering*, 2004.

Paper 5 Peter Davidsson, Göran Sandberg, Gunnar Björkman and Johan Svenningstorp, Structure-acoustic analysis in an integrated modelling environment, *WCCM V congress in Vienna*, 2002.

Paper 6 Peter Davidsson, Jonas Brunskog, Per-Anders Wernberg, Göran Sandberg and Per Hammer, Analysis of sound transmission loss of double-leaf walls in the low-frequency range using the finite element method, Submitted to *Building Acoustics*, 2004.

Paper 7 Jonas Brunskog and Peter Davidsson, Sound transmission of structures; a finite element approach with simplified room description, Accepted for publication in *Acta acustica united with Acustica*, 2004.

Summary of papers

Paper 1 The problem in which a flexible structure interacts with an acoustic fluid is analysed by use of the finite element method. With increasing complexity of the geometry and when increasing the frequency limit is of interest, the number of degrees of freedom needed to describe the system becomes very large. To reduce the coupled system, modal analysis is performed in the structural and in the fluid domain separately. The subdomain eigenvectors are then used to reduce the coupled problem. A method for choosing which of these subdomain eigenvectors to include in this operation is derived based on the coupling between the structural and fluid modes, further reducing the system. The coupling depends on similarity in the natural frequencies and in the shapes of the subdomain modes.

Paper 2 The unsymmetrical eigenvalue problem involved in analysing structure-acoustic problems by use of the finite element method with a pressure formulation in the fluid domain can be reduced by transforming it into a symmetric standard eigenvalue problem. The paper shows that when hysteretic damping is introduced in both the structural and the fluid domain, the problem can still be treated as a symmetric standard eigenvalue problem, which becomes complex-valued due to the damping. This provides a simple method for including damping in the frequency response analysis of structure-acoustic problems.

Paper 3 A structure-poroelastic system, consisting of a porous material domain bounded to a flexible structural domain, is studied. The porous material is modelled by Biot's theory, where both the flexible frame material and the fluid in the open pores are described by coupled equations of motion. The component mode synthesis method is used to derive a reduced set of basis vectors for the system. This is done by dividing the system into three physical domains, the flexible structure, and the fluid and structural partitions of the porous material. The displacement continuity between the flexible structural domain and the porous material is fulfilled by interface modes. These modes are derived by studying the two structural subdomains, the flexible structure and the structural partition of the porous material, in vacuo. The interface modes are used together with a set of basis vectors for each of the uncoupled domains, derived by modal analysis with the interface degrees of freedom fixed, to reduce the coupled system.

Paper 4 A reduction method is proposed for the analysis of structure-acoustic and poroelastic–acoustic problems within the finite element framework. This includes systems consisting of an acoustic fluid domain in contact with a flexible structural domain and/or a porous sound absorbing material domain. The problem studied is reduced by dividing the system into a number of physical domains. A set of basis vectors is derived for each of these domains both including eigenvectors of the uncoupled domain and interface-dependent vectors including the influence from connecting domains. The proposed method is compared to solving the total system for both a structure-acoustic eigenvalue problem and a frequency response analysis of a poroelastic–acoustic system.

Paper 5 This paper, which is based on the results reported in Papers 1 and 2, describes the implementation of structure-acoustic finite element analysis in an integrated modelling environment, one which has interfaces to programs for meshing and for finite element analysis. The aim is to determine the vehicle interior noise on the basis of the force applied to the structure.. An interface is created to a code developed for performing structure-acoustic analysis involving coupled modal analysis and frequency response analysis. The possibilities this modelling environment provides are demonstrated. Use of this approach simplifies cooperation between researchers and their interaction with industrial groups.

Paper 6 The sound transmission loss of double-leaf walls in the low-frequency range is evaluated by means of structure-acoustic finite element analysis. A parametric study is performed to investigate the influence on the sound transmission loss of various material and geometric properties of the wall and the dimensions of the connecting rooms. It is found that a very detailed description of the system is needed in order to describe sound transmission loss in the low-frequency range. The model confirms the importance of primary structural resonance and the size of the wall and the connecting rooms in determining the sound transmission loss in the low-frequency range.

Paper 7 A prediction model within the finite element framework for the sound insulation of a wall is proposed. The connecting rooms are described as infinite-long tubes and the influence of the rooms becomes loading terms on the wall, reducing the model to the two-dimensional wall. The analysis can thereby be conducted higher in the frequency range compared to having to include the modal bases of the connecting rooms. The same method is developed to study the sound insulation of lightweight double-leaf walls, and the numerical results are presented.

Contents

Chapter 1

Introduction

This thesis investigates structure-acoustic systems by use of finite element analysis. The systems studied here are limited to those that consist of an enclosed acoustic fluid cavity, which is coupled to a flexible structure and/or a porous sound absorbing material domain.

The introduction gives the background and objective for the thesis and also describes a number of applications where this type of analysis can be employed. The typical procedure of structure-acoustic analysis is discussed, including the generation of the governing system of equations and the solution of the generated systems using substructuring and modal reduction.

The introduction also contains a description of the work conducted, as based on the included papers where the main contributions of this thesis are stated.

1.1 Background

The demand for building lighter and thereby more fuel efficient vehicles is very likely to be in conflict with the comfort of the passengers in terms of a low level of interior noise. Reducing the weight could increase the structural vibrations, leading to higher noise levels in the passenger compartment. To deal with this problem in the design stage, detailed structure-acoustic analyses need to be performed. The governing equations for structure-acoustic analysis are presented in Chapter 2, where also a short review of the literature of interest is presented. The interior noise comfort can also be in conflict with other vehicle properties such as safety (crashworthiness), so the design process must be conducted in an integrated fashion that addresses various vehicle properties – such as safety, reliability and comfort – in the process. Also, with a decreasing weight of the vehicle, the dimensioning and thereby the modelling of porous sound absorbing materials becomes very important. The modelling of porous sound absorbing materials is described in Chapter 4, also including a literature review.

The use of lightweight constructions in buildings increases the need for prediction models in the low-frequency range. For example, the sound transmission loss of a double wall, in the low frequency range, is not only dependent on wall type and wall material properties but also the dimensions of both the wall and the connecting rooms. Also, the modelling of the porous sound absorbing material inside the double wall cavities is of great importance in predicting the sound transmission loss of the wall. The literature

pertaining to predicting sound transmission loss in walls can be found in Paper 7 and in the Doctoral thesis by Brunskog [1].

The number of degrees of freedom of the finite element model, i.e. the size of the system of equations, when solving structure-acoustic systems is likely to become very large. The geometric complexity of the systems under study and the frequency limit of interest determine the size of the system. The constant aim to have a more detailed description of the geometry and an increased frequency limit of validity for the model result in increasing number of degrees of freedom. Thus, the need for efficient solution strategies in structure-acoustic analysis and methods to reduce the size of the model, i.e. the size of the system of equations to be solved, is therefore large. Different modal reduction techniques are described in Chapter 3.

The modelling of porous sound absorbing materials increases the solution time due to both increased number of degrees of freedom and the frequency dependent material properties. Therefore, it would be desirable to be able to include the porous material description in the reduction methods.

1.2 Objective

In this thesis, the coupled structure-acoustic problem is studied using the finite element method. The objective is twofold: to develop the analysis methods and to study engineering applications.

To increase the possibility of including a detailed geometrical description of the studied system and advanced material descriptions in the analysis, the thesis develops efficient methods, using substructuring and modal reduction, for the analysis of structure-acoustic

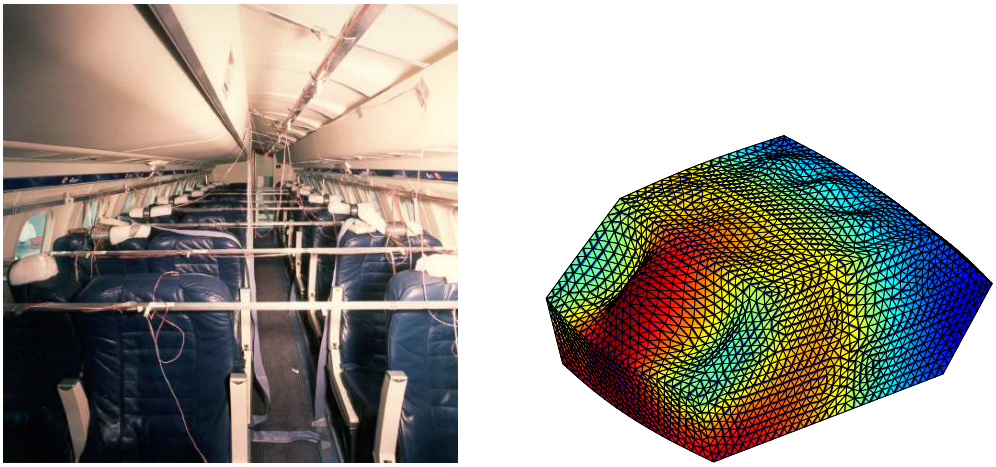

Figure 1.1: *Vehicle interior noise: a) Measurement setup for determining the level of interior noise in the SAAB 340 airplane (M. Gustavsson [2], A2 Acoustics AB, project performed at SAAB AB during 1995), b) A coupled structure-acoustic mode of the vehicle model that was analysed in VIVS-lab (P. Davidsson, project with Volvo Technological Development, 2001), paper 5.*

problems. The aim is also to be able to increase the frequency limit of validity for the analysis. The geometric problem domain is divided into a number of subdomains and reduced set of basis vectors is derived for each of these subdomains. The main objective is to be able to perform as large part of the analysis on the subdomain level as possible, before assembling the total system. The set of basis vectors for each domain is derived to include information about both the internal behaviour of the subdomain and the coupling to the other subdomains. The reduced description enables efficient solution of the total system. An important feature is to include the description of porous sound absorbing materials in the reduction process of the structure-acoustic problems.

Another objective for the thesis is to use the derived procedures in engineering applications; particularly in the study of sound transmission of lightweight double-leaf walls in the low-frequency range. The objective is to include a detailed geometric description of the problem enabling a structured evaluation of the influence of various geometrical and material properties of the studied wall on the predicted sound transmission loss.

1.3 Problem description

This section presents a short discussion on the realisation of finite element analysis of structure-acoustic systems. This type of analysis is applicable to a wide range of engineering problems. Figure 1.1 displays two vehicle applications. The first is the measurement setup used to determine the interior noise level in the SAAB 340 airplane. The second is a structure-acoustic analysis of the generic car cavity model developed in VIVS-lab, see Paper 5. The behaviour within the low frequency range of a wall consisting of sheet-metal wall studs covered by plaster boards is studied in Figure 1.2 (see Papers 6 and 7). Another example of structure-acoustic analysis is a fluid-filled tank being exposed to an earthquake, shown in Figure 1.3. The typical damage, being elephant foot buckling, can be seen at the base. (Note however that large deformations and damage is not investigated

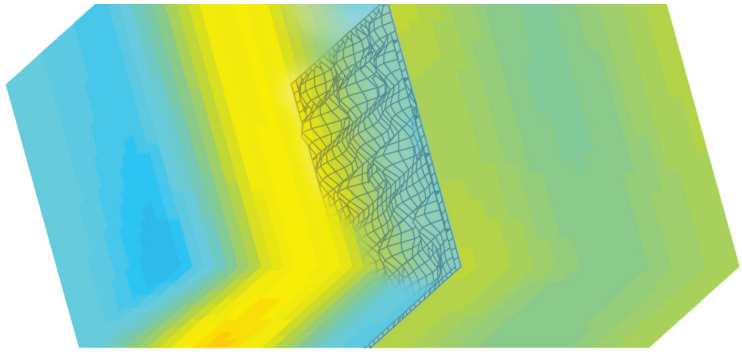

Figure 1.2: *Building acoustics: The acoustic behaviour of double leaf walls is studied in the low frequency range. The figure shows the frequency response to a point source in the room-wall-room system simulating the measurement setup used for determining the sound reduction index of the wall (P. Davidsson, project together with Lindab Profil AB, 2001), paper 6.*

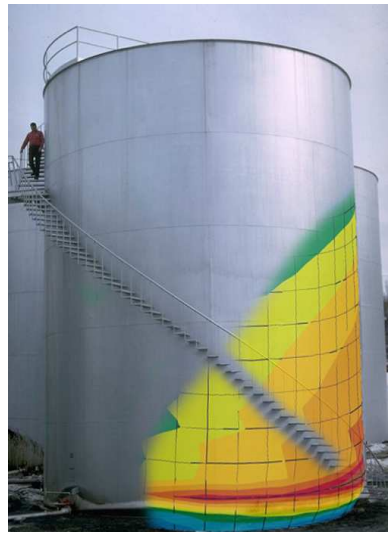

Figure 1.3: *Earthquake analysis: A fluid filled tank exposed to an earthquake. The typical damage, elephant foot buckling, is seen at the base of the tank (P. Davidsson, Structural Mechanics, Report TVSM-5083, 1998).*

in this thesis.)

Finite element analysis

In the mathematical description of the structure-acoustic problem, one differential equation governs the behaviour of each of the structural and fluid domains. The two domains are coupled through boundary conditions ensuring continuity in displacement and pressure. Finite element formulation of the governing equations including the coupling conditions yields that the system of equation of motion for an undamped structure-acoustic problem can be written in the form

$$\begin{bmatrix} \mathbf{M}_S & \mathbf{0} \\ \rho_0 c_0^2 \mathbf{H}_{SF}^T & \mathbf{M}_F \end{bmatrix} \begin{bmatrix} \ddot{\mathbf{d}}_S \\ \ddot{\mathbf{p}}_F \end{bmatrix} + \begin{bmatrix} \mathbf{K}_S & -\mathbf{H}_{SF} \\ 0 & \mathbf{K}_F \end{bmatrix} \begin{bmatrix} \mathbf{d}_S \\ \mathbf{p}_F \end{bmatrix} = \begin{bmatrix} \mathbf{f}_b \\ \mathbf{f}_q \end{bmatrix} \tag{1.1}$$

which is derived in Chapter 2, where the matrices and material parameters are defined. The primary variables are the displacements, $\mathbf{d}_S$, in the structural domain and the acoustic pressure, $\mathbf{p}_F$, in the fluid domain. The two domains are described by the corresponding mass and stiffness matrices, $\langle \mathbf{M}_S, \mathbf{K}_S \rangle$ and $\langle \mathbf{M}_F, \mathbf{K}_F \rangle$, respectively. The coupling between the domains is given by the spatial coupling matrix $\mathbf{H}_{SF}$. The right side of the equation describes the external forces. The number of equations, equal to the number of degrees of freedom, is denoted n. The Doctoral theses by Sandberg [3] and Carlsson [4] investigate the finite element formulation of the structure-acoustic problem.

The structure-acoustic system is solved for a specific force field. In a time domain analysis, the system of equations can be solved in a stepping procedure throughout the time interval studied. This is carried out when studying the water tank exposed to an

earthquake, for example. In frequency domain analysis, a harmonic motion is assumed, i.e. the motion of the system is described by the displacement and pressure amplitudes, $\hat{\mathbf{d}}_S$ and $\hat{\mathbf{p}}_F$,

$$\begin{bmatrix} \mathbf{d}_S \\ \mathbf{p}_F \end{bmatrix} = \begin{bmatrix} \hat{\mathbf{d}}_S \\ \hat{\mathbf{p}}_F \end{bmatrix} \mathrm{e}^{\mathrm{i}\omega t} \tag{1.2}$$

where $\omega = 2\pi f$ (f is the studied frequency in Hz), $\mathrm{i} = \sqrt{-1}$, and t denotes time. The vehicle interior noise problem in Figure 1.1 and the sound transmission loss in a double wall in Figure 1.2 are two examples of this type of frequency response analysis. Introducing equation (1.2) in equation (1.1), the response to a harmonic excitation at a number of frequency steps in the frequency interval of interest can be determined. Due to the frequency dependence of the dynamic stiffness matrix, a new system of equations must be solved in each of these steps. Also, when frequency dependent material properties are used to, for example, describe porous materials or internal damping, the system matrices must also be reassembled in each frequency step. In the mathematical description, the porous sound absorbing materials can either be included as a part of the acoustic fluid domain, using an equivalent fluid model, or as a part of the structural domain, using displacement formulation of the porous material domain. The modelling of porous materials is studied in Chapter 4. Solution strategies for the frequency response of structure-acoustic problems are studied in the Licentiate thesis by Gustavsson [2].

Size of the system of equations

An important problem encountered in structure-acoustic analysis is that the number of degrees of freedom easily becomes very large. This, together with the lack of symmetry in the system of equations and the large bandwidth of the system matrices, due to the coupling matrix, $\mathbf{H}_{SF}$, in equation (1.1), all adds up to long computational times. The large number of degrees of freedom is mainly due to the fact that the wavelengths of the structure and acoustic fluid must be resolved in the finite element model. Figure 1.4,

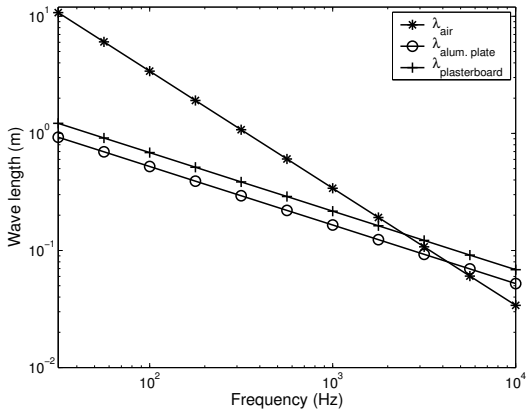

Figure 1.4: *The longitudinal wavelength in air and the bending wave lengths of a 3 mm aluminium panel and a 12.5 mm plasterboard.*

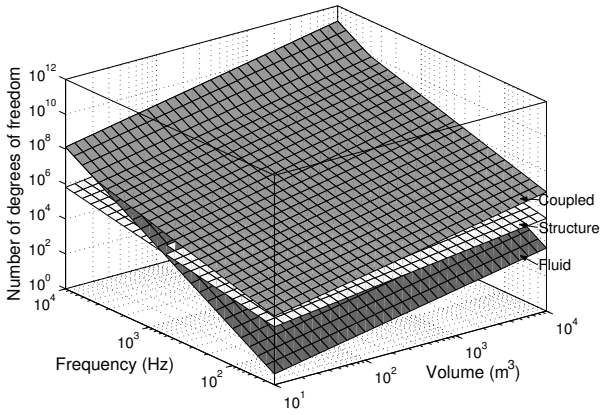

Figure 1.5: *The required number of degrees of freedom when studying the fluid domain, the structural domain and the coupled problem.*

displays how the bending wavelengths of two typical structural members, a 3 mm thick aluminium plate and a 12.5 mm thick plasterboard, and the longitudinal wavelength in air varies with frequency. Note, at low frequencies the wavelength in air is much larger compared to the wavelengths of the structural members, but the wavelength in air decreases more rapidly with increasing frequency.

A simple measure of the number of degrees of freedom needed in dynamic analysis is illustrated in Figure 1.5. An enclosed cube-shaped cavity with all boundary sides flexible is investigated, where it is assumed that 8 degrees of freedom are satisfactory to resolve each wavelength, both for the structural and fluid domains. The total number of degrees of freedom needed to describe the system is determined both with respect to the frequency limit of interest and the volume of the system under study. As for the size of the system, for comparison, the volume of a passenger compartment in a car is typically a few cubic metres, a room in an apartment $\sim 10^2$ m^3, a large airplane fuselage $\sim 10^3$ m^3, and a concert hall $\sim 10^4$ m^3. To describe the fluid domain at low frequencies, only a few degrees of freedom are needed; the wavelength is of the same magnitude as the dimensions of the system. For the structural domain, the wavelength is much shorter and more degrees of freedom are needed to resolve it. With increasing frequency, the number of degrees of freedom increases more rapidly for the three-dimensional acoustic fluid domain compared to the two-dimensional structure.

For the coupled structure-acoustic analysis, it is assumed that both domains must be able to describe the shortest wavelength that can appear. This is the structural wavelength up to the point where the lines cross in Figure 1.5 a), at the, so called, coincidence frequency. Thus, even for the low-frequency range and small volumes of the acoustic cavity, a large number of degrees of freedom is needed for the acoustic fluid domain compared to an uncoupled analysis. For example, at 1000 Hz and a volume of 10 m^3, a few million degrees of freedom are needed to describe the system. From this simple problem, the need for modal reduction, where a reduced set of basis vectors is derived, is evident.

Modal reduction

The aim of a modal reduction technique is that m, which is the number of basis vectors that is used for describing the system, is much smaller then the number of degrees of freedom, n,. This leads to a speed-up of the analysis since the system of equations to be solved is smaller. For the studied system in equation (1.1), a reduced set of basis vectors can be derived

$$\begin{bmatrix} \mathbf{d}_S \\ \mathbf{p}_F \end{bmatrix} = \mathbf{\Psi}\boldsymbol{\xi} \tag{1.3}$$

where $\mathbf{\Psi}$ contains a number of basis vectors, or modes, and $\boldsymbol{\xi}$ contains the modal coordinates. Modal reduction techniques are investigated in Chapter 3. The most frequently used basis vectors are the normal modes, denoted $\mathbf{\Phi}$, which are derived in solving the eigenvalue problem of the system. This analysis also achieves an understanding of the dynamic behaviour of the system. The eigenvalue problem is also studied in Chapter 3. An important technique in modal reduction is substructuring, where the system is divided into subdomains, which are first analysed separately. In structure-acoustic analysis, the natural choice of subdomains are the structural and fluid domains, i.e. the reduced base becomes

$$\mathbf{\Psi} = \begin{bmatrix} \mathbf{\Psi}_S & \mathbf{0} \\ \mathbf{0} & \mathbf{\Psi}_F \end{bmatrix} \tag{1.4}$$

where the basis vectors, $\mathbf{\Psi}_S$ and $\mathbf{\Psi}_F$ are derived separately. When analysing the gain in solution time from solving the system using the reduced set of basis vectors, compared to solving the total system, one must also consider the time to derive this reduced base. The reduced set of basis vectors must also be able to describe the motion of the system without restricting the motion into too few displacement modes. Reduction procedures for structure-acoustic problems are studied in the Doctoral thesis by Carlsson [4] and the Licentiate thesis by Hansson [5].

A short numerical investigation

To investigate the finite element analysis of structure-acoustic systems, numerical experiments were carried out using the finite element program MSC/Nastran [6]. (All analyses were performed on a computer with an Intel P4 2.53 Ghz processor and 1 Gb DDR SDRAM main memory.) A box-shaped structure used for the study was constructed of aluminium panels, with dimensions $1.7 \times 1.2 \times 0.8$ m^3, surrounding an acoustic cavity filled with either air or water. The computational time for solving the eigenvalue problem of the fluid domain was first studied, varying the number of degrees of freedom and the number of normal modes required, see Figure 1.6. The number of normal modes required determined how many times the iterative procedure, using the factorised system matrix, needed to be performed, while the number of degrees of freedom determined the time for each step in the iteration. As can be seen in Figure 1.6, the number of degrees of freedom is very important to the solution time.

The method of substructuring and modal reduction was also studied (see Figure 1.7). The structure-acoustic eigenvalue problem was solved, studying the convergence of the eigenvalues when increasing the number of subdomain modes included. In this analysis, the acoustic fluid was water. The calculated natural frequencies using the substructuring and modal reduction converged towards the results from direct solution of the total

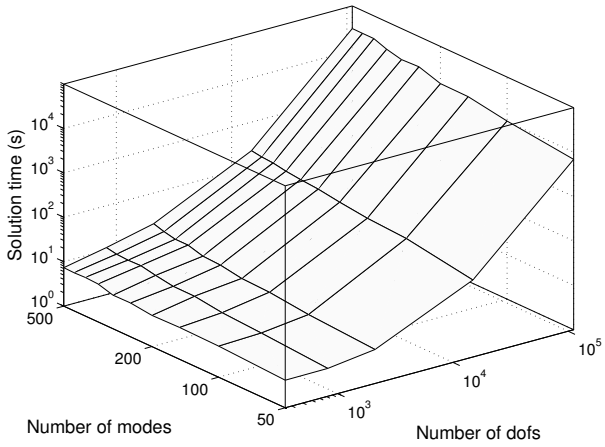

Figure 1.6: *Time to solve the eigenvalue problem for the acoustic fluid domain.*

system. However, a very large number of subdomain modes are needed to describe the coupled system.

The time consumption in a frequency response analysis of the structural domain was also studied (see Figure 1.8). One of two solution procedures can be used: either the total system is solved in each frequency step or a reduced set of basis vectors is derived and used in a modal frequency response only requiring the solution of a system with the size equal to the number of modes included. The maximum frequency of interest and the number of frequency steps to be solved are important factors in the choice of the type of analysis. Modal frequency response is very efficient when the number of frequency steps

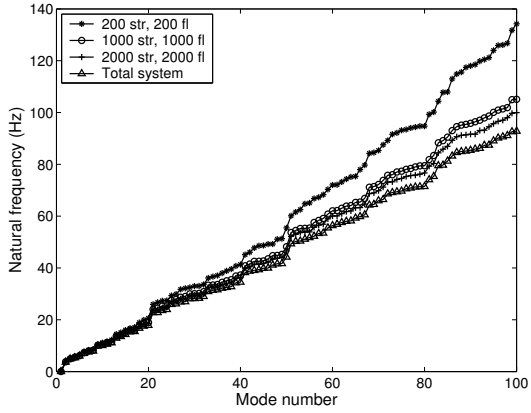

Figure 1.7: *The natural frequencies of the coupled system calculated when varying the number of structural and fluid modes used for describing the subdomains and also when solving the total system.*

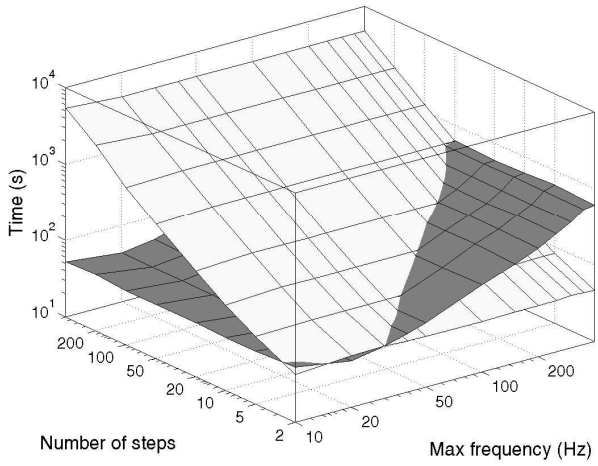

Figure 1.8: *The time for solving the frequency response of the structural domain, when solving the problem direct (the white surface) and using modal reduction (grey surface). The number of frequency steps and the maximum frequency of interest are varied.*

is large and the number of excited modes is low. If only a few frequency steps are of interest, it is more efficient to solve the system directly, without first deriving the reduced set of basis vectors.

Summary

In this section, the procedure of structure-acoustic analysis was discussed, see Figures 1.5 – 1.8. With increasing frequency of interest and dimensions of the studied problem, the degrees of freedom needed for describing the problem increases rapidly. Also, the time for solving the derived system of equations is very dependent on the size of this system, i.e., the number of degrees of freedom. Using a reduced set of basis vectors, or modes, the size of the system of equations is decreased and this can be very effective for speeding up the computations, especially when the system of equations is to be solved in large number of frequency steps (or time steps). However, a large number of modes can be needed to describe the system. Methods to calculate these subdomain modes using available information of the studied subdomain and the connecting subdomains are an important part of this thesis.

1.4 Contents of the thesis

The contents of this thesis are presented in two main parts:

- Development of analysis methods using substructuring and modal reduction for structure-acoustic and poroelastic-acoustic systems. The procedures that were developed divide the studied systems into a number of physical subdomains. These subdomains, which may be an acoustic cavity, a flexible structure and/or a porous

sound absorbing material domain, are described by a reduced set of basis vectors including both the free motion of the subdomain and the influence from the connecting subdomains.

- The investigation of sound transmission loss of double walls in the low-frequency range using a detailed geometric description of the system. The detailed description is used to study the influence of both geometric and material properties of the wall.

As a basis for the work presented in the papers included in the thesis, different aspects of structure-acoustic analysis are discussed. In Chapter 2, the governing equations of the structure-acoustic problem are given. The finite element formulation is derived for the structural and acoustic fluid domains, using the structural displacements and acoustic pressure as the primary variables, and for the coupled problem. In Chapter 3, modal reduction techniques are described and evaluated with focus on different variants of the Rayleigh-Ritz procedure. In Chapter 4, the modelling of porous sound absorbing materials within the finite element method is investigated. Different formulations of porous materials can be employed, either a full description of both the structural and fluid partitions or simplified equivalent fluid models. The different formulations are described and some typical problems are solved to evaluate for which cases the different descriptions should be employed.

1.4.1 Methods for substructuring and reduction

Papers 1–4 contain development of modal reduction techniques for structure-acoustic systems. Paper 1 proposes a procedure to determine which subdomain normal modes – derived from separate analyses of the structural and fluid domains – are most important

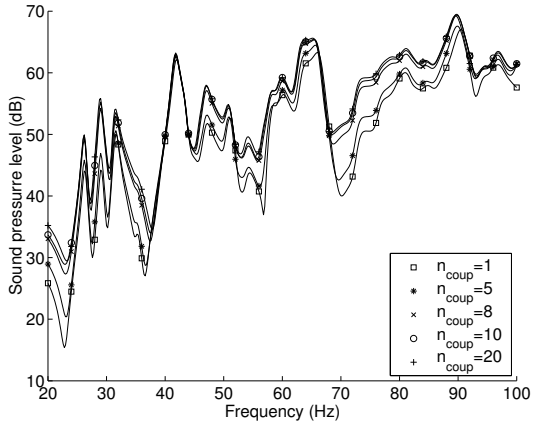

Figure 1.9: *Papers 1, 2 and 5: The sound level at the drivers ear in a generic car model. The number of subdomain modes included in the reduction is varied by increasing the number of subdomain modes with strong coupling included in the reduction. Small deviations can be seen between using* $n_{coup} = 10$ *and* $n_{coup} = 20$*. This analysis is described in Paper 5 and based on the work in Papers 1 and 2.*

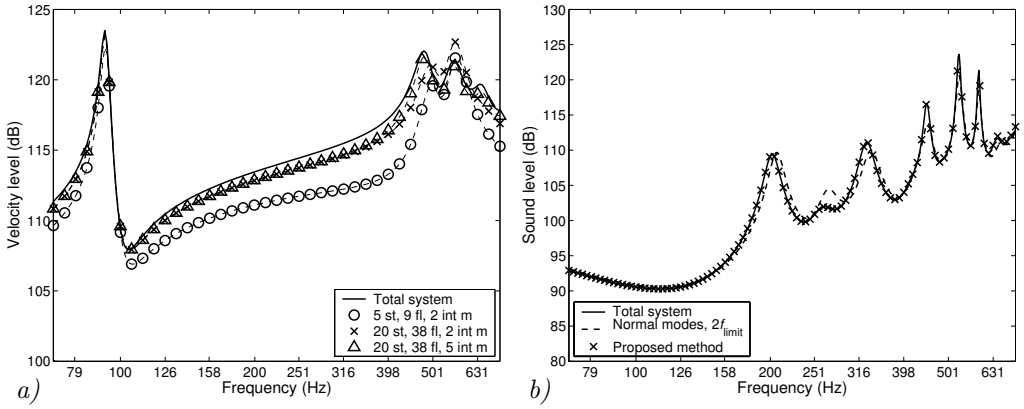

Figure 1.10: *a) Paper 3: Velocity level calculated when using the reduced set of basis vectors or solving the total system. b) Paper 4: The calculated mean pressure pressure level in the acoustic cavity. See the papers for details.*

to describe the coupled system. Only these normal modes with strong coupling need to be included in the reduced set of basis vectors for the coupled system and the system is further reduced. Paper 2 is a study of the same problem but here describes a procedure to include a simple description of damping in the system. The results of Papers 1 and 2 are implemented in an integrated modelling environment in Paper 5, where a generic car model is studied. For example, the calculated sound level at the driver's ear, varying the number of subdomain modes with strong coupling that are included in the description of

Table 1.1: *Paper 4: The calculated natural frequencies of the coupled problem using the proposed method, employing interface-dependent subdomain modes, and the typical procedure of including normal modes with natural frequency below "$2f_{limit}$" are compared to solving the total system. Note the low number of modes used for the proposed method.*

	"$2f_{limit}$"	Lanczos vectors, m			Direct
		0	1	2	
Mode	Natural frequencies (Hz)				
1	73.2197	73.3166	73.0821	73.0820	73.0820
2	89.2792	89.4187	89.0880	89.0879	89.0879
3	148.0841	148.9089	147.5391	147.5310	147.5306
4	163.9861	163.9952	163.9601	163.9600	163.9600
5	246.5600	246.5605	246.4992	246.4990	246.4990
6	252.0476	252.6919	251.1389	251.1246	251.1242
7	263.4865	263.6686	262.4484	262.4178	262.4121
Domain	Number of degrees of freedom				
Structural	4	4	5	6	243
Fluid	20	4	8	12	1377
Sum	24	8	13	18	1620

the coupled problem, is plotted in Figure 1.9.

The inclusion of porous absorbing materials in the modal reduction is investigated in Papers 3 and 4. Paper 3 describes a study of a flexible structure with porous material bounded to its surface. Substructuring and modal reduction is employed to derive a reduced set of basis vectors for these types of problems. The results from using this reduced set of basis vectors are compared to solving the total system, as shown in Figure 1.10 a). In Paper 4, a reduction method is proposed which can be used for both plain structure-acoustic systems and for systems with an acoustic cavity in contact with a porous material domain. Interface-dependent modes, which include the influence of the connecting domains, enable a very efficient reduced set of basis vectors to be derived for each subdomain. The natural frequencies of a structure-acoustic eigenvalue problem using the proposed method are presented in Table 1.1, and the frequency response in a damped rectangular acoustic cavity is shown in Figure 1.10 b).

1.4.2 Sound transmission loss

In Papers 6 and 7, the sound transmission loss of double walls is studied by use of the finite element method. Paper 6 comprises the study of the low-frequency range with a detailed geometrical description of the wall and the two connecting rooms. The detailed description is used to study the influence of both geometric properties, for example, the distance between the wall studs, the length of the wall and the dimensions of the rooms acoustically coupled to the wall, and material properties; for example, varying the modulus of elasticity of the plasterboards as is displayed in Figure 1.11 a). In Paper 7, a simplified tube-like description of the rooms is proposed. The rooms are included as loading terms on the wall and the size of the system of equations to be solved is only dependent on the finite element model of the wall. This enables the sound transmission loss to be determined in a wider frequency range, as shown in Figure 1.11 b).

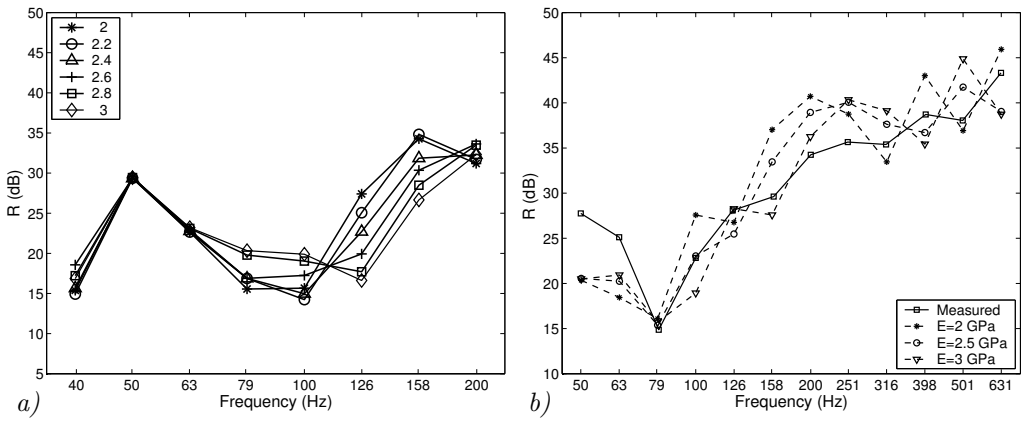

Figure 1.11: *a) Paper 6: Sound transmission loss when varying the plasterboard modulus of elasticity, E, for the wall type* R120 202 s450. *b) Paper 7: The transmission loss for a double wall with thickness 95 mm, comparing calculations and measurements.*

Chapter 2

Structure-acoustic analysis

This chapter investigates the analysis of structure-acoustic systems, here limited to systems consisting of a flexible structure in contact with an enclosed acoustic cavity, within the finite element environment. A short literature review is presented here which focuses on the need for this type of analysis and where different formulations in the finite element analysis are discussed. In the sections following, the governing equations of the structure-acoustic problem are given and the finite element formulation of this problem is derived.

2.1 Literature review

Vibrating structures inducing pressure waves in a connecting acoustic fluid and the opposite case of acoustic pressure waves inducing structural vibrations constitute a thoroughly investigated field of research (see for example the texts by Cremer and Heckl [7], and Fahy [8]). In [9, 10, 11, 12, 13, 14, 15], the structure-acoustic problem is studied using analytical expressions for the two domains. It is evident that the two connecting domains, the flexible structure and the enclosed acoustic cavity, can be strongly coupled and in that case the structure-acoustic system must be studied in a coupled system to evaluate the natural frequencies and the response to dynamic excitation.

The systems studied often have complex shapes, leading to the conclusion that analytical functions cannot be used for describing the spatial distribution of the primary variables. Numerical methods must be employed. A review of different solution strategies for structure-acoustic problems is given by Atalla [16], where analytical methods and two numerical approaches: the finite element method and the boundary element method, are discussed. The development of structure-acoustic analysis using the finite element method for the study of vehicle interior noise is reviewed by Nefske et al. [17]. The basics of the finite element method are described in, for example, Ottosen and Petersson [18]. A more thorough investigation of the finite element method is found in, for example, the cited works of Bathe [19] or Zienkiewicz and Taylor [20], while a focus on dynamic problems is provided in Clough [21] or Chopra [22].

The formulation of coupled structure-acoustic problems using the finite element method is described, for example, in [3, 4, 23, 24]. In the finite element formulation, a system of equations describing the motion of the system is developed, with the number of equations

equal to the number of degrees of freedom introduced in the finite element discretisation. One important property of the equation system derived is the sparsity of the system matrices, i.e. only a few positions in these matrices are populated. This property results in that the time for solving the system of equations is much shorter, compared to solving a fully populated system of equations with equal size.

In the structural domain, the primary variable is displacement. For the fluid domain, several different primary variables can be used to describe the motion. Using the fluid displacement as the primary variable, both the structural and fluid domains can be described with the same type of solid elements. The fluid domain has no shear stiffness and normal modes with pure rotational motion are introduced. All rotational modes should have the eigenvalue equal to zero. However, spurious non-zero, and thereby non-physical, modes are introduced when using full integration of the solid element. Reduced integration can be used to make all eigenvalues of rotational modes equal to zero [25]. The hourglass modes due to the reduced integration can however interact with the correct modes giving spurious modes with the same frequencies as the correct ones. In [26], the element mass matrix was modified to account for this and the eigenvalue of all spurious modes becomes zero. A mixed displacement based finite element formulation was presented by Bathe [19], also removing the spurious modes. Using displacement to describe the fluid domain can be called an one-field formulation, with only the displacement field is used to describe the structure-acoustic system.

In order to remove the problem with non-physical modes and to arrive at a more compact system of equations, a potential description of the fluid domain can be used, such as the acoustic pressure or fluid displacement potential. The pressure formulation was used in [27, 28] to determine normal modes and eigenvalues of complex shaped rigid-wall enclosures and also in [29] to study the transient response of structure-acoustic systems. A two-field formulation, with structural displacements and fluid potential function is achieved with only one degree of freedom per fluid node. The derived system of equations using pressure or displacement potential yields an unsymmetric system of equations. A fluid velocity potential can also be used, where a matrix proportional to velocity is introduced [30]. To solve the structure-acoustic eigenvalue problem using the two field formulation, one needs an eigenvalue solver that either can handle unsymmetric matrices or can solve quadratic eigenvalue problems. Solving these problems are more computational intensive compared to solving the generalised eigenvalue problem for symmetric systems [31].

In order to achieve a symmetric system of equations describing the structure-acoustic system, a three field formulation with structural displacement, fluid pressure and fluid displacement potential can be used [32, 33]. By condensation of one of the fluid potentials, a symmetric two field system of equations can be achieved [4]. However, the system matrices then lose the positive property of being sparse.

Different types of methods for model reduction are often employed in structure-acoustic analysis. (For details about the model reduction techniques, see Chapter 3.) The most commonly used method is to reduce the system using the normal modes for the structural and fluid domains, derived in separate eigenvalue analysis of the two subdomains [34, 35]. In a paper by Sandberg [36], the un-symmetric eigenvalue problem, achieved when using the structural displacement and fluid pressure as primary variables, is made symmetric using the subdomain modes and matrix scaling. Reduction methods using component mode synthesis were also proposed in, for example, [37, 38]. In the thesis by Carlsson [4], the Lanczos procedure was used in investigating structure-acoustic

problems.

2.2 Governing equations

For the structure-acoustic system, the structure is (here) described by the differential equation of motion for a continuum body assuming small deformations and the fluid by the acoustic wave equation. Coupling conditions at the boundary between the structural and fluid domains ensure the continuity in displacement and pressure between the domains. The governing equations and boundary conditions can, as for example, was described in detail by Carlsson [4], be written:

$$\begin{aligned}
&\text{Structure}: && \begin{cases} \tilde{\boldsymbol{\nabla}}^T \boldsymbol{\sigma}_S + \mathbf{b}_S = \rho_S \dfrac{\partial^2 \mathbf{u}_S}{\partial t^2} & \Omega_S \\ + \text{ Boundary and initial conditions} \end{cases} \\
&\text{Fluid}: && \begin{cases} \dfrac{\partial^2 p_F}{\partial^2 t} - c_0^2 \boldsymbol{\nabla}^2 p_F = c_0^2 \dfrac{\partial q_F}{\partial t} & \Omega_F \\ + \text{ Boundary and initial conditions} \end{cases} \\
&\text{Coupling}: && \begin{cases} u_S|_n = u_F|_n & \partial\Omega_{FS} \\ \sigma_S|_n = -p_F & \partial\Omega_{FS} \end{cases}
\end{aligned} \tag{2.1}$$

The variables and material parameters are defined in the following sections, where also the finite element formulation of this coupled problem derived.

In Chapter 4, the finite element formulation of both the continuum body and the acoustic fluid are used for the modelling of porous sound absorbing materials. The structure of interest in most structure-acoustic problems is two dimensional and is therefore often described by plate or shell theory. For derivation of the system matrices for these problems, see, for example, [19, 20].

2.3 Finite element formulation

2.3.1 Structural domain

The structure is described by the equation of motion for a continuum body. The finite element formulation is derived with the assumption of small displacements. This presentation follows the matrix notation used by Ottosen and Petersson [18].

For a continuum material the equation of motion can be written

$$\tilde{\boldsymbol{\nabla}}^T \boldsymbol{\sigma}_S + \mathbf{b}_S = \mathbf{q}_S \tag{2.2}$$

with the displacement, $\mathbf{u}_S$, the body force, $\mathbf{b}_S$, and the inertia force, $\mathbf{q}_S$,

$$\mathbf{u}_S = \begin{bmatrix} u_1^S \\ u_2^S \\ u_3^S \end{bmatrix}; \quad \mathbf{b}_S = \begin{bmatrix} b_1^S \\ b_2^S \\ b_3^S \end{bmatrix}; \quad \mathbf{q}_S = \rho_S \frac{\partial^2 \mathbf{u}_S}{\partial t^2} \tag{2.3}$$

where ρ_S is the density of the material. The differential operator $\tilde{\boldsymbol{\nabla}}$ can be written

$$\tilde{\boldsymbol{\nabla}} = \begin{bmatrix} \dfrac{\partial}{\partial x_1} & 0 & 0 \\ 0 & \dfrac{\partial}{\partial x_2} & 0 \\ 0 & 0 & \dfrac{\partial}{\partial x_3} \\ \dfrac{\partial}{\partial x_2} & \dfrac{\partial}{\partial x_1} & 0 \\ \dfrac{\partial}{\partial x_3} & 0 & \dfrac{\partial}{\partial x_1} \\ 0 & \dfrac{\partial}{\partial x_3} & \dfrac{\partial}{\partial x_2} \end{bmatrix}; \tag{2.4}$$

The Green-Lagrange strain tensor, $\mathbf{E}_S$, and the Cauchy stress tensor $\mathbf{S}_S$ are defined as

$$\mathbf{E}_S = \begin{bmatrix} \varepsilon_{11}^S & \varepsilon_{12}^S & \varepsilon_{13}^S \\ & \varepsilon_{22}^S & \varepsilon_{23}^S \\ sym. & & \varepsilon_{33}^S \end{bmatrix}; \quad \mathbf{S}_S = \begin{bmatrix} \sigma_{11}^S & \sigma_{12}^S & \sigma_{13}^S \\ & \sigma_{22}^S & \sigma_{23}^S \\ sym. & & \sigma_{33}^S \end{bmatrix} \tag{2.5}$$

and in matrix notations the strains and stresses can be written

$$\boldsymbol{\varepsilon}_S = \begin{bmatrix} \varepsilon_{11}^S \\ \varepsilon_{22}^S \\ \varepsilon_{33}^S \\ \gamma_{12}^S \\ \gamma_{13}^S \\ \gamma_{23}^S \end{bmatrix} \quad \boldsymbol{\sigma}_S = \begin{bmatrix} \sigma_{11}^S \\ \sigma_{22}^S \\ \sigma_{33}^S \\ \sigma_{12}^S \\ \sigma_{13}^S \\ \sigma_{23}^S \end{bmatrix} \tag{2.6}$$

where $\gamma_{12}^S = 2\varepsilon_{12}^S$, $\gamma_{13}^S = 2\varepsilon_{13}^S$ and $\gamma_{23}^S = 2\varepsilon_{23}^S$. The kinematic relations, the relations between the displacements and strains, can be written

$$\boldsymbol{\varepsilon}_S = \tilde{\nabla}\mathbf{u}_S \tag{2.7}$$

For an isotropic material, the stresses and strains are related by the constitutive matrix $\mathbf{D}_S$ given by

$$\boldsymbol{\sigma}_S = \mathbf{D}_S\boldsymbol{\varepsilon}_S \tag{2.8}$$

where

$$\mathbf{D}_S = \begin{bmatrix} \lambda+2\mu & \lambda & \lambda & 0 & 0 & 0 \\ \lambda & \lambda+2\mu & \lambda & 0 & 0 & 0 \\ \lambda & \lambda & \lambda+2\mu & 0 & 0 & 0 \\ 0 & 0 & 0 & \mu & 0 & 0 \\ 0 & 0 & 0 & 0 & \mu & 0 \\ 0 & 0 & 0 & 0 & 0 & \mu \end{bmatrix} \tag{2.9}$$

The Lamé coefficients, λ and μ, are expressed in the modulus of elasticity, E, the shear modulus, G, and Poisson's ratio, ν by

$$\lambda = \frac{\nu E}{(1+\nu)(1-2\nu)} \tag{2.10}$$

$$\mu = G = \frac{E}{2(1+\nu)} \tag{2.11}$$

To arrive at the finite element formulation for the structural domain, the weak form of the differential equation is derived. This can be done by multiplying equation (2.2) with a weight function, $\mathbf{v}_S = [v_1\ v_2\ v_3]^T$, and integrating over the material domain, Ω_S,

$$\int_{\Omega_S} \mathbf{v}_S^T (\tilde{\boldsymbol{\nabla}}^T \boldsymbol{\sigma}_S - \rho_S \frac{\partial^2 \mathbf{u}_S}{\partial t^2} + \mathbf{b}_S) dV = 0 \tag{2.12}$$

Using Green-Gauss theorem on the first term in equation (2.12) gives

$$\int_{\Omega_S} \mathbf{v}_S^T \tilde{\boldsymbol{\nabla}}^T \boldsymbol{\sigma}_S dV = \int_{\partial\Omega_S} (\mathbf{v}_S)^T \mathbf{t}_S dS - \int_{\Omega_S} (\tilde{\boldsymbol{\nabla}} \mathbf{v}_S)^T \boldsymbol{\sigma}_S dV \tag{2.13}$$

The surface traction vector $\mathbf{t}_S$ related to the Cauchy stress tensor, $\mathbf{S}_S$, by

$$\mathbf{t}_S = \mathbf{S}_S \mathbf{n}_S \tag{2.14}$$

where $\mathbf{n}_S$ is the boundary normal vector pointing outward from the structural domain. The weak form of the problem can be written

$$\int_{\Omega_S} \mathbf{v}_S^T \rho_S \frac{\partial^2 \mathbf{u}_S}{\partial t^2} dV + \int_{\Omega_S} (\tilde{\boldsymbol{\nabla}} \mathbf{v}_S)^T \boldsymbol{\sigma}_S dV - \int_{\partial\Omega_S} (\mathbf{v}_S)^T \mathbf{t}_S dS - \int_{\Omega_S} \mathbf{v}_S^T \mathbf{b}_S dV = 0 \tag{2.15}$$

Introducing the finite element approximations of the displacements $\mathbf{d}_S$ and weight functions $\mathbf{c}_S$ by

$$\mathbf{u}_S = \mathbf{N}_S \mathbf{d}_S; \quad \mathbf{v}_S = \mathbf{N}_S \mathbf{c}_S \tag{2.16}$$

where $\mathbf{N}_S$ contains the finite element shape functions for the structural domain, the strains can be expressed as

$$\boldsymbol{\varepsilon}_S = \tilde{\boldsymbol{\nabla}} \mathbf{N}_S \mathbf{d}_S \tag{2.17}$$

This gives the finite element formulation for the structural domain, when described as a continuum body

$$\int_{\Omega_S} \mathbf{N}_S^T \rho_S \mathbf{N}_S dV \ddot{\mathbf{d}}_S + \int_{\Omega_S} (\tilde{\boldsymbol{\nabla}} \mathbf{N}_S)^T \mathbf{D}_S \tilde{\boldsymbol{\nabla}} \mathbf{N}_S dV \mathbf{d}_S = \int_{\partial\Omega_S} \mathbf{N}_S^T \mathbf{t}_S dS + \int_{\Omega_S} \mathbf{N}_S^T \mathbf{b}_S dV \tag{2.18}$$

and the governing system of equations can be written

$$\mathbf{M}_S \ddot{\mathbf{d}}_S + \mathbf{K}_S \mathbf{d}_S = \mathbf{f}_F + \mathbf{f}_b \tag{2.19}$$

where

$$\begin{aligned} \mathbf{M}_S &= \int_{\Omega_S} \mathbf{N}_S^T \rho_S \mathbf{N}_S dV; \quad \mathbf{K}_S = \int_{\Omega_S} (\tilde{\boldsymbol{\nabla}} \mathbf{N}_S)^T \mathbf{D}_S \tilde{\boldsymbol{\nabla}} \mathbf{N}_S dV \\ \mathbf{f}_F &= \int_{\partial\Omega_S} \mathbf{N}_S^T \mathbf{t}_S dS \qquad \mathbf{f}_b = \int_{\Omega_S} \mathbf{N}_S^T \mathbf{b}_S dV \end{aligned} \tag{2.20}$$

2.3.2 Acoustic fluid domain

The governing equations for an acoustic fluid are derived using the following assumptions for the compressible fluid [4]:

- The fluid is inviscid.
- The fluid only undergoes small translations.
- The fluid is irrotational.

Thereby, the governing equations for an acoustic fluid are, the equation of motion,

$$\rho_0 \frac{\partial^2 \mathbf{u}_F(t)}{\partial t^2} + \boldsymbol{\nabla} p_F(t) = 0 \tag{2.21}$$

the continuity equation,

$$\frac{\partial \rho_F(t)}{\partial t} + \rho_0 \boldsymbol{\nabla} \frac{\partial \mathbf{u}_F(t)}{\partial t} = q_F(t) \tag{2.22}$$

and the constitutive equation,

$$p_F(t) = c_0^2 \rho_F(t) \tag{2.23}$$

Here $\mathbf{u}_F(t)$ is the displacement, $p_F(t)$ is the dynamic pressure, $\rho_F(t)$ is the dynamic density and $q_F(t)$ is the added fluid mass per unit volume. ρ_0 is the static density and c_0 is the speed of sound. $\boldsymbol{\nabla}$ denotes a gradient of a variable, i.e.,

$$\boldsymbol{\nabla} = \left[\begin{array}{ccc} \dfrac{\partial}{\partial x_1} & \dfrac{\partial}{\partial x_2} & \dfrac{\partial}{\partial x_3} \end{array} \right]^T ; \tag{2.24}$$

The nonhomogeneous wave equation can be derived from equations (2.21) – (2.23). Differentiating equation (2.22) with respect to time and using (2.23) gives

$$\frac{1}{c_0^2} \frac{\partial^2 p_F}{\partial^2 t} + \rho_0 \boldsymbol{\nabla} \left(\rho_0 \frac{\partial^2 \mathbf{u}_F}{\partial t^2} \right) = \frac{\partial q_F}{\partial t} \tag{2.25}$$

Substituting (2.21) into this expression gives the nonhomogeneous wave equation expressed in acoustic pressure p_F.

$$\frac{\partial^2 p_F}{\partial^2 t} - c_0^2 \boldsymbol{\nabla}^2 p_F = c_0^2 \frac{\partial q_F}{\partial t} \tag{2.26}$$

where $\boldsymbol{\nabla}^2 = \partial^2/\partial x_1^2 + \partial^2/\partial x_2^2 + \partial^2/\partial x_3^2$.

The finite element formulation of equation (2.26) is derived by multiplying with a test function, v_F, and integrating over a volume Ω_F.

$$\int_{\Omega_F} v_F \left(\frac{\partial^2 p_F}{\partial^2 t} - c_0^2 \boldsymbol{\nabla}^2 p_F - c_0^2 \frac{\partial q_F}{\partial t} \right) dV = 0 \tag{2.27}$$

and with Green's theorem the weak formulation is achieved

$$\int_{\Omega_F} v_F \frac{\partial^2 p_F}{\partial^2 t} dV + c_0^2 \int_{\Omega_F} \boldsymbol{\nabla} v_F \boldsymbol{\nabla} p_F dV = c_0^2 \int_{\partial\Omega_F} v_F \boldsymbol{\nabla} p_F \mathbf{n}_F dA + c_0^2 \int_{\Omega_F} v_F \frac{\partial q_F}{\partial t} dV \tag{2.28}$$

where the boundary normal vector $\mathbf{n}_F$ points outward from the fluid domain. The finite element method approximates the pressure field and the weight function by

$$p_F = \mathbf{N}_F \mathbf{p}_F; \quad v_F = \mathbf{N}_F \mathbf{c}_F \tag{2.29}$$

where $\mathbf{p}_F$ contains the nodal pressures, $\mathbf{c}_F$ the nodal weights and $\mathbf{N}_F$ contains the finite element shape functions for the fluid domain. Inserting this into equation (2.28) and noting that $\mathbf{c}_F$ is arbitrary gives

$$\begin{aligned} \int_{\Omega_F} \mathbf{N}_F^T \mathbf{N}_F dV \ddot{\mathbf{p}}_F + c_0^2 \int_{\Omega_F} (\boldsymbol{\nabla} \mathbf{N}_F)^T \boldsymbol{\nabla} \mathbf{N}_F dV \mathbf{p}_F = \\ = c_0^2 \int_{\partial\Omega_F} \mathbf{N}_F^T \boldsymbol{\nabla} p_F \mathbf{n}_F dS + c_0^2 \int_{\Omega_F} \mathbf{N}_F^T \frac{\partial q_F}{\partial t} dV \end{aligned} \tag{2.30}$$

The system of equations for an acoustic fluid domain becomes

$$\mathbf{M}_F \ddot{\mathbf{p}} + \mathbf{K}_F \mathbf{p} = \mathbf{f}_q + \mathbf{f}_S \tag{2.31}$$

where

$$\begin{aligned} \mathbf{M}_F &= \int_{\Omega_F} \mathbf{N}_F^T \mathbf{N}_F dV; \qquad \mathbf{K}_F = c_0^2 \int_{\Omega_F} (\boldsymbol{\nabla} \mathbf{N}_F)^T \boldsymbol{\nabla} \mathbf{N}_F dV \\ \mathbf{f}_S &= c_0^2 \int_{\partial\Omega_F} \mathbf{N}_F^T \mathbf{n}_F^T \boldsymbol{\nabla} p dS; \quad \mathbf{f}_q = c_0^2 \int_{\Omega_F} \mathbf{N}_F^T \frac{\partial q}{\partial t} dV \end{aligned} \tag{2.32}$$

2.3.3 The coupled structure-acoustic system

At the boundary between the structural and fluid domains, denoted $\partial\Omega_{SF}$, the fluid particles and the structure moves together in the normal direction of the boundary. Introducing the normal vector $\mathbf{n} = \mathbf{n}_F = -\mathbf{n}_S$, the displacement boundary condition can be written

$$\mathbf{u}_S \mathbf{n}|_{\partial\Omega_{SF}} = \mathbf{u}_F \mathbf{n}|_{\partial\Omega_{SF}} \tag{2.33}$$

and the continuity in pressure

$$\sigma_S|_n = -p_F \tag{2.34}$$

where p_F is the acoustic fluid pressure. The structural stress tensor at the boundary $\partial\Omega_{SF}$ thus becomes

$$\mathbf{S}_S = -p_F \begin{bmatrix} 1 & 0 & 0 \\ 0 & 1 & 0 \\ 0 & 0 & 1 \end{bmatrix} \tag{2.35}$$

and the structural force term providing the coupling to the fluid domain, $\mathbf{f}_F$ (in equation (2.19)), can be written

$$\mathbf{f}_F = \int_{\partial\Omega_{SF}} \mathbf{N}_S^T (-p_F) \begin{bmatrix} 1 & 0 & 0 \\ 0 & 1 & 0 \\ 0 & 0 & 1 \end{bmatrix} \mathbf{n}_S dS = \int_{\partial\Omega_{SF}} \mathbf{N}_S^T \mathbf{n} p_F dS = \int_{\partial\Omega_{SF}} \mathbf{N}_S^T \mathbf{n} \mathbf{N}_F dS \mathbf{p}_F \tag{2.36}$$

Note that the structural boundary normal vector $\mathbf{n}_S$ is replaced with the normal vector $\mathbf{n}$ pointing in the opposite direction. The force acting on the structure is expressed in the acoustic fluid pressure.

For the fluid partition the coupling is introduced in the force term $\mathbf{f}_S$ (in equation (2.31)). Using the relation between pressure and acceleration in the fluid domain

$$\boldsymbol{\nabla} p_F = -\rho_0 \frac{\partial^2 \mathbf{u}_F(t)}{\partial t^2} \tag{2.37}$$

and the boundary condition in equation (2.33), the force acting on the fluid can be described in terms of structural acceleration

$$\mathbf{n}^T \boldsymbol{\nabla} p_F|_{\partial\Omega_{SF}} = -\rho_0 \mathbf{n}^T \frac{\partial^2 \mathbf{u}_F}{\partial t^2}|_{\partial\Omega_{SF}} = -\rho_0 \mathbf{n}^T \frac{\partial^2 \mathbf{u}_S}{\partial t^2}|_{\partial\Omega_{SF}} = -\rho_0 \mathbf{n}^T \mathbf{N}_S \ddot{\mathbf{d}}_S|_{\partial\Omega_{SF}} \tag{2.38}$$

and the boundary force term of the acoustic fluid domain, $\mathbf{f}_S$, can be expressed in structural acceleration

$$\mathbf{f}_S = -c_0^2 \int_{\partial\Omega_{FS}} \mathbf{N}_F^T \mathbf{n}^T \boldsymbol{\nabla} p_F dS = -\rho_0 c_0^2 \int_{\partial\Omega_{FS}} \mathbf{N}_F^T \mathbf{n}^T \mathbf{N}_S dS \ddot{\mathbf{d}}_S \tag{2.39}$$

The introduction of a spatial coupling matrix

$$\mathbf{H}_{SF} = \int_{\partial\Omega_{SF}} \mathbf{N}_S^T \mathbf{n} \mathbf{N}_F dS \tag{2.40}$$

allows the coupling forces to be written as

$$\mathbf{f}_F = \mathbf{H}_{SF} \mathbf{p}_F \tag{2.41}$$

and

$$\mathbf{f}_S = -\rho_0 c_0^2 \mathbf{H}_{SF}^T \ddot{\mathbf{d}}_S \tag{2.42}$$

The structure-acoustic problem can then be described by an unsymmetrical system of equations

$$\begin{bmatrix} \mathbf{M}_S & \mathbf{0} \\ \rho_0 c_0^2 \mathbf{H}_{SF}^T & \mathbf{M}_F \end{bmatrix} \begin{bmatrix} \ddot{\mathbf{d}}_S \\ \ddot{\mathbf{p}}_F \end{bmatrix} + \begin{bmatrix} \mathbf{K}_S & -\mathbf{H}_{SF} \\ 0 & \mathbf{K}_F \end{bmatrix} \begin{bmatrix} \mathbf{d}_S \\ \mathbf{p}_F \end{bmatrix} = \begin{bmatrix} \mathbf{f}_b \\ \mathbf{f}_q \end{bmatrix} \tag{2.43}$$

This system is studied through out this thesis. In Chapter 3, different model reduction techniques are described with focus on the structural domain, which also can be applied to the acoustic fluid domain. The porous sound absorbing materials, investigated in Chapter 4, can be modelled using an equivalent fluid model, i.e. modifying the material properties of the acoustic fluid, or using the equations for the continuum body. In the papers included in this thesis, procedures for reducing this system of equations is described and developed.

2.4 Summary

The governing equations of the structure-acoustic problem was presented. The finite element formulation of this problem was also derived. This formulation is adopted both in the following chapters as well as in the papers included in the thesis.

Chapter 3

Modal reduction techniques

This chapter comprises an investigation of different methods for reducing the size of the equation system to be solved in structural vibration problems, when using the finite element method. The chapter is a basis for the papers included in the theses, where modal reduction techniques are adopted and developed for the study of structure-acoustic systems. Using the finite element method to analyse the dynamic behaviour of a structure, the size of the equation system of motion often becomes very large. Increasing the complexity of the model or the maximum frequency of interest leads to an increasing number of degrees of freedom and thereby an increasing size of the system of equations. Solving the problem becomes computation-intensive, so it is desirable to reduce the size of the system by use of modal reduction techniques, with as little loss of information about dynamic behaviour of the system as possible. First, a literature review of the studied problem is presented. The problem of interest is then described and after that the different reduction methods are discussed. In parallel with the description of the methods, a numerical example is studied.

3.1 Literature review

Finite element formulation of the structural vibration problem can be found in [19, 20, 21, 22]. The system is studied either in free vibration solving the eigenvalue problem, or for some type of force excitation. The studied modal reduction techniques are divided into three different – although closely related – methods: introducing generalised coordinates, condensation methods and component mode synthesis. All three methods are variants of a Rayleigh-Ritz procedure [19].

When introducing generalised coordinates, a reduced set of basis vectors, compared to the original (physical) coordinates, are derived. For example, after solving the eigenvalue problem, only a few of the calculated normal modes with the lowest natural frequency are needed to describe the system [19, 21, 22]. Types of modes other then normal can also be used. When using Ritz vectors [39, 40, 41, 42], or Lanczos vectors [4, 43, 44], a very efficient modal reduction of the system can be performed.

In condensation methods, a large number of the degrees of freedom, that are not needed in describing the dynamic behaviour of the system, is removed. This can be done by static (Guyan) condensation [45], where the choice of the kept degrees of freedom is

very important [46, 47, 48]. The reduction of the problem can also achieved by dynamic condensation, where the influence of the internal degrees of freedom are accounted for in a simplified manner [49, 50, 51, 52, 53].

A frequently used method for substructuring and modal reduction is the component mode synthesis method. The research conducted to develop this method was reviewed by Seshu [54] and detailed description of the method can be found in, for example, the book by Craig [55]. The problem domain under study is divided into a number of components, or subdomains, and a set of basis vectors is derived for each component to be included in the description of the whole system. Using generalised coordinates or condensation methods can be seen as special cases of the component mode synthesis method.

Component mode methods are usually divided into the fixed-interface component mode method and the free-interface component mode method. The fixed-interface mode method uses static condensation of each component, only keeping the degrees of freedom at the interface between components [56]. These basis vectors, which fulfil the displacement and force continuity at the interface boundary, are expanded with internal modes calculated with the interface degrees of freedom fixed. The eigenvalue problem of the static-reduced system, only including the interface degrees of freedom, can first be solved. The inclusion of only a number of these modes reduces the size of the reduced system further [57, 58]. The convergence of the fixed-interface mode method can be improved in a certain frequency range using quasi-static constraint modes as basis vectors [59].

Using the free interface mode method, the internal modes are calculated without constraints on the interface degrees of freedom, see [60, 61, 62] for recent developments of this method. The continuity over the interface is achieved by including attachment modes, which are calculated by applying a unit force on each of the interface degrees of freedom with the other interface degrees of freedom unconstrained.

3.2 Problem formulation

The system of equations of the finite element formulated structural vibration problem can be written

$$\mathbf{M}\ddot{\mathbf{d}} + \mathbf{C}\dot{\mathbf{d}} + \mathbf{K}\mathbf{d} = \mathbf{f} \tag{3.1}$$

where $\mathbf{d}$ contains the displacements, $\mathbf{M}$ is the mass matrix, $\mathbf{C}$ is the viscous damping matrix, $\mathbf{K}$ is the stiffness matrix and $\mathbf{f}$ is the nodal force vector. The system of equations has n degrees of freedom. This system is solved for two typical loading conditions. Solving the system for a transient excitation, a time stepping technique, for example the Newmark method [21, 22], is often adopted. Assuming harmonic excitation, a steady-state solution is sought, where the force and corresponding response are expressed as harmonic functions,

$$\begin{aligned} \mathbf{f} &= \hat{\mathbf{f}}\mathrm{e}^{\mathrm{i}\omega t} \\ \mathbf{d} &= \hat{\mathbf{d}}\mathrm{e}^{\mathrm{i}\omega t} \end{aligned} \tag{3.2}$$

where $\hat{\mathbf{f}}$ and $\hat{\mathbf{d}}$ are the complex force and displacement amplitudes. Also, ω is the angular frequency, t denotes time and $\mathrm{i} = \sqrt{-1}$. Inserting these expressions into equation (3.1), and suppressing the time dependance $\mathrm{e}^{\mathrm{i}\omega t}$, the equation of motion in the frequency domain becomes

$$\mathbf{D}(\omega)\hat{\mathbf{d}} = \hat{\mathbf{f}} \tag{3.3}$$

where the dynamic stiffness matrix $\mathbf{D}(\omega)$, dependent on excitation frequency, determine the response,

$$\mathbf{D}(\omega) = -\omega^2\mathbf{M} + \mathrm{i}\omega\mathbf{C} + \mathbf{K} \tag{3.4}$$

The eigenvalue problem

The eigenvalue problem is solved in order to describe the dynamic behaviour in free motion of the studied system in equation (3.3). The derived eigenvectors, or normal modes, are employed in the modal reduction techniques described below. For free motion, the force term is zero and when neglecting damping, the freely vibrating system can be written

$$\left(\mathbf{K} - \omega^2\mathbf{M}\right)\hat{\mathbf{d}} = \mathbf{0} \tag{3.5}$$

This system has a non-trivial solution if

$$\det\left(\mathbf{K} - \omega^2\mathbf{M}\right) = 0 \tag{3.6}$$

which is called the characteristic equation. This equation, has the same order as the number of degrees of freedom of the system. The roots of the characteristic equation are the n eigenvalues of the system. For each eigenvalue, $\lambda_i = \omega_i^2$, a displacement shape fulfil equation (3.5). This is the corresponding eigenvector, or normal mode, $\boldsymbol{\phi}_i$. The system can be written

$$\left(\mathbf{K} - \lambda_i\mathbf{M}\right)\boldsymbol{\phi}_i = \mathbf{0} \tag{3.7}$$

Premultiplying equation (3.7) with the transposed eigenvector, $\boldsymbol{\phi}_i^T$, the eigenvalue, λ_i, can be determined by

$$\lambda_i = \frac{\boldsymbol{\phi}_i^T\mathbf{K}\boldsymbol{\phi}_i}{\boldsymbol{\phi}_i^T\mathbf{M}\boldsymbol{\phi}_i} \tag{3.8}$$

which is called the Rayleigh quotient. Introducing the matrix $\boldsymbol{\Lambda}$, with the eigenvalues of the system in the diagonal and the matrix $\boldsymbol{\Phi}$, with the corresponding normal modes as column vectors, the generalised eigenvalue problem can be written

$$\left(\mathbf{K} - \boldsymbol{\Lambda}\mathbf{M}\right)\boldsymbol{\Phi} = \mathbf{0} \tag{3.9}$$

With mass-normalised eigenvectors the following properties can be noted

$$\boldsymbol{\Phi}^T\mathbf{M}\boldsymbol{\Phi} = \mathbf{I} \qquad \boldsymbol{\Phi}^T\mathbf{K}\boldsymbol{\Phi} = \boldsymbol{\Lambda} \tag{3.10}$$

Using the finite element method, the system of equations (3.9) often has a very large number of degrees of freedom, n, and usually only m of the lowest eigenvalues are wanted, where $m \ll n$. Some type of iterative procedure can be adopted to solve the eigenvalue problem [19]. The solution of this problem is studied in Section 3.3.

Rayleigh-Ritz procedure

In the Rayleigh-Ritz procedure, it is assumed that the motion of the system can be described using a reduced set of basis vectors, or modes,

$$\mathbf{d} = \boldsymbol{\Psi}_1\xi_1 + \boldsymbol{\Psi}_2\xi_2 + ... + \boldsymbol{\Psi}_m\xi_m = \boldsymbol{\Psi}\boldsymbol{\xi} \tag{3.11}$$

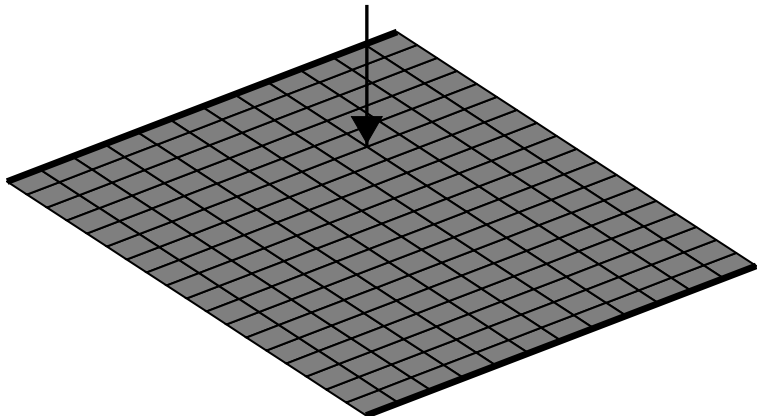

Figure 3.1: *The plate studied in the numerical example. The bold lines show where the plate is fixed and the force applied in the frequency response example is also displayed.*

where $\mathbf{\Psi}_1$, ..., $\mathbf{\Psi}_m$ are the mode shapes and ξ_1, .., ξ_m the corresponding modal coordinates. The keystone in the procedure is that the number of introduced modes m is much smaller then the total number of degrees of freedom, n. Introducing equation (3.11) in the equation system of motion (3.1), and multiplying from left with $\mathbf{\Psi}^T$ the system is reduced to

$$\mathbf{\Psi}^T\mathbf{M}\mathbf{\Psi}\ddot{\boldsymbol{\xi}} + \mathbf{\Psi}^T\mathbf{C}\mathbf{\Psi}\dot{\boldsymbol{\xi}} + \mathbf{\Psi}^T\mathbf{K}\mathbf{\Psi}\boldsymbol{\xi} = \mathbf{\Psi}^T\mathbf{f} \tag{3.12}$$

It can here be noted that in the following sections, $\mathbf{\Phi}$ is used to denote normal modes derived from an eigenvalue analysis of the system while $\mathbf{\Psi}$ contains any suitable vectors to be used in the Rayleigh-Ritz procedure. Three main approaches for the Rayleigh-Ritz procedure are described:

- Introducing generalised coordinates, for example normal modes or Krylov vectors, Section 3.3.
- Condensation methods where the model is divided into master (kept) degrees of freedom and internal degrees of freedom which can be condensed using either static or dynamic condensation, Section 3.4.
- The component mode synthesis method where the studied problem domain is divided into subdomains. For each domain so called component modes are derived which are then coupled together for the whole structure using Lagrange multipliers, Section 3.5.

In parallel with the description of the reduction methods, a numerical example, being an aluminium plate (see Figure 3.1), is studied. The plate, with the thickness 3 mm, is 0.3 m long (x direction) and 0.2 m wide (y direction). The plate boundaries are fixed in both translation and rotation at $x = 0$ m and $x = 0.3$ m and free at $y = 0$ m and $x = 0.2$ m. The modulus of elasticity $E = 70$ GPa, Poisson's ratio $\nu = 0.3$, density $\rho = 2700$ kg/m^3 and the hysteretic damping factor $\eta = 0.02$.

3.3 Generalised coordinates

The system is reduced by introducing vectors which limits the possible movement of the system to certain mode shapes. These vectors should fulfil the Dirchlet boundary conditions (displacements) and the Neumann boundary conditions (applied forces) are introduced by computing modal forces. The system is here reduced using two types of generalised coordinates, either using normal modes, derived in an eigenvalue analysis, or Krylov modes, which are derived in an iterative procedure discussed below. The Krylov modes are often used to reduce the system when performing eigenvalue analysis.

3.3.1 Normal modes

For a system with n degrees of freedom, the eigenvalue problem, in equation (3.9), can be solved and n normal modes can be calculated, which describes all possible movement of the system. In an analysis it is however often only necessary to include m number of the lowest modes, where $m \ll n$, based on two assumptions:

- The dynamic force only excites the modes included.
- The finite element model introduces a frequency limit above which the model ceases to be valid, the modes over this limit being nonphysical.

Also, when only a limited number of modes are needed, the iterative procedures using Krylov methods, described in the next section, are very effective in solving the eigenvalue problem. Using the normal modes to reduce the system in equation (3.12), the mass and stiffness matrices are reduced to two diagonal matrices. With mass-normalised normal modes the system can be written

$$\mathbf{I}\ddot{\boldsymbol{\xi}} + \boldsymbol{\Phi}^T\mathbf{C}\boldsymbol{\Phi}\dot{\boldsymbol{\xi}} + \boldsymbol{\Lambda}\boldsymbol{\xi} = \boldsymbol{\Phi}^T\mathbf{f} \tag{3.13}$$

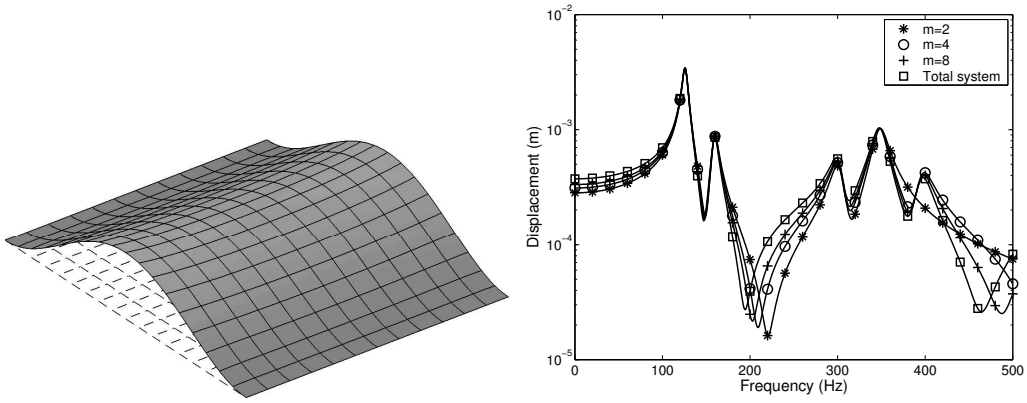

a) b)

Figure 3.2: *a) First normal mode, with natural frequency 126 Hz, of the plate. b) Displacement response of the point force using m normal modes to describe the system.*

where $\mathbf{I}$ is the unity matrix, $\mathbf{\Lambda}$ contains the eigenvalues in the diagonal and $\mathbf{\Phi}$ the eigenvectors, or normal modes. With general damping, the modal damping matrix becomes fully populated. Using simplified damping descriptions – being either proportional Rayleigh damping or hysteretic damping – the damping matrix becomes diagonal ending up with an uncoupled system of equations [22]. For the example problem, the normal mode with the lowest natural frequency is displayed in Figure 3.2 a) and the frequency response to the point force, with the amplitude 100 N, applied according to Figure 3.1, when varying the number of normal modes included in the system of equations (3.13).

3.3.2 Krylov modes

For a given matrix, $\mathbf{A}$, and a non-zero start vector, $\mathbf{r}_0$, m linear independent Krylov vectors, i.e. the columns in the Krylov matrix $\mathbf{\Psi}_K$, can be derived by a sequence of multiplications

$$\mathbf{\Psi}_K = \left[\begin{array}{cccc} \mathbf{r}_0, & \mathbf{A}\mathbf{r}_0, & ..., & \mathbf{A}^{m-1}\mathbf{r}_0 \end{array} \right] \tag{3.14}$$

Performing these multiplications, the last column of the matrix converges towards the wanted eigenvector, non-orthogonal to the start vector $\mathbf{r}_0$, corresponding to the largest eigenvalue of the matrix. This can be employed for solving the eigenvalue problem of interest here, given in equation (3.9), by rewriting it on the form

$$\mathbf{K}^{-1}\mathbf{M}\mathbf{\Phi} = \boldsymbol{\mu}\mathbf{\Phi} \tag{3.15}$$

A standard eigenvalue problem of the matrix $\mathbf{K}^{-1}\mathbf{M}$ is achieved. The eigenvectors of this system is equal to the eigenvectors of equation (3.9) and the eigenvalues, λ_i, of the original system relates to μ_i by

$$\lambda_i = \frac{1}{\mu_i} \tag{3.16}$$

Replacing the matrix $\mathbf{A}$ with $\mathbf{K}^{-1}\mathbf{M}$ in equation (3.14), the Krylov matrix becomes

$$\mathbf{\Psi}_K = \left[\begin{array}{cccc} \mathbf{r}_0, & \mathbf{K}^{-1}\mathbf{M}\mathbf{r}_0, & ..., & (\mathbf{K}^{-1}\mathbf{M})^{m-1}\mathbf{r}_0 \end{array} \right] \tag{3.17}$$

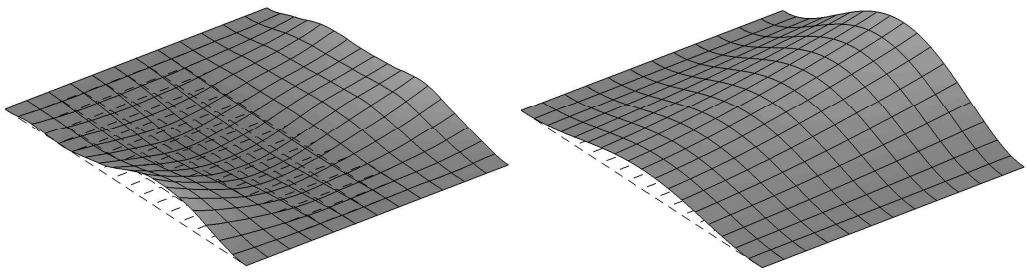

Figure 3.3: *The first and fourth Krylov vector generated from a random pressure distribution over the plate.*

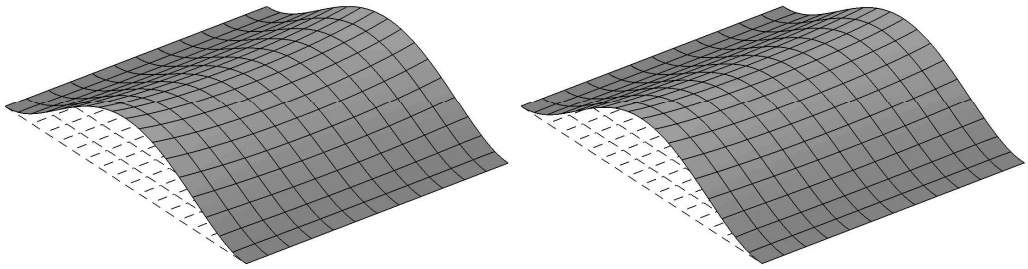

Figure 3.4: *The first and fourth Krylov vector generated from an uniform pressure distribution over the plate.*

The last column converges to the eigenvector, $\boldsymbol{\phi}_1$, corresponding to the largest eigenvalue of this matrix, μ_1. The eigenvalue, μ_1, can be calculated using the Rayleigh quotient in equation (3.8). The eigenvalue, λ_1, of the original system of equation (3.9) can be determined by $\lambda_1 = 1/\mu_1$ (see equation (3.16)). That is, the lowest eigenvalue of the problem in equation (3.9) is derived. To find the lowest eigenvalue of the system only the last column of the Krylov matrix is needed. However, the Krylov matrix in equation (3.17) can also be used as an reduced base for the original problem by it self; m vectors is generated as the Rayleigh-Ritz base in equation (3.11). Two different, but similar, approaches are described in the following sections using the Krylov method, the first using Ritz vectors based on static deformation, and the second method being the Lanczos method. First, the choice of static force vector used for deriving the start vector and the method of shifting stiffness matrix to avoid singularities are discussed.

Calculating the start vector

The start vector $\mathbf{r}_0$ is calculated by applying a static force vector, $\mathbf{f}_0$, on the system

$$\mathbf{r}_0 = \mathbf{K}^{-1}\mathbf{f}_0 \tag{3.18}$$

The choice of the force vector determines how fast the Krylov vectors converges towards the first normal mode. Examples of the Krylov vectors derived when applying a random or uniform pressure to calculate the start vector are plotted in Figures 3.3 and 3.4, respectively. For both force vectors, the vectors converge towards the mode shape with the lowest natural frequency, which is displayed in Figure 3.2 a). However, when the response to the force vector, $\mathbf{f}_0$, is similar to the first mode shape the converges is more rapid, i.e. fewer columns in the Krylov matrix have to be calculated before the last calculated Krylov vector is equal to the normal mode, for a certain tolerance. The force vector achieved for uniformly distributed pressure, resembles the inertia forces excited by the mode shape in free vibration and the convergence is faster. In eigenvalue analysis, the force vector must be chosen non-orthogonal to all eigenvectors desired, i.e. as a random vector. For response analysis, the force vector can be chosen as the static part of the dynamic force vector. All derived Krylov vectors are thereby non-orthogonal to the force vector, and an efficient reduced base can be derived.

Shifting

In the Krylov methods, the stiffness matrix is inverted and in the above description it has been assumed that this is possible, i.e. that the stiffness matrix is not singular. If it is singular, a shift point can be introduced. The shifted stiffness matrix can be written

$$\mathbf{K}_\sigma = \mathbf{K} - \sigma\mathbf{M} \tag{3.19}$$

and the eigenvalue problem rewritten using the inverted shifted stiffness matrix becomes

$$\mathbf{K}_\sigma^{-1}\mathbf{M}\boldsymbol{\Phi} = \boldsymbol{\tau}\boldsymbol{\Phi} \tag{3.20}$$

The normal modes are not affected by this shift and the eigenvalue λ_i in equation (3.9) is related to eigenvalue τ_i by

$$\lambda_i = \frac{1}{\tau_i} + \sigma \tag{3.21}$$

The shift point can also be used to improve convergence in a certain frequency range; the eigenvalues closest to the shift point converge first, as can be seen in Figure 3.7.

Ritz vectors based on static deformation

A set of mass-orthogonal Ritz vectors, $\boldsymbol{\Psi}_R = [\mathbf{x}_1 ... \mathbf{x}_m]$, can be derived using the procedure described in Table 3.1. The first Ritz-vector is the response to a static force applied to the system. The force vector is non-orthogonal to all the derived Ritz vectors. The (needed) Ritz vectors are then derived in an iterative fashion based on the Krylov method. In each step, the new Krylov vector is mass-orthogonalised to the previous ones. The two first Ritz vectors derived when applying a random pressure are displayed in Figure 3.5 and when applying an uniform pressure in Figure 3.6. Note that the uniform pressure only produces symmetric Ritz vectors. The generated vectors can be used to perform the reduction in equation (3.12).

Lanczos vectors

The Lanczos procedure is a very efficient method for deriving a few of the eigenvalues and eigenvectors of a large matrix based on the Krylov subspace method [4, 19, 63, 64]. The

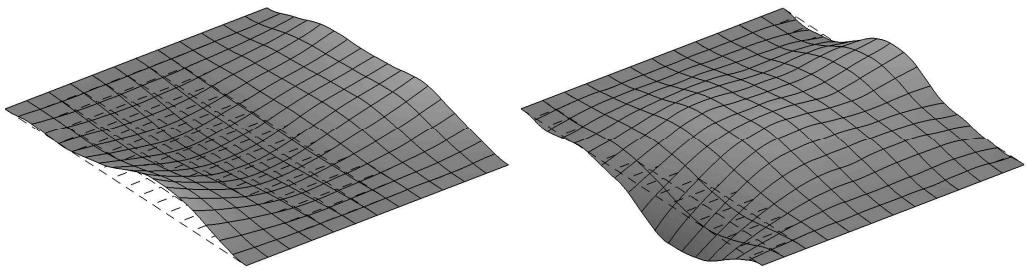

Figure 3.5: *The two first Ritz vectors derived when the force vector is generated from a random pressure distribution over the plate.*

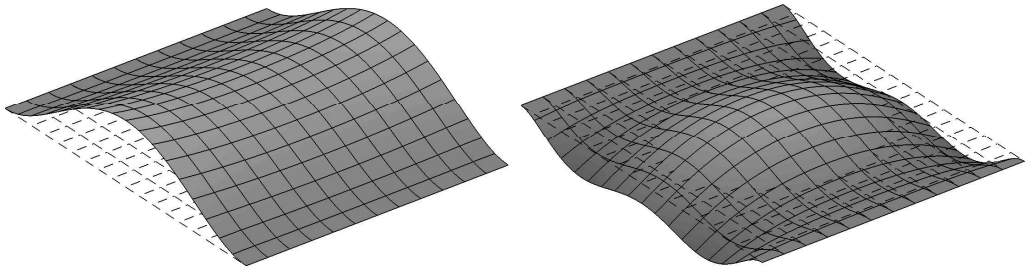

Figure 3.6: *The two first Ritz vectors derived when the force vector is generated from an uniform pressure distribution over the plate.*

studied system can be written

$$\mathbf{K}_\sigma^{-1}\mathbf{M}\ddot{\mathbf{d}} + \mathbf{K}_\sigma^{-1}\mathbf{C}\dot{\mathbf{d}} + (\mathbf{I} + \sigma\mathbf{K}_\sigma^{-1}\mathbf{M})\mathbf{d} = \mathbf{K}_\sigma^{-1}\mathbf{f} \tag{3.22}$$

where the system in equation (3.1) is multiplied with the shifted and inverted stiffness matrix. The aim is to perform the change of base

$$\mathbf{d} = \mathbf{\Psi}_L \boldsymbol{\xi}_L \tag{3.23}$$

Table 3.1: *Algorithm to generate m Ritz vectors*

1. Known stiffness and mass matrices $\mathbf{M}$ and $\mathbf{K}$.
2. Generate force vector $\mathbf{f}$.
3. Factorise the stiffness matrix,
   $$\mathbf{K} = \mathbf{LU} \text{ or } \mathbf{K} = \mathbf{LDL}^T.$$
4. Generate the first vector, $\mathbf{x}_1$:
   a) Solve for the first vector,
   $$\mathbf{K}\hat{\mathbf{x}}_1 = \mathbf{f}.$$
   b) Mass-normalise the vector,
   $$\mathbf{x}_1 = (\hat{\mathbf{x}}_1^T\mathbf{M}\hat{\mathbf{x}}_1)^{-1/2}\hat{\mathbf{x}}_1.$$
5. Loop for achieving the additional vectors, $i = 2, ..., m$:
   a) Solve for vector $\hat{\mathbf{x}}_i$,
   $$\mathbf{K}\hat{\mathbf{x}}_i = \mathbf{M}\mathbf{x}_{i-1}$$
   b) Mass-orthogonality of the new vector using Gram-Schmidt method.
   $$\hat{\mathbf{x}}_i = \hat{\mathbf{x}}_i - \sum_{j=1}^{i-1}(\mathbf{x}_j^T\mathbf{M}\hat{\mathbf{x}}_i)\mathbf{x}_j$$
   c) Mass-normalise the vector,
   $$\mathbf{x}_i = (\hat{\mathbf{x}}_i^T\mathbf{M}\hat{\mathbf{x}}_i)^{-1/2}\hat{\mathbf{x}}_i.$$

where $\mathbf{\Psi}_L = [\mathbf{q}_1 \ ... \ \mathbf{q}_m]$ contains the Lanczos vectors, which are mass-orthogonal, i.e.

$$\mathbf{\Psi}_L^T \mathbf{M} \mathbf{\Psi}_L = \mathbf{I} \tag{3.24}$$

In deriving the Lanczos vectors, it can be shown, as described by Nour-Omid [63], that the new vector in the Krylov sequence can be expressed by the two previous Lanczos vectors and a residual vector

$$\mathbf{K}_\sigma^{-1} \mathbf{M} \mathbf{q}_j = \mathbf{r}_j + \mathbf{q}_j \alpha_j + \mathbf{q}_{j-1} \beta_{j-1} \tag{3.25}$$

where the residual vector can be expressed

$$\mathbf{r}_j = \mathbf{q}_{j+1} \beta_j \tag{3.26}$$

and

$$\begin{aligned} \alpha_j &= \mathbf{q}_j^T \mathbf{M} \mathbf{K}_\sigma^{-1} \mathbf{M} \mathbf{q}_j \\ \beta_{j-1} &= \mathbf{q}_{j-1}^T \mathbf{M} \mathbf{K}_\sigma^{-1} \mathbf{M} \mathbf{q}_j \end{aligned} \tag{3.27}$$

The residual vector, $\mathbf{r}_j$ is calculated in each step and then normalised using β_j to arrive at the new Lanczos vector, $\mathbf{q}_{i+1}$. After m steps the system can be written

$$\mathbf{K}_\sigma^{-1} \mathbf{M} \mathbf{\Psi}_L = \mathbf{\Psi}_L \mathbf{T} + \mathbf{R}_m \tag{3.28}$$

where $\mathbf{T}$, with a tri-diagonal form, can be written

$$\mathbf{T} = \begin{bmatrix} \alpha_1 & \beta_1 & & & \\ \beta_1 & \alpha_2 & & & \\ & & ... & & \\ & & & \alpha_{m-1} & \beta_{m-1} \\ & & & \beta_{m-1} & \alpha_m \end{bmatrix} \tag{3.29}$$

and

$$\mathbf{R}_m = \begin{bmatrix} \mathbf{0} & \mathbf{0} & ... & \mathbf{0} & \mathbf{r}_m \end{bmatrix} \tag{3.30}$$

The residual $\mathbf{R}_m$ is orthogonal to the derived Lanczos vectors. Multiplying on the left side of equation (3.28) with $\mathbf{\Psi}_L^T \mathbf{M}$ and using the mass-orthogonality in equation (3.24) the system can be written

$$\mathbf{\Psi}_L^T \mathbf{M} \mathbf{K}_\sigma^{-1} \mathbf{M} \mathbf{\Psi}_L = \mathbf{T} \tag{3.31}$$

Introducing the change of base of equation (3.23) in the eigenvalue problem (3.20), i.e. expressing the normal modes in original coordinates by use of the Lanczos vectors,

$$\mathbf{\Phi} = \mathbf{\Psi}_L \hat{\mathbf{\Phi}} \tag{3.32}$$

and multiplying the system from left with $\mathbf{\Psi}_L^T \mathbf{M}$, the problem can be written

$$\mathbf{T}_m \hat{\mathbf{\Phi}} = \boldsymbol{\mu} \hat{\mathbf{\Phi}} \tag{3.33}$$

The eigenvalues of the original system can still be determined by (3.21). The procedure to derive the Lanczos vectors is described in Table 3.2 and performs a Lanczos step for each start vector. Using one start vector the algorithm is used in deriving m Lanczos vectors, $\mathbf{\Psi}_L = [\mathbf{q}_1 \ ... \ \mathbf{q}_m]$. However, a restart of the procedure – i.e. another Lanczos step with a

Table 3.2: *Algorithm to generate the Lanczos vectors.*

1. Input:
   Stiffness matrix $\mathbf{K}$, mass matrix $\mathbf{M}$ and boundary conditions.
2. Choose a shift point, σ, and factorise the system matrix,
   $$\mathbf{K} - \sigma\mathbf{M} = \mathbf{LU} \text{ or } \mathbf{K} - \sigma\mathbf{M} = \mathbf{LDL}^T.$$
3. Generate arbitrary force vector $\mathbf{f}_0$.
4. Generate the start vector, $\mathbf{r}_0$,
   $$(\mathbf{K} - \mu\mathbf{M})\mathbf{r}_0 = \mathbf{f}_0.$$
5. Compute the first Lanczos vector, $\mathbf{q}_1$,
   a) Compute,
   $$\beta_0 = \mathbf{r}_0^T\mathbf{M}\mathbf{r}_0.$$
   b) Compute the first Lanczos vector,
   $$\mathbf{q}_1 = \mathbf{r}_0/\beta_0$$
6. Loop for achieving the additional Lanczos vectors $i = 1, ..., m$,
   where m is the maximum number of Lanczos vectors to be derived.
   a) Solve for vector $\hat{\mathbf{r}}_i$,
   $$(\mathbf{K} - \mu\mathbf{M})\hat{\mathbf{r}}_i = \mathbf{M}\mathbf{q}_i$$
   b) Compute α_i,
   $$\alpha_i = \hat{\mathbf{r}}_i^T\mathbf{M}\mathbf{q}_i$$
   c) Compute the residual vector
   $$\mathbf{r}_i = \hat{\mathbf{r}}_i - \alpha_i\mathbf{q}_i - \beta_{i-1}\mathbf{q}_{i-1}$$
   d) Mass-orthogonality of the vector using Gram-Schmidt method
   $$\mathbf{r}_i = \mathbf{r}_i - \sum_{k=1}^{i}(\mathbf{r}_i\mathbf{M}\mathbf{q_k})\mathbf{q}_k$$
   e) Check for orthogonality
   $$\beta_i = \mathbf{r}_i^T\mathbf{M}\mathbf{r}_i.$$
   If $\beta_i < \tau$, the orthogonality is lost and the loop is ended,
   τ is a selected tolerance, for example, $\tau = 10^{-12}$.
   f) Compute the $(i+1)'th$ Lanczos vector
   $$\mathbf{q}_{i+1} = \mathbf{r}_i/\beta_i$$

new start vector and shift point – can be needed due to the fact that only eigenvectors that are non-orthogonal to the start vector can be determined. The method of shifting the stiffness matrix can also be used to improve convergence of the eigenvectors towards the correct ones, the eigenvalues closest to the shift point converges first.

The Lanczos procedure can be used in direct analysis using the Lanczos vectors, with a start vector derived from the geometrical distribution of the dynamic force, as the Rayleigh-Ritz base. Performing the same change of basis vectors in equation (3.22) as

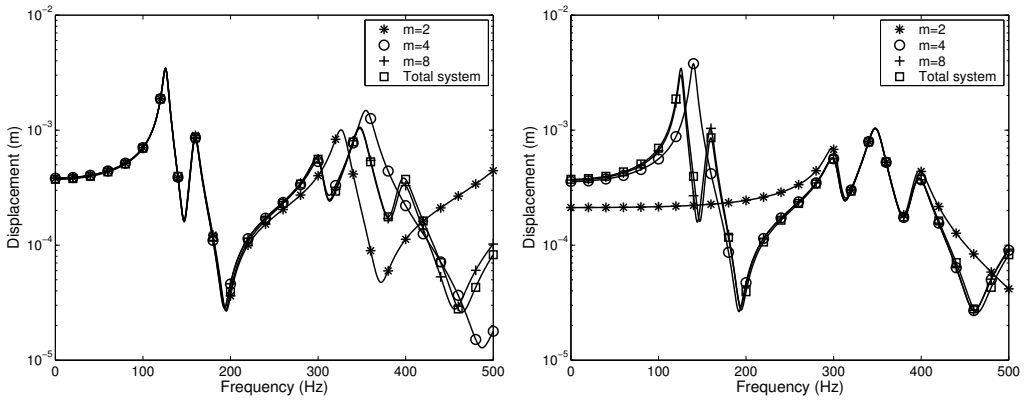

Figure 3.7: *The displacement calculated at the applied point force when varying the number of Lanczos vectors, in the left figure, the shift point* $\sigma = 0$ *and in the right figure,* $\sigma = (2\pi 350)^2$.

was done for the eigenvalue problem (3.33), the reduced system becomes

$$\mathbf{T}\ddot{\boldsymbol{\xi}}_L + \boldsymbol{\Psi}_L^T \mathbf{M}\mathbf{K}_\sigma^{-1}\mathbf{C}\boldsymbol{\Psi}_L\dot{\boldsymbol{\xi}}_L + (\mathbf{I}+\sigma\mathbf{T})\boldsymbol{\xi}_L = \boldsymbol{\Psi}_L^T\mathbf{M}\mathbf{K}_\sigma^{-1}\mathbf{f} \tag{3.34}$$

Having proportional damping, the system is reduced to a tri-diagonal form having m degrees of freedom. The plate in Figure 3.1 is studied in a frequency response analysis using the Lanczos vectors to reduce the dynamic system, see Figure 3.7. Two different shift points are used in the derivation of the Lanczos vectors. Choosing $\sigma = 0$ gives the first Lanczos vector equal to the static response, which shows that the response at zero frequency is exact. With $\sigma = (2\pi 350)^2$, i.e. the Lanczos vectors are calculated at the frequency 350 Hz, the calculated response at this frequency is exact as compared to solving the total system.

3.4 Condensation of degrees of freedom

The number of physical degrees of freedom can be reduced by either static (Guyan) or dynamic condensation. The system of equations (3.1) is partitioned into master degrees of freedom, $\mathbf{d}_b$, which are retained, and slave degrees of freedom, $\mathbf{d}_s$, which are to be condensed, as (when neglecting damping)

$$\begin{bmatrix} \mathbf{M}_{bb} & \mathbf{M}_{bs} \\ \mathbf{M}_{sb} & \mathbf{M}_{ss} \end{bmatrix} \begin{bmatrix} \ddot{\mathbf{d}}_b \\ \ddot{\mathbf{d}}_s \end{bmatrix} + \begin{bmatrix} \mathbf{K}_{bb} & \mathbf{K}_{bs} \\ \mathbf{K}_{sb} & \mathbf{K}_{ss} \end{bmatrix} \begin{bmatrix} \mathbf{d}_b \\ \mathbf{d}_s \end{bmatrix} = \begin{bmatrix} \mathbf{f}_b \\ \mathbf{0} \end{bmatrix} \tag{3.35}$$

The boundary conditions and external forces are applied at the physical degrees of freedom of the reduced model.

3.4.1 Static Condensation

The static condensation was introduced by Guyan, [45], only studying the stiffness matrix

$$\begin{bmatrix} \mathbf{K}_{bb} & \mathbf{K}_{bs} \\ \mathbf{K}_{sb} & \mathbf{K}_{ss} \end{bmatrix} \begin{bmatrix} \mathbf{d}_b \\ \mathbf{d}_s \end{bmatrix} = \begin{bmatrix} \mathbf{f}_b \\ \mathbf{0} \end{bmatrix} \tag{3.36}$$

The displacements can thereby be expressed using the master degrees of freedom

$$\begin{bmatrix} \mathbf{d}_b \\ \mathbf{d}_s \end{bmatrix} = \begin{bmatrix} \mathbf{I} \\ -\mathbf{K}_{ss}^{-1}\mathbf{K}_{sb} \end{bmatrix} \mathbf{d}_b = \mathbf{\Phi}_{sc}\mathbf{d}_b \tag{3.37}$$

Introducing this equation as the change of base in equation (3.11), the system of equations is reduced to

$$\tilde{\mathbf{M}}_{sc}\ddot{\mathbf{d}}_b + \tilde{\mathbf{K}}_{sc}\mathbf{d}_b = \mathbf{f}_b \tag{3.38}$$

where

$$\tilde{\mathbf{K}}_{sc} = \mathbf{\Phi}_{sc}^T\mathbf{K}\mathbf{\Phi}_{sc} \qquad \tilde{\mathbf{M}}_{sc} = \mathbf{\Phi}_{sc}^T\mathbf{M}\mathbf{\Phi}_{sc} \tag{3.39}$$

The inertia effect of the condensed degrees of freedom is neglected. The linear eigenvalue problem of the reduced system becomes

$$\tilde{\mathbf{K}}_{sc}\mathbf{\Phi} = \boldsymbol{\lambda}\tilde{\mathbf{M}}_{sc}\mathbf{\Phi} \tag{3.40}$$

The choice of master degrees of freedom has a large influence on the frequency limit where the reduced model ceases to be valid. This limit in frequency is at the point when the dynamic effect of the condensed degrees of freedom becomes of importance. As a simple measure, the reduced model is valid up to the lowest natural frequency of the model with the master degrees of freedom constrained. Methods how to choose which degrees of freedom to be included as been proposed by several authors [46, 47, 48].

3.4.2 Dynamic Condensation

Dynamic condensation is performed in the same fashion as static condensation but including inertia effects, [49]. The dynamic stiffness matrix $\mathbf{D}(\omega)$, see equation (3.4), is partitioned into master and slave degrees of freedom

$$\begin{bmatrix} \mathbf{D}_{bb} & \mathbf{D}_{bs} \\ \mathbf{D}_{sb} & \mathbf{D}_{ss} \end{bmatrix} \begin{bmatrix} \hat{\mathbf{d}}_b \\ \hat{\mathbf{d}}_s \end{bmatrix} = \begin{bmatrix} \hat{\mathbf{f}}_b \\ \mathbf{0} \end{bmatrix} \tag{3.41}$$

The displacements can thereby be expressed using the master degrees of freedom

$$\begin{bmatrix} \hat{\mathbf{d}}_b \\ \hat{\mathbf{d}}_s \end{bmatrix} = \begin{bmatrix} \mathbf{I} \\ -\mathbf{D}_{ss}^{-1}\mathbf{D}_{sb} \end{bmatrix} \hat{\mathbf{d}}_b = \mathbf{\Phi}_{dc}\mathbf{d}_b \tag{3.42}$$

and the system of equations is reduced to

$$\tilde{\mathbf{D}}_{dc}(\omega)\hat{\mathbf{d}}_b = \hat{\mathbf{f}}_b \tag{3.43}$$

where

$$\tilde{\mathbf{D}}_{dc}(\omega) = \mathbf{\Phi}_{dc}^T\mathbf{D}\mathbf{\Phi}_{dc} = \mathbf{D}_{bb} - \mathbf{D}_{bs}\mathbf{D}_{ss}^{-1}\mathbf{D}_{sb} \tag{3.44}$$

The non-linear eigenvalue problem ($\omega^2 \rightarrow \lambda$ and $\hat{\mathbf{d}}_b \rightarrow \mathbf{\Phi}_b$ in equation (3.43)) of the reduced system becomes

$$\tilde{\mathbf{D}}_{dc}(\lambda)\mathbf{\Phi}_b = \mathbf{0} \tag{3.45}$$

where the nonlinearity depends on the the term $\mathbf{D}_{ss}^{-1} = (-\lambda\mathbf{M}_{ss} + \mathbf{K}_{ss})^{-1}$. To use dynamic condensation in an efficient way, the description of the inertia effects of the slave degrees of freedom must be simplified since the dynamic stiffness matrix must be inverted at each frequency step [50, 51, 52, 53, 65].

3.5 Component Mode Synthesis

The component mode synthesis method, which is a frequently used method for reducing the size of the system of equations to be solved, is here investigated. In this method the studied domain is divided into components, or subdomains, and each subdomain is described by a set of displacement modes. For the i'th subdomain of a system, described by the displacement $\mathbf{d}_i$ and with the stiffness matrix $\mathbf{K}_i$, mass matrix $\mathbf{M}_i$ and force vector $\mathbf{f}_i$, the system of equations is written

$$\mathbf{M}_i\ddot{\mathbf{d}}_i + \mathbf{K}_i\mathbf{d}_i = \mathbf{f}_i \tag{3.46}$$

or partitioned into boundary (master) degrees of freedom, $\mathbf{d}_b$, and internal (slave) degrees of freedom, $\mathbf{d}_s$.

$$\left[\begin{array}{cc} \mathbf{M}_{bb} & \mathbf{M}_{bs} \\ \mathbf{M}_{sb} & \mathbf{M}_{ss} \end{array}\right]_i \left[\begin{array}{c} \ddot{\mathbf{d}}_b \\ \ddot{\mathbf{d}}_s \end{array}\right]_i + \left[\begin{array}{cc} \mathbf{K}_{bb} & \mathbf{K}_{bs} \\ \mathbf{K}_{sb} & \mathbf{K}_{ss} \end{array}\right]_i \left[\begin{array}{c} \mathbf{d}_b \\ \mathbf{d}_s \end{array}\right]_i = \left[\begin{array}{c} \mathbf{f}_b \\ \mathbf{f}_s \end{array}\right]_i \tag{3.47}$$

A change of base is introduced by

$$\mathbf{d}_i = \mathbf{\Psi}_i\boldsymbol{\xi}_i \tag{3.48}$$

where $\mathbf{\Psi}_i$ is the set of displacement modes for the subdomain and $\boldsymbol{\xi}_i$ the corresponding modal amplitudes. Thus, equation (3.46) can be written

$$\mathbf{\Psi}_i^T\mathbf{M}_i\mathbf{\Psi}_i\ddot{\boldsymbol{\xi}}_i + \mathbf{\Psi}_i^T\mathbf{K}_i\mathbf{\Psi}_i\boldsymbol{\xi}_i = \mathbf{\Psi}_i^T\mathbf{f}_i \tag{3.49}$$

Two types of component mode methods are most frequently used, being either the fixed interface mode method or the free interface mode method [55]. For each method one set of modes is derived to fulfill the continuity in displacements and forces between the subdomains and one set to describe the internal behaviour of the subdomain. In Section 3.5.1, the different modes derived for the subdomains are described and then the method to couple these subdomains together using Lagrange multipliers is described in Section 3.5.2.

In the previously described numerical example, see Figure 3.1, the plate is divided into two subdomains and the different included modes are exemplified.

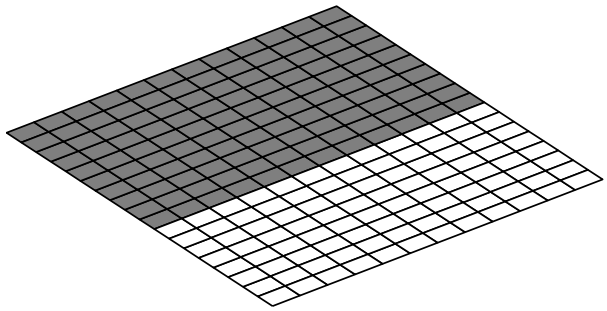

Figure 3.8: *The plate divided into two subdomains. The shaded subdomain is used to exemplify the modes included in the component mode synthesis method.*

3.5.1 Included modes

Fixed-interface mode method

In the component mode synthesis method using fixed interface modes, static reduction is performed for each subdomain, only retaining the boundary degrees of freedom in contact with the connecting subdomains. A number of internal normal modes, $\mathbf{\Phi}_s$, calculated with the boundary degrees of freedom fixed, are added to the basis vectors from the static reduction, $\mathbf{\Psi}_c$, in order to improve the description of the dynamic behaviour of the system. The internal modes could be of any shape fulfilling the the boundary conditions, see for example, [41, 43]. The change of base using the reduced set of basis vectors can be written

$$\begin{bmatrix} \mathbf{d}_b \\ \mathbf{d}_s \end{bmatrix} = \begin{bmatrix} \mathbf{\Psi}_c & \mathbf{\Phi}_s \end{bmatrix} \begin{bmatrix} \mathbf{d}_b \\ \boldsymbol{\xi}_s \end{bmatrix} \tag{3.50}$$

All the degrees of freedom that lies on the interface boundary are included in the reduced system.

Constraint modes

The modes from the static reduction

$$\mathbf{\Psi}_c = \begin{bmatrix} \mathbf{I}_{bb} \\ -\mathbf{K}_{ss}^{-1}\mathbf{K}_{sb} \end{bmatrix} \tag{3.51}$$

are called component constraint modes and can be derived by applying a unit displacement to each interface degree of freedom while keeping the other interface degrees of freedom fixed. Note that if only including these constraint modes in the reduction, the method reduces to the static condensation method. Two examples of constraint modes are displayed in Figure 3.9.

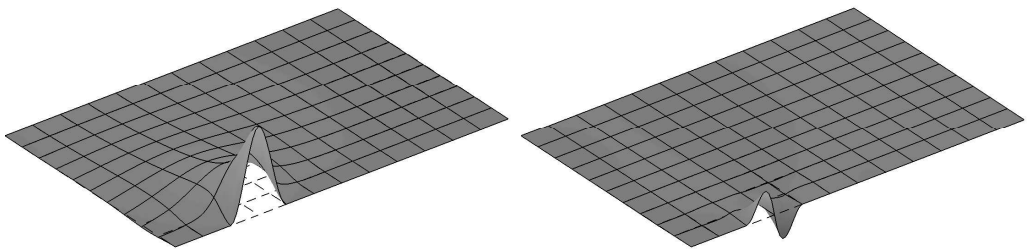

Figure 3.9: *Two of the constraint modes at one node.*

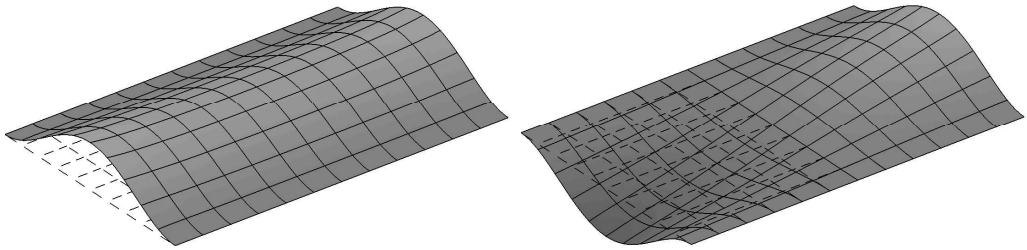

Figure 3.10: *Two of the fixed normal modes of the subdomain.*

Fixed interface normal modes

The added normal modes with the interface degrees of freedom fixed are calculated from the eigenvalue problem with the boundary degrees of freedom condensed

$$\mathbf{K}_{ss}\mathbf{\Phi}_{ss} = \boldsymbol{\lambda}_{ss}\mathbf{M}_{ss}\mathbf{\Phi}_{ss} \tag{3.52}$$

and by adding the zeros at boundary degrees of freedom, the fixed interface normal modes can be written

$$\mathbf{\Phi}_s = \begin{bmatrix} \mathbf{0}_{bb} \\ \mathbf{\Phi}_{ss} \end{bmatrix} \tag{3.53}$$

Two examples of normal modes calculated with the boundary degrees of freedom fixed are displayed in Figure 3.10.

Free-interface mode method

Another approach is to reduce the system with free interface modes, i.e. the normal modes describing the subdomain, $\mathbf{\Phi}_k$, are calculated without imposing boundary conditions at the interface between subdomains. To fulfill the displacement and force continuity between the subdomains, attachment modes, $\mathbf{\Psi}_a$, of the subdomain are derived and the subdomain is described by

$$\begin{bmatrix} \mathbf{d}_b \\ \mathbf{d}_s \end{bmatrix} = \begin{bmatrix} \mathbf{\Psi}_a & \mathbf{\Phi}_k \end{bmatrix} \begin{bmatrix} \boldsymbol{\xi}_a \\ \boldsymbol{\xi}_k \end{bmatrix} \tag{3.54}$$

Attachment modes

The attachment modes are calculated by applying an unit force at each interface degree of freedom while keeping the other interface degrees of freedom free. A matrix containing the corresponding force vectors can be written

$$\mathbf{f}_a = \begin{bmatrix} \mathbf{I}_{bb} \\ \mathbf{0}_{sb} \end{bmatrix} \tag{3.55}$$

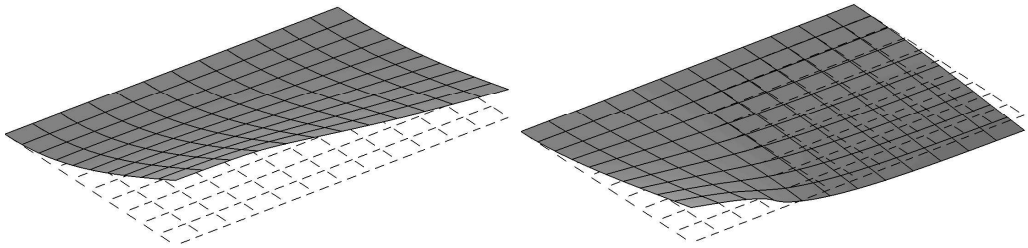

Figure 3.11: *Two of the attachment modes at one node.*

and with the flexibility matrix, $\mathbf{G} = \mathbf{K}^{-1}$, i.e. the inverse of the non-singular stiffness matrix, the attachment modes can be calculated by

$$\mathbf{\Psi}_a = \mathbf{G}\mathbf{f}_a = \mathbf{G} \begin{bmatrix} \mathbf{I}_{bb} \\ \mathbf{0}_{sb} \end{bmatrix} \tag{3.56}$$

Two examples of attachment modes are displayed in Figure 3.11.

Free interface normal modes

The normal modes of the sub-structure is calculated by

$$\mathbf{K}\mathbf{\Phi}_k = \boldsymbol{\lambda}_{kk}\mathbf{M}\mathbf{\Phi}_k \tag{3.57}$$

including Dirchlet boundary conditions. Two examples of normal modes calculated with the boundary degrees of freedom free are displayed in Figure 3.12.

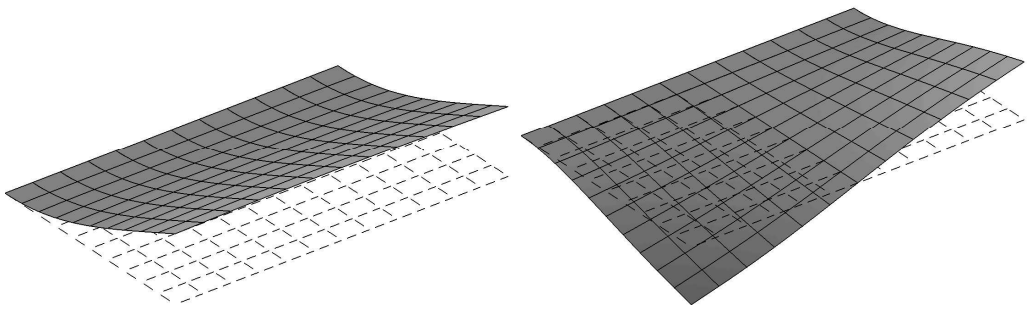

Figure 3.12: *Two of the free normal modes of the subdomain.*

Residual attachment modes

The flexibility matrix, i.e. the inverse of the stiffness matrix, $\mathbf{G} = \mathbf{K}^{-1}$, can be written

$$\mathbf{G} = \mathbf{\Phi}_n \boldsymbol{\lambda}_{nn}^{-1} \mathbf{\Phi}_n^T = \mathbf{\Phi}_k \boldsymbol{\lambda}_{kk}^{-1} \mathbf{\Phi}_k^T + \mathbf{\Phi}_d \boldsymbol{\lambda}_{dd}^{-1} \mathbf{\Phi}_d^T \tag{3.58}$$

where $\mathbf{\Phi}_n$ contains all the flexible normal modes of the subdomain in the free interface method, $\mathbf{\Phi}_k$ the actual calculated flexible normal modes and $\mathbf{\Phi}_d$ the residual normal modes not calculated. The residual flexibility of the structure can be written

$$\mathbf{G}_d = \mathbf{\Phi}_d \boldsymbol{\lambda}_{dd}^{-1} \mathbf{\Phi}_d^T = \mathbf{G} - \mathbf{\Phi}_k \boldsymbol{\lambda}_{kk}^{-1} \mathbf{\Phi}_k^T \tag{3.59}$$

The residual attachment modes then becomes

$$\mathbf{\Psi}_d = \mathbf{G}_d \mathbf{f}_a = \left[\mathbf{G} - \mathbf{\Phi}_k \boldsymbol{\lambda}_{kk}^{-1} \mathbf{\Phi}_k^T \right] \begin{bmatrix} \mathbf{I}_{bb} \\ \mathbf{0}_{sb} \end{bmatrix} \tag{3.60}$$

Two examples of residual attachment modes calculated are displayed in Figure 3.13. Performing the change of base using the calculated normal modes and the residual attachment modes

$$\mathbf{d} = \begin{bmatrix} \mathbf{\Phi}_k & \mathbf{\Psi}_d \end{bmatrix} \begin{bmatrix} \boldsymbol{\xi}_k \\ \boldsymbol{\xi}_d \end{bmatrix} \tag{3.61}$$

equation (3.1) can be written

$$\begin{aligned} \mathbf{I}\boldsymbol{\xi}_k + \mathbf{\Lambda}_k \boldsymbol{\xi}_k &= \mathbf{\Phi}_k^T \mathbf{f} \\ \mathbf{\Psi}_d^T \mathbf{M} \mathbf{\Psi}_d \boldsymbol{\xi}_d + \mathbf{\Psi}_d^T \mathbf{K} \mathbf{\Psi}_d \boldsymbol{\xi}_d &= \mathbf{\Psi}_d^T \mathbf{f} \end{aligned} \tag{3.62}$$

The two parts can be separated due to the orthogonality of the used modes. It is then assumed that the attachment modes are only determined by the stiffness contribution, neglecting inertia effects, and the second line of equation (3.62) can be written

$$\mathbf{\Psi}_d^T \mathbf{K} \mathbf{\Psi}_d \boldsymbol{\xi}_d = \mathbf{\Psi}_d^T \mathbf{f} \tag{3.63}$$

The residual attachment modes can then be written

$$\mathbf{\Psi}_d = \mathbf{\Phi}_d \mathbf{\Lambda}_d^{-1} \mathbf{\Phi}_d^T \begin{bmatrix} \mathbf{I}_{bb} \\ \mathbf{0}_{sb} \end{bmatrix} = \mathbf{\Phi}_d \mathbf{\Lambda}_d^{-1} \mathbf{\Phi}_{bd}^T \tag{3.64}$$

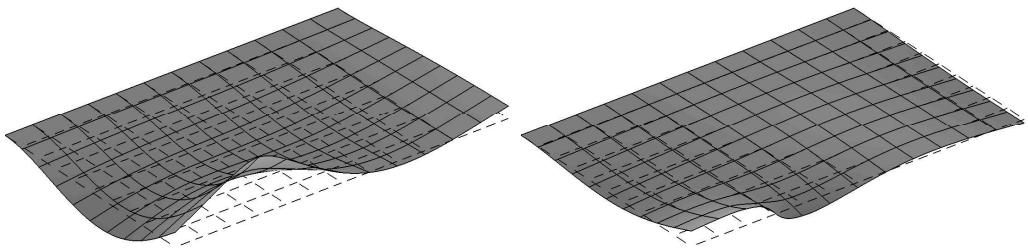

Figure 3.13: *Two of the residual attachment modes at one node.*

Introducing this in equation (3.63) gives

$$\mathbf{\Phi}_{bd}\mathbf{\Lambda}_d^{-1}\mathbf{\Phi}_d^T\mathbf{K}\mathbf{\Phi}_d\mathbf{\Lambda}_d^{-1}\mathbf{\Phi}_{bd}^T\boldsymbol{\xi}_d = \mathbf{\Phi}_{bd}\mathbf{\Lambda}_d^{-1}\mathbf{\Phi}_d^T\mathbf{f} \tag{3.65}$$

Noting that $\mathbf{\Phi}_d^T\mathbf{K}\mathbf{\Phi}_d = \mathbf{\Lambda}_d$ and because the forces that act at the boundary degrees of freedom can be written

$$\mathbf{f} = \mathbf{f}_a = \begin{bmatrix} \mathbf{I}_{bb} \\ \mathbf{0}_{sb} \end{bmatrix} \tag{3.66}$$

the system becomes

$$\mathbf{\Phi}_{bd}\mathbf{\Lambda}_d^{-1}\mathbf{\Phi}_{bd}^T(\boldsymbol{\xi}_d - \mathbf{f}_a) = 0 \tag{3.67}$$

This gives a condition between the forces acting on the boundary degrees of freedom and the residual attachment mode coordinate

$$\boldsymbol{\xi}_d = \mathbf{f}_a \tag{3.68}$$

This will be used in the procedure to couple the subdomains together, giving additional constraint equations, see Section 3.5.2.

Rigid body modes

If the subdomain have rigid body modes these can be determined as constraint modes by partition the stiffness matrix as follows

$$\begin{bmatrix} \mathbf{K}_{rr} & \mathbf{K}_{rb} & \mathbf{K}_{rs} \\ \mathbf{K}_{br} & \mathbf{K}_{bb} & \mathbf{K}_{bs} \\ \mathbf{K}_{sr} & \mathbf{K}_{sb} & \mathbf{K}_{ss} \end{bmatrix} \begin{bmatrix} \mathbf{d}_r \\ \mathbf{d}_b \\ \mathbf{d}_s \end{bmatrix} = \begin{bmatrix} \mathbf{f}_r \\ \mathbf{f}_b \\ \mathbf{f}_s \end{bmatrix} \tag{3.69}$$

where $\mathbf{d}_r$ contains exactly as many degrees of freedom that are needed to remove the rigid body motion. Only retaining these degrees of freedom in a static condensation, the rigid body modes can be written

$$\mathbf{\Psi}_r = \begin{bmatrix} \mathbf{I}_{rr} \\ -\begin{bmatrix} \mathbf{K}_{bb} & \mathbf{K}_{bs} \\ \mathbf{K}_{sb} & \mathbf{K}_{ss} \end{bmatrix}^{-1} \begin{bmatrix} \mathbf{K}_{br} \\ \mathbf{K}_{sr} \end{bmatrix} \end{bmatrix} \tag{3.70}$$

The degrees of freedom included in $\mathbf{d}_r$ can not be part of the boundary degrees of freedom $\mathbf{d}_b$.

Inertia relief attachment modes

If the subdomain has rigid body modes, these must be considered when calculating the attachment modes. The total displacements of the subdomain is divided into a rigid body motion, $\mathbf{d}_0$, and deformation of the flexible structure, $\mathbf{d}_f$,

$$\mathbf{d} = \mathbf{d}_0 + \mathbf{d}_f \tag{3.71}$$

or expressed in modal coordinates

$$\mathbf{d} = \mathbf{\Psi}_r\boldsymbol{\xi}_r + \mathbf{\Phi}_f\boldsymbol{\xi}_f \tag{3.72}$$

Note the following properties

$$\begin{aligned} \boldsymbol{\Psi}_r^T \mathbf{M} \boldsymbol{\Psi}_r &= \mathbf{I}_r & \boldsymbol{\Psi}_r^T \mathbf{K} \boldsymbol{\Psi}_r &= \mathbf{0} \\ \boldsymbol{\Phi}_f^T \mathbf{M} \boldsymbol{\Phi}_f &= \mathbf{I}_f & \boldsymbol{\Phi}_f^T \mathbf{K} \boldsymbol{\Phi}_f &= \boldsymbol{\Lambda}_f \\ \boldsymbol{\Psi}_r^T \mathbf{M} \boldsymbol{\Phi}_f &= \mathbf{0} & \boldsymbol{\Psi}_r^T \mathbf{K} \boldsymbol{\Phi}_f &= \mathbf{0} \end{aligned} \tag{3.73}$$

Introducing the change of base given in equation (3.72) in the equation of motion (3.46), it can be divided in two parts

$$\begin{aligned} \mathbf{I}_r \ddot{\boldsymbol{\xi}}_r &= \boldsymbol{\Psi}_r^T \mathbf{f} \\ \mathbf{I}_f \ddot{\boldsymbol{\xi}}_f + \boldsymbol{\Lambda} \boldsymbol{\xi}_f &= \boldsymbol{\Phi}_f^T \mathbf{f} \end{aligned} \tag{3.74}$$

Also, the external force is divided into two parts, the one exciting the rigid body motion, $\mathbf{f}_0$, and the other exciting the flexible system, $\mathbf{f}_f$,

$$\mathbf{f} = \mathbf{f}_0 + \mathbf{f}_f \tag{3.75}$$

The force acting on the rigid body can be written

$$\mathbf{f}_0 = \mathbf{M} \ddot{\mathbf{d}}_0 = \mathbf{M} \boldsymbol{\Psi}_r \ddot{\boldsymbol{\xi}}_r = \mathbf{M} \boldsymbol{\Psi}_r \boldsymbol{\Psi}_r^T \mathbf{f} \tag{3.76}$$

From this, the force acting on the flexible body can be expressed

$$\mathbf{f}_f = \mathbf{f} - \mathbf{f}_0 = \mathbf{f} - \mathbf{M} \boldsymbol{\Psi}_r \boldsymbol{\Psi}_r^T \mathbf{f} = (\mathbf{I} - \mathbf{M} \boldsymbol{\Psi}_r \boldsymbol{\Psi}_r^T) \mathbf{f} = \mathbf{P}_r \mathbf{f} \tag{3.77}$$

where $\mathbf{P}_r$ is called the inertia-relief projection matrix; any force vector multiplied with this matrix gives a self balanced force vector not imposing rigid body motion of the system. The attachment modes can be calculated by

$$\boldsymbol{\Psi}_a = \mathbf{P}_r^T \mathbf{G}_r \mathbf{P}_r \begin{bmatrix} \mathbf{I}_{bb} \\ \mathbf{0}_{sb} \end{bmatrix} \tag{3.78}$$

where the flexibility matrix, $\mathbf{G}_r$, is calculated with the degrees of freedom $\mathbf{d}_r$ in equation (3.69) condensed. Due to the self balanced force vector, no constraint forces are present at these degrees of freedom.

Residual inertia relief attachment modes

For a subdomain having rigid body modes, the residual attachment modes can be combined with the inertia relief modes. The residual inertia relief attachment modes then becomes

$$\boldsymbol{\Psi}_d = \left[\mathbf{P}_r^T \mathbf{G}_r \mathbf{P}_r - \boldsymbol{\Phi}_k \boldsymbol{\lambda}_{kk}^{-1} \boldsymbol{\Phi}_k^T \right] \begin{bmatrix} \mathbf{I}_{bb} \\ \mathbf{0}_{sb} \end{bmatrix} \tag{3.79}$$

Quasi-static mode compensation

As suggested in [59], instead of using the static constraint modes the shifted problem can be used and the solution at a certain angular frequency, ω_{qs}, can be used in equation (3.51), where $\boldsymbol{\Psi}_c$ is replaced by

$$\boldsymbol{\Psi}_c = \begin{bmatrix} \mathbf{I}_{bb} \\ -(\mathbf{K}_{ss} - \omega_{qs}^2 \mathbf{M}_{ss})^{-1} (\mathbf{K}_{sb} - \omega_{qs}^2 \mathbf{M}_{sb}) \end{bmatrix} \tag{3.80}$$

This can also be used to make the stiffness matrix non-singular, removing the need to calculate the inertia relief attachment modes. Also, for an acoustic fluid domain, the wave equation do not provide a static solution, and the quasi-static method can be used to determine constraint or attachment modes.

3.5.2 Subdomain synthesis

A procedure to assemble the subdomains using Lagrange multiplier – which can be used for both the fixed and free interface methods – is now to investigated. The use of Lagrange multipliers was described by, for example, Bathe [19] or Craig [55]. Each subdomain is described by a set of basis vectors that can be divided into a set of vectors that are linearly dependent to the basis vectors of the connecting domains and a set of linearly independent vectors. The linear dependent vectors describes the coupling between the domains and the number of these vectors is equal to the number of degrees of freedom at the interface boundary between the domains. A set of linearly independent vectors is also included to describe the internal behaviour of the subdomain. Note that in the fixed interface method the physical degrees of freedom at the interface are retained in the reduced model and a direct assembling procedure can be conducted.

Assume that a structure is divided into two subdomains I and II. The degrees of freedom are partitioned into boundary and slave degrees of freedom and the displacement can be described by the linearly dependent vectors, $\boldsymbol{\Psi}_d^i$, and independent vectors, $\boldsymbol{\Psi}_l^i$, of the two domains

$$\begin{bmatrix} \mathbf{d}_{\mathrm{I}} \\ \mathbf{d}_{\mathrm{II}} \end{bmatrix} = \begin{bmatrix} \mathbf{d}_b^{\mathrm{I}} \\ \mathbf{d}_s^{\mathrm{I}} \\ \mathbf{d}_b^{\mathrm{II}} \\ \mathbf{d}_s^{\mathrm{II}} \end{bmatrix} = \begin{bmatrix} \boldsymbol{\Psi}_{db}^{\mathrm{I}} & \boldsymbol{\Psi}_{lb}^{\mathrm{I}} & \mathbf{0} & \mathbf{0} \\ \boldsymbol{\Psi}_{ds}^{\mathrm{I}} & \boldsymbol{\Psi}_{ls}^{\mathrm{I}} & \mathbf{0} & \mathbf{0} \\ \mathbf{0} & \mathbf{0} & \boldsymbol{\Psi}_{db}^{\mathrm{II}} & \boldsymbol{\Psi}_{lb}^{\mathrm{II}} \\ \mathbf{0} & \mathbf{0} & \boldsymbol{\Psi}_{ds}^{\mathrm{II}} & \boldsymbol{\Psi}_{ls}^{\mathrm{II}} \end{bmatrix} \begin{bmatrix} \boldsymbol{\xi}_d^{\mathrm{I}} \\ \boldsymbol{\xi}_l^{\mathrm{I}} \\ \boldsymbol{\xi}_d^{\mathrm{II}} \\ \boldsymbol{\xi}_l^{\mathrm{II}} \end{bmatrix} = \begin{bmatrix} \boldsymbol{\Psi}_{\mathrm{I}} & \mathbf{0} \\ \mathbf{0} & \boldsymbol{\Psi}_{\mathrm{II}} \end{bmatrix} \begin{bmatrix} \boldsymbol{\xi}_{\mathrm{I}} \\ \boldsymbol{\xi}_{\mathrm{II}} \end{bmatrix} \tag{3.81}$$

The two domains are described separately. The displacement and force continuity at the boundary between the domains introduce conditions that couple the two domains together.

Displacement continuity

At the boundary between two subdomains, the displacement must be continuous

$$\mathbf{d}_b^{\mathrm{I}} = \mathbf{d}_b^{\mathrm{II}} \tag{3.82}$$

This displacement condition can be written using a matrix equation

$$\mathbf{B}\mathbf{d} = \mathbf{B} \begin{bmatrix} \boldsymbol{\Psi}_{\mathrm{I}} & \mathbf{0} \\ \mathbf{0} & \boldsymbol{\Psi}_{\mathrm{II}} \end{bmatrix} \begin{bmatrix} \boldsymbol{\xi}_{\mathrm{I}} \\ \boldsymbol{\xi}_{\mathrm{II}} \end{bmatrix} = \mathbf{C} \begin{bmatrix} \boldsymbol{\xi}_{\mathrm{I}} \\ \boldsymbol{\xi}_{\mathrm{II}} \end{bmatrix} = 0 \tag{3.83}$$

where the matrix $\mathbf{B}$ can be written

$$\mathbf{B} = \begin{bmatrix} \mathbf{I}_{bb}^{\mathrm{I}} & \mathbf{0} & -\mathbf{I}_{bb}^{\mathrm{II}} & \mathbf{0} \end{bmatrix} \tag{3.84}$$

The displacement continuity can be expressed using equation (3.81), which gives

$$\begin{bmatrix} \mathbf{I}^{\mathrm{I}}_{bb} & \mathbf{0} & -\mathbf{I}^{\mathrm{II}}_{bb} & \mathbf{0} \end{bmatrix} \begin{bmatrix} \mathbf{d}^{\mathrm{I}}_{b} \\ \mathbf{d}^{\mathrm{I}}_{s} \\ \mathbf{d}^{\mathrm{II}}_{b} \\ \mathbf{d}^{\mathrm{II}}_{s} \end{bmatrix} = \begin{bmatrix} \mathbf{I}_{bb} & \mathbf{0} & -\mathbf{I}_{bb} & \mathbf{0} \end{bmatrix} \begin{bmatrix} \boldsymbol{\Psi}^{\mathrm{I}}_{db} & \boldsymbol{\Psi}^{\mathrm{I}}_{lb} & \mathbf{0} & \mathbf{0} \\ \boldsymbol{\Psi}^{\mathrm{I}}_{ds} & \boldsymbol{\Psi}^{\mathrm{I}}_{ls} & \mathbf{0} & \mathbf{0} \\ \mathbf{0} & \mathbf{0} & \boldsymbol{\Psi}^{\mathrm{II}}_{db} & \boldsymbol{\Psi}^{\mathrm{II}}_{lb} \\ \mathbf{0} & \mathbf{0} & \boldsymbol{\Psi}^{\mathrm{II}}_{ds} & \boldsymbol{\Psi}^{\mathrm{II}}_{ls} \end{bmatrix} \begin{bmatrix} \boldsymbol{\xi}^{\mathrm{I}}_{d} \\ \boldsymbol{\xi}^{\mathrm{I}}_{l} \\ \boldsymbol{\xi}^{\mathrm{II}}_{d} \\ \boldsymbol{\xi}^{\mathrm{II}}_{l} \end{bmatrix} \tag{3.85}$$

Thus, the constraint matrix $\mathbf{C}$ becomes

$$\mathbf{C} = \begin{bmatrix} \boldsymbol{\Psi}^{\mathrm{I}}_{db} & \boldsymbol{\Psi}^{\mathrm{I}}_{lb} & -\boldsymbol{\Psi}^{\mathrm{II}}_{db} & -\boldsymbol{\Psi}^{\mathrm{II}}_{lb} \end{bmatrix} \tag{3.86}$$

Using the fixed interface method, the set of basis vectors in equation (3.50) describes the motion in each subdomain and the constraint system of equations becomes

$$\begin{bmatrix} \mathbf{I}^{\mathrm{I}}_{bb} & \mathbf{0} & -\mathbf{I}^{\mathrm{II}}_{bb} & \mathbf{0} \end{bmatrix} \begin{bmatrix} \mathbf{I}^{\mathrm{I}}_{bb} & \mathbf{0} & \mathbf{0} & \mathbf{0} \\ -(\mathbf{K}^{\mathrm{I}}_{ss})^{-1}\mathbf{K}^{\mathrm{I}}_{sb} & \boldsymbol{\Psi}^{\mathrm{I}}_{ss} & \mathbf{0} & \mathbf{0} \\ \mathbf{0} & \mathbf{0} & \mathbf{I}^{\mathrm{II}}_{bb} & \mathbf{0} \\ \mathbf{0} & \mathbf{0} & -(\mathbf{K}^{\mathrm{II}}_{ss})^{-1}\mathbf{K}^{\mathrm{II}}_{sb} & \boldsymbol{\Psi}^{\mathrm{II}}_{ss} \end{bmatrix} \begin{bmatrix} \mathbf{d}^{\mathrm{I}}_{b} \\ \boldsymbol{\xi}^{\mathrm{I}}_{s} \\ \mathbf{d}^{\mathrm{II}}_{b} \\ \boldsymbol{\xi}^{\mathrm{II}}_{s} \end{bmatrix} \tag{3.87}$$

thus

$$\mathbf{C} = \begin{bmatrix} \mathbf{I}^{\mathrm{I}}_{bb} & \mathbf{0} & -\mathbf{I}^{\mathrm{II}}_{bb} & \mathbf{0} \end{bmatrix} \tag{3.88}$$

For the free interface method, the subdomains are described by equation (3.54) and $\mathbf{C}$ becomes

$$\mathbf{C} = \begin{bmatrix} \boldsymbol{\Psi}^{\mathrm{I}}_{ab} & \boldsymbol{\Phi}^{\mathrm{I}}_{kb} & -\boldsymbol{\Psi}^{\mathrm{II}}_{ab} & -\boldsymbol{\Phi}^{\mathrm{II}}_{kb} \end{bmatrix} \tag{3.89}$$

Force equilibrium

The reaction forces that acts at the boundary degrees of freedom must be in equilibrium

$$\mathbf{f}^{\mathrm{I}}_{b} + \mathbf{f}^{\mathrm{II}}_{b} = \mathbf{0} \tag{3.90}$$

Equations of motion

The equation system describing a problem domain consisting of two subdomains can be written

$$\begin{bmatrix} \mathbf{M}_{\mathrm{I}} & \mathbf{0} \\ \mathbf{0} & \mathbf{M}_{\mathrm{II}} \end{bmatrix} \begin{bmatrix} \ddot{\mathbf{d}}_{\mathrm{I}} \\ \ddot{\mathbf{d}}_{\mathrm{II}} \end{bmatrix} + \begin{bmatrix} \mathbf{K}_{\mathrm{I}} & \mathbf{0} \\ \mathbf{0} & \mathbf{K}_{\mathrm{II}} \end{bmatrix} \begin{bmatrix} \mathbf{d}_{\mathrm{I}} \\ \mathbf{d}_{\mathrm{II}} \end{bmatrix} = \mathbf{B}^T\boldsymbol{\lambda} + \begin{bmatrix} \mathbf{f}_{\mathrm{I}} \\ \mathbf{f}_{\mathrm{II}} \end{bmatrix} \tag{3.91}$$

where $\mathbf{B}^T\boldsymbol{\lambda}$ impose the Lagrange multipliers imposing the constraints described by the displacement continuity between the two subdomains. The number of Lagrange multipliers, n_d (d for dependent), is equal to the number of degrees of freedom at the connecting boundary between the two domains. Introducing the change of base in equation (3.81) the system is described by

$$\begin{bmatrix} \tilde{\mathbf{M}}_{\mathrm{I}} & \mathbf{0} \\ \mathbf{0} & \tilde{\mathbf{M}}_{\mathrm{II}} \end{bmatrix} \begin{bmatrix} \ddot{\boldsymbol{\xi}}_{\mathrm{I}} \\ \ddot{\boldsymbol{\xi}}_{\mathrm{II}} \end{bmatrix} + \begin{bmatrix} \tilde{\mathbf{K}}^{\mathrm{I}} & \mathbf{0} \\ \mathbf{0} & \tilde{\mathbf{K}}^{\mathrm{II}} \end{bmatrix} \begin{bmatrix} \boldsymbol{\xi}_{\mathrm{I}} \\ \boldsymbol{\xi}_{\mathrm{II}} \end{bmatrix} = \mathbf{C}^T\boldsymbol{\lambda} + \begin{bmatrix} \boldsymbol{\Psi}_{\mathrm{I}} & \mathbf{0} \\ \mathbf{0} & \boldsymbol{\Psi}_{\mathrm{II}} \end{bmatrix}^T \begin{bmatrix} \mathbf{f}_{\mathrm{I}} \\ \mathbf{f}_{\mathrm{II}} \end{bmatrix} \tag{3.92}$$

Because n_d constraint equations as been introduced, there exists $n - n_d$ linearly independent degrees of freedom. $\mathbf{C}$ is partitioned into the dependent and linearly independent degrees of freedom

$$\mathbf{C} = \begin{bmatrix} \mathbf{C}_{dd} & \mathbf{C}_{ld} \end{bmatrix} \tag{3.93}$$

and a change of base can be introduced

$$\boldsymbol{\xi} = \begin{bmatrix} -\mathbf{C}_{dd}^{-1}\mathbf{C}_{ld} \\ \mathbf{I} \end{bmatrix} \boldsymbol{\eta} = \mathbf{T}\boldsymbol{\eta} \tag{3.94}$$

For the fixed interface mode method, assuming that the constraint modes of the second subdomain are linearly dependent on the other modes, the matrix, $\mathbf{T}$ becomes

$$\mathbf{T} = \begin{bmatrix} \mathbf{I}_{bb} & \mathbf{0} & \mathbf{0} \\ \mathbf{0} & \mathbf{I}_l^{\mathrm{I}} & \mathbf{0} \\ \mathbf{I}_{bb} & \mathbf{0} & \mathbf{0} \\ \mathbf{0} & \mathbf{0} & \mathbf{I}_l^{\mathrm{II}} \end{bmatrix} \tag{3.95}$$

The two domains are coupled through the boundary degrees of freedom. For the free interface mode method, assuming that the attachment modes of the second subdomain is linearly dependent on the other modes, the matrix $\mathbf{T}$ becomes

$$\mathbf{T} = \begin{bmatrix} \mathbf{I}_{bb} & \mathbf{0} & \mathbf{0} \\ \mathbf{0} & \mathbf{I}_l^{\mathrm{I}} & \mathbf{0} \\ (\boldsymbol{\Psi}_{ab}^{\mathrm{II}})^{-1}\boldsymbol{\Psi}_{ab}^{\mathrm{I}} & (\boldsymbol{\Psi}_{ab}^{\mathrm{II}})^{-1}\boldsymbol{\Phi}_{kb}^{\mathrm{I}} & -(\boldsymbol{\Psi}_{ab}^{\mathrm{II}})^{-1}\boldsymbol{\Phi}_{kb}^{\mathrm{II}} \\ \mathbf{0} & \mathbf{0} & \mathbf{I}_l^{\mathrm{II}} \end{bmatrix} \tag{3.96}$$

Using equation (3.94) in equation (3.92) and because

$$\mathbf{T}^T\mathbf{C}^T = 0 \tag{3.97}$$

the total system can be written

$$\tilde{\mathbf{M}}\ddot{\boldsymbol{\eta}} + \tilde{\mathbf{K}}\boldsymbol{\eta} = \mathbf{T}^T\mathbf{f} \tag{3.98}$$

where

$$\tilde{\mathbf{M}} = \mathbf{T}^T \begin{bmatrix} \tilde{\mathbf{M}}_{\mathrm{I}} & \mathbf{0} \\ \mathbf{0} & \tilde{\mathbf{M}}_{\mathrm{II}} \end{bmatrix} \mathbf{T} \quad \tilde{\mathbf{K}} = \mathbf{T}^T \begin{bmatrix} \tilde{\mathbf{K}}_{\mathrm{I}} & \mathbf{0} \\ \mathbf{0} & \tilde{\mathbf{K}}_{\mathrm{II}} \end{bmatrix} \mathbf{T} \tag{3.99}$$

Either the transformation matrix $\mathbf{T}$ of equation (3.95) or equation (3.96) can be used. The size of the coupled system in equation (3.92) is the sum of the number of boundary degrees of freedom and the number of kept normal modes of the subdomains. With many interface degrees of freedom the reduced system still is quite large but can be reduced further by two methods described below. The first focus on the fixed interface method and calculates interface modes which describes the behaviour of the interface degrees of freedom in a reduced fashion. The second method uses the extra constraint derived when using residual attachment modes which removes the attachment modes from the reduced problem and only keeping the free interface normal modes.

Synthesis using interface modes

Using the fixed interface mode method and only including the substructure constraint modes for each subdomain in the reduction, the eigenvalue problem can be written

$$\tilde{\mathbf{K}}_B\boldsymbol{\Phi}_B = \boldsymbol{\lambda}_B\tilde{\mathbf{M}}_B\boldsymbol{\Phi}_B \tag{3.100}$$

where $\boldsymbol{\lambda}_B$ contains the eigenvalues in the diagonal, $\boldsymbol{\Phi}_B$ the corresponding eigenvectors and

$$\begin{aligned}\tilde{\mathbf{M}}_B &= \begin{bmatrix} \mathbf{I}_{bb} \\ \mathbf{I}_{bb} \end{bmatrix}^T \begin{bmatrix} \boldsymbol{\Psi}_c^{\mathrm{I}} & \mathbf{0} \\ \mathbf{0} & \boldsymbol{\Psi}_c^{\mathrm{II}} \end{bmatrix}^T \begin{bmatrix} \mathbf{M}_{\mathrm{I}} & \mathbf{0} \\ \mathbf{0} & \mathbf{M}_{\mathrm{II}} \end{bmatrix} \begin{bmatrix} \boldsymbol{\Psi}_c^{\mathrm{I}} & \mathbf{0} \\ \mathbf{0} & \boldsymbol{\Psi}_c^{\mathrm{II}} \end{bmatrix} \begin{bmatrix} \mathbf{I}_{bb} \\ \mathbf{I}_{bb} \end{bmatrix} \\ \tilde{\mathbf{K}}_B &= \begin{bmatrix} \mathbf{I}_{bb} \\ \mathbf{I}_{bb} \end{bmatrix}^T \begin{bmatrix} \boldsymbol{\Psi}_c^{\mathrm{I}} & \mathbf{0} \\ \mathbf{0} & \boldsymbol{\Psi}_c^{\mathrm{II}} \end{bmatrix}^T \begin{bmatrix} \mathbf{K}_{\mathrm{I}} & \mathbf{0} \\ \mathbf{0} & \mathbf{K}_{\mathrm{II}} \end{bmatrix} \begin{bmatrix} \boldsymbol{\Psi}_c^{\mathrm{I}} & \mathbf{0} \\ \mathbf{0} & \boldsymbol{\Psi}_c^{\mathrm{II}} \end{bmatrix} \begin{bmatrix} \mathbf{I}_{bb} \\ \mathbf{I}_{bb} \end{bmatrix}\end{aligned} \tag{3.101}$$

The eigenvectors derived from solving this problem can then be transformed back to original coordinates

$$\boldsymbol{\Psi}_B = \begin{bmatrix} \boldsymbol{\Psi}_c^{\mathrm{I}} & \mathbf{0} \\ \mathbf{0} & \boldsymbol{\Psi}_c^{\mathrm{II}} \end{bmatrix} \begin{bmatrix} \mathbf{I}_{bb} \\ \mathbf{I}_{bb} \end{bmatrix} \boldsymbol{\Phi}_B \tag{3.102}$$

The system in equation (3.91) can then be reduced by the change of base

$$\mathbf{d} = \begin{bmatrix} \boldsymbol{\Psi}_{Bb}^{\mathrm{I}} & \mathbf{0} & \mathbf{0} \\ \boldsymbol{\Psi}_{Bs}^{\mathrm{I}} & \boldsymbol{\Phi}_{ss}^{\mathrm{I}} & \mathbf{0} \\ \boldsymbol{\Psi}_{Bb}^{\mathrm{II}} & \mathbf{0} & \mathbf{0} \\ \boldsymbol{\Psi}_{Bs}^{\mathrm{II}} & \mathbf{0} & \boldsymbol{\Phi}_{ss}^{\mathrm{II}} \end{bmatrix} \begin{bmatrix} \boldsymbol{\xi}_B \\ \boldsymbol{\xi}^{\mathrm{I}} \\ \boldsymbol{\xi}^{\mathrm{II}} \end{bmatrix} \tag{3.103}$$

The coupling between the two domains is accounted for by the interface modes and the number of degrees of freedom in the reduced problem is the sum of the number of retained interface modes and the number of uncoupled modes of the subdomains. This is efficient when a large number of boundary degrees of freedom is present.

Synthesis using the method of Craig and Chang

Using residual attachment modes, the number of kept modes can be reduced by not having to include modes for each interface degree of freedom. This is done by including an additional number of Lagrange multipliers equal to the number of interface degrees of freedom. The force equilibrium in equation (3.90) and the relationship between the residual attachment mode coordinates and forces at the boundary, in equation (3.68), introduce additional constraint equations

$$\boldsymbol{\xi}_b^{\mathrm{I}} + \boldsymbol{\xi}_b^{\mathrm{II}} = \mathbf{0} \tag{3.104}$$

This gives the number of boundary interface degrees of freedom additional constraints and the constraint matrix can be written

$$\mathbf{C} = \begin{bmatrix} \boldsymbol{\Psi}_{db}^{\mathrm{I}} & \boldsymbol{\Phi}_{kb}^{\mathrm{I}} & -\boldsymbol{\Psi}_{db}^{\mathrm{II}} & -\boldsymbol{\Phi}_{kb}^{\mathrm{II}} \\ \mathbf{I}_{bb}^{\mathrm{I}} & \mathbf{0} & \mathbf{I}_{bb}^{\mathrm{II}} & \mathbf{0} \end{bmatrix} \tag{3.105}$$

Partitioning the matrix into linear dependent and independent coordinates

$$\mathbf{C} = \left[\begin{array}{c|c} \mathbf{C}_{dd} & \mathbf{C}_{ld} \end{array} \right] = \left[\begin{array}{cc|cc} \boldsymbol{\Psi}_{db}^{\mathrm{I}} & -\boldsymbol{\Psi}_{db}^{\mathrm{II}} & \boldsymbol{\Phi}_{kb}^{\mathrm{I}} & -\boldsymbol{\Phi}_{kb}^{\mathrm{II}} \\ \mathbf{I}_{bb}^{\mathrm{I}} & \mathbf{I}_{bb}^{\mathrm{I}} & \mathbf{0} & \mathbf{0} \end{array} \right] \tag{3.106}$$

The transformation matrix then becomes

$$\mathbf{T} = \begin{bmatrix} -\mathbf{C}_{dd}^{-1}\mathbf{C}_{dl} \\ \mathbf{I} \end{bmatrix} = \begin{bmatrix} -\begin{bmatrix} \boldsymbol{\Psi}_{db}^{\mathrm{I}} & -\boldsymbol{\Psi}_{db}^{\mathrm{II}} \\ \mathbf{I}_{bb}^{\mathrm{I}} & \mathbf{I}_{bb}^{\mathrm{II}} \end{bmatrix}^{-1} \begin{bmatrix} \boldsymbol{\Phi}_{kb}^{\mathrm{I}} & -\boldsymbol{\Phi}_{kb}^{\mathrm{II}} \\ \mathbf{0} & \mathbf{0} \end{bmatrix} \\ \begin{matrix} \mathbf{I}_l^{\mathrm{I}} & \mathbf{0} \\ \mathbf{0} & \mathbf{I}_l^{\mathrm{II}} \end{matrix} \end{bmatrix} \tag{3.107}$$

Using the same transformation as in equation (3.94), a reduced system is achieved having the number of degrees of freedom equal to the number of included subdomain modes.

3.6 Summary

Modal reduction techniques for structural vibration problems were investigated. The procedures of deriving the reduced set of basis vectors are described for three methods: Introducing generalised coordinates, condensation methods and component mode synthesis method. The two first methods can be seen as special cases of the third one. In the component mode synthesis method, the studied problem domain is divided into a number of subdomains and the procedure of coupling these subdomains together, using Lagrange multipliers, is described. A number of the described reduction procedures are adopted in the papers included in the thesis.

Chapter 4

Porous sound absorbing materials

The modelling of porous materials within the finite element method is now to be investigated. This modelling is very important when, for example, predicting the sound pressure level in a passenger compartment of a vehicle due to the engine vibrations, or evaluating the sound transmission loss of double-walls.

The aim of this chapter is to investigate the implementation of the porous material descriptions in the finite element environment, with an emphasis on the boundary conditions when coupling the porous materials with a flexible structure or an acoustic cavity. (A detailed description of the theories describing porous materials can be found in the referenced publications.) The finite elements, that describe the porous material using either two different equivalent fluid models or Biot's theory, are implemented as an extension to the Matlab [66] toolbox CALFEM [67].

The implemented elements are verified in a number of one-dimensional test problems where the results using the implemented element are compared to the analytical solutions. Two three dimensional problems are also studied to investigate the effect of using different porous material descriptions. The two problems of interest are the sound transmission loss in a double wall lined with porous material and an enclosed acoustic cavity with one of the walls covered by porous material.

The chapter also includes a review of the literature investigating the modelling of porous sound absorbing materials, with focus on the description of the porous material within the finite element framework. Also, the material parameters for the porous material, for both the frame and air inside the pores, are described.

4.1 Literature review

In the modelling of sound propagation in sound absorbing materials, the porous material can be divided into two partitions: the fluid partition (the fluid in the open pores) and the structural partition (the flexible porous material frame).

Assuming a simplified description of the structural partition, the sound propagation can be described by an equivalent fluid with frequency dependent bulk modulus and

density. These material properties can be determined from measurements, as where done by Delany and Bazley [68], or by analytical models. The empirical model in [68] was improved by Mechel [69] by describing the low frequency behaviour by an analytical model. A similar procedure was adopted by Kirby and Cummings [70]. In the analytical models, the structural frame is either assumed to be rigid, as described in the book by Allard [71], or limp, i.e. the inertia effects of the structural frame are included, as in the models by Ingard [72] and Göransson [73, 74]. Finite element analysis of porous sound absorbing materials using an equivalent fluid model was performed by, for example, Craggs [75], using the assumption that the frame is rigid. A scalar primary variable, for example the pressure, is used for the porous material domain and a system with only one degree of freedom in each node is achieved in the finite element formulation. The equivalent fluid models and the inclusion of the models within in the finite element environment are studied in the following sections.

Biot derived a theory for studying sound propagation in porous materials [76], see also the book by Allard [71]. The theory accounts for the sound propagation in both the fluid partition and in the flexible frame (structural partition) as well as the coupling between the two partitions. The motion in the two partitions is described by the equations of linear continuum mechanics, with the displacements in the structural and fluid partitions, $\mathbf{u}_s$ and $\mathbf{u}_f$ respectively, as the primary variables. Finite element formulation of Biot's equations [77, 78, 79] gives six degrees of freedom, three displacement components for each partition, in each node. Since the shear stresses in the fluid partition are zero, a formulation using the acoustic pressure as the variable in the fluid partition can be derived [80, 81], a $\langle \mathbf{u}_s, p_f \rangle$-formulation is achieved. Finite element formulation gives four degrees of freedom in each node, the displacement components for the structure and the pressure for the fluid. Both formulations are described in this chapter.

4.2 Porous material properties

The porous material can be divided into two partitions. The structural frame material and the air in the open pores. The properties for these partitions are here divided into the properties of the air in the pores, the properties that depend on the geometry of the porous material frame and the mechanical properties of the frame.

Air properties

The air can be considered as an ideal gas for which the ideal gas law reads

$$PV = nRT \tag{4.1}$$

where P is the pressure, V the volume, n is the number of moles and T the temperature of the gas in Kelvin (K). R is the universal gas constant, $R = 8.31144$ J/(mol K). Introducing the molar mass, m, which is given for air in Table 4.1, and the density, ρ, the ideal gas law can be written

$$P = \frac{\rho RT}{m} \tag{4.2}$$

The density of air is dependent on the ambient pressure and temperature. The static density, ρ_0, at standard air pressure, $P_0 = 1.01 \cdot 10^5$ Pa and the temperature 20 °C is

given in Table 4.1. The speed of sound, c, in a gas is defined as

$$c^2 = \frac{dP}{d\rho} \tag{4.3}$$

Two conditions are of interest. At isothermal conditions, the temperature is constant and the ratio between the pressure and density at the static configuration, P_0 and ρ_0, is equal to the ratio at any state, P and ρ,

$$\frac{P_0}{\rho_0} = \frac{P}{\rho} \tag{4.4}$$

The speed of sound in air at isothermal conditions becomes

$$c^2_{isothermal} = c^2_t = \left(\frac{d}{d\rho}\left(\frac{P_0\rho}{\rho_0}\right)\right)_0 = \frac{P_0}{\rho_0} \tag{4.5}$$

At adiabatic conditions, i.e. no heat is exchanged with the surroundings, the relation between pressure and density becomes, see [4],

$$\frac{P_0}{\rho_0^\gamma} = \frac{P}{\rho^\gamma} \tag{4.6}$$

with

$$\gamma = \frac{c_p}{c_v} \tag{4.7}$$

being the ratio between the specific heat at constant pressure, c_p, and at constant volume, c_v. For air, $\gamma = 1.4$. and the speed of sound at adiabatic conditions is

$$c^2_{adiabatic} = c^2_0 = \left(\frac{d}{d\rho}\left(\frac{P_0\rho^\gamma}{\rho_0^\gamma}\right)\right)_0 = \frac{\gamma P_0}{\rho_0} \tag{4.8}$$

Sound propagation in free air is assumed to be adiabatic, i.e. there is no heat exchange with the surroundings. However, in porous materials the heat exchange with the frame material leads to that the isothermal assumption is more correct. The speed of sound in air, at 20 °C for both adiabatic, c_0, and isothermal conditions, c_t, is presented in Table 4.1. The viscosity of air η (Nms/m^3) and the Prandtl number, Pr, are also given for air in Table 4.1.

Table 4.1: *Material data for air at standard pressure,* $P_0 = 1.01 \cdot 10^5$ *Pa and temperature* $20°$ *C.*

Air:				
	ρ_0	=	1.21	kg/m^3
	c_0	=	343	m/s
	c_t	=	290	m/s
	γ	=	1.4	
	Pr	=	0.71	
	η	=	$1.84 \cdot 10^{-5}$	Ns/m^2
	m	=	29.0	g/mol

Geometric properties of the frame

The following properties dependent on the geometry of the porous frame material are introduced to describe the sound propagation in porous materials. A thorough description of these properties can be found in Allard [71], where also methods to determine these parameters experimentally are discussed. The porosity, ϕ, of a material is the ratio between the air volume in the open pores, V_a, and the total volume V_t, i.e. $\phi = V_a/V_t$. The flow resistivity σ (Ns/m^4) introduces viscous losses in the sound propagation in the porous material. The tortuosity, α_∞, relates the actual distance the sound has to propagate to pass through a layer to the thickness of the layer. The tortuosity increases the real part of the fluid density since the acceleration of the fluid particles is increased when they have to move around the solid frame. The viscous characteristic length, Λ, and the thermal characteristic length, Λ', also depend on the geometry of the frame and are coupled to the viscous and thermal losses, respectively.

The five measurable porous material properties, ϕ, σ, α_∞, Λ and Λ', together with the properties of air in Table 4.1, describe the sound propagation in fluid partition of the porous absorbing material.

Mechanical properties of the frame

The isotropic structural partition of the porous material is described by two of the related modulus of elasticity, E_s, Poisson's ratio, ν_s and shear modulus, G_s together with the density, ρ_s. The damping in the structural partition is introduced by a loss factor η_s, which is independent of frequency, giving a complex modulus of elasticity, $\tilde{E}_s$

$$\tilde{E}_s = (1 + \mathrm{i}\eta_s)E_s \tag{4.9}$$

Material properties used in the numerical investigation

In the numerical investigation presented in Section 4.8, three different porous materials are investigated and the material properties are given in Table 4.2. Material 1 is chosen to have a structural frame that is very weak and Material 2 to have a very stiff structural frame. These two materials can be found in [80]. Material 3 has the properties of a typical foam and can be found in [79].

Table 4.2: *Material data for the porous materials.*

Porous material:		1	2	3
ϕ		0.95	0.94	0.96
σ	Ns/m^4	25000	40000	32000
α_∞		1.4	1.06	1.7
Λ	μm	93.2	56	90
Λ'	μm	93.2	110	165
E_s	kPa	42	4400	845
ν_s		0	0	0.3
η_s		0.05	0.1	0.1
ρ_s	kg/m^3	30	130	30

4.3 Boundary conditions for a porous material

Using the primary variables $\langle \mathbf{u}_s, \mathbf{u}_f \rangle$ – being the displacements in the structural and fluid partitions – for describing the sound propagation in porous material the following boundary conditions can arise ($\mathbf{n}_P$ is a normal vector at the boundary directed outward from the porous material domain):

1. The boundary in contact with an acoustic fluid with the pressure p_F and displacement $\mathbf{u}_F$ at the boundary. Here the following conditions must be satisfied

$$\begin{aligned} -\phi p_F &= \mathbf{n}_P^T \mathbf{t}_f \\ -(1-\phi) p_F &= \sigma_s|_{n_P} = \mathbf{n}_P^T \mathbf{t}_s \\ \mathbf{n}_P^T \mathbf{u}_F &= (1-\phi)\mathbf{n}_P^T \mathbf{u}_s + \phi \mathbf{n}_P^T \mathbf{u}_f \end{aligned} \tag{4.10}$$

2. The porous material bounded to a flexible structure with the displacement $\mathbf{u}_S$

$$\begin{aligned} \mathbf{u}_s &= \mathbf{u}_S \\ \mathbf{n}_P^T \mathbf{u}_f &= \mathbf{n}_P^T \mathbf{u}_S \end{aligned} \tag{4.11}$$

   For a rigid wall

$$\begin{aligned} \mathbf{u}_s &= \mathbf{0} \\ \mathbf{n}_P^T \mathbf{u}_f &= 0 \end{aligned} \tag{4.12}$$

3. The porous material is in contact with a flexible structure, but the coupling is unbounded, i.e. the structural partition of the porous material and the flexible structure is not in contact with each other. In this case a thin acoustic fluid layer is placed between the flexible structure and porous material and the coupling conditions in equation (4.10) can be used.

4.4 Equivalent fluid models for porous materials

In the equivalent fluid models, the sound propagation in the porous material is described by the acoustic equation (2.26) with $\tilde{c}$, the speed of sound, calculated by

$$\tilde{c} = \sqrt{\frac{\tilde{K}}{\tilde{\rho}}} \tag{4.13}$$

where $\tilde{\rho}$ is the density and $\tilde{K}$ is the bulk modulus. These parameters are complex and frequency dependent. The finite element formulation for an acoustic fluid is stated in equation (2.31). The subscript F, denoting the acoustic fluid domain in the finite element formulation, is replaced with P, to specify that the porous material is studied. The porous material domain is denoted Ω_P, the nodal pressures and finite element shape functions are denoted $\mathbf{p}_P$ and $\mathbf{N}_P$, respectively. The studied equivalent fluid models are derived in detail in the cited references. In this presentation, only the density and bulk modulus are stated together with an investigation concerning the boundary conditions.

When describing porous materials using an equivalent fluid model, the volume displacements in the fluid can be used. The actual fluid displacements in the pores, $\mathbf{u}_f$, are related to the volume displacements through the porosity, ϕ,

$$\mathbf{u}_{fv} = \phi \mathbf{u}_f \tag{4.14}$$

This gives simplified expressions in the boundary conditions.

The structural frame of the porous material is either considered to be rigid or limp and one model for each of these assumptions is studied.

4.4.1 Porous material with a rigid frame

This model is based on describing the sound propagation in porous materials as propagation of sound in cylindrical tubes with the frame considered rigid. A detailed description of this model was presented by Allard [71]. The frequency dependent density and bulk modulus are derived by including the viscosity of the air and the thermal exchange with the connecting frame in the model. The density of the porous material is given by

$$\tilde{\rho}(\omega) = \alpha_\infty \rho_0 \left[1 + \frac{\sigma\phi}{\mathrm{i}\omega\rho_0\alpha_\infty} G_J(\omega) \right] \tag{4.15}$$

and the bulk modulus

$$\tilde{K}(\omega) = \frac{\gamma P_0}{\gamma - (\gamma - 1)\left[1 + \frac{\sigma'\phi}{\mathrm{iPr}\omega\rho_0\alpha_\infty} G'_J(\mathrm{Pr}\omega) \right]^{-1}} \tag{4.16}$$

with

$$G_J(\omega) = \left[1 + \frac{4\mathrm{i}\alpha_\infty^2 \eta\rho_0\omega}{\sigma^2\Lambda^2\phi^2} \right]^{1/2} \tag{4.17}$$

and

$$G'_J(\mathrm{Pr}\omega) = \left[1 + \frac{4\mathrm{i}\alpha_\infty^2 \eta\rho_0\omega\mathrm{Pr}}{\sigma'^2\Lambda'^2\phi^2} \right]^{1/2} \tag{4.18}$$

where

$$\sigma' = \frac{\Lambda^2}{\Lambda'^2}\sigma \tag{4.19}$$

The density and bulk modulus are derived from the fluid displacements in the pores. Using the volume displacements, the density and the bulk modulus becomes

$$\begin{aligned} \tilde{\rho}_v(\omega) &= \frac{\tilde{\rho}(\omega)}{\phi} \\ \tilde{K}_v(\omega) &= \frac{\tilde{K}(\omega)}{\phi} \end{aligned} \tag{4.20}$$

with $\tilde{\rho}(\omega)$ and $\tilde{K}(\omega)$ from equations (4.15) and (4.16).

Simplification by Brennan

In the paper by Brennan et al. [82], the complicated expressions for the density and bulk modulus in equations (4.15) and (4.16) are simplified by neglecting the thermal damping and with a low frequency assumption. The equivalent fluid density becomes

$$\tilde{\rho}(\omega) = \alpha_\infty \rho_0 + \frac{\sigma\phi}{\mathrm{i}\omega} \tag{4.21}$$

and the bulk modulus

$$\tilde{K}(\omega) = P_0 \tag{4.22}$$

4.4.2 Porous material with a limp frame

Assuming the frame material to be limp, i.e. the frame material has no stiffness but the inertia effects are included, a material model was derived by Göransson [73]. In this model the acoustic wave propagates at constant temperature conditions inside the porous material and the speed of sound is given the isothermal value in Table 4.1. Introducing the bulk mass density of the material

$$M = \phi\rho_0 + (1-\phi)\rho_s \tag{4.23}$$

where ρ_s is the density of the frame material, the relation between the volume displacements of the fluid particles, $\mathbf{u}_{vf}$ and the limp frame $\mathbf{u}_s$ becomes

$$\frac{\mathbf{u}_s}{\mathbf{u}_{vf}} = \frac{1}{1 + \mathrm{i}\omega M/\sigma\phi} \tag{4.24}$$

The density and the bulk modulus of the porous material can be written

$$\tilde{\rho}_v = \frac{\alpha_\infty\rho_0/\phi - \mathrm{i}\sigma/\omega}{1 - \mathrm{i}\phi\sigma/\omega M} \tag{4.25}$$

and

$$\tilde{K}_v = \frac{c_t^2\rho_0}{\phi} \tag{4.26}$$

The subscript, v, denotes that the model is derived using the fluid volume displacements. Note that when $M \to \infty$, this model approaches the simplified model by Brennan, presented in the previous section.

4.4.3 Boundary conditions

Studying the boundary conditions between the porous material domain, Ω_P, described by an equivalent fluid and a connecting structural or fluid domain, the continuity of pressure and fluid displacements over the boundary must be fulfilled. The continuity in pressure, when in contact with an acoustic domain, is fulfilled through the assembling process. The same degrees of freedom at the interface between the domains can be used for both the acoustic and the porous material domains. The continuity of displacements, of interest when the fluid is in contact with a flexible structure, is fulfilled using the condition of preserved normal volume displacements together with the relation between displacements

and pressure in the acoustic fluid describing the porous material ($\mathbf{n}_P$ is the boundary vector pointing outward from the porous material domain.)

$$\mathbf{n}_P^T \nabla p_P = \omega^2 \tilde{\rho} \mathbf{n}_P^T \mathbf{u}_f = \omega^2 \tilde{\rho}_v \mathbf{n}_P^T \mathbf{u}_{fv} \tag{4.27}$$

This is used in the boundary term in the finite element formulation of the porous material domain, i.e.

$$\mathbf{f}_S = \tilde{\rho}\tilde{c}^2 \int_{\partial\Omega_{SP}} \mathbf{N}_P^T \mathbf{n}_P^T \mathbf{u}_f dS = \tilde{\rho}_v \tilde{c}^2 \int_S \mathbf{N}_P^T \mathbf{n}_P^T \mathbf{u}_{fv} dS \tag{4.28}$$

with the conditions derived below. The boundary conditions in the equivalent fluid are:

1. At boundary in contact with an acoustic fluid the conditions in Eq. (4.10) must be fulfilled. Using the equivalent fluid with a rigid frame the boundary conditions can be written

$$\begin{aligned} p_F &= p_P \\ \mathbf{n}_P^T \mathbf{u}_F &= \mathbf{n}_P^T \phi \mathbf{u}_f = \mathbf{n}_P^T \mathbf{u}_{fv} \end{aligned} \tag{4.29}$$

   When the frame is assumed to be limp, the boundary conditions can be derived using equations (4.14), (4.24) and (4.10) giving

$$\begin{aligned} p_F &= p_P \\ \mathbf{n}_P^T \mathbf{u}_F &= \gamma_b \mathbf{n}_P^T \mathbf{u}_{fv} \end{aligned} \tag{4.30}$$

   where

$$\gamma_b = \frac{1 - \mathrm{i}\sigma/M\omega}{1 - \mathrm{i}\phi\sigma/M\omega} \tag{4.31}$$

2. With the boundary in contact with a flexible structure, the conditions in equation (4.11) are valid. The continuity between the structural frame and the flexible structure can not be fulfilled using the equivalent fluid models. It is assumed that there is an air gap between the flexible wall and the porous material and the flexible wall displacement in the normal direction is equal to the displacement in the acoustic fluid, i.e., $\mathbf{n}_P^T \mathbf{u}_S = \mathbf{n}_P^T \mathbf{u}_F$. The boundary conditions for the porous material in contact with the acoustic domain then gives, for the rigid frame

$$\mathbf{n}_P^T \mathbf{u}_S = \mathbf{n}_P^T \phi \mathbf{u}_f = \mathbf{n}_P^T \mathbf{u}_{fv} \tag{4.32}$$

   and for the limp frame assumption

$$\mathbf{n}_P^T \mathbf{u}_S = \gamma_b \mathbf{n}_P^T \mathbf{u}_{fv} \tag{4.33}$$

   For a rigid wall, $\mathbf{n}_P^T \mathbf{u}_f = \mathbf{n}_P^T \mathbf{u}_{fv} = 0$.

4.5 Biot's theory

When the sound transmission in a porous material both occurs in the air in the pores and in the flexible frame, Biot's theory can be used [76]. This theory describes the fluid and structural partitions and the coupling between them using the equations of linear continuum mechanics.

The implementation of Biot's theory consists of three main parts, the finite element formulation of the equation of motion for a continuum body, described in Section 2.3.1. The sound propagation in the pores when the frame is considered rigid, described in Section 4.4.1. The third part is Biot's relations consisting of the stress-strain relationships of the structural and fluid partitions, described in Section 4.5.1, the inertia coupling, Section 4.5.2, and viscous forces, Section 4.5.3. Based on these sections the finite element formulation of Biot's theory is derived.

4.5.1 Stress-strain relation

The stress-strain relationship in Biot's theory can, in order to fit into the finite element formulation, be written in matrix notation as

$$\boldsymbol{\sigma}_s = \mathbf{D}_s \boldsymbol{\varepsilon}_s + \mathbf{Q} \boldsymbol{\varepsilon}_f \tag{4.34}$$

$$\boldsymbol{\sigma}_f = \mathbf{Q}^T \boldsymbol{\varepsilon}_s + \mathbf{D}_f \boldsymbol{\varepsilon}_f \tag{4.35}$$

where

$$\begin{aligned} \mathbf{D}_s &= \begin{bmatrix} P & P-2G & P-2G & 0 & 0 & 0 \\ P-2G & P & P-2G & 0 & 0 & 0 \\ P-2G & P-2G & P & 0 & 0 & 0 \\ 0 & 0 & 0 & G & 0 & 0 \\ 0 & 0 & 0 & 0 & G & 0 \\ 0 & 0 & 0 & 0 & 0 & G \end{bmatrix} \\ \mathbf{D}_f &= R \begin{bmatrix} 1 & 1 & 1 & 0 & 0 & 0 \\ 1 & 1 & 1 & 0 & 0 & 0 \\ 1 & 1 & 1 & 0 & 0 & 0 \\ 0 & 0 & 0 & 0 & 0 & 0 \\ 0 & 0 & 0 & 0 & 0 & 0 \\ 0 & 0 & 0 & 0 & 0 & 0 \end{bmatrix}; \quad \mathbf{Q} = Q \begin{bmatrix} 1 & 1 & 1 & 0 & 0 & 0 \\ 1 & 1 & 1 & 0 & 0 & 0 \\ 1 & 1 & 1 & 0 & 0 & 0 \\ 0 & 0 & 0 & 0 & 0 & 0 \\ 0 & 0 & 0 & 0 & 0 & 0 \\ 0 & 0 & 0 & 0 & 0 & 0 \end{bmatrix} \end{aligned} \tag{4.36}$$

For large values of the bulk modulus of the material in the porous frame, the effective bulk modulus of the fluid partition is

$$R = \phi K_f \tag{4.37}$$

where the frequency dependent bulk modulus of the fluid, K_f, is previously defined for the porous material having a rigid frame, equation (4.16). The volume change in the fluid partition is related to the volume change in the structural partition by the dilatational coupling coefficient

$$Q = (1-\phi) K_f \tag{4.38}$$

The bulk modulus of the structural partition, P, can be expressed

$$P = \frac{4}{3} G + K_b + \frac{(1-\phi)^2}{\phi} K_f \tag{4.39}$$

where K_b is the in vacuo bulk modulus of the structural frame

$$K_b = \frac{2G(\nu+1)}{3(1-2\nu)} \tag{4.40}$$

With no coupling between the structure and fluid ($Q = 0$) then $P = \lambda + 2\mu$ and $R = \phi K_f$. The four material parameters G, P, R and Q can be determined from experiments.

4.5.2 Inertia forces

There also exists a coupling in the inertia terms. When the structure vibrates the fluid acts as an added mass increasing the density of the frame. In the opposite, vibrating fluid particles has to move around the structural frame which can be seen as an increase in density of the fluid. The inertia forces can be written

$$\mathbf{q}_s = \rho_{11}\ddot{\mathbf{u}}_s + \rho_{12}\ddot{\mathbf{u}}_f \tag{4.41}$$

$$\mathbf{q}_f = \rho_{12}\ddot{\mathbf{u}}_s + \rho_{22}\ddot{\mathbf{u}}_f \tag{4.42}$$

where

$$\begin{aligned} \rho_{11} &= \rho_1 + \rho_a \\ \rho_{12} &= -\rho_a \\ \rho_{22} &= \phi\rho_0 + \rho_a \end{aligned} \tag{4.43}$$

and ρ_a is the inertial coupling term

$$\rho_a = \phi\rho_0(\alpha_\infty - 1) \tag{4.44}$$

4.5.3 Viscous forces

The flow resistivity for the air particles in the pores introduces a body force proportional to the difference in the velocities between the structural partition and fluid partition. This can be written

$$\mathbf{b}_s^{visc} = -\sigma\phi^2 G_J(\omega)\frac{\partial}{\partial t}(\mathbf{u}_s - \mathbf{u}_f) \tag{4.45}$$

and

$$\mathbf{b}_f^{visc} = \sigma\phi^2 G_J(\omega)\frac{\partial}{\partial t}(\mathbf{u}_s - \mathbf{u}_f) \tag{4.46}$$

4.5.4 Strong form of Biot's equations

The equation of motions in the frequency domain for a porous material can now be written

$$\tilde{\boldsymbol{\nabla}}^T\boldsymbol{\sigma}_s - \mathrm{i}\omega\sigma\phi^2 G_J(\omega)(\mathbf{u}_s - \mathbf{u}_f) = -\omega^2(\rho_{11}\mathbf{u}_s + \rho_{12}\mathbf{u}_f) \tag{4.47}$$

$$\tilde{\boldsymbol{\nabla}}^T\boldsymbol{\sigma}_f + \mathrm{i}\omega\sigma\phi^2 G_J(\omega)(\mathbf{u}_s - \mathbf{u}_f) = -\omega^2(\rho_{22}\mathbf{u}_f + \rho_{12}\mathbf{u}_s) \tag{4.48}$$

This can be compared with the governing equation for a continuum body in Section 2.3.1. Introducing the complex densities including the inertia and viscous effects

$$\begin{aligned} \tilde{\rho}_{11} &= \rho_1 + \rho_a - i\sigma\phi^2\frac{G(\omega)}{\omega} \\ \tilde{\rho}_{12} &= -\rho_a + i\sigma\phi^2\frac{G(\omega)}{\omega} \\ \tilde{\rho}_{22} &= \phi\rho_0 + \rho_a - i\sigma\phi^2\frac{G(\omega)}{\omega} \end{aligned} \tag{4.49}$$

the equations of motion can be written

$$\tilde{\boldsymbol{\nabla}}^T \boldsymbol{\sigma}_s = -\omega^2(\tilde{\rho}_{11}\mathbf{u}_s + \tilde{\rho}_{12}\mathbf{u}_f) \tag{4.50}$$

$$\tilde{\boldsymbol{\nabla}}^T \boldsymbol{\sigma}_f = -\omega^2(\tilde{\rho}_{22}\mathbf{u}_f + \tilde{\rho}_{12}\mathbf{u}_s) \tag{4.51}$$

In the finite element formulation of these equations, described in Section 4.6, both partitions have the displacement as the primary variable, an $\langle \mathbf{u}_s\text{-}\mathbf{u}_f \rangle$-formulation is achieved. The fluid domain can be described by the acoustic wave equation, which gives a $\langle \mathbf{u}_s\text{-}p_f \rangle$-formulation. This formulation is described in Section 4.7.

4.6 $\mathbf{u}_s$-$\mathbf{u}_f$-formulation

4.6.1 Finite element formulation

Following the procedure in the finite element formulation of the continuum material described in Section 2.3.1, multiplying with a weight function, integrating over the domain Ω_{PF} and using the Green-Gauss theorem, the weak form of the equations of motion for the two partitions can be derived

$$-\omega^2 \int_{\Omega_P} \mathbf{v}_s^T(\tilde{\rho}_{11}\mathbf{u}_s + \tilde{\rho}_{12}\mathbf{u}_f)dV + \int_{\Omega_P} (\tilde{\boldsymbol{\nabla}}\mathbf{v}_s)^T \boldsymbol{\sigma}_s dV - \int_{\partial\Omega_P} \mathbf{v}_s^T \mathbf{t}_s dS = 0 \tag{4.52}$$

$$-\omega^2 \int_{\Omega_P} \mathbf{v}_f^T(\tilde{\rho}_{22}\mathbf{u}_f + \tilde{\rho}_{12}\mathbf{u}_s)dV + \int_{\Omega_P} (\tilde{\boldsymbol{\nabla}}\mathbf{v}_f)^T \boldsymbol{\sigma}_f dV - \int_{\partial\Omega_P} \mathbf{v}_f^T \mathbf{t}_f dS = 0 \tag{4.53}$$

where $\mathbf{t}_s$ and $\mathbf{t}_f$ are the surface traction vectors of the structural and fluid partitions, respectively. With this weak formulation of the poroelastic problem the finite element equations of motion can be derived. The finite element approximation of the structural and fluid displacements, $\mathbf{u}_s$ and $\mathbf{u}_f$, and the weight functions, $\mathbf{v}_s$ and $\mathbf{v}_f$, can be written

$$\begin{aligned} \mathbf{u}_s &= \mathbf{N}_s\mathbf{d}_s; \quad \mathbf{u}_f = \mathbf{N}_f\mathbf{d}_f \\ \mathbf{v}_s &= \mathbf{N}_s\mathbf{c}_s; \quad \mathbf{v}_f = \mathbf{N}_f\mathbf{c}_f \end{aligned} \tag{4.54}$$

where $\mathbf{d}_s$ and $\mathbf{d}_f$ are the nodal displacements and the $\mathbf{c}_s$ and $\mathbf{c}_f$ the corresponding nodal weights. The kinematic relations can be expressed in the finite element displacements

$$\boldsymbol{\varepsilon}_s = \tilde{\boldsymbol{\nabla}}\mathbf{N}_s\mathbf{d}_s; \quad \boldsymbol{\varepsilon}_f = \tilde{\boldsymbol{\nabla}}\mathbf{N}_f\mathbf{d}_f \tag{4.55}$$

Introducing the stress-strain relations in equations (4.34) and (4.35), and noting that $\mathbf{c}_s$ and $\mathbf{c}_f$ are arbitrary, give the finite element formulation; for the structural partition

$$\begin{aligned} &-\omega^2(\tilde{\rho}_{11}\int_{\Omega_P} \mathbf{N}_s^T\mathbf{N}_s dV\mathbf{d}_s + \tilde{\rho}_{12}\int_{\Omega_P} \mathbf{N}_s^T\mathbf{N}_f dV\mathbf{d}_f) + \\ &+\int_{\Omega_P} (\tilde{\boldsymbol{\nabla}}\mathbf{N}_s)^T\mathbf{D}_s\tilde{\boldsymbol{\nabla}}\mathbf{N}_s dV\mathbf{d}_s + \int_{\Omega_P} (\tilde{\boldsymbol{\nabla}}\mathbf{N}_s)^T\mathbf{Q}\tilde{\boldsymbol{\nabla}}\mathbf{N}_f dV\mathbf{d}_f = \\ &= \int_{\partial\Omega_P} \mathbf{N}_s^T\mathbf{t}_s dS \end{aligned} \tag{4.56}$$

and for the fluid partition

$$
\begin{aligned}
&-\omega^2(\tilde{\rho}_{22}\int_{\Omega_P}\mathbf{N}_f^T\mathbf{N}_f dV\mathbf{d}_f+\tilde{\rho}_{12}\int_{\Omega_P}\mathbf{N}_f^T\mathbf{N}_s dV\mathbf{d}_s+\\
&+\int_{\Omega_P}(\tilde{\boldsymbol{\nabla}}\mathbf{N}_f)^T\mathbf{D}_f\tilde{\boldsymbol{\nabla}}\mathbf{N}_f dV+\int_{\Omega_P}(\tilde{\boldsymbol{\nabla}}\mathbf{N}_f)^T\mathbf{Q}\tilde{\boldsymbol{\nabla}}\mathbf{N}_s dV\mathbf{d}_s=\\
&=\int_{\partial\Omega_P}\mathbf{N}_f^T\mathbf{t}_f dS
\end{aligned}
\tag{4.57}
$$

The system of equations describing the sound propagation in porous material can be written

$$
\left(-\omega^2\begin{bmatrix}\mathbf{M}_{ss} & \mathbf{M}_{sf}\\ \mathbf{M}_{fs} & \mathbf{M}_{ff}\end{bmatrix}+\begin{bmatrix}\mathbf{K}_{ss} & \mathbf{K}_{sf}\\ \mathbf{K}_{fs} & \mathbf{K}_{ff}\end{bmatrix}\right)\begin{bmatrix}\mathbf{d}_s\\ \mathbf{d}_f\end{bmatrix}=\begin{bmatrix}\mathbf{f}_{bs}\\ \mathbf{f}_{bf}\end{bmatrix}
\tag{4.58}
$$

with the following matrices derived

$$
\begin{aligned}
&\mathbf{M}_{ss}=\tilde{\rho}_{11}\int_{\Omega_P}\mathbf{N}_s^T\mathbf{N}_s dV && \mathbf{M}_{sf}=\tilde{\rho}_{12}\int_{\Omega_P}\mathbf{N}_s^T\mathbf{N}_f dV\\
&\mathbf{K}_{ss}=\int_{\Omega_P}(\tilde{\boldsymbol{\nabla}}\mathbf{N}_s)^T\mathbf{D}_s\tilde{\boldsymbol{\nabla}}\mathbf{N}_s dV && \mathbf{K}_{sf}=\int_{\Omega_P}(\tilde{\boldsymbol{\nabla}}\mathbf{N}_s)^T\mathbf{Q}\tilde{\boldsymbol{\nabla}}\mathbf{N}_f dV\\
&\mathbf{f}_{bs}=\int_{\partial\Omega_P}\mathbf{N}_s^T\mathbf{t}_s dS
\end{aligned}
\tag{4.59}
$$

$$
\begin{aligned}
&\mathbf{M}_{ff}=\tilde{\rho}_{22}\int_{\Omega_P}\mathbf{N}_f^T\mathbf{N}_f dV && \mathbf{M}_{fs}=\tilde{\rho}_{12}\int_{\Omega_P}\mathbf{N}_f^T\mathbf{N}_s dV\\
&\mathbf{K}_{ff}=\int_{\Omega_P}(\tilde{\boldsymbol{\nabla}}\mathbf{N}_f)^T\mathbf{D}_f\tilde{\boldsymbol{\nabla}}\mathbf{N}_f dV && \mathbf{K}_{fs}=\int_{\Omega_P}(\tilde{\boldsymbol{\nabla}}\mathbf{N}_f)^T\mathbf{Q}^T\tilde{\boldsymbol{\nabla}}\mathbf{N}_s dV\\
&\mathbf{f}_{bf}=\int_{\partial\Omega_P}\mathbf{N}_f^T\mathbf{t}_f dS
\end{aligned}
\tag{4.60}
$$

The procedure to couple the porous material to an acoustic fluid domain or a flexible structure is studied in the next sections.

4.6.2 Coupling with an acoustic fluid

If the porous material is in contact with an acoustic fluid, at the boundary $\partial\Omega_{PF}$, the conditions in equation (4.10) can be introduced through the boundary force terms $\mathbf{f}_{bs}$ and $\mathbf{f}_{bf}$ in equations (4.59) and (4.60) for the porous material. Noting that the boundary normal vector $\mathbf{n}$ points outward from the acoustic fluid domain, i.e. $\mathbf{n}=\mathbf{n}_F=-\mathbf{n}_P$, the force terms can be written

$$
\begin{aligned}
\mathbf{f}_{sF}&=\int_{\partial\Omega_{PF}}\mathbf{N}_s^T\mathbf{t}_s dS=\int_{\partial\Omega_{PF}}(\mathbf{N}_s)^T\mathbf{n}(1-\phi)p_F dS=(1-\phi)\int_{\partial\Omega_{PF}}(\mathbf{N}_s)^T\mathbf{n}\mathbf{N}_F dS\mathbf{p}_F\\
\mathbf{f}_{fF}&=\int_{\partial\Omega_{PF}}\mathbf{N}_f^T\mathbf{t}_f dS=\int_{\partial\Omega_{PF}}(\mathbf{N}_f)^T\mathbf{n}\phi p_F dS=\phi\int_{\partial\Omega_{PF}}(\mathbf{N}_f)^T\mathbf{n}\mathbf{N}_F dS\mathbf{p}_F
\end{aligned}
\tag{4.61}
$$

The boundary force term in the acoustic fluid domain, $\mathbf{f}_{bF}$ in equation (2.31), is

$$\begin{aligned}\mathbf{f}_{FP} = c_0^2 \int_{\partial\Omega_{PF}} \mathbf{N}_F^T \nabla p_F \mathbf{n} dS = \omega^2 \rho_0 c_0^2 \int_{\partial\Omega_{PF}} \mathbf{N}_F^T \mathbf{n}^T \left((1-\phi)\mathbf{u}_s + \phi \mathbf{u}_f\right) dS = \\ \omega^2 \rho_0 c_0^2 \left((1-\phi) \int_{\partial\Omega_{PF}} \mathbf{N}_F^T \mathbf{n}^T \mathbf{N}_s dS \mathbf{d}_s + \phi \int_{\partial\Omega_{PF}} \mathbf{N}_F^T \mathbf{n}^T \mathbf{N}_f dS \mathbf{d}_f \right)\end{aligned} \tag{4.62}$$

The following coupling matrices can be introduced

$$\begin{aligned}\mathbf{H}_{sF} &= \int_{\partial\Omega_{PF}} \mathbf{N}_s^T \mathbf{n} \mathbf{N}_F dS \\ \mathbf{H}_{fF} &= \int_{\partial\Omega_{PF}} \mathbf{N}_f^T \mathbf{n} \mathbf{N}_F dS\end{aligned} \tag{4.63}$$

whereby the force terms can be written

$$\begin{aligned}\mathbf{f}_{sF} &= (1-\phi)\mathbf{H}_{sF}\bar{\mathbf{p}}_F \\ \mathbf{f}_{fF} &= \phi \mathbf{H}_{fF}\bar{\mathbf{p}}_F \\ \mathbf{f}_{FP} &= \omega^2 \rho_0 c_0^2 \left((1-\phi)\mathbf{H}_{sF}^T \mathbf{d}_s + \phi \mathbf{H}_{fF}^T \mathbf{d}_f \right)\end{aligned} \tag{4.64}$$

And the coupled system becomes

$$\left(-\omega^2 \begin{bmatrix} \mathbf{M}_{ss} & \mathbf{M}_{sf} & 0 \\ \mathbf{M}_{fs} & \mathbf{M}_{ff} & 0 \\ (1-\phi)\rho_0 c_0^2 \mathbf{H}_{sF}^T & \phi \rho_0 c_0^2 \mathbf{H}_{fF}^t & \mathbf{M}_F \end{bmatrix} + \begin{bmatrix} \mathbf{K}_{ss} & \mathbf{K}_{sf} & -(1-\phi)\mathbf{H}_{sF} \\ \mathbf{K}_{fs} & \mathbf{K}_{ff} & -\phi \mathbf{H}_{fF} \\ 0 & 0 & \mathbf{K}_F \end{bmatrix} \right) \begin{bmatrix} \mathbf{d}_s \\ \mathbf{d}_f \\ \bar{\mathbf{p}}_F \end{bmatrix} = \begin{bmatrix} \mathbf{f}_{ls} \\ \mathbf{f}_{lf} \\ \mathbf{f}_{Fq} \end{bmatrix} \tag{4.65}$$

4.6.3 Coupling with a flexible structure

If the boundary is in contact with a flexible structure the porous material can be either bounded or unbounded to the surface. If bounded, the structural partition of the porous material and the flexible structure have common degrees of freedom at the interface,

$$\mathbf{u}_s = \mathbf{u}_S \tag{4.66}$$

The displacements in the normal direction, $\mathbf{n}_P$, at the boundary is the same for the connecting flexible structure and the fluid partition

$$\mathbf{n}_P^T \mathbf{u}_S = \mathbf{n}_P^T \mathbf{u}_f \tag{4.67}$$

If unbounded, a thin layer of an acoustic fluid is placed between the flexible structure and the porous material. The procedure in Section 4.6.2 for the coupling with the acoustic fluid can be adopted.

4.7 $\mathbf{u}_s$-p_f – formulation

In Ref. [80], a mixed formulation using the structural displacements and the fluid pressure as the variables for describing the porous material using Biot's theory, is derived. The advantage is that only four degrees of freedom, three structural displacement components and one fluid pressure component, are needed in each node instead of, when using the displacement formulation for both partitions, six degrees of freedom. The derivation enables the equations of motion, (4.50) and (4.51), to expressed without using the fluid displacements. The total stresses, $\boldsymbol{\sigma}_t$, in the porous material can be written

$$\boldsymbol{\sigma}_t = \boldsymbol{\sigma}_s + \boldsymbol{\sigma}_f \tag{4.68}$$

where $\boldsymbol{\sigma}_s$ denotes the stresses in the frame and $\boldsymbol{\sigma}_f$ the stresses in the fluid, which is related to the fluid pressure by

$$\boldsymbol{\sigma}_f = -\phi p_f \mathbf{1} \tag{4.69}$$

where $\mathbf{1} = \begin{bmatrix} 1 & 1 & 1 & 0 & 0 & 0 \end{bmatrix}^T$. The stress-strain relationship in Biot's theory can be written

$$\boldsymbol{\sigma}_s = \mathbf{D}_s \boldsymbol{\varepsilon}_s + Q\mathrm{div}(\mathbf{u}_f)\mathbf{1} \tag{4.70}$$

$$\boldsymbol{\sigma}_f = -\phi p_f \mathbf{1} = Q\mathrm{div}(\mathbf{u}_s)\mathbf{1} + R\mathrm{div}(\mathbf{u}_f)\mathbf{1} \tag{4.71}$$

Introducing $\tilde{\boldsymbol{\sigma}}_s$, which contains the stresses in the frame depending on the frame displacements, the stresses in the frame can be written

$$\boldsymbol{\sigma}_s = \tilde{\boldsymbol{\sigma}}_s - \phi \frac{Q}{R} p_f \mathbf{1} \tag{4.72}$$

where

$$\tilde{\boldsymbol{\sigma}}_s = \mathbf{D}_s \boldsymbol{\varepsilon}_s - \frac{Q^2}{R}\mathrm{div}(\mathbf{u}_s)\mathbf{1} \tag{4.73}$$

The total stresses can thereby be expressed as

$$\boldsymbol{\sigma}_t = \tilde{\boldsymbol{\sigma}}_s - \phi \left(1 + \frac{Q}{R}\right) p_f \mathbf{1} \tag{4.74}$$

without using the fluid displacements. The equation of motion for the structural partition becomes

$$\tilde{\boldsymbol{\nabla}}^T \tilde{\boldsymbol{\sigma}}_s = -\omega^2 \tilde{\rho} \mathbf{u}_s - \tilde{\gamma} \boldsymbol{\nabla} p_f \tag{4.75}$$

where

$$\tilde{\boldsymbol{\sigma}}_s = \tilde{\mathbf{D}}_s \boldsymbol{\varepsilon}_s \tag{4.76}$$

with

$$\tilde{\mathbf{D}}_s = \begin{bmatrix} \left(P - \frac{Q^2}{R}\right) & \left(P - \frac{Q^2}{R}\right) - 2N & \left(P - \frac{Q^2}{R}\right) - 2N & 0 & 0 & 0 \\ \left(P - \frac{Q^2}{R}\right) - 2N & \left(P - \frac{Q^2}{R}\right) & \left(P - \frac{Q^2}{R}\right) - 2N & 0 & 0 & 0 \\ \left(P - \frac{Q^2}{R}\right) - 2N & \left(P - \frac{Q^2}{R}\right) - 2N & \left(P - \frac{Q^2}{R}\right) & 0 & 0 & 0 \\ 0 & 0 & 0 & N & 0 & 0 \\ 0 & 0 & 0 & 0 & N & 0 \\ 0 & 0 & 0 & 0 & 0 & N \end{bmatrix} \tag{4.77}$$

and

$$\tilde{\rho} = \tilde{\rho}_{11} - \frac{\tilde{\rho}_{12}^2}{\tilde{\rho}_{22}} \qquad \tilde{\gamma} = \phi\left(\frac{\tilde{\rho}_{12}}{\tilde{\rho}_{22}} - \frac{Q}{R}\right) \tag{4.78}$$

For the fluid partition, the equation of motion becomes

$$\boldsymbol{\nabla}^T \boldsymbol{\sigma}_f = -\phi \boldsymbol{\nabla} p_f = -\omega^2(\tilde{\rho}_{22}\mathbf{u}_f + \tilde{\rho}_{12}\mathbf{u}_s) \tag{4.79}$$

Taking the divergence of this equation and together with equation (4.71), the acoustic equation describing the fluid partition is achieved,

$$\frac{\phi^2}{\tilde{\rho}_{22}}\nabla^2 p_f = -\omega^2 \frac{\phi^2}{R} p_f + \omega^2 \tilde{\gamma} \mathrm{div}(\mathbf{u}_s) \tag{4.80}$$

The primary variable is the fluid pressure and the contribution from the structural partition is present in the last term.

4.7.1 Finite element formulation

The weak form is derived, multiplying with weight functions, $\mathbf{v}_s$ and v_f, integrating over a region Ω_{PF} and using the Green-Gauss theorem, for the structural partition

$$\begin{aligned} -\omega^2\tilde{\rho}\int_{\Omega_P} \mathbf{v}_s^T \mathbf{u}_s dV + \int_{\Omega_P} \tilde{\boldsymbol{\nabla}}(\mathbf{v}_s)^T \tilde{\boldsymbol{\sigma}}_s dV - \tilde{\gamma}\int_{\Omega_P} \mathbf{v}_s^T \boldsymbol{\nabla} p_f dV - \\ - \int_{\partial\Omega_P} \mathbf{v}_s^T \mathbf{S}^t \mathbf{n}_P dS - \int_{\partial\Omega_P} \mathbf{v}_s^T \phi\left(1 + \frac{Q}{R}\right) p_f \mathbf{I}\mathbf{n}_P dS = 0 \end{aligned} \tag{4.81}$$

where $\mathbf{I}$ is a identity tensor, $\mathbf{n}_P$ is the boundary normal vector directed outward from the porous material domain and the relation

$$\tilde{\mathbf{t}}_s = \tilde{\mathbf{S}}^s \mathbf{n}_P = \left(\mathbf{S}^t + \phi\left(1 + \frac{Q}{R}\right) p_f \mathbf{I}\right)\mathbf{n}_P \tag{4.82}$$

has been used. For the fluid partition

$$\begin{aligned} -\omega^2\frac{\phi^2}{R}\int_{\Omega_P} v_p p_f dV + \frac{\phi^2}{\tilde{\rho}_{22}}\int_{\Omega_P} \nabla v_p \nabla p dV - \omega^2\tilde{\gamma}\int_{\Omega_P} \nabla v_p \mathbf{u}_s dV - \\ - \frac{\phi^2}{\tilde{\rho}_{22}}\int_{\partial\Omega_P} v_p \mathbf{n}_P^T \nabla p_f dS + \omega^2\tilde{\gamma}\int_{\partial\Omega_P} v_p \mathbf{n}_P^T \mathbf{u}_s dS = 0 \end{aligned} \tag{4.83}$$

The finite element approximation of the structural displacement, $\mathbf{u}_s$ and fluid pressure p_f, and the weight functions, $\mathbf{v}_s$ and v_p, are

$$\begin{aligned} \mathbf{u}_s &= \mathbf{N}_s \mathbf{d}_s; \quad p_f = \mathbf{N}_p \mathbf{p}_f \\ \mathbf{v}_s &= \mathbf{N}_s \mathbf{c}_s; \quad v_p = \mathbf{N}_p \mathbf{c}_p \end{aligned} \tag{4.84}$$

where $\mathbf{d}_s$ and $\mathbf{p}_f$ are the nodal displacement and pressure, respectively, and the $\mathbf{c}_s$ and $\mathbf{c}_p$ the corresponding nodal weights. Using that $\mathbf{c}_s$ and $\mathbf{c}_f$ are arbitrary, introducing the stress strain relation in equation (4.76) and with

$$\boldsymbol{\varepsilon}_s = \tilde{\boldsymbol{\nabla}} \mathbf{N}_s \mathbf{d}_s \tag{4.85}$$

the finite element formulation becomes; for the structural partition

$$-\omega^2\tilde{\rho}\int_{\Omega_P}\mathbf{N}_s^T\mathbf{N}_s dV\mathbf{d}_s+\int_{\Omega_P}(\tilde{\boldsymbol{\nabla}}\mathbf{N}_s)^T\tilde{\mathbf{D}}_s\tilde{\boldsymbol{\nabla}}\mathbf{N}_s dV\mathbf{d}_s-\tilde{\gamma}\int_{\Omega_P}\mathbf{N}_s^T\nabla\mathbf{N}_p dV\mathbf{p}_f- \\ -\int_{\partial\Omega_P}\mathbf{N}_s^T\mathbf{S}^t\mathbf{n}_P dS-\phi\left(1+\frac{Q}{R}\right)\int_{\partial\Omega_P}\mathbf{N}_s^T\mathbf{n}_P p_f dS=0 \tag{4.86}$$

and for the fluid partition

$$-\omega^2\frac{\phi^2}{R}\int_{\Omega_P}\mathbf{N}_p^T\mathbf{N}_p dV\mathbf{p}_f+\frac{\phi^2}{\tilde{\rho}_{22}}\int_{\Omega_P}(\nabla\mathbf{N}_p)^T\nabla\mathbf{N}_p dV\mathbf{p}_f-\omega^2\tilde{\gamma}\int_{\Omega_P}(\nabla\mathbf{N}_p)^T\mathbf{N}_s dV\mathbf{d}_s- \\ -\frac{\phi^2}{\tilde{\rho}_{22}}\int_{\partial\Omega_P}\mathbf{N}_p^T\mathbf{n}_P^T\nabla p_f dS+\omega^2\tilde{\gamma}\int_{\partial\Omega_P}\mathbf{N}_p^T\mathbf{n}_P^T\mathbf{N}_s dS\mathbf{d}_s=0 \tag{4.87}$$

The finite element system of equations can be written

$$\begin{bmatrix}-\omega^2\mathbf{M}_{ss}+\mathbf{K}_{ss} & -\mathbf{C}_{sp}\\ -\omega^2\mathbf{C}_{sp}^T & -\omega^2\mathbf{M}_{pp}+\mathbf{K}_{pp}\end{bmatrix}\begin{bmatrix}\mathbf{d}_s\\ \mathbf{p}_f\end{bmatrix}=\begin{bmatrix}\mathbf{f}_{bs}\\ \mathbf{f}_{bp}\end{bmatrix} \tag{4.88}$$

where the system matrices for the structural and fluid partition are

$$\begin{aligned}\mathbf{M}_{ss}&=\tilde{\rho}\int_{\Omega_P}\mathbf{N}_s^T\mathbf{N}_s dV & \mathbf{K}_{ss}&=\int_{\Omega_P}\tilde{\boldsymbol{\nabla}}\mathbf{N}_s^T\tilde{\mathbf{D}}_s\tilde{\boldsymbol{\nabla}}\mathbf{N}_s dV\\ \mathbf{M}_{pp}&=\frac{\phi^2}{R}\int_{\Omega_P}\mathbf{N}_p^T\mathbf{N}_p dV & \mathbf{K}_{pp}&=\frac{\phi^2}{\tilde{\rho}_{22}}\int_{\Omega_P}(\nabla\mathbf{N}_p)^T\nabla\mathbf{N}_p dV\end{aligned} \tag{4.89}$$

The coupling matrix is

$$\mathbf{C}_{sp}=\tilde{\gamma}\int_{\Omega_{PF}}\mathbf{N}_s^T\nabla\mathbf{N}_p dV \tag{4.90}$$

The boundary term of the structural partition can be written

$$\mathbf{f}_{bs}=\int_{\partial\Omega_P}\mathbf{N}_s^T\mathbf{S}^t\mathbf{n}_P dS+\phi\left(1+\frac{Q}{R}\right)\int_{\partial\Omega_P}\mathbf{N}_s^T\mathbf{n}_P p_f dS \tag{4.91}$$

and for the boundary term of the fluid partition, the relation in equation (4.79) is used in order to apply the appropriate boundary conditions

$$\begin{aligned}\mathbf{f}_{bp}&=\frac{\phi^2}{\tilde{\rho}_{22}}\int_{\partial\Omega_P}\mathbf{N}_p^T\mathbf{n}_P^T\nabla p_f dS-\omega^2\tilde{\gamma}\int_{\partial\Omega_P}\mathbf{N}_p^T\mathbf{n}_P^T\mathbf{u}_s dS=\\ &=\frac{\phi^2}{\tilde{\rho}_{22}}\int_{\partial\Omega_P}\mathbf{N}_p^T\mathbf{n}_P^T\frac{\omega^2}{\phi}(\tilde{\rho}_{12}\mathbf{u}_s+\tilde{\rho}_{22}\mathbf{u}_f)dS-\omega^2\tilde{\gamma}\int_{\partial\Omega_P}\mathbf{N}_p^T\mathbf{n}_P^T\mathbf{u}_s dS=\\ &=\omega^2\int_{\partial\Omega_P}\mathbf{N}_p^T\mathbf{n}_P^T\phi\left(\mathbf{u}_f-\mathbf{u}_s\right)dS+\omega^2\int_{\partial\Omega_P}\mathbf{N}_p^T\mathbf{n}_P^T\phi\left(1+\frac{Q}{R}\right)\mathbf{u}_s dS\end{aligned} \tag{4.92}$$

4.7.2 Boundary conditions

A thorough investigation of the boundary conditions when using the $\langle\mathbf{u}_s,p_f\rangle$-formulation for describing the sound propagation in porous material was given by Debergue et al. [83]. The following boundary conditions can arise ($\mathbf{n}_P$ is a normal vector at the boundary directed outward from the porous material domain), :

1. The boundary in contact with an acoustic fluid with the pressure p_F and displacement $\mathbf{u}_F$ at the boundary. Only the following condition must be satisfied

$$p_F = p_f \tag{4.93}$$

This condition is fulfilled in the assembling process using the same degrees of freedom for the acoustic fluid domain and the fluid partition of the porous material domain at the connecting boundary.

2. The boundary in contact with a flexible structure

$$\begin{aligned} \mathbf{u}_s &= \mathbf{u}_S \\ \mathbf{n}_P^T \mathbf{u}_f &= \mathbf{n}_P^T \mathbf{u}_s = \mathbf{n}_P^T \mathbf{u}_S \end{aligned} \tag{4.94}$$

The continuity in displacements between the flexible structure and the structural partition of the porous material is accounted for in the assembling. The condition in normal displacement of the fluid partition is imposed in the second term of the last step in equation (4.92).

$$\mathbf{f}_{bp} = \omega^2 \int_{\partial\Omega_{SP}} \mathbf{N}_p^T \mathbf{n}^T \mathbf{N}_S^T dS \mathbf{u}_S = \mathbf{H}_{Sp}^T \mathbf{u}_S \tag{4.95}$$

This is the usual structure-acoustic coupling condition.

4.8 Finite element analysis including porous materials

The implemented finite elements describing the sound propagation of porous materials are employed in the investigation of a number of numerical examples. The porous material is described using the equivalent fluid models and Biot's theory. For Biot's theory, both the $\langle \mathbf{u}_s, \mathbf{u}_f \rangle$- and the $\langle \mathbf{u}_s, p_f \rangle$-formulation, are evaluated. A number of one-dimensional problems are studied to verify the implemented elements with the analytical solutions. Two three-dimensional problems, being the sound transmission loss of a double wall lined with porous material and an enclosed cavity with one wall covered with porous material, are also investigated. These problems include a discussion of which description to be adopted in the modelling of the porous material.

4.8.1 Implementation of finite elements

The porous material finite elements are implemented as extensions to the Matlab [66] finite element toolbox CALFEM [67]. An eight node isoparametric solid element is used. The equivalent fluid models use the pressure formulation giving one degree of freedom in each node. The displacement formulation of Biot's theory have six degrees of freedom in each node, see Figure 4.1. The mixed displacement-pressure formulation gives four degrees of freedom in each node.

4.8.2 One-dimensional sound propagation

A porous material layer, with thickness $L = 0.1$ m and placed between $x = -L$ and $x = 0$, is studied. Four one-dimensional problems, displayed in Figure 4.2, are investigated,

exciting both the two compressional waves and the shear wave. Problems 1–3 were studied by Dauchez et al. [79], comparing finite element results with the analytical solutions. In all problems, 8 elements are used in the x direction. The results using the implemented elements are compared with the analytical solutions.

The one-dimensional sound propagation in porous materials modelled by Biot's theory can be described by two compressional waves and one shear wave [71]. The compressional waves, which are uncoupled to the shear wave, can propagate in the porous material having the wave numbers

$$k_1 = \sqrt{\frac{\omega^2\left(P\tilde{\rho}_{22} + R\tilde{\rho}_{11} - 2Q\tilde{\rho}_{12} - \sqrt{\Delta}\right)}{2PR - 2Q^2}} \tag{4.96}$$

and

$$k_2 = \sqrt{\frac{\omega^2\left(P\tilde{\rho}_{22} + R\tilde{\rho}_{11} - 2Q\tilde{\rho}_{12} + \sqrt{\Delta}\right)}{2PR - 2Q^2}} \tag{4.97}$$

where

$$\Delta = \left(P\tilde{\rho}_{22} + R\tilde{\rho}_{11} - 2Q\tilde{\rho}_{12}\right)^2 - 4\left(PR - Q^2\right)\left(\tilde{\rho}_{11}\tilde{\rho}_{22} - \tilde{\rho}_{12}^2\right) \tag{4.98}$$

The two compressional waves can propagate in positive or negative x direction, denoted by the superscripts + and −, and the motion in the structural partition can be written

$$u_s(x) = u_{s1}^{+}(0)\mathrm{e}^{-\mathrm{i}k_1 x} + u_{s1}^{-}(0)\mathrm{e}^{\mathrm{i}k_1 x} + u_{s2}^{+}(0)\mathrm{e}^{-\mathrm{i}k_2 x} + u_{s2}^{-}(0)\mathrm{e}^{\mathrm{i}k_2 x} \tag{4.99}$$

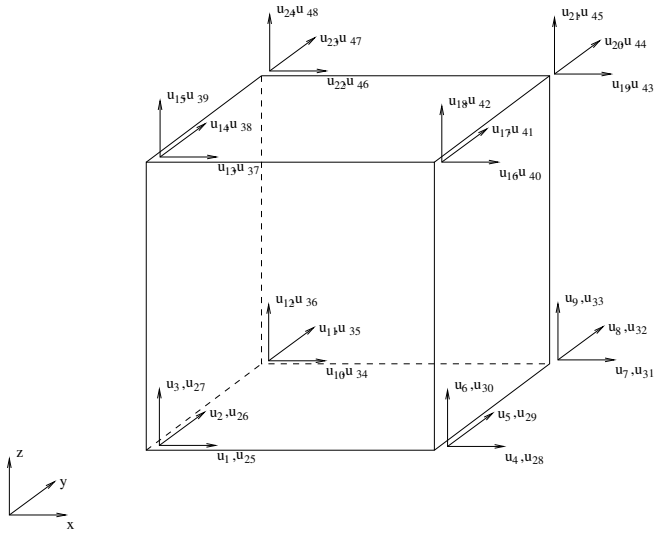

Figure 4.1: *Displacement formulated element describing Biot's theory. Six degrees of freedom are present at each node. Degree 1 to 24 contains the structural displacements and 25 to 48 the fluid displacements.*

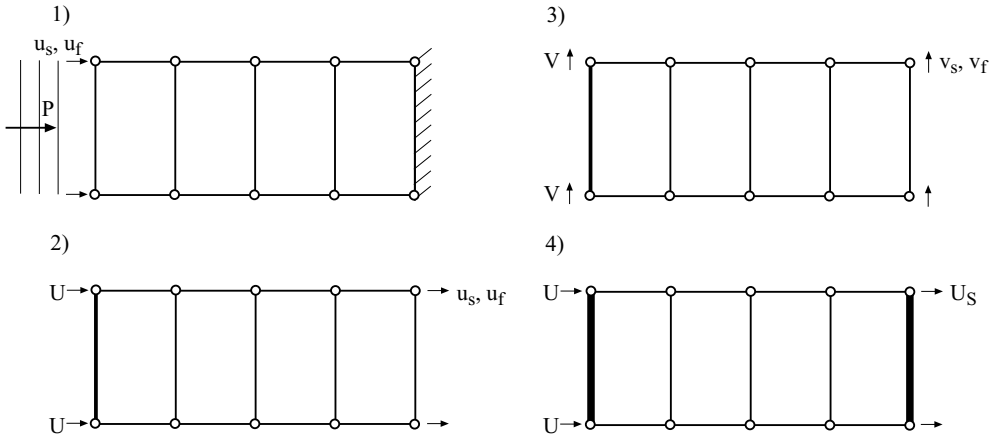

Figure 4.2: *The four one-dimensional problems for which the results using the implemented finite elements are compared with the analytical solutions, 1) normal impedance, 2) prescribed normal displacement, 3) prescribed shear displacement, 4) double wall.*

and for the fluid partition

$$\begin{aligned} u_f(x) &= u_{f1}^+(0)\mathrm{e}^{-\mathrm{i}k_1 x} + u_{f1}^-(0)\mathrm{e}^{\mathrm{i}k_1 x} + u_{f2}^+(0)\mathrm{e}^{-\mathrm{i}k_2 x} + u_{f2}^-(0)\mathrm{e}^{\mathrm{i}k_2 x} = \\ &= \mu_1 u_{s1}^+\mathrm{e}^{-\mathrm{i}k_1 x} + \mu_1 u_{s1}^-\mathrm{e}^{\mathrm{i}k_1 x} + \mu_2 u_{s2}^+\mathrm{e}^{-\mathrm{i}k_2 x} + \mu_2 u_{s2}^-\mathrm{e}^{\mathrm{i}k_2 x} \end{aligned} \tag{4.100}$$

where the ratios between the displacements in the structural partition and fluid partition, μ_1 and μ_2, are given by

$$\mu_1 = \frac{u_{f1}^+(0)}{u_{s1}^+(0)} = \frac{Pk_1^2 - \omega^2\tilde{\rho}_{11}}{\omega^2\tilde{\rho}_{12} - Qk_1^2}; \qquad \mu_2 = \frac{u_{f2}^+(0)}{u_{s2}^+(0)} = \frac{Pk_2^2 - \omega^2\tilde{\rho}_{11}}{\omega^2\tilde{\rho}_{12} - Qk_2^2} \tag{4.101}$$

Also, the shear wave can propagate with the wave number

$$k_3 = \sqrt{\frac{\omega^2(\tilde{\rho}_{11}\tilde{\rho}_{22} - \tilde{\rho}_{12}^2)}{G_0\tilde{\rho}_{22}}} \tag{4.102}$$

The shear wave can be written

$$v_s(x) = v_{s1}^+(0)\mathrm{e}^{-\mathrm{i}k_3 x} + v_{s1}^-(0)\mathrm{e}^{\mathrm{i}k_3 x} \tag{4.103}$$

$$v_f(x) = v_{f1}^+(0)\mathrm{e}^{-\mathrm{i}k_3 x} + v_{f1}^-(0)\mathrm{e}^{\mathrm{i}k_3 x} = \mu_3 v_{s1}^+(0)\mathrm{e}^{-\mathrm{i}k_3 x} + \mu_3 v_{s1}^-(0)\mathrm{e}^{\mathrm{i}k_3 x} \tag{4.104}$$

where the ratios between the displacement in the structural partition and fluid partition

$$\mu_3 = \frac{v_{f1}^+(0)}{v_{s1}^+(0)} = -\frac{\tilde{\rho}_{12}}{\tilde{\rho}_{22}} \tag{4.105}$$

The four one-dimensional problems displayed in Figure 4.2 are studied. The materials used are described in Table 4.2.

1) Normal impedance

The porous material is excited by an unit pressure at $x = -L$ and the end at $x = 0$ is fixed. The velocity level at $x = -L$ is calculated and the normal impedance can be determined. The governing boundary conditions are

$$\begin{aligned} u_s(0) &= 0 \\ u_f(0) &= 0 \\ P\frac{\partial u_s(-L)}{\partial x} + Q\frac{\partial u_f(-L)}{\partial x} &= (1-\phi)p \\ Q\frac{\partial u_s(-L)}{\partial x} + R\frac{\partial u_f(-L)}{\partial x} &= \phi p \end{aligned} \tag{4.106}$$

and the solution becomes

$$u_s(-L) = -2\mathrm{i}\left(u_{s1}^+(0)\sin(-k_1L) + u_{s2}^+(0)\sin(-k_2L)\right) \tag{4.107}$$

$$u_f(-L) = -2\mathrm{i}\left(\mu_1 u_{s1}^+(0)\sin(-k_1L) + \mu_2 u_{s2}^+(0)\sin(-k_2L)\right) \tag{4.108}$$

where

$$u_{s1}^+(0) = \frac{1}{2}\frac{\mathrm{i}p\left(P\phi + Q\mu_2\phi - Q - R\mu_2 + \phi Q + \phi R\mu_2\right)}{\cos(k_1L)\,k_1\left(-PR\mu_1 - Q^2\mu_2 + PR\mu_2 + Q^2\mu_1\right)} \tag{4.109}$$

$$u_{s2}^+(0) = -\frac{1}{2}\frac{\mathrm{i}p\left(R\mu_1\phi - R\mu_1 + P\phi - Q + \mu_1\phi Q + \phi Q\right)}{k_2\cos(k_2L)\left(-PR\mu_1 - Q^2\mu_2 + PR\mu_2 + Q^2\mu_1\right)} \tag{4.110}$$

The impedance, Z, can be determined as

$$Z = \frac{1}{\mathrm{i}\omega\left(\phi u_f(-L) + (1-\phi)u_s(-L)\right)} \tag{4.111}$$

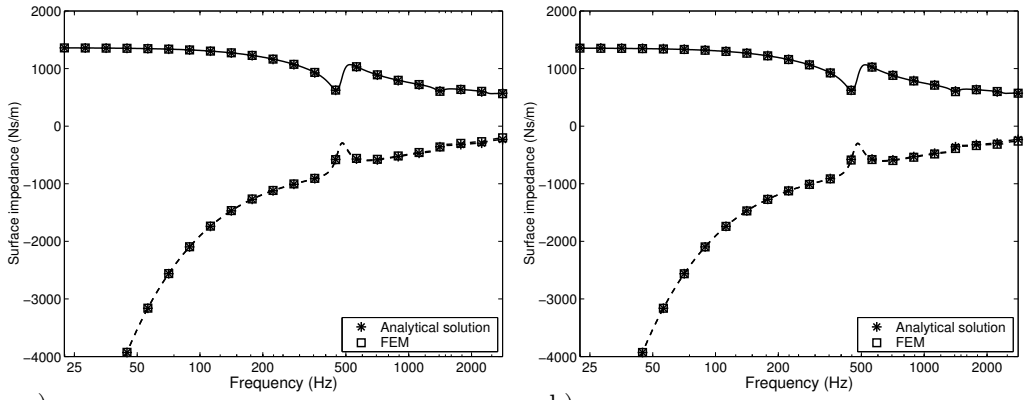

Figure 4.3: *Normal impedance for Material 2 using, a) the* $\langle \mathbf{u}_s, \mathbf{u}_f \rangle$*- and b) the* $\langle \mathbf{u}_s, p_f \rangle$*-formulation formulation. The solid lines displays the real part, and the dotted line the imaginary part, of the normal impedance.*

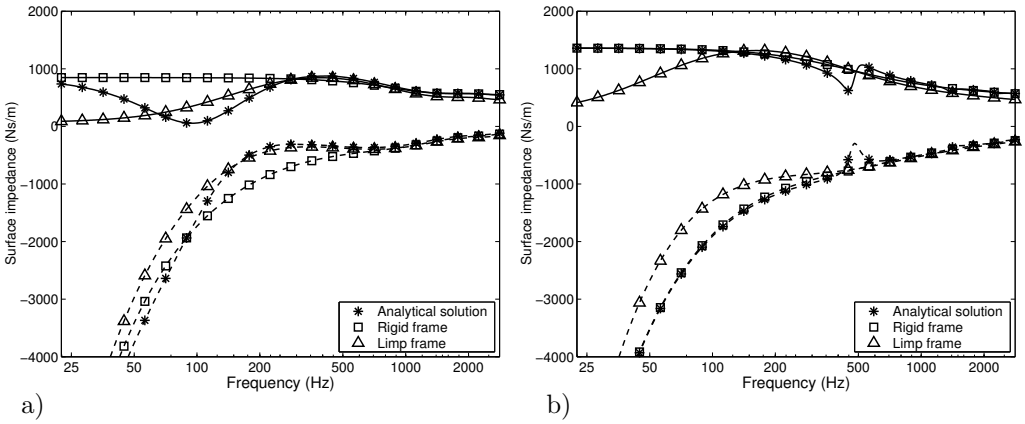

Figure 4.4: *Normal impedance when using the equivalent fluid models, a) Material 1 and b) Material 2. The solid lines displays the real part, and the dotted line the imaginary part, of the normal impedance.*

The real and imaginary parts of the impedance are displayed comparing the analytical and the finite element solutions using both the $\langle \mathbf{u}_s, \mathbf{u}_f \rangle$-formulation, in Figure 4.3 a), and the $\langle \mathbf{u}_s, p_f \rangle$-formulation, in Figure 4.3 b). The solutions are practically identical.

In Figure 4.4, the normal impedance is determined using the equivalent fluid models. The limp assumption provides a better description of Material 1, which has a low structural stiffness, and the rigid assumption for Material 2, which have a high structural stiffness. Resonances in the frame material can not be described by the equivalent fluid models.

2) Prescribed normal displacement

A prescribed normal displacement, U, excites the porous material at $x = -L$ and the end at $x = 0$ is free. The velocity level at $x = 0$ is determined. Boundary conditions:

$$\begin{aligned} u_s(-L) &= U \\ u_f(-L) &= U \\ \frac{\partial u_s(0)}{\partial x} &= 0 \\ \frac{\partial u_f(0)}{\partial x} &= 0 \end{aligned} \tag{4.112}$$

The solution becomes:

$$u_s(0) = \frac{U\,(\mu_2 - 1)}{\cos(k_1\,L)\,(\mu_2 - \mu_1)} - \frac{(\mu_1 - 1)\,U}{\cos(k_2\,L)\,(\mu_2 - \mu_1)} \tag{4.113}$$

and

$$u_f(0) = \frac{\mu_1\,U\,(\mu_2 - 1)}{\cos(k_1\,L)\,(\mu_2 - \mu_1)} - \frac{\mu_2\,(\mu_1 - 1)\,U}{\cos(k_2\,L)\,(\mu_2 - \mu_1)} \tag{4.114}$$

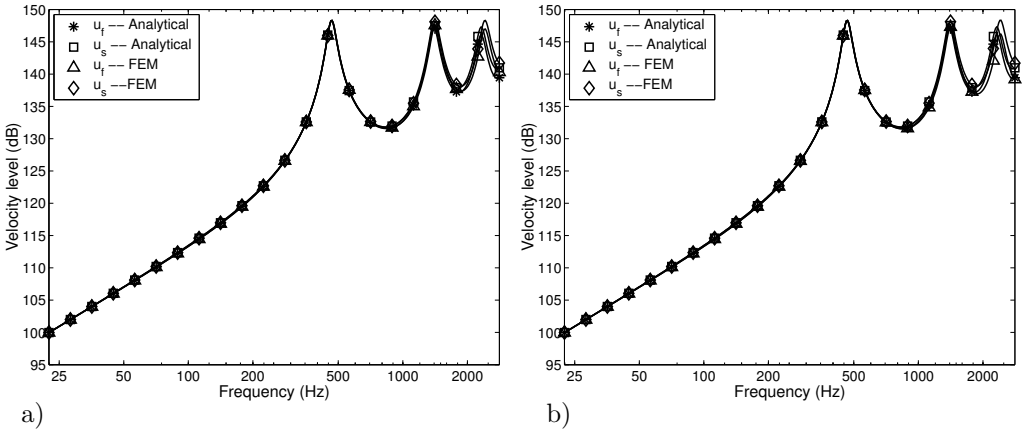

Figure 4.5: *Normal displacement for material 2 using, a) the* $\langle \mathbf{u}_s, \mathbf{u}_f \rangle$*- and b) the* $\langle \mathbf{u}_s, p_f \rangle$*-formulation.*

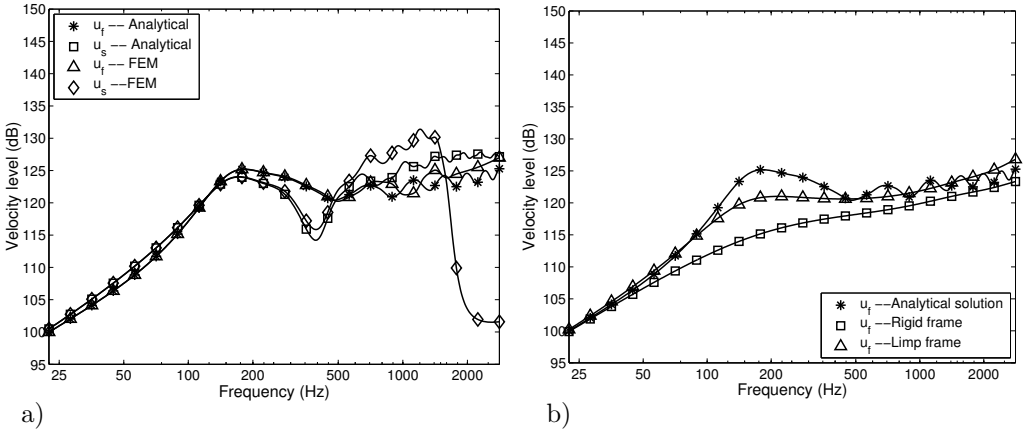

Figure 4.6: *Normal displacement for material 1 using, a) the* $\langle \mathbf{u}_s, \mathbf{u}_f \rangle$*-formulation and b) equivalent fluid models.*

The normal velocity level calculated using the implemented elements – based on both $\langle \mathbf{u}_s, \mathbf{u}_f \rangle$- and $\langle \mathbf{u}_s, p_f \rangle$-formulation of Biot's theory – and the corresponding analytical solution are displayed in Figure 4.5. The results agree well with the analytical solution when Material 2, with a stiff structural frame, is used. In Figure 4.6, Material 1 is studied using both Biot's theory and equivalent fluid models. The resonances in the structural frame can not be captured in the equivalent fluid models. Also, as can be seen in Figure4.6 a), the weak frame leads to a large number of resonances in the frequency range studied. More elements are therefore needed in the x direction, in order to describe the structural behaviour when employing Biot's theory.

3) Prescribed shear displacement

A prescribed transverse displacement, V, excites the porous material at $x = -L$ and the end at $x = 0$ is free. The velocity level at the free end is determined. Boundary conditions:

$$\begin{aligned} v_s(-L) &= V \\ \frac{\partial v_s(0)}{\partial x} &= 0 \end{aligned} \tag{4.115}$$

The solution becomes:

$$v_s(0) = \frac{V}{\cos\left(k_3\, L\right)} \tag{4.116}$$

$$v_f(0) = \frac{\mu_3\, V}{\cos\left(k_3\, L\right)} \tag{4.117}$$

The shear velocity level calculated using the implemented elements based on Biot's theory and the corresponding analytical solution are displayed in Figure 4.7. Both $\langle \mathbf{u}_s, \mathbf{u}_f \rangle$- and $\langle \mathbf{u}_s, p_f \rangle$-formulation are used and the results agree well with the analytical solution. No shear stresses are present in the equivalent fluid models, only the elements based on Biot's theory are studied.

4) One dimensional double wall

An aluminium panel, with the thickness 2 mm, is bounded to each side of the porous material and, at $x = -L$ the plate is excited with a prescribed normal displacement, U, and the end at $x = 0$ is free. The velocity level difference of the plate at $x = 0$, and at

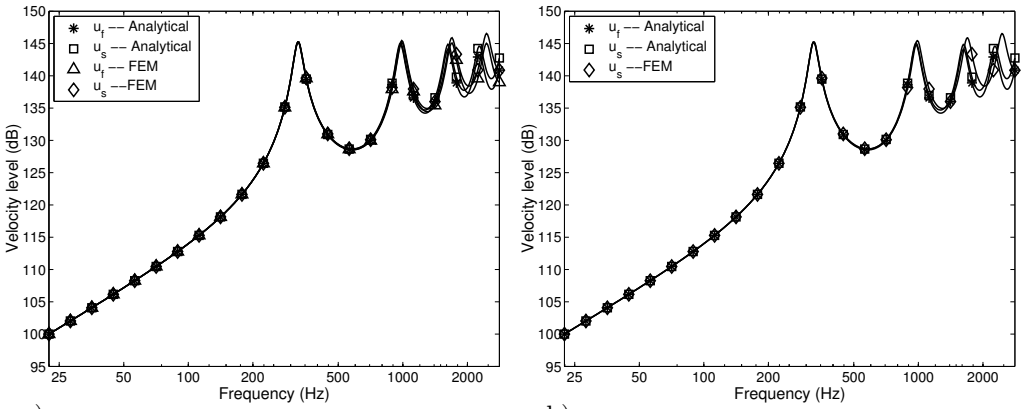

Figure 4.7: *Shear displacement for material 2 using, a) the* $\langle \mathbf{u}_s, \mathbf{u}_f \rangle$*- and b) the* $\langle \mathbf{u}_s, p_f \rangle$*-formulation.*

$x = -L$ is determined. Boundary conditions:

$$\begin{aligned} u_s(-L) &= U \\ u_f(-L) &= U \end{aligned} \tag{4.118}$$

The equation of motion of the sheet at $x = 0$ is also needed,

$$-\omega^2 m_S u_S = p(0) \tag{4.119}$$

where m_S is the sheet mass (kg/m^2) and $p(0)$ the pressure acting on the sheet from the porous structural and fluid domain, which is given by

$$p(0) = -\left(P\frac{\partial u_s(0)}{\partial x} + Q\frac{\partial u_f(0)}{\partial x} + Q\frac{\partial u_s(0)}{\partial x} + R\frac{\partial u_f(0)}{\partial x} \right) \tag{4.120}$$

There are five unknowns and five equations to solve and the velocity can be determined. The velocity level difference calculated using the implemented elements based on Biot's theory and the analytical solution is displayed in Figure 4.8. Three configurations including the different materials in Table 4.2 are investigated. The velocity level difference is accurately calculated using the implemented elements.

The equivalent fluid models are evaluated in Figure 4.9. The rigid and limp frame assumption is compared with Biot's theory. The case where the porous material is described by Biot's theory and the material is unbounded to the panels is also evaluated. If the porous material is bounded to the panels, the full Biot's description must be employed. When the porous material is unbounded, the equivalent fluid models gives results similar to using Biot's theory.

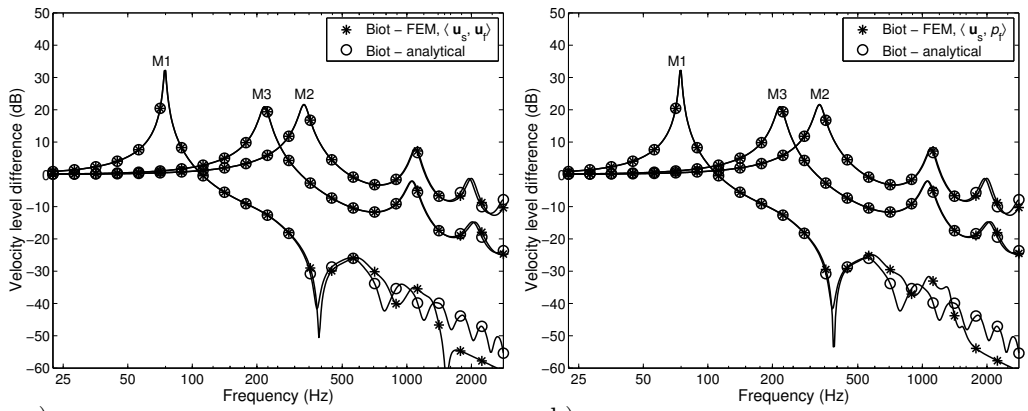

a) b)

Figure 4.8: *Velocity level difference using the implemented finite elements compared to the analytical solution, for the three different materials, using a) the* $\langle \mathbf{u}_s, \mathbf{u}_f \rangle$*- and b) the* $\langle \mathbf{u}_s, p_f \rangle$*-formulation.*

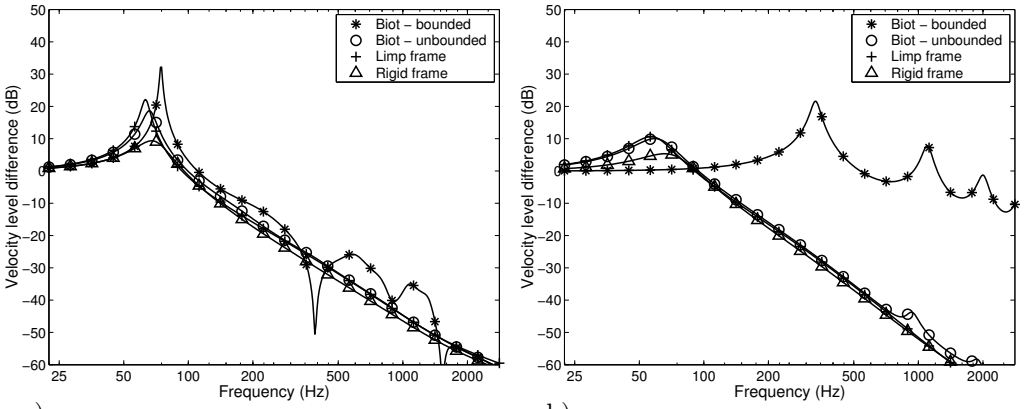

Figure 4.9: *Velocity level difference using different descriptions of the porous sound absorbing material, a) Material 1 b) Material 2.*

4.8.3 Sound transmission loss of a double wall

The sound transmission loss in a double wall lined with porous sound absorbing material, adopting the procedure described in Paper 7, is evaluated. The double wall is considered to be an ideal double wall, i.e. only the structural and fluid partitions of the porous material provides the coupling between the panels. The wall is 0.5 m long and 0.3 m high and with the distance 0.1 m between the panels. The panels are 2 mm thick and made of aluminium. The porous material is described by Biot's theory or an equivalent fluid model using either a rigid frame or limp frame assumption. The porous material is bounded to the panels and two different materials are studied: Material 1, with relatively low structural stiffness, and Material 2, with a relatively high structural stiffness, see Table 4.2. A study of the sound transmission loss of a multilayered structure including porous material was studied by Panneton et. al. [84], which can be seen as the basis of the study presented here. In [84], the panels were described by plate theory, not including the longitudinal stiffness of the panels in the model. This stiffness is included here, modelling the panels using 4-node shell elements, which are derived by combing a quadrilateral plate element [85] and a membrane element with drilling degrees of freedom [86].

The sound transmission loss of the ideal double wall, when the porous material is bounded to the panels, is displayed in Figure 4.10. Even for the low stiffness of the frame material (Material 1), when the static stiffness of the wall is not affected, it is important to include the structural partition of the porous material when determining the sound transmission loss. The equivalent fluid models can not describe the behaviour of the system.

In Figure 4.11 the ideal double wall is studied for the case of the porous material being modelled by Biot's theory and assumed to be bounded or unbounded to the panels and also using the limp equivalent fluid model. It can be seen that if the porous material is not bounded to the panels, the equivalent fluid model gives reasonable agreement with the full Biot's description.

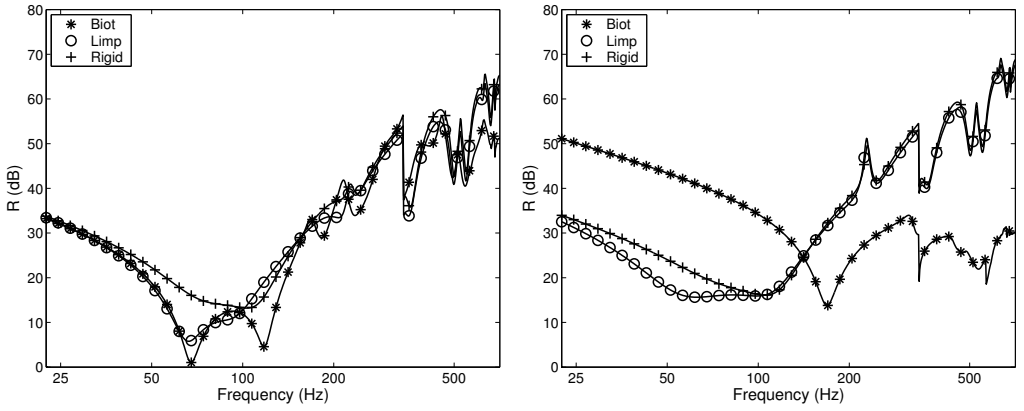

Figure 4.10: *Sound transmission loss of an ideal double wall lined with porous material. a) Material 1, b) Material 2.*

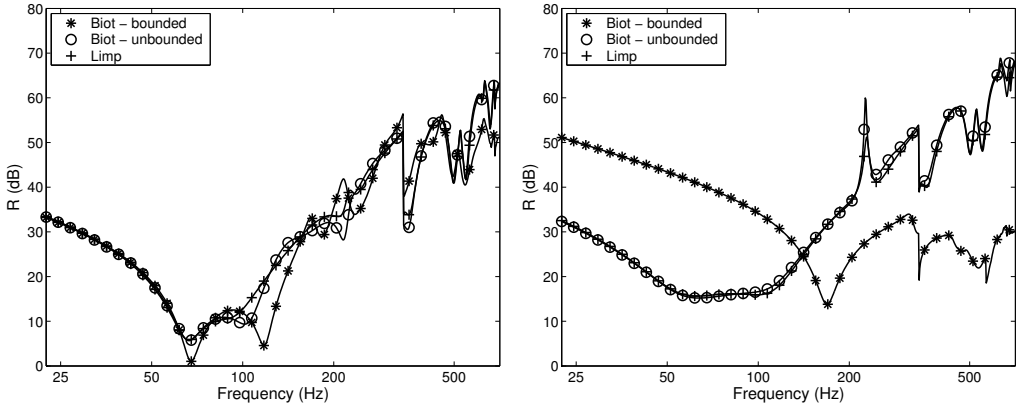

Figure 4.11: *Sound transmission loss of an ideal double wall lined with porous material, which is either bounded or unbounded to the panels, a) Material 1, b) Material 2.*

4.8.4 Enclosed cavity

An enclosed cavity with one wall covered with porous absorbing material is studied, see Figure 4.12. This problem was studied Kang et. al. [78]. The cavity is 0.6 m long and 0.4 m wide and 0.75 in depth. The porous material domain is 0.05 m wide. The cavity is excited by a volume velocity source placed in a corner and the mean sound pressure level is evaluated. Three different formulations for the porous material is used. It is described by Biot's theory or by an equivalent fluid model using either a rigid frame or limp frame assumption. The sound pressure level calculated for Material 1 and 2, using the tree

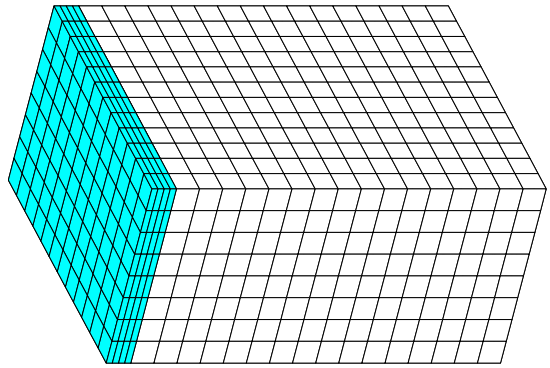

Figure 4.12: *The enclosed cavity with one wall covered with porous material.*

different formulations, is displayed in Figure 4.13. The different material descriptions gives similar results. However, at the first cavity resonance peak for, the response level predicted when Material 1 is modelled by Biot's theory is much higher, compared for the equivalent fluid models. A possible explanation of this behaviour can be achieved by comparing the with the normal impedance displayed in Figures 4.3 and 4.4. For Material 1, the real part of the normal impedance has a low value at the first response peak. Note that the material thickness is 0.1 m for the normal impedance calculations, whereas the thickness is 0.05 m in the analysis presented in this section. The low real-valued impedance is due to a structural resonance in the frame material partition which results in that the fluid and structural partitions moves in phase with each other. The damping provided due to the flow resistivity, which is proportional to the velocity difference of the two partitions, is therefor low. This resonance can not be described by the equivalent

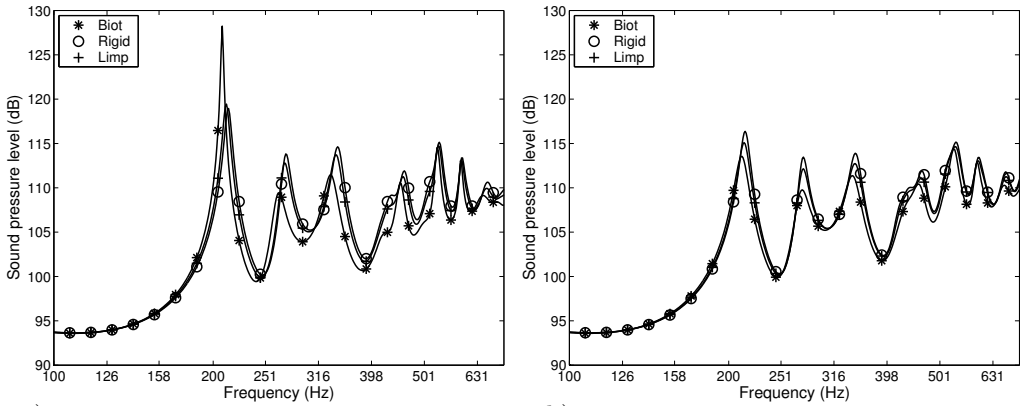

Figure 4.13: *Calculated mean sound pressure level using different formulations for the porous material, a) Material 1, b) Material 2.*

fluid models. For Material 2, with a stiffer frame material, this resonance occurs at a higher frequency and the equivalent fluid models can capture the behaviour of the porous material.

4.9 Summary

The modelling of porous materials within the finite element framework was investigated. The governing equations and the finite element formulation of these equations were described. Different material descriptions was implemented and compared to analytical solutions for a number of one-dimensional problems. Two three-dimensional problems were also investigated to evaluate which porous material model to be used. The porous material descriptions are employed in the included papers.

Bibliography

[1] J. Brunskog. Acoustic excitation and transmission of lightweight structures. TVBA 1009, Engineering Acoustics, LTH, Lund University, Box 118, SE-221 00 Lund, Sweden, 2002.

[2] M. Gustavsson. Methods for aircraft noise and vibration analysis. TVSM 3035, Structural Mechanics, LTH, Lund University, Box 118, SE-221 00 Lund, Sweden, 1998.

[3] G. Sandberg. Finite element modelling of fluid-structure interaction. TVSM 1002, Structural Mechanics, LTH, Lund University, Box 118, SE-221 00 Lund, Sweden, 1986.

[4] H. Carlsson. Finite element analysis of structure-acoustic systems; formulations and solution strategies. TVSM 1005, Structural Mechanics, LTH, Lund University, Box 118, SE-221 00 Lund, Sweden, 1992.

[5] P.-A. Hansson. Finite element analysis of fluid-structure systems; element formulations and decompostion strategies. TVSM 3028, Structural Mechanics, LTH, Lund University, Box 118, SE-221 00 Lund, Sweden, 1999.

[6] MSC/NASTRAN - V2001. The MacNeal-Schwendler Corporation, 2001.

[7] L. Cremer, M. Heckl, and E. Ungar. *Structure-Borne Sound*. Springer-Verlag, Berlin, 1988.

[8] F. Fahy. *Sound and structural vibration*. Academic Press, London, 1985.

[9] A. J. Pretlove. Free vibrations of a rectangular panel backed by a closed rectangular cavity. *Journal of Sound and Vibration*, 2(3):197–209, 1965.

[10] A. J. Pretlove. Forced vibrations of a rectangular panel backed by a closed rectangular cavity. *Journal of Sound and Vibration.*, 3(3):252–261, 1966.

[11] R. W. Guy. The response of a cavity backed panel to external airborne excitation: A general analysis. *The Journal of the Acoustical Society of America*, 65(3):719–731, 1979.

[12] E. H. Dowell, G. F. Gorman, and D. A. Smith. Acoustoelasticity: General theory, acoustic natural modes and forced response to sinusodal excitation, including comparasons with experiments. *Journal of Sound and Vibration*, 52(4):519–542, 1977.

[13] J. Pan and D. A. Bies. The effect of fluid-structural coupling on sound waves in an enclosure–theoretical part. *The Journal of the Acoustical Society of America*, 87(2):691–707, 1990.

[14] Hong K. L. and Kim J. Analysis of free vibration of structural-acoustic coupled systems, part i: Development and verification of the procedure. *Journal of Sound and Vibration.*, 188(4):561–575, 1995.

[15] Hong K. L. and Kim J. Analysis of free vibration of structural-acoustic coupled systems, part ii: Two- and three-dimensional examples. *Journal of Sound and Vibration.*, 188(4):577–600, 1995.

[16] Atalla N. and Bernhard R. J. Review of numerical solutions for low-frequency structural-acoustic problems. *Applied Acoustics*, 43(2):271–294, 1994.

[17] D. J. Nefske, J. A. Wolf, and L. J. Howell. Structural-acoustic finite element analysis of the automobile compartment: A review of current practice. *Journal of Sound and Vibration*, 80(2):247–266, 1982.

[18] N. Ottosen and H. Peterson. *Introduction to the Finite Element Method*. Prentice Hall, New York, 1992.

[19] K.-J. Bathe. *Finite Element Procedures*. Prentice Hall, New York, 1996.

[20] O. C. Zienkiewicz and R. L.Taylor. *The Finite Element Method*, volume 1 and 2. MacGraw-Hill, London, 1994.

[21] R. Clough and J. Penzien. *Dynamics of Structures*. McGraw-Hill, London, 1993.

[22] A. Chopra. *Dynamics of Structures*. Prentice Hall, New York, 2001.

[23] H. Morand and R. Ohayon. *Fluid structure interaction*. John Wiley & sons, Chichester, 1995.

[24] Everstine G. C. Finite element formulations of structural acoustics problems. *Computers & Structures*, 65(2):307–321, 1997.

[25] N. Akkas, H. U. Akay, and C. Yilmaz. Applicability of general-purpose finite element programs in solid-fluid interaction problems. *Computers & Structures*, 10:773–783, 1979.

[26] H. C. Chen and R. L. Taylor. Vibration analysis of fluid-solid systems using a finite element displacement formulation. *International Journal of Numerical Methods in Engineering*, 29:683–698, 1990.

[27] A. Craggs. The use of three-dimensional acoustic finite elements for determining the natural modes and frequencies of complex shaped enclosures. *Journal of Sound and Vibration*, 23(3):331–339, 1972.

[28] M. Petyt, J. Lea, and G. H. Koopmann. A finite element method for determining the acoustic modes of irregular shaped cavities. *Journal of Sound and Vibration*, 45(4):495–502, 1976.

[29] A. Craggs. The transient response of a coupled plate-acoustic system using plate and acoustic finite elements. *Journal of Sound and Vibration*, 15(4):509–528, 1971.

[30] G. C. Everstine. A symmetric potential formulation for fluid-structure interaction. *Journal of Sound and Vibration*, 71(1):157–160, 1981.

[31] G. H. Golub and C. F. Van Loan. *Matrix Computations*. The Johns Hopkins University Press, Baltimore, 1990.

[32] H. Morand and R. Ohayon. Substructure variational analysis of the vibrations of coupled fluid-structure systems. finite elemtent results. *International Journal of Numerical Methods in Engineering*, 14:741–755, 1979.

[33] G. Sandberg and P. Göransson. A symmetric finite element formulation for acosutic fluid-structure interaction analysis. *Journal of Sound and Vibration*, 123(3):507–515, 1988.

[34] J. A. Wolf. Modal synthesis for combined structural-acoustic systems. *AIAA Journal*, 15:743–745, 1977.

[35] R. Ohayon. Reduced symmetric models for modal analysis of internal structural-acoustic and hydroelastic-sloshing systems. *Computer methods in applied mechanics and engineering*, 190:3009–3019, 2001.

[36] G. Sandberg. A new strategy for solving fluid-structure problems. *International Journal of Numerical Methods in Engineering*, 38:357–370, 1995.

[37] W. J. T. Daniel. Modal methods in finite element fluid-structure eigenvalue problems. *International Journal of Numerical Methods in Engineering*, 15:1161–1175, 1980.

[38] J. Wandinger. A symmetric Craig-Bampton method of coupled fluid-structure systems. *Engineering Computation*, 15(4):450–461, 1998.

[39] R. R. Arnold, R. L. Citerley, M. Chargin, and D. Galant. Application of Ritz vectors for dynamic analysis of large structures. *Computers & Structures*, 21(3):461–467, 1985.

[40] E. L. Wilson and E. P. Bayo. Use of special Ritz vectors in dynamic substructure analysis. *Journal of Structural Engineering*, 112(8):1944–1954, 1986.

[41] A. A. Abdallah and A. A. Huckelbridge. Boundary flexibility method of component mode synthesis using static Ritz vectors. *Computers & Structures*, 35(1):51–61, 1990.

[42] M. Lou, A. Ghobarah, and T. S. Aziz. Application of Wilson-Ritz vectors in dynamic substructuring. *International Journal of Solids and Structures*, 30(22):3159–3170, 1993.

[43] B. Häggblad and L. Eriksson. Model reduction methods for dynamic analyses of large structures. *Computers & Structures*, 47(4/5):735–749, 1993.

[44] H. C. Chen and L. Taylor. Solution of eigenproblems for damped structural systems by the Lanczos algorithm. *Computers & Structures*, 30(1/2):151–161, 1988.

[45] R. Guyan. Reduction of stiffness and mass matrices. *AIAA*, 3:380, 1965.

[46] V. N. Shah. Analytical selection of masters for the reduced eigenvalue problem. *International Journal of Numerical Methods in Engineering*, 18:89–98, 1982.

[47] E. J. Haug and W. Pan. Optimal inertia lumping from modal mass matrices for structural dynamics. *Computer methods in applied mechanics and engineering*, 163:171–191, 1998.

[48] N. Bouhaddi and R. Fillod. A method for selecting master dof in dynamic substructuring using the Guyan condensation method. *Computers & Structures*, 45(5/6):941–946, 1992.

[49] A. Y. T. Leung. An accurate method of dynamic condensation in structural analysis. *International Journal of Numerical Methods in Engineering*, 12:1705–1715, 1978.

[50] A. Y. T. Leung. An accurate method of dynamic substructuring with simpified computation. *International Journal of Numerical Methods in Engineering*, 14:1241–1256, 1979.

[51] N. Bouhaddi and R. Fillod. Substructuring using a linearized dynamic condensation method. *Computers & Structures*, 45(4):679–683, 1992.

[52] N. Bouhaddi and R. Fillod. Substructuring by a two level dynamic condensation method. *Computers & Structures*, 60(3):403–409, 1996.

[53] N. Bouhaddi and R. Fillod. Model reduction by a simplified variant of dynamic condensation. *Journal of Sound and Vibration.*, 191(2):233–250, 1996.

[54] P. Seshu. Substructuring and component mode synthesis. *Shock and Vibration*, 4(3):199–210, 1997.

[55] R. R. Craig. *Structural Dynamics; An introduction to computer methods.* John Wiley & Sons Inc., New York, 1981.

[56] R. R. Jr. Craig and M. C. C. Bampton. Coupling of substructures for dynamic analyses. *AIAA Journal*, 6(7):1313–1319, 1968.

[57] F. Bourquin and F. d'Hennezel. Numerical study of an intrinsic component mode synthesis method. *Computer methods in applied mechanics and engineering*, 97:49–76, 1992.

[58] F. Bourquin and F. d'Hennezel. Intrinsic component mode synthesis and plate vibrations. *Computers & Structures*, 44:315–324, 1992.

[59] W.-H. Shyu, Z.-D. Ma, and G. M. Hulbert. A new component mode synthesis method: Quasi-static mode compensation. *Finite elements in Analysis and Design*, 24:271–281, 1997.

[60] N. Bouhaddi and J.P. Lombard. Improved free-interface substructures representation method. *Computers & Structures*, 77:269–283, 2000.

[61] D.-M. Tran. Component mode synthesis methods using interface modes. *Computers & Structures*, 79:209–222, 2001.

[62] M. A. Tournour, N. Atalla, O. Chiello, and F. Sgard. Validation, performance, convergence and applicaion of free interface component mode synthesis. *Computers & Structures*, 79:1861–1876, 2001.

[63] T. J. R. Hughes. *The Finite Element Method; Linear Static and Dynamic Finite Element Analysis*. Prentice-Hall International, Inc., New Jersy, 1987.

[64] B. Nour-Omid, B. N. Parlett, and R. L. Taylor. Lanczos versus subspace iteration for solution of eigenvalue problems. *International Journal of Numerical Methods in Engineering*, 12:1705–1715, 1978.

[65] A. Y. T. Leung. Multilevel dynamic substructures. *International Journal of Numerical Methods in Engineering*, 28:181–191, 1989.

[66] Matlab user's manual. Mathworks Inc., 2002.

[67] CALFEM – a finite element toolbox to matlab. Technical Report Report TVSM–9001, Lund University, 1996.

[68] M. E. Delany and E. N. Bazley. Acoustical properties of fibrous absorbent materials. *Applied Acoustics*, 3:105–116, 1970.

[69] F. P. Mechel. Ausweitung der absorberformel von delany and bazley zu tiefen frequenzen. *Acustica*, 35:210–213, 1976.

[70] R. Kirby and A. Cummings. Prediction of the bulk acoustic properties of fibrious materials at low frequencies. *Applied Acoustics*, 56:101–125, 1999.

[71] J. F. Allard. *Propagation of sound in porous media; modelling sound absorbing matarials*. Elsevier Science Publishers Ltd, London, 1993.

[72] K. U. Ingard. Locally and nonlocally reacting flexible porous layers; A comparison of acoustical properties. *Journal of Engineering for Industry*, 103:302–313, 1981.

[73] P. Göransson. Acoustic finite element formulation of a flexible porous material– a correction for inertial effects. *Journal of Sound and Vibration*, 185(4):559–580, 1995.

[74] P. Göransson. Numerical modelling of dynamics of light porous materials. TVBA 1006, Engineering Acoustics, LTH, Lund University, Box 118, SE-221 00 Lund, Sweden, 1998.

[75] A. Craggs. A finite element model for rigid porous absorbing materials. *Journal of Sound and Vibration*, 61(1):101–111, 1978.

[76] M. A. Biot. Theory of propagation of elastic waves in fluid-saturated porous solid. i. low frequency range. *The Journal of the Acoustical Society of America*, 28(2):168–178, 1956.

[77] J. P. Coyette. The use of finite-element and boundary-element models for predicting the vibro-acoustic behaviour of layered structures. *Adv. Eng. Soft.*, 30(1):133–139, 1999.

[78] Y. J. Kang and J. S. Bolton. Finite element modeling of isotropic elastic porous materials coupled with coustical finite elements. *The Journal of the Acoustical Society of America*, 98(1):635–643, 1995.

[79] N. Dauchez, S. Sahraoui, and N. Atalla. Convergence of poroelastic finite elements based on biot displacement formulation. *The Journal of the Acoustical Society of America*, 109(1):33–40, 2001.

[80] N. Atalla, R. Panneton, and P. Debergue. A mixed displacement pressure formulation for poroelastic materials. *The Journal of the Acoustical Society of America*, 104(3):1444–1452, 1998.

[81] P. Göransson. A 3-d, symmetric, finite element formulation of the biot equations with application to acoustic wave propagation through an elastic porous medium. *International Journal of Numerical Methods in Engineering*, 41:167–192, 1998.

[82] M.J. Brennan and W. M. To. Acoustic properties of rigid-frame porous materials – an engineering perspective. *Applied Acoustics*, 62:793–811, 2001.

[83] P. Debergue, R. Panneton, and N. Atalla. Boundary conditions for the weak formulation of the mixed (u,p) poroelasticity problem. *The Journal of the Acoustical Society of America*, 106(5):2383–2390, 1999.

[84] R. Panneton and N. Atalla. Numerical prediction of sound transmission through finite multilayer systems with poroelastic materials. *The Journal of the Acoustical Society of America*, 100(1):346–354, 1996.

[85] J.-L. Batoz and M. B. Tahar. Evaluation of a new quadrilateral thin plate element. *International Journal of Numerical Methods in Engineering*, 18:1655–1677, 1982.

[86] R.-H. MacNeal and L. H. Harder. A refined four-noded membrane element with rotational degrees of freedom. *Computers & Structures*, 28(1):75–84, 1988.

The included papers

Paper 1

A strategy for modal reduction of structure-acoustic systems

Göran Sandberg and Peter Davidsson
Division of Structural Mechanics,
Lund University

A strategy for modal reduction of structure-acoustic systems

Göran Sandberg, Peter Davidsson
Division of Structural Mechanics, Lund University, Sweden

Abstract

A strategy for choosing a modal basis for the reduction of structure-acoustic systems based on the finite element method is investigated. The coupled system is set up using a displacement formulation in the structural domain and a pressure formulation in the fluid domain, resulting in an unsymmetrical system. This system is reduced by the structural and fluid normal modes, which are derived in separate eigenvalue analyses of the two domains. The paper emphasises the need to include a large number of normal modes in the reduction for proper description of the coupled problem and therefor proposes a method for choosing which of these structural and fluid modes to include in the reduced model. This is performed by evaluating the characteristics of the coupling between the normal modes of the two domains. The structural and fluid modes with strong coupling that depends on similarity in the natural frequencies or similarity in the mode shapes are included in the reduction. This enables the structure-acoustic system to be described accurately using a very limited number of structural and fluid modes. A numerical example is given for verifying the method proposed.

1 Introduction

The coupled problem of a flexible structure interacting with an acoustic fluid is of interest in many fields of engineering. It can concern a fluid-filled tank exposed to an earthquake or the noise level due to structural vibrations in a vehicle compartment. Many different formulations for describing the structure-acoustic problem have been proposed [1, 2, 3, 4]. In the present paper the primary variable in the structural domain is the displacement and in the fluid domain the acoustic pressure. Using a finite element formulation gives an unsymmetrical system of equations, the lack of symmetry being due to the coupling terms between the structural and the fluid subdomains.
Problems involving fluid-structure interaction typically generate very large systems of equations. In performing modal analysis, the system can be reduced by using the structural and fluid normal modes derived in separate eigenvalue analyses of the two domains [5, 6]. These modes are in this paper referred to as subdomain modes and the normal modes of the coupled structure-acoustic system are referred to as the coupled modes. The coupled modes are dominated by either the structure or the fluid, each subdomain mode providing

a corresponding coupled mode. The system can be made symmetric by matrix transformations [7, 8, 9].
The need for only including a selected portion of the subdomain modes in the reduction of the coupled problem was stated in [5]. In [10] a possible way of choosing these structural and fluid modes was outlined.
In the present paper, a set of basis vectors is derived for each domain by including those of the subdomain modes that are of most importance in describing the coupled structure-acoustic system. In [11], a similar procedure was used to determine which modes are of importance for the interior noise in a vehicle. By including only the important modes in the reduction of the coupled problem, the size of the system of equations can be reduced further. The paper elaborates on the importance of a correct choice of modal basis in structure-acoustic calculations and obtaining a proper understanding of the coupling phenomena which links the two domains.
A numerical example is presented based on the work described in [12] where the structure-acoustic behaviour of an aircraft fuselage was studied.

2 Finite element analysis

The structure-acoustic problem with a flexible structure in contact with an enclosed acoustic fluid involves one differential equation describing the structure, typically from plate or shell theory, and one describing the fluid, the acoustic wave equation. The fluid domain is assumed to be both inviscid and irrotational and the motions involved are small. A finite element formulation of the governing equations gives the equations of motion for the structural domain

$$\mathbf{M}_S\ddot{\mathbf{d}}_S + \mathbf{K}_S\mathbf{d}_S = \mathbf{f}_b + \mathbf{f}_F \tag{1}$$

where $\mathbf{d}_S$ denotes the nodal displacements, $\mathbf{M}_S$ and $\mathbf{K}_S$ are the structural mass and stiffness matrices. $\mathbf{f}_b$ includes the external forces and $\mathbf{f}_F$ is the force vector describing the coupling to the fluid domain. For the fluid domain

$$\mathbf{M}_F\ddot{\mathbf{p}}_F + \mathbf{K}_F\mathbf{p}_F = \mathbf{f}_q + \mathbf{f}_S \tag{2}$$

where $\mathbf{p}_F$ denotes the nodal pressures, $\mathbf{M}_F$ and $\mathbf{K}_F$ are the fluid mass and stiffness matrices. $\mathbf{f}_q$ includes the added mass term and $\mathbf{f}_S$ the force vector describing the coupling to the structural domain. For a further account of the system matrices, see [7].
The coupling between the domains is, as mentioned, described by the boundary force terms, the structure is subjected to a force at the boundary between the domains, $\partial\Omega_{SF}$, due to the fluid pressure

$$\mathbf{f}_F = \int_{\partial\Omega_{SF}} \mathbf{N}_S^T p_F \mathbf{n} dS \tag{3}$$

where $\mathbf{n} = [n_x\ n_y\ n_z]^T$ is the boundary surface normal vector pointing outward from the fluid domain and $\mathbf{N}_S$ denotes the structural shape functions. The force acting on the fluid due to displacement of the structure can be derived from the boundary term

$$\mathbf{f}_S = c_0^2 \int_{\partial\Omega_{SF}} \mathbf{N}_F^T \mathbf{n}^T \nabla p_F dS \tag{4}$$

where $\nabla = [\partial/\partial x \ \partial/\partial y \ \partial/\partial z]^T$, $\mathbf{N}_F$ contains the fluid shape functions and c_0 is the speed of sound in the fluid. At the connecting boundary the movement of the two domains in the normal direction is equal, $\mathbf{u}_S\mathbf{n}|_S = \mathbf{u}_F\mathbf{n}|_S$. Using the relation between pressure and acceleration in the fluid domain enables the force acting on the fluid due to structural movement to be written in terms of structural acceleration. The component of the pressure gradient at the interface boundary, $\partial\Omega_{SF}$, in the direction of the normal vector $\mathbf{n}$ can be expressed

$$\mathbf{n}^T\nabla p_F|_{\partial\Omega_{SF}} = -\rho_0\mathbf{n}^T\frac{\partial^2\mathbf{u}_F}{\partial t^2}|_{\partial\Omega_{SF}} = -\rho_0\mathbf{n}^T\frac{\partial^2\mathbf{u}_S}{\partial t^2}|_{\partial\Omega_{SF}} = -\rho_0\mathbf{n}^T\mathbf{N}_S\ddot{\mathbf{d}}_S|_{\partial\Omega_{SF}} \tag{5}$$

where ρ_0 is the fluid density. In the final step the structural accelerations are approximated by a finite element formulation. Using this to express $\mathbf{f}_S$ gives

$$\mathbf{f}_S = -\rho_0 c_0^2\int_{\partial\Omega_{SF}}\mathbf{N}_F^T\mathbf{n}^T\mathbf{N}_S dS\ddot{\mathbf{d}}_S = -\rho_0 c_0^2\mathbf{H}_{SF}^T\ddot{\mathbf{d}}_S \tag{6}$$

The spatial coupling matrix $\mathbf{H}_{SF}$ that is introduced can also be used to describe $\mathbf{f}_F$

$$\mathbf{f}_F = \int_{\partial\Omega_{SF}}\mathbf{N}_S^T\mathbf{n}\mathbf{N}_F dS\mathbf{p}_F = \mathbf{H}_{SF}\mathbf{p}_F \tag{7}$$

Equations (1) and (2) can now be written in matrix form to yield the system of equations describing the structure-acoustic problem

$$\begin{bmatrix} \mathbf{M}_S & \mathbf{0} \\ \rho_0 c_0^2\mathbf{H}_{SF}^T & \mathbf{M}_F \end{bmatrix}\begin{bmatrix} \ddot{\mathbf{d}}_S \\ \ddot{\mathbf{p}}_F \end{bmatrix} + \begin{bmatrix} \mathbf{K}_S & -\mathbf{H}_{SF} \\ 0 & \mathbf{K}_F \end{bmatrix}\begin{bmatrix} \mathbf{d}_S \\ \mathbf{p}_F \end{bmatrix} = \begin{bmatrix} \mathbf{f}_b \\ \mathbf{f}_q \end{bmatrix} \tag{8}$$

The matrix $\mathbf{H}_{SF}$ makes the system matrices unsymmetrical and therefore both the left and right eigenvectors need to be calculated in order to diagonalise the system. A procedure for establishing a reduced symmetric system of equations has been described in a previous paper [7]. The normal modes of the subdomains are first calculated and are normalised according to

$$\begin{aligned} \mathbf{\Phi}_S^T\mathbf{M}_S\mathbf{\Phi}_S &= \mathbf{I}_S & \mathbf{\Phi}_S^T\mathbf{K}_S\mathbf{\Phi}_S &= \mathbf{\Lambda}_S \\ \mathbf{\Phi}_F^T\mathbf{M}_F\mathbf{\Phi}_F &= \mathbf{I}_F & \mathbf{\Phi}_F^T\mathbf{K}_F\mathbf{\Phi}_F &= \mathbf{\Lambda}_F \end{aligned} \tag{9}$$

where $\mathbf{\Phi}_S$ and $\mathbf{\Phi}_F$ are the normal modes of the structural and the fluid domain and $\mathbf{\Lambda}_S$ and $\mathbf{\Lambda}_F$ contain the corresponding eigenvalues of the two domains in the diagonal. Introducing the change of base

$$\begin{bmatrix} \mathbf{d}_S \\ \mathbf{p}_F \end{bmatrix} = \begin{bmatrix} \mathbf{\Phi}_S & \mathbf{0} \\ \mathbf{0} & \mathbf{\Phi}_F \end{bmatrix}\begin{bmatrix} \boldsymbol{\xi}_S \\ \boldsymbol{\xi}_F \end{bmatrix} \tag{10}$$

the coupled system in equation (8) can be reformulated, according to the procedure in [7], to arrive at a reduced symmetric system

$$\begin{bmatrix} \ddot{\boldsymbol{\zeta}}_S \\ \ddot{\boldsymbol{\zeta}}_F \end{bmatrix} + \begin{bmatrix} \mathbf{\Lambda}_S & -\sqrt{\rho c^2}\sqrt{\mathbf{\Lambda}_S}\mathbf{\Phi}_S^T\mathbf{H}_{SF}\mathbf{\Phi}_F \\ -\sqrt{\rho c^2}\mathbf{\Phi}_F^T\mathbf{H}_{SF}^T\mathbf{\Phi}_S\sqrt{\mathbf{\Lambda}_S} & \mathbf{\Lambda}_F + \rho c^2\mathbf{\Phi}_F^T\mathbf{H}_{SF}^T\mathbf{\Phi}_S\mathbf{\Phi}_S^T\mathbf{H}_{SF}\mathbf{\Phi}_F \end{bmatrix}\begin{bmatrix} \boldsymbol{\zeta}_S \\ \boldsymbol{\zeta}_F \end{bmatrix} = \begin{bmatrix} \sqrt{\rho c^2}\sqrt{\mathbf{\Lambda}_S}\mathbf{\Phi}_S^T\mathbf{f}_b \\ \mathbf{\Phi}_F^T\mathbf{f}_q - \rho c^2\mathbf{\Phi}_F^T\mathbf{H}_{SF}^T\mathbf{\Phi}_S\mathbf{\Phi}_S^T\mathbf{f}_b \end{bmatrix} \tag{11}$$

which gives the right eigenvectors. Setting up a system with the transposed system matrices gives the left eigenvectors.

3 Choosing subdomain modes.

In the change of base in equation (10), the number of structural and fluid modes included can become very large. The motion at the boundary for a certain subdomain mode of one of the domains must be captured by the included modes of the opposite domain. That is, the static behaviour due to the loading from a mode of the opposite domain must be described correctly. Having, as for a typical low frequency structure-acoustic problem, much smaller wave lengths of the structural domain than for the fluid domain, this leads to that high frequency modes of the fluid domain must be included to capture the pressure distribution at the boundary interface. In opposite, the pressure distribution can excite structural modes with high natural frequency.
In this section, a method for using information about the coupling between the structural and fluid normal modes to determine which of these modes are important in describing the coupled problem and to only include them in equation (10).
For a principal discussion of the structure–acoustic problem, an illustrative example problem, being a simply supported plate in contact with an acoustic cavity, is investigated. A similar discussion can be found in Refs. [4, pp. 14-18]) and [13, pp. 252-256]. Only the structural normal mode, ψ_{S1}, and fluid normal mode, ψ_{F1}, with the lowest (non-zero) natural frequencies (see Figure 1), are included in the analysis. These natural frequencies are denoted f_{S1} and f_{F1}, respectively. The coupling between the two domains is given by the spatial coupling coefficient C_{11},

$$C_{11} = \int_{\partial\Omega_{SF}} \psi_{S1}(x,y)\psi_{F1}(x,y)dS = \mathbf{\Phi}_{S1}^T \mathbf{H}_{SF} \mathbf{\Phi}_{F1} \tag{12}$$

where the finite element approximation of the modes is introduced in the last step.
For the studied problem, the natural frequencies of the coupled problem, f_{c1} and f_{c2}, are calculated while varying the coupling coefficient, C_{11} in equation (12) and the natural frequency of the structural domain f_{S1}, see Figure 2. C_{11} is varied by changing the area of the boundary, $\partial\Omega_{SF}$, with acoustical coupling between the two domains. The natural frequency of the fluid domain f_{F1} is held constant. The coupled natural frequencies are affected by the strength in mode shape coupling and are more sensitive to changes in the coupling strength when the natural frequencies of the subdomain modes are of similar magnitude.
From this brief discussion it can be concluded that when using the normal modes, calculated for the structural and fluid domains separately, in the reduction of the coupled problem, the

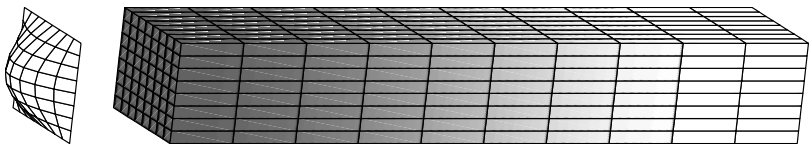

Figure 1: *A flexible panel backed by an acoustic cavity is studied. The two subdomain normal modes, with the lowest (non-zero) natural frequencies, are displayed. The figure shows the displacement shape of the structural domain and the pressure distribution in the fluid domain.*

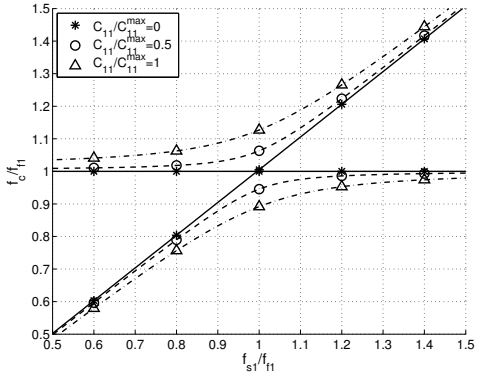

Figure 2: *Natural frequencies, f_c, of the coupled structure-acoustic problem with two degrees of freedom when varying the coupling strength. The calculated natural frequencies are normalised by the natural frequency of the fluid domain, f_{F1}, which is held constant. C_{11}^{max} is calculated with the whole interface area, $\partial\Omega_{SF}$, coupled.*

similarity between the natural frequencies, f_{Si} and f_{Fj}, as well as strength of the coupling C_{ij}, determine the influence of each of these modes on the coupled modes.
To determine which of the structural and fluid modes are strongly coupled, the following expression is used

$$B_{ij} = \frac{\mathbf{\Phi}_{Si}^T \mathbf{H}_{SF} \mathbf{\Phi}_{Fj}}{\omega_{Si}^2 - \omega_{Fj}^2} \tag{13}$$

The numerator corresponds to the coefficient C_{ij} in equation (12). In the denominator, natural frequencies of the i'th structural mode and the j'th fluid mode are introduced, similar frequencies giving a value of denominator close to zero. This expression allows the coupling between the structural domain and the fluid domain to be determined creating the possibility of choosing the most important subdomain modes to include in the reduced coupled problem. Equation (13) was used in [11] to determine which structural and fluid modes participate in generating vehicle interior noise. Similarity in the mode shapes and similarity in the natural frequencies gives a large value for B_{ij}, the corresponding modes being included in the coupled analysis. The following variables are defined, see also Figure 3:

$\mathbf{\Phi}_S$ denotes all available structural modes. n_S being the number of these modes
$\mathbf{\Phi}_F$ denotes all available fluid modes. n_F being the number of these modes
$\hat{\mathbf{\Phi}}_S = \{\mathbf{\Phi}_{Si} \in \mathbf{\Phi}_S; \omega_{Si} \leq \hat{\omega}\}$
$\hat{\mathbf{\Phi}}_F = \{\mathbf{\Phi}_{Fi} \in \mathbf{\Phi}_F; \omega_{Fi} \leq \hat{\omega}\}$

where $\hat{\omega} = 2\pi\hat{f}$ and $\hat{f}$ is the maximum frequency of interest.
The scheme for choosing which subdomain modes to include in the analysis is as follows:

1. Perform modal analyses of the structural and fluid domains separately, calculating $\mathbf{\Phi}_S$ and $\mathbf{\Phi}_F$.

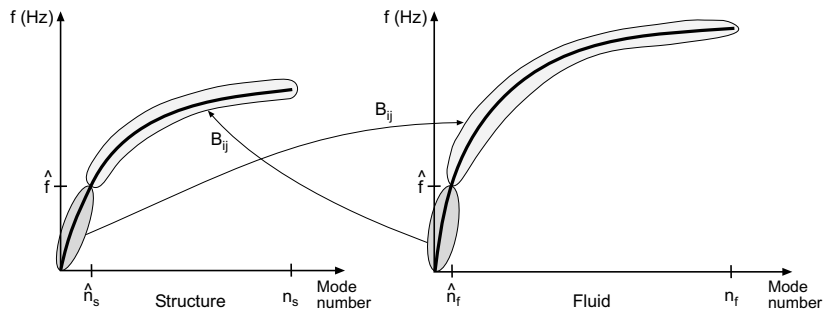

Figure 3: *Natural frequencies of the two domains plotted against the mode number. Uncoupled modes of the two domains are compared using equation (13) and the most important modes to describe the coupled system can be included in the reduced coupled analysis, equation (11).*

2. On the basis of the maximum frequency of interest, $\hat{f}$, determine $\hat{\mathbf{\Phi}}_S$ and $\hat{\mathbf{\Phi}}_F$. All of these modes are included in the reduction of the coupled problem.

3. Determine the coupling between $\hat{\mathbf{\Phi}}_S$ and $\mathbf{\Phi}_F$ using equation (13). A number n_{coup} of fluid modes with the strongest coupling for each structural mode is determined. These fluid modes above the frequency range of interest are also included in the reduction, see Figure 3. The effect of the value of n_{coup} is studied in the numerical example.

4. Use the same method for the fluid modes $\hat{\mathbf{\Phi}}_F$ comparing them with $\mathbf{\Phi}_S$ for determining which structural modes above the frequency range of interest should be included in the reduction.

5. Perform the reduced coupled modal analysis, based on equation (11), using the structural and fluid modes chosen.

Because all the modes below the frequency limit $\hat{f}$ are included the numerator has only a small effect on the choice of modes in the upper frequency range, assuming that the condition $\omega_{Si} \gg \omega_{Fj}$ or $\omega_{Si} \ll \omega_{Fj}$ is satisfied. Instead of using equation (13) a simplified expression

$$\hat{B}_{ij} = \mathbf{\Phi}_{Si}^T \mathbf{H}_{SF} \mathbf{\Phi}_{Fj} \tag{14}$$

in which only the similarity in mode shapes is calculated, can be used to determine the modes to include in the analysis. These two methods, method I represented by equation (13) and method II represented by equation (14), are evaluated in the numerical example in the next section.

4 Numerical example

In this section the two methods for choosing the subdomain modes described above are evaluated and the number of these modes needed for describing the coupled system is examined.

Table 1: *Material data for the body.*

Steel:	E	=	210	GPa
	ν	=	0.30	
	ρ	=	7800	kg/m^3
Aluminum:	E	=	70	GPa
	ν	=	0.30	
	ρ	=	2700	kg/m^3
Air:	ρ	=	1.21	kg/m^3
	c	=	340	m/s.

4.1 Model

A simple three-dimensional body is analysed, Figure 4. The model employed is based on [12], in which numerical and experimental work was performed. It involves a cylindrical steel shell 1.2 mm thick with a 0.183 m radius. The length of the cylinder is 1.01 m and circular aluminum plates 25.4 mm thick are attached to the ends. The material properties are listed in Table 1 and the number of degrees of freedom for the domains being shown in Table 2. Eigenvalue analysis of the fluid domain and the structural domain is performed using MSC/Nastran [14] and the coupled modal analysis in Matlab/CALFEM [15, 16]. The results are compared with a direct solution of the coupled problem using MSC/Nastran. The total number of subdomain modes needed to describe the coupled system is evaluated.

Table 2: *Finite element model data.*

Domain	Degrees of freedom
Structure	4620
Acoustic fluid	2465
Total	7085

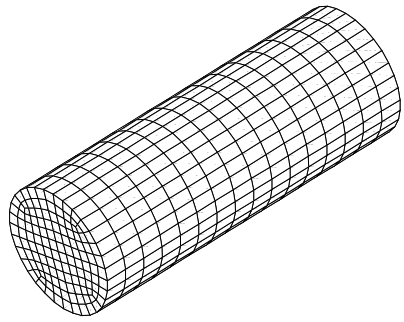

Figure 4: *Finite element model of the three-dimensional body.*

The methods described for choosing modes are studied by varying the number of subdomain modes with strong coupling that are included, i.e. the number n_{coup}. The mode shapes calculated, $\mathbf{\Phi}_{reduced}$, are compared with the modes obtained in solving the total system, $\mathbf{\Phi}_{total}$, using the expression

$$\kappa = \frac{\mathbf{\Phi}_{reduced}^T \cdot \mathbf{\Phi}_{total}}{|\mathbf{\Phi}_{reduced}| \cdot |\mathbf{\Phi}_{total}|} \tag{15}$$

The value of κ is between 0 to 1 where 1 represents exact agreement between the modes that are compared.

4.2 Coupled analysis without choosing modes

The effect of the number of structural modes, n_S, and fluid modes, n_F, included in the analysis is shown in Figure 5. The maximum frequency of interest is set to 500 Hz , the similarity of the eigenvectors of the reduced model and the total model, κ, being plotted for the 22 coupled modes with natural frequency below this value. Four cases are shown in the Figure, differing in the number of structural and fluid modes included, namely: 1) all structural and fluid modes up to 1.2 times the highest frequency of interest, which gives $n_S = 39, n_F = 9$ ($\circ$); 2) $n_S = 100, n_F = 200$ ($*$); 3) $n_S = 200, n_F = 500$ ($\triangle$); 4) $n_S = 500, n_F = 1000$ ($\times$). The similarity in mode shapes is plotted for the structural and fluid parts of the coupled eigenvectors separately. For the structural part of the mode, the shape is accurate for those modes dominated by the structure. In contrast, modes 1 and 12 are dominated by the fluid. Thus, a large number of structural modes are needed to describe the behaviour of the coupled modes. The same is true for the fluid domain, where the modes dominated by the fluid are represented accurately. From this it is obvious that many of the subdomain modes do not contribute to the coupled solution and can thus be sorted out. When the 22 lowest coupled modes are calculated, based on originally 500

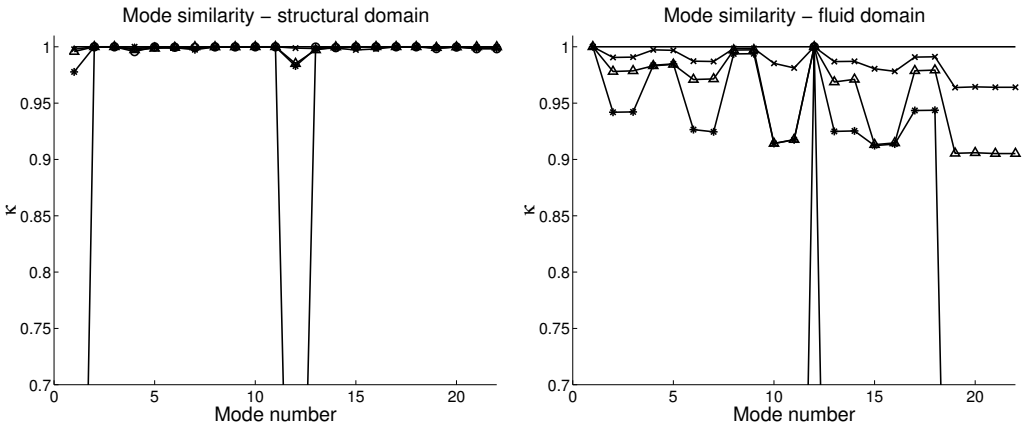

Figure 5: *Similarity between modes in the reduced model and in the total model: a) structural part, b) fluid part. Modes included:* $n_S = 39, n_F = 9$*, all subdomain modes with a natural frequency of up to 600 Hz* ($\circ$)*;* $n_S = 100, n_F = 200$ ($*$)*;* $n_S = 200, n_F = 500$ ($\triangle$)*;* $n_S = 500, n_F = 1000$ ($\times$)

structural modes and 1000 fluid modes, the minimum values are $\kappa = 0.997$ for the structure and $\kappa = 0.964$ for the fluid.

4.3 Proposed method

The methods for selecting modes are evaluated by making selections from the 500 structural modes, $\mathbf{\Phi}_S$, and the 1000 fluid modes, $\mathbf{\Phi}_F$, that are lowest. Since the highest frequency of interest is 500 Hz, $\hat{\mathbf{\Phi}}_S$ represents the 26 lowest structural modes (including 6 zero-modes). $\hat{\mathbf{\Phi}}_F$ represents the 3 lowest fluid modes (including one zero-mode).

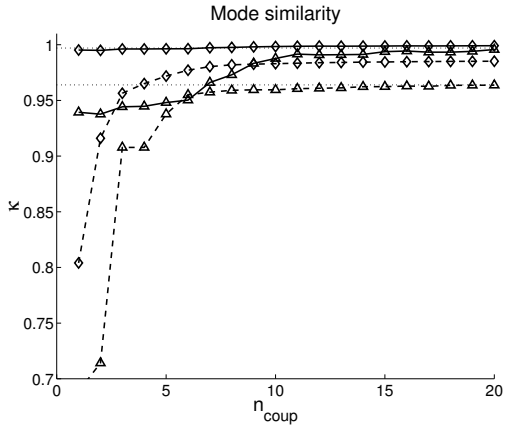

Figure 6: *Method I (equation 13). Similarity between modes in the reduced model and in the total model: Solid line - structural domain. Dashed line - fluid domain. △ - minimum value of κ, ◇ - mean value of κ.*

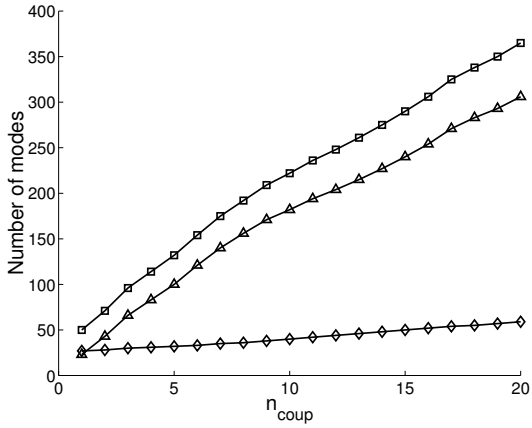

Figure 7: *Method I (equation 13). Number of modes from the subdomains included: ◇ - structural domain, △ - fluid domain, □ - Total number.*

Figure 6 displays the similarity in mode shapes for each domain as obtained for method I when n_{coup}, according to the suggested scheme, is increased from one to twenty. The mean and the minimum value of κ for the first 22 coupled modes (below 500 Hz) are displayed for the structural and the fluid part of the coupled eigenvector separately. The horizontal dotted lines denote κ for the structural and fluid domains, obtained when all 500 structural and 1000 fluid modes are included. In Figure 7, the corresponding number of subdomain modes included in the coupled analysis is plotted. The results for method II are displayed in Figures 8 and 9. Note that all the modes below 500 Hz from each subdomain are included in the coupled analysis. The first method provides very close

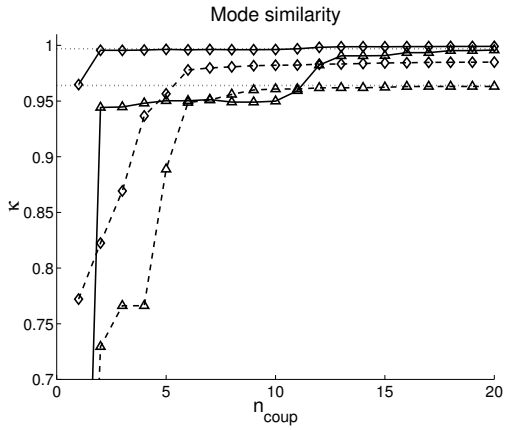

Figure 8: *Method II (equation 14). Similarity between modes in the reduced model and in the total model: Solid line - structural domain. Dashed line - fluid domain.* △ *- minimum value of* κ*,* ◇ *- mean value of* κ*.*

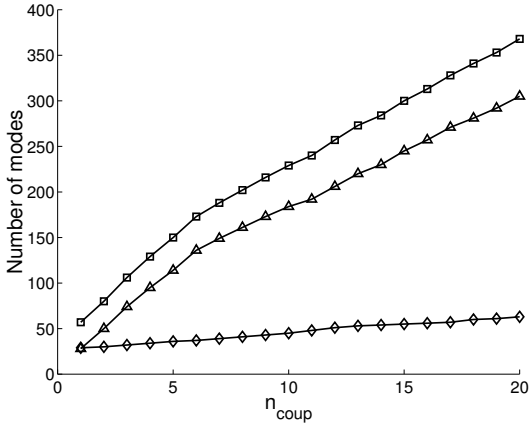

Figure 9: *Method II (equation 14). Number of modes from the subdomains included:* ◇ *- structural domain,* △ *- fluid domain,* □ *- Total number.*

agreement for $n_{coup} = 11$, where 236 subdomain modes (42 structural and 194 fluid modes) are included in the coupled analysis. The number of degrees of freedom for the coupled system is thus reduced from 7085 to 236, with very high accuracy being maintained. The eigenvalue problem is also of a standard symmetric form which makes it easy to solve. The second method which uses a simpler method, also yields good results, but since the frequency dependence is neglected a less smooth curve of convergence is obtained.

5 Conclusions

A structure-acoustic system is analysed using a strategy for substructuring and reducing the coupled problem by the structural and the fluid normal modes derived in separate analyses. Since a large number of modes from the subdomains is needed to describe the coupled system, a method for choosing the structural and the fluid normal modes that contribute most strongly to a description of the coupled problem in the frequency range of interest is studied. The paper proposes two methods which are similar, Method I involves selecting the subdomain modes on the basis of strong coupling using resemblance in terms both of natural frequency and of mode shapes. Method II involves determining the most important subdomain modes on the basis of the similarity in mode shapes only. The numerical example shows Method I to give the best results. That method allows the coupled system to be reduced from 7085 to 236 degrees of freedom, with only a small loss of accuracy. Comparing the results for the reduced system using a selected set of modes with those obtained using all the modes available shows the results to be almost identical. For the case analysed here the number of modes included is reduced from 1500 to 236.

References

[1] O. C. Zienkiewicz and R. L.Taylor. *The Finite Element Method*, volume 1 and 2. MacGraw-Hill, London, 1994.

[2] G. Sandberg. Finite element modelling of fluid-structure interaction. TVSM 1002, Structural Mechanics, LTH, Lund University, Box 118, SE-221 00 Lund, Sweden, 1986.

[3] H. Carlsson. Finite element analysis of structure-acoustic systems; formulations and solution strategies. TVSM 1005, Structural Mechanics, LTH, Lund University, Box 118, SE-221 00 Lund, Sweden, 1992.

[4] H. Morand and R. Ohayon. *Fluid structure interaction*. John Wiley & sons, Chichester, 1995.

[5] J. A. Wolf. Modal synthesis for combined structural-acoustic systems. *AIAA Journal*, 15:743–745, 1977.

[6] D. J. Nefske, J. A. Wolf, and L. J. Howell. Structural-acoustic finite element analysis of the automobile compartment: A review of current practice. *Journal of Sound and Vibration*, 80(2):247–266, 1982.

[7] G. Sandberg. A new strategy for solving fluid-structure problems. *International Journal of Numerical Methods in Engineering*, 38:357–370, 1995.

[8] G. Sandberg. Acoustic and interface elements for structure-acoustic analysis in calfem. TVSM 7113, Structural Mechanics, LTH, Lund University, Box 118, SE-221 00 Lund, Sweden, 1996.

[9] G. Sandberg, P. Hansson, and M. Gustavsson. Domain decomposition in acoustic and structure-acoustic analysis. *Computer methods in applied mechanics and engineering*, 190:2979–2988, 2001.

[10] G. Sandberg. Domain decomposition in structure-acoustic analysis. *In S. N. Atluri, G. Yagawa, and T.A. Cruse, editors, Proc. of the International Conference on Computational Engineering Science '95*, pages 857–862, 1995.

[11] S. H. Kim and J. M. Lee. A practical method for noise reduction in a vehicle passenger compartment. *Journal of Vibration and Acoustics*, 120(3):199–205, 1998.

[12] S. Boily and F. Charron. The vibroacoustic response of a cylindrical shell structure with viscoelastic and poroelastic materials. *Applied Acoustics*, 58:131–152, 1999.

[13] F. Fahy. *Sound and structural vibration*. Academic Press, London, 1985.

[14] MSC/NASTRAN - V2001. The MacNeal-Schwendler Corporation, 2001.

[15] Matlab user's manual. Mathworks Inc., 2002.

[16] CALFEM – a finite element toolbox to matlab. Technical Report Report TVSM–9001, Lund University, 1996.

Paper 2

Reduction of structure-acoustic systems that include hysteretic damping

Peter Davidsson and Göran Sandberg
Division of Structural Mechanics,
Lund University

Reduction of structure-acoustic systems that include hysteretic damping

Peter Davidsson, Göran Sandberg
Division of Structural Mechanics, Lund University, Sweden

Abstract

The structure-acoustic fluid problem is studied by use of the finite element method. In a previous paper the unsymmetrical system obtained by use of a pressure formulation for the fluid domain was reduced by use of the uncoupled modes of the structural and the fluid domain and was transformed into a symmetric standard eigenvalue problem. In the present paper the possibility of including hysteretic damping in this transformation, resulting in a complex-valued symmetric standard eigenvalue problem, is described. This provides a simple method for including damping in the frequency response analysis of structure-acoustic problems.

1 Introduction

In structure-acoustic finite element analysis the number of degrees of freedom can easily becomes very large. The element size needs to be small enough for the model to be able to describe the dynamic behaviour of the system below the frequency limit of interest. In [1, 2], the size of the problem is reduced by sub-structuring of the coupled problem followed by modal reduction of it. The normal modes of the structural domain and of the fluid domain are calculated separately, the coupled system then being reduced by use of these modes. After matrix scaling, the symmetric standard eigenvalue problem can be solved.

Damping is of considerable importance in the dynamic behaviour of the system and needs to be accounted for in the structure-acoustic analysis. This is a very complex phenomena and advanced models must be used in the description of typical damping materials, for example, rubber, see [3, 4] or porous sound absorbtion material, see [5, 6]. In these models, a large number of material parameters are needed and in a frequency response analysis, the frequency dependance in the parameters leads to that the system matrices must be generated in each frequency step. The normal mode approach, which arrive at an uncoupled system of equations, can not be used. However, at certain circumstances, for example, when determining the effect of structural modifications on the sound pressure level in the compartment in the early design process of a vehicle, a rough description of the damping is often adopted.

The reduction of the coupled system is performed here including hysteretic damping in both the structural and the fluid domain. This provides an averaged measure of the damping

in each domain by use of two damping factors, η_S and η_F, both of them independent of frequency. The modal analysis of the damped coupled problem yields complex eigenvalues and eigenvectors. These eigenmodes can then be used in a modal frequency response analysis.
The ability of this approach is investigated in predicting the sound transmission loss in a flexible panel coupled to an acoustic cavity.

2 Sub-structuring and reduction

The damping is included at a constitutive level in the structural domain as a complex modulus of elasticity

$$\tilde{E}_S = (1 + \mathrm{i}\eta_S)E_S \tag{1}$$

and in the fluid domain a complex bulk modulus

$$\tilde{B}_0 = (1 + \mathrm{i}\eta_F)B_0 \tag{2}$$

After finite element formulation has been performed the coupled structure-acoustic system can be described by an unsymmetrical equation system using a displacement formulation for the structural domain and a pressure formulation for the fluid domain, The displacements are denoted $\mathbf{d}_F$ and the pressure $\mathbf{p}_F$. Harmonic motion is assumed

$$\begin{bmatrix} \mathbf{d}_F \\ \mathbf{p}_F \end{bmatrix} = \begin{bmatrix} \hat{\mathbf{d}}_F \\ \hat{\mathbf{p}}_F \end{bmatrix} \mathrm{e}^{\mathrm{i}\omega t} \tag{3}$$

where $\mathrm{i} = \sqrt{-1}$, ω is the angular frequency and t denotes time. With the time dependency suppressed the system of equations becomes

$$\left(-\omega^2 \begin{bmatrix} \mathbf{M}_S & \mathbf{0} \\ \rho c^2 \mathbf{H}_{SF}^T & \mathbf{M}_F \end{bmatrix} + \begin{bmatrix} \tilde{\mathbf{K}}_S & -\mathbf{H}_{SF} \\ 0 & \tilde{\mathbf{K}}_F \end{bmatrix} \right) \begin{bmatrix} \hat{\mathbf{d}}_F \\ \hat{\mathbf{p}}_F \end{bmatrix} = \begin{bmatrix} \hat{\mathbf{f}}_b \\ \hat{\mathbf{f}}_q \end{bmatrix} \tag{4}$$

where

$$\tilde{\mathbf{K}}_S = (1 + \mathrm{i}\eta_S)\mathbf{K}_S; \qquad \tilde{\mathbf{K}}_F = (1 + \mathrm{i}\eta_F)\mathbf{K}_F \tag{5}$$

are the complex stiffness matrices, which means an imaginary part due to damping being included in the structural and fluid stiffness matrices. $\mathbf{M}_S$ and $\mathbf{M}_F$ are the mass matrices and $\mathbf{H}_{SF}$ describes the spatial coupling between the two domains. The right hand side of the equation describes the amplitude of the harmonic external forces acting on the system. The aim is now to calculate the eigenvalues, $\tilde{\mathbf{\Lambda}}$, and the left and right eigenvectors,$\tilde{\mathbf{v}}_L$ and $\tilde{\mathbf{v}}_R$, of the coupled system in order to end up with a diagonal equation system in the frequency domain, i.e.

$$\begin{aligned} \tilde{\mathbf{v}}_L^T \begin{bmatrix} \mathbf{M}_S & \mathbf{0} \\ \rho c^2 \mathbf{H}_{SF}^T & \mathbf{M}_F \end{bmatrix} \tilde{\mathbf{v}}_R &= \mathbf{I} \\ \tilde{\mathbf{v}}_L^T \begin{bmatrix} \tilde{\mathbf{K}}_S & -\mathbf{H}_{SF} \\ 0 & \tilde{\mathbf{K}}_F \end{bmatrix} \tilde{\mathbf{v}}_R &= \tilde{\mathbf{\Lambda}} \end{aligned} \tag{6}$$

where $\mathbf{I}$ is an identity matrix and $\tilde{\mathbf{\Lambda}}$ contains the eigenvalues of the coupled system in the diagonal. The coupled system is solved by first a reduction through use of uncoupled

modes of the structural and fluid domains. The two domains are analysed separately [1]. When hysteretic damping is included, this gives

$$\begin{aligned} \boldsymbol{\Phi}_S^T \mathbf{M}_S \boldsymbol{\Phi}_S &= \mathbf{I}_S & \boldsymbol{\Phi}_S^T \tilde{\mathbf{K}}_S \boldsymbol{\Phi}_S &= \tilde{\boldsymbol{\Lambda}}_S \\ \boldsymbol{\Phi}_F^T \mathbf{M}_F \boldsymbol{\Phi}_F &= \mathbf{I}_F & \boldsymbol{\Phi}_F^T \tilde{\mathbf{K}}_F \boldsymbol{\Phi}_F &= \tilde{\boldsymbol{\Lambda}}_F \end{aligned} \tag{7}$$

where the eigenvectors $\boldsymbol{\Phi}_S$ and $\boldsymbol{\Phi}_F$ are real and the eigenvalues of the two domains $diag(\tilde{\boldsymbol{\Lambda}}_S)$ and $diag(\tilde{\boldsymbol{\Lambda}}_F)$ are complex. By introducing the change of base

$$\begin{bmatrix} \hat{\mathbf{d}}_F \\ \hat{\mathbf{p}}_F \end{bmatrix} = \begin{bmatrix} \boldsymbol{\Phi}_S & \mathbf{0} \\ \mathbf{0} & \boldsymbol{\Phi}_F \end{bmatrix} \begin{bmatrix} \hat{\boldsymbol{\xi}}_S \\ \hat{\boldsymbol{\xi}}_F \end{bmatrix} \tag{8}$$

in equation (4) and through matrix scaling of the reduced problem, a symmetric standard eigenvalue problem is obtained

$$\begin{bmatrix} \tilde{\boldsymbol{\Lambda}}_S & -\sqrt{\rho c^2}\sqrt{\tilde{\boldsymbol{\Lambda}}_S}\boldsymbol{\Phi}_S^T \mathbf{H}_{SF} \boldsymbol{\Phi}_F \\ -\sqrt{\rho c^2}\boldsymbol{\Phi}_F^T \mathbf{H}_{SF}^T \boldsymbol{\Phi}_S \sqrt{\tilde{\boldsymbol{\Lambda}}_S} & \boldsymbol{\Lambda}_F + \rho c^2 \boldsymbol{\Phi}_F^T \mathbf{H}_{SF}^T \boldsymbol{\Phi}_S \boldsymbol{\Phi}_S^T \mathbf{H}_{SF} \boldsymbol{\Phi}_F \end{bmatrix} \begin{bmatrix} \hat{\boldsymbol{\zeta}}_S \\ \hat{\boldsymbol{\zeta}}_F \end{bmatrix}_R = \tilde{\boldsymbol{\Lambda}} \begin{bmatrix} \hat{\boldsymbol{\zeta}}_S \\ \hat{\boldsymbol{\zeta}}_F \end{bmatrix}_R \tag{9}$$

$\tilde{\boldsymbol{\Lambda}}$ now contains n eigenvalues of the coupled system in the diagonal where n is the total number of structural and fluid eigenvectors used in reduction of the coupled system. This system gives the eigenvalues and the right eigenvectors expressed in terms of the transformed coordinates. In terms of the original coordinates the right eigenvectors become

$$\tilde{\mathbf{v}}_R = \begin{bmatrix} \boldsymbol{\Phi}_S & 0 \\ 0 & \boldsymbol{\Phi}_F \end{bmatrix} \begin{bmatrix} \left(\sqrt{\rho c^2}\sqrt{\tilde{\boldsymbol{\Lambda}}_S}\right)^{-1} & 0 \\ 0 & \mathbf{I}_F \end{bmatrix} \begin{bmatrix} \hat{\boldsymbol{\zeta}}_S \\ \hat{\boldsymbol{\zeta}}_F \end{bmatrix}_R \tag{10}$$

For the left system, the coupled system matrices are transposed prior to reduction, i.e.

$$\begin{gathered} \tilde{\mathbf{v}}_L^T \begin{bmatrix} \tilde{\mathbf{K}}_S & -\mathbf{H}_{SF} \\ 0 & \tilde{\mathbf{K}}_F \end{bmatrix} = \tilde{\lambda} \tilde{\mathbf{v}}_L^T \begin{bmatrix} \mathbf{M}_S & \mathbf{0} \\ \rho c^2 \mathbf{H}_{SF}^T & \mathbf{M}_F \end{bmatrix} \\ \Leftrightarrow \\ \begin{bmatrix} \tilde{\mathbf{K}}_S & -\mathbf{H}_{SF} \\ 0 & \tilde{\mathbf{K}}_F \end{bmatrix}^T \tilde{\mathbf{v}}_L = \tilde{\lambda} \begin{bmatrix} \mathbf{M}_S & \mathbf{0} \\ \rho c^2 \mathbf{H}_{SF}^T & \mathbf{M}_F \end{bmatrix}^T \tilde{\mathbf{v}}_L \end{gathered} \tag{11}$$

The system matrices $\mathbf{M}_S$, $\tilde{\mathbf{K}}_S$, $\mathbf{M}_F$ and $\tilde{\mathbf{K}}_F$ are symmetric and the standard eigenvalue problem that yields the left eigenvectors can be written as

$$\begin{bmatrix} \tilde{\boldsymbol{\Lambda}}_S + \rho c^2 \boldsymbol{\Phi}_S^T \mathbf{H}_{SF} \boldsymbol{\Phi}_F \boldsymbol{\Phi}_F^T \mathbf{H}_{SF}^T \boldsymbol{\Phi}_S & -\sqrt{\rho c^2}\boldsymbol{\Phi}_S^T \mathbf{H}_{SF} \boldsymbol{\Phi}_F \sqrt{\tilde{\boldsymbol{\Lambda}}_F} \\ -\sqrt{\rho c^2}\sqrt{\tilde{\boldsymbol{\Lambda}}_F}\boldsymbol{\Phi}_F^T \mathbf{H}_{SF}^T \boldsymbol{\Phi}_S & \tilde{\boldsymbol{\Lambda}}_F \end{bmatrix} \begin{bmatrix} \hat{\boldsymbol{\zeta}}_S \\ \hat{\boldsymbol{\zeta}}_F \end{bmatrix}_L = \tilde{\boldsymbol{\Lambda}} \begin{bmatrix} \hat{\boldsymbol{\zeta}}_S \\ \hat{\boldsymbol{\zeta}}_F \end{bmatrix}_L . \tag{12}$$

In terms of the original coordinates the left eigenvectors become

$$\tilde{\mathbf{v}}_L = \begin{bmatrix} \boldsymbol{\Phi}_S & 0 \\ 0 & \boldsymbol{\Phi}_F \end{bmatrix} \begin{bmatrix} \mathbf{I}_S & 0 \\ 0 & \left(\sqrt{\rho c^2}\sqrt{\tilde{\boldsymbol{\Lambda}}_F}\right)^{-1} \end{bmatrix} \begin{bmatrix} \hat{\boldsymbol{\zeta}}_S \\ \hat{\boldsymbol{\zeta}}_F \end{bmatrix}_L \tag{13}$$

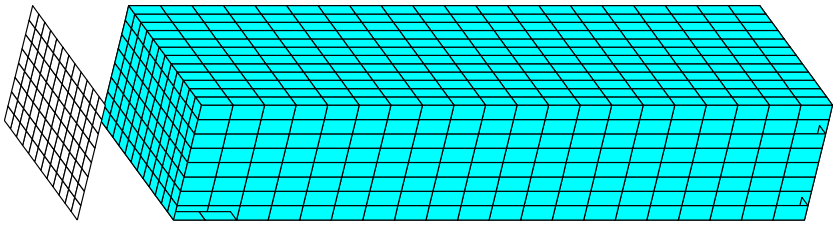

Figure 1: *A flexible panel backed by an acoustic cavity is studied.*

Introducing the change of base with the right eigenvectors

$$\begin{bmatrix} \hat{\mathbf{d}}_F \\ \hat{\mathbf{p}}_F \end{bmatrix} = \tilde{\mathbf{v}}_R \hat{\boldsymbol{\xi}} \tag{14}$$

in equation (4) and multiplying with the left eigenvectors $\tilde{\mathbf{v}}_L$ from the left gives the reduced system of equations

$$(-\bar{\omega}^2 \mathbf{I} + \tilde{\boldsymbol{\Lambda}})\hat{\boldsymbol{\xi}} = \tilde{\mathbf{v}}_L^T \begin{bmatrix} \hat{\mathbf{f}}_b \\ \hat{\mathbf{f}}_q \end{bmatrix} \tag{15}$$

A system of uncoupled equations describing the structure-acoustic problem including hysteretic damping is achieved.

3 Numerical example

The numerical part of the analysis was performed in Matlab using the finite element toolbox CALFEM [7]. An aluminium panel of 3 mm in thickness behind which a rectangular acoustic cavity is located has been analysed, see Fig. 1. The panel is 0.60 m long and 0.40 m wide. The air filled cavity is 2.1 m in depth. All the walls of the cavity except for the panel are rigid. The material data is given in Tab. 1.
A normal incident pressure wave in the frequency range of 1-700 Hz impinges on the outside of the panel. The sound transmission loss is measured between the outside and inside of the midpoint of the panel. The structural domain is described in use of 4-node quadrilateral plate elements derived in [8], and for the acoustic domain 8-node isoparametric elements with pressure formulation are used, see [2]. The analysis, which involves 910 degrees-of-freedom follows the steps described in the previous section. The sound transmission loss

Table 1: *Material data for the panel and cavity.*

Aluminum:	E	=	70	GPa
	ν	=	0.30	
	ρ	=	2700	kg/m^3
Air:	ρ	=	1.21	kg/m^3
	c	=	340	m/s.

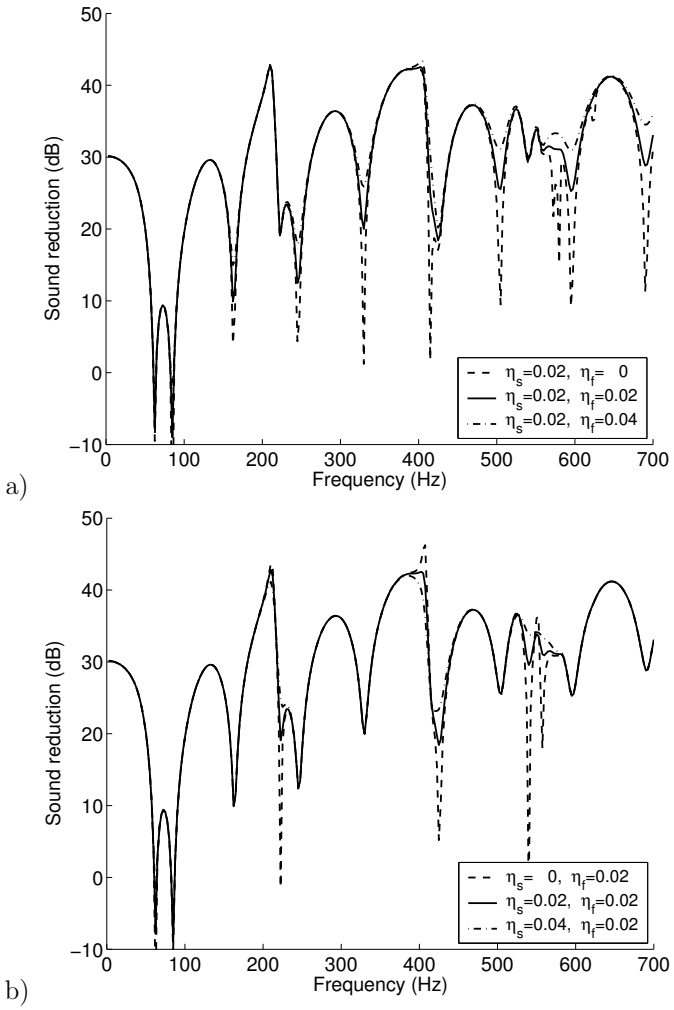

Figure 2: *Sound transmission loss* $20^{10}log\frac{\hat{p}_0}{\hat{p}_{back}}$. *a) The damping in the fluid domain is varied, b) the damping in the structural domain is varied.*

when the damping factors for the two domains are varied is plotted in Fig. 2. It can be concluded which subdomain dominate the behaviour at each transmission peak. For example, the first transmission peak, at 70 Hz, is dominated by a structural mode and increasing the structural damping increases the sound transmission loss. However, varying the damping in the fluid domain has little effect at this peak. The opposite behaviour can be seen at the second transmission peak, at 90 Hz, which is dominated by the fluid domain.

4 Conclusions

The reduction of a structure-acoustic system presented earlier [1] is conducted here with inclusion of hysteretic damping in both the structural and the fluid domain. The reduction of the coupled problem can be performed as in the undamped case, except that the damping introduces complex arithmetics that yields imaginary parts for both the eigenvalues and the eigenvectors. Although the description of the damping this provides is very much simplified it is efficient from an engineering point of view since accurate estimates of damping are often difficult to obtain. The proposed method can for example be used in the early design stage when detailed properties of the system is not known. The simplified damping description can be used to evaluate in which domain the effort must be put to reduce a certain response peak.

References

[1] G. Sandberg. A new strategy for solving fluid-structure problems. *International Journal of Numerical Methods in Engineering*, 38:357–370, 1995.

[2] G. Sandberg. Acoustic and interface elements for structure-acoustic analysis in calfem. TVSM 7113, Structural Mechanics, LTH, Lund University, Box 118, SE-221 00 Lund, Sweden, 1996.

[3] T. Pritz. Frequency dependences of complex moduli and complex Poisson's ratio of real solid materials. *Journal of Sound and Vibration*, 214(1):83–104, 1998.

[4] C. W. Bert. Material dmping: An introductory review of mathematical models, measures and experemental techniques. *Journal of Sound and Vibration*, 29(2):129–153, 1973.

[5] J. F. Allard. *Propagation of sound in porous media; modelling sound absorbing matarials*. Elsevier Science Publishers Ltd, London, 1993.

[6] P. Göransson. Acoustic finite element formulation of a flexible porous material– a correction for inertial effects. *Journal of Sound and Vibration*, 185(4):559–580, 1995.

[7] CALFEM – a finite element toolbox to matlab. Technical Report Report TVSM–9001, Lund University, 1996.

[8] J.-L. Batoz and M. B. Tahar. Evaluation of a new quadrilateral thin plate element. *International Journal of Numerical Methods in Engineering*, 18:1655–1677, 1982.

Paper 3

Substructuring and modal reduction of finite element formulated poroelastic systems

Peter Davidsson and Göran Sandberg
Division of Structural Mechanics,
Lund University

Substructuring and modal reduction of finite element formulated poroelastic systems

Peter Davidsson, Göran Sandberg
Division of Structural Mechanics, Lund University, Sweden

Abstract

A method, using substructuring and modal reduction, is proposed for the finite element analysis of the dynamic behaviour of porous sound absorption material bounded to a flexible structure; the porous material is described by Biot's theory. The system is divided into three physical subdomains: the flexible structural domain, and the structural and fluid partitions of the porous material. The interface modes, studying the structural subdomains in vacuo, are derived to fulfil the displacement continuity between the subdomains. These modes are used, together with a set of fixed interface normal modes for each of the subdomains, to describe the total system.

1 Introduction

The accurate description of porous absorption material, and its interaction with a flexible structure, is very important when studying various acoustical applications. For example, in attempting to improve passenger comfort regarding interior noise in vehicles, a very detailed description of the acoustic cavity (the compartment) and its boundaries – which can incorporate absorption material – are needed. Another example is the description of absorption material inside wall cavities when investigating sound transmission loss in lightweight double walls.

Porous sound absorption material can be modelled using Biot's theory [1, 2], in which the material is divided into two partitions: the structural partition, being the flexible frame material, and the fluid partition, being the fluid in the open pores. Both these partitions are described by the equations of continuum mechanics. The two partitions are coupled through Biot's stress–strain relationships, viscous forces and inertial forces. This problem has been studied within the finite element environment using displacement formulation in both partitions, a $\langle \mathbf{u}_s, \mathbf{u}_f \rangle$ formulation [3, 4, 5], or by a mixed displacement pressure formulation, a $\langle \mathbf{u}_s, p_f \rangle$ formulation [6, 7, 8]. Depending on the properties of the structural frame of the porous material, the modelling of the porous material can be simplified to that of an equivalent fluid. This is done by assuming the frame to be either rigid [2] or limp [9]. In this paper it is assumed that the flexibility of the structural frame must be included in the description. Biot's theory together with displacement formulation for both the structural and the fluid partition is used.

The poroelastic problem has been studied using a reduced base, starting from the $\langle \mathbf{u}_s, p_f \rangle$ formulation [10, 11]. The system matrices are complex and frequency dependent, which implies that a set of normal modes that uncouple the equations of motion cannot easily be derived. The analysis can be sped up, however, by deriving a set of basis vectors that can reduce the size of the equation system to be solved.

An efficient and widely used method for model reduction is the component mode synthesis (CMS) method [12]. In this method the studied problem domain is divided into a number of components, or subdomains, and a set of basis vectors is derived for each subdomain describing its behaviour as well as its coupling to the other subdomains. The degrees of freedom for each subdomain can be divided into interface and internal degrees of freedom. The interface degrees of freedom ensure that continuity of displacement between the subdomains is accomplished. Two main methods are used to calculate the basis vectors, either using fixed interface modes or free interface modes [13]. The present study uses the fixed interface method, where the set of basis vectors for each domain contains the constraint modes, calculated by applying a unit displacement at each interface degree of freedom while keeping the other interface degrees of freedom fixed, and the normal modes, calculated with the interface degrees of freedom fixed. Assembling the system using only the constraint modes, i.e. only retaining the interface degrees of freedom, and solving the eigenvalue problem of this system, allows the interface modes to be calculated [14, 15]. These modes give an efficient description of the displacement continuity, especially when a large number of interface degrees of freedom are present.

In this paper the studied system is divided into three physical subdomains: the flexible structural domain, and the two partitions of the porous material (being the structural and fluid partitions of this material). Each domain is described by the interface modes fulfilling the displacement continuity between the domains and by the fixed interface normal modes. The interface modes are derived by studying the structure in vacuo, i.e. the flexible structure and structural partition of the porous material. The fluid partition is not included in this analysis, but the interface vectors are also used in order to fulfil the displacement continuity between the flexible structure and the fluid partition of the porous material.

For the porous material, the fixed interface normal modes are calculated for the structural and fluid partitions by solving the eigenvalue problems of the two partitions separately, ignoring the coupling terms in Biot's theory. For the fluid partition, reduced integration and projection of the mass matrix is used to remove spurious non-zero modes [16, 17]. By using this procedure, all purely rotational modes will have the eigenvalue zero. The normal modes can be used as a reduced base for the poroelastic problem. However, due to the viscous and inertial coupling terms in Biot's theory, all purely rotational fluid modes must be included. This could lead to numerical problems and is moreover inefficient, because a large number of modes must be included. Instead, a number of modes having non-zero eigenvalues from both the structural and fluid partitions are combined into a set of basis vectors describing the fluid partition. This ensures that the rotational motion in the fluid partition induced by motion in the structural partition can be described correctly.

This method, that divides the system into physical subdomains, enables a large part of the analysis to be performed at the subdomain level before generating the total system. This aims at both faster computational times and increasing the frequency of interest.

The paper is organised as follows: After the introduction, the governing equations of Biot's theory are described and the finite element formulation of the problem is given. Then the

proposed method for substructuring and reduction is described. This is followed by a numerical example, where a porous material, bounded to a flexible panel, is excited by pressure distributions simulating the porous material being in contact with an acoustic cavity. The paper ends with a discussion and conclusions.

2 Method

2.1 Biot's theory

The porous material is described by Biot's theory, which includes sound propagation in both the flexible frame (the structural partition), and the fluid in the pores (the fluid partition). Both partitions are described using continuum mechanics and are coupled through volume preserving (dilatational), inertial and viscous coupling terms. The description of Biot's theory is based on the derivation in [2], and the matrix notation used to write the equations for easy implementation in the finite element analysis follows the example of [18].
The equations of motion in the frequency domain for a porous material without any body forces can be written, for the structural partition

$$\tilde{\boldsymbol{\nabla}}^T \boldsymbol{\sigma}_s = -\omega^2(\tilde{\rho}_{11}\mathbf{u}_s + \tilde{\rho}_{12}\mathbf{u}_f) \tag{1}$$

and for the fluid partition

$$\tilde{\boldsymbol{\nabla}}^T \boldsymbol{\sigma}_f = -\omega^2(\tilde{\rho}_{22}\mathbf{u}_f + \tilde{\rho}_{12}\mathbf{u}_s) \tag{2}$$

where $\omega = 2\pi f$ is the angular frequency (f is the frequency in Hz); the stress–strain relationship according to Biot's theory can be written in matrix notation, for the structural partition

$$\boldsymbol{\sigma}_s = \mathbf{D}_s\boldsymbol{\varepsilon}_s + \mathbf{Q}\boldsymbol{\varepsilon}_f \tag{3}$$

and for the fluid partition

$$\boldsymbol{\sigma}_f = \mathbf{Q}^T\boldsymbol{\varepsilon}_s + \mathbf{D}_f\boldsymbol{\varepsilon}_f \tag{4}$$

The stress and strain components in the three-dimensional partitions are

$$\boldsymbol{\sigma}_i = \begin{bmatrix} \sigma^i_{11} \\ \sigma^i_{22} \\ \sigma^i_{33} \\ \sigma^i_{12} \\ \sigma^i_{13} \\ \sigma^i_{23} \end{bmatrix};\ \boldsymbol{\varepsilon}_i = \begin{bmatrix} \varepsilon^i_{11} \\ \varepsilon^i_{22} \\ \varepsilon^i_{33} \\ \gamma^i_{12} \\ \gamma^i_{13} \\ \gamma^i_{23} \end{bmatrix} \tag{5}$$

where $i = \{s, f\}$ denotes the structural and fluid partitions. The displacements in the structural and fluid partitions are denoted

$$\mathbf{u}_i = \begin{bmatrix} u^i_1 \\ u^i_2 \\ u^i_3 \end{bmatrix} \tag{6}$$

and the matrix differential operator is

$$\tilde{\boldsymbol{\nabla}} = \begin{bmatrix} \dfrac{\partial}{\partial x_1} & 0 & 0 \\ 0 & \dfrac{\partial}{\partial x_2} & 0 \\ 0 & 0 & \dfrac{\partial}{\partial x_3} \\ \dfrac{\partial}{\partial x_2} & \dfrac{\partial}{\partial x_1} & 0 \\ \dfrac{\partial}{\partial x_3} & 0 & \dfrac{\partial}{\partial x_1} \\ 0 & \dfrac{\partial}{\partial x_3} & \dfrac{\partial}{\partial x_2} \end{bmatrix} \tag{7}$$

The constitutive matrices $\mathbf{D}_s$ and $\mathbf{D}_f$ and the coupling matrix $\mathbf{Q}$ are given by

$$\begin{gathered} \mathbf{D}_s = \begin{bmatrix} P & P-2G_s & P-2G_s & 0 & 0 & 0 \\ P-2G_s & P & P-2G_s & 0 & 0 & 0 \\ P-2G_s & P-2G_s & P & 0 & 0 & 0 \\ 0 & 0 & 0 & G_s & 0 & 0 \\ 0 & 0 & 0 & 0 & G_s & 0 \\ 0 & 0 & 0 & 0 & 0 & G_s \end{bmatrix} \\ \mathbf{D}_f = R \begin{bmatrix} 1 & 1 & 1 & 0 & 0 & 0 \\ 1 & 1 & 1 & 0 & 0 & 0 \\ 1 & 1 & 1 & 0 & 0 & 0 \\ 0 & 0 & 0 & 0 & 0 & 0 \\ 0 & 0 & 0 & 0 & 0 & 0 \\ 0 & 0 & 0 & 0 & 0 & 0 \end{bmatrix}; \quad \mathbf{Q} = Q \begin{bmatrix} 1 & 1 & 1 & 0 & 0 & 0 \\ 1 & 1 & 1 & 0 & 0 & 0 \\ 1 & 1 & 1 & 0 & 0 & 0 \\ 0 & 0 & 0 & 0 & 0 & 0 \\ 0 & 0 & 0 & 0 & 0 & 0 \\ 0 & 0 & 0 & 0 & 0 & 0 \end{bmatrix} \end{gathered} \tag{8}$$

where G_s is the shear modulus of the frame material related to the modulus of elasticity, E_s, and Poisson's ratio, ν_s. P and R are the bulk modulus of the structural and fluid partitions, respectively. The bulk modulus, P, of the structural partition can be expressed

$$P = \frac{4}{3}G_s + K_b + \frac{(1-\phi)^2}{\phi}K_f \tag{9}$$

and the bulk modulus, R, of the fluid partition

$$R = \phi K_f \tag{10}$$

The dilatational coupling coefficient, Q, is given by

$$Q = (1-\phi)K_f \tag{11}$$

The bulk modulus of the frame in vacuo is determined from

$$K_b = \frac{2G_s(\nu_s+1)}{3(1-2\nu_s)} \tag{12}$$

and the frequency-dependent bulk modulus of the fluid

$$K_f(\omega) = \frac{\gamma P_0}{\gamma - (\gamma - 1)\left[1 + \frac{\sigma'\phi}{\mathrm{i}\,\mathrm{Pr}\,\omega\rho_0\alpha_\infty} G'_J(\mathrm{Pr}\,\omega)\right]^{-1}} \tag{13}$$

where $\mathrm{i} = \sqrt{-1}$ and

$$G'_J(\mathrm{Pr}\,\omega) = \left[1 + \frac{4\mathrm{i}\alpha_\infty^2\eta\rho_0\omega\,\mathrm{Pr}}{\sigma'^2\Lambda'^2\phi^2}\right]^{1/2} \tag{14}$$

which is related to the thermal losses in the fluid to the solid frame. The material parameters for air, used in the description of the porous material, are density, ρ_0, mean pressure, P_0, viscosity, η, and the ratio between specific heat of unit mass at constant pressure and constant volume, γ. Pr denotes the Prandtl number. The values of these parameters for air, at the temperature 18°C, are given in Table 1. The porous material parameters depending on the geometry of the material are porosity, ϕ, flow resistivity, σ, tortuosity, α_∞, viscous characteristic length, Λ, and thermal characteristic length, Λ'. These material parameters are described in detail in [2] and are presented for the studied porous material in Table 1. The complex and frequency-dependent densities are

$$\begin{aligned}
\tilde{\rho}_{11} &= \rho_s + \rho_a - \mathrm{i}\sigma\phi^2\frac{G_J(\omega)}{\omega} \\
\tilde{\rho}_{12} &= -\rho_a + \mathrm{i}\sigma\phi^2\frac{G_J(\omega)}{\omega} \\
\tilde{\rho}_{22} &= \phi\rho_0 + \rho_a - \mathrm{i}\sigma\phi^2\frac{G_J(\omega)}{\omega}
\end{aligned} \tag{15}$$

where ρ_s is the structural density. These densities includes the inertial and viscous coupling between the structural and fluid partitions. $G_J(\omega)$ is related to the viscous losses and is given by

$$G_J(\omega) = \left[1 + \frac{4\mathrm{i}\alpha_\infty^2\eta\rho_0\omega}{\sigma^2\Lambda^2\phi^2}\right]^{1/2} \tag{16}$$

2.2 Boundary conditions

The conditions at the boundary between the flexible structure and the porous material bounded to the structure are

$$\begin{aligned}
\mathbf{u}_s &= \mathbf{u}_S \\
\mathbf{u}_f\mathbf{n} &= \mathbf{u}_S\mathbf{n}
\end{aligned} \tag{17}$$

where $\mathbf{n}$ denotes a boundary normal vector pointing outward from the porous material domain. The subscript, S, denotes the flexible structure, and s and f, denote the structural and fluid partitions of the porous material,respectively.

2.3 Finite element formulation

A flexible structure can be described using the finite element method by the system of equations

$$\left(-\omega^2 \mathbf{M}_S + \mathbf{K}_S\right) \mathbf{d}_S = \mathbf{f}_{bS} \tag{18}$$

where $\mathbf{d}_S$ contains the structural displacements, $\mathbf{M}_S$ and $\mathbf{K}_S$ are the mass and stiffness matrices and $\mathbf{f}_{bS}$ is the force vector.
For the porous material, by multiplying equations (1) and (2) by the weight functions, $\mathbf{v}_s$ and $\mathbf{v}_\mathbf{f}$, and integrating the results over region Ω, the weak formulation of the poroelastic problem can be derived. The next step is to introduce the finite element approximations of the structural and fluid displacements and the weight functions

$$\begin{aligned} \mathbf{u}_s &= \mathbf{N}_s \mathbf{d}_s; \quad \mathbf{u}_f = \mathbf{N}_f \mathbf{d}_f \\ \mathbf{v}_s &= \mathbf{N}_s \mathbf{c}_s; \quad \mathbf{v}_f = \mathbf{N}_f \mathbf{c}_f \end{aligned} \tag{19}$$

where $\mathbf{d}_s$ and $\mathbf{d}_f$ are the finite element displacements and $\mathbf{N}_s$ and $\mathbf{N}_f$ are the shape functions. The conditions at the boundary between the flexible structural domain and the porous material domain given in equation (17) can be expressed as a matrix equation

$$\mathbf{B} \begin{bmatrix} \mathbf{d}_S \\ \mathbf{d}_s \\ \mathbf{d}_f \end{bmatrix} = \mathbf{0} \tag{20}$$

The finite element system of equations for a porous material attached to a flexible structure can then be written

$$\left(-\omega^2 \begin{bmatrix} \mathbf{M}_S & \mathbf{0} & \mathbf{0} \\ \mathbf{0} & \mathbf{M}_{ss} & \mathbf{M}_{sf} \\ \mathbf{0} & \mathbf{M}_{fs} & \mathbf{M}_{ff} \end{bmatrix} + \begin{bmatrix} \mathbf{K}_S & \mathbf{0} & \mathbf{0} \\ \mathbf{0} & \mathbf{K}_{ss} & \mathbf{K}_{sf} \\ \mathbf{0} & \mathbf{K}_{fs} & \mathbf{K}_{ff} \end{bmatrix} \right) \begin{bmatrix} \mathbf{d}_S \\ \mathbf{d}_s \\ \mathbf{d}_f \end{bmatrix} = \begin{bmatrix} \mathbf{f}_{bS} \\ \mathbf{f}_{bs} \\ \mathbf{f}_{bf} \end{bmatrix} + \mathbf{B}^T \boldsymbol{\lambda}_{lagr} \tag{21}$$

where the last term includes Lagrange multipliers to fulfil the displacement continuity between the domains. The system matrices for the porous material are

$$\begin{aligned} \mathbf{M}_{ss} &= \tilde{\rho}_{11} \int_\Omega \mathbf{N}_s^T \mathbf{N}_s dV \qquad \mathbf{M}_{sf} = \tilde{\rho}_{12} \int_\Omega \mathbf{N}_s^T \mathbf{N}_f dV \\ \mathbf{K}_{ss} &= \int_\Omega \tilde{\boldsymbol{\nabla}} \mathbf{N}_s^T \mathbf{D}_s \tilde{\boldsymbol{\nabla}} \mathbf{N}_s dV \quad \mathbf{K}_{sf} = \int_\Omega \tilde{\boldsymbol{\nabla}} \mathbf{N}_s^T \mathbf{Q} \tilde{\boldsymbol{\nabla}} \mathbf{N}_f dV \\ \mathbf{f}_{bs} &= \int_{\partial\Omega} \mathbf{N}_s^T \mathbf{t}_s dS \end{aligned} \tag{22}$$

$$\begin{aligned} \mathbf{M}_{ff} &= \tilde{\rho}_{22} \int_\Omega \mathbf{N}_f^T \mathbf{N}_f dV \qquad \mathbf{M}_{fs} = \tilde{\rho}_{12} \int_\Omega \mathbf{N}_f^T \mathbf{N}_s dV \\ \mathbf{K}_{ff} &= \int_\Omega \tilde{\boldsymbol{\nabla}} \mathbf{N}_f^T \mathbf{D}_f \tilde{\boldsymbol{\nabla}} \mathbf{N}_f dV \quad \mathbf{K}_{fs} = \int_\Omega \tilde{\boldsymbol{\nabla}} \mathbf{N}_f^T \mathbf{Q}^T \tilde{\boldsymbol{\nabla}} \mathbf{N}_s dV \\ \mathbf{f}_{bf} &= \int_{\partial\Omega} \mathbf{N}_f^T \mathbf{t}_f dS \end{aligned} \tag{23}$$

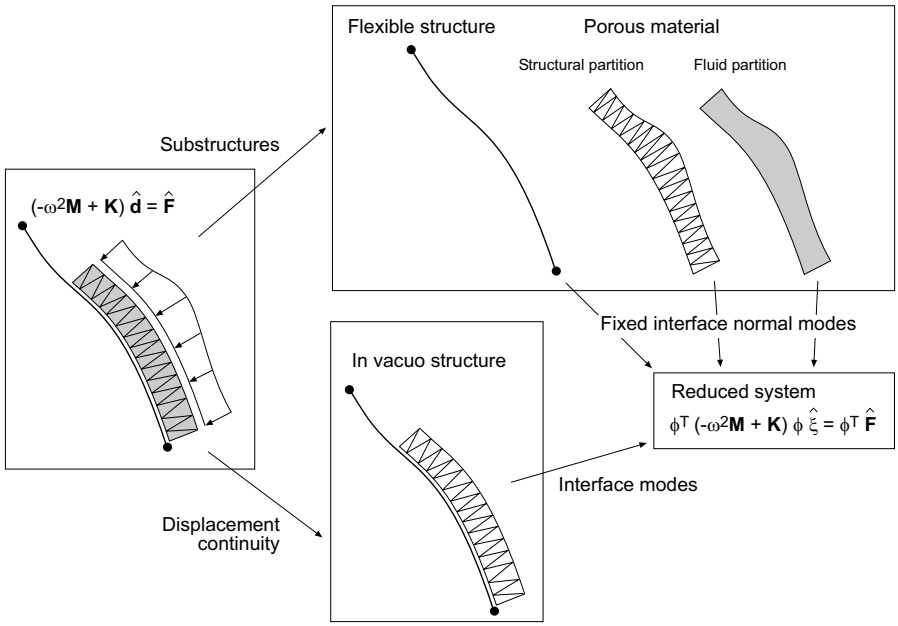

Figure 1: *Analysis method that generates the reduced system. A set of fixed interface modes is derived for each domain and the in vacuo structural interface modes are derived to fulfil the displacement continuity in equation (17).*

The external force terms $\mathbf{f}_{bs}$ and $\mathbf{f}_{bf}$ include the pressure exciting the system.
Performing frequency response analysis of poroelastic systems can often be very computationally intensive. The frequency limit of interest and the geometric complexity of the system determine the number of degrees of freedom of the model, and due to the frequency dependence of the system matrices, these must be regenerated in each step. However, in analysing large poroelastic systems most time is consumed in solving the system of equations. In the next section a method is proposed that reduces the size of the equation system and thereby speeds up the analysis.

2.4 Substructuring and modal reduction

A reduced set of basis vectors is derived for the system in equation (21) by means of substructuring and modal reduction. The component mode synthesis (CMS) method with fixed interface modes is used.
The proposed method is described in Figure 1. For each partition the constraint modes, $\boldsymbol{\psi}_{bi}$, derived by applying a unit force at each interface degree of freedom while keeping the other interface degrees of freedom fixed, and the fixed interface normal modes, $\boldsymbol{\phi}_i$, derived by modal analysis with the interface degrees of freedom fixed, are used in the reduction,

$$\mathbf{d}_i = \begin{bmatrix} \boldsymbol{\psi}_{bi} & \boldsymbol{\phi}_i \end{bmatrix} \begin{bmatrix} \mathbf{d}_{bi} \\ \boldsymbol{\xi}_i \end{bmatrix} \tag{24}$$

where $i = \{S, s, f\}$. In the method, the structural domains (the flexible structural domain and the structural partition of the porous material) are first examined in vacuo, i.e. the fluid partition of the porous material is not included. The displacements are partitioned into boundary degrees of freedom connecting to the opposite domain, $\mathbf{d}_{bi}$, and degrees of freedom of the interior of the domain, $\mathbf{d}_{di}$. The continuity between the flexible structure and the structural partition of the porous material can be written

$$\left[\begin{array}{cc} \mathbf{I} & -\mathbf{I} \end{array} \right] \left[\begin{array}{c} \mathbf{d}_{bS} \\ \mathbf{d}_{bs} \end{array} \right] = \mathbf{C} \left[\begin{array}{c} \mathbf{d}_{bS} \\ \mathbf{d}_{bs} \end{array} \right] \tag{25}$$

where the the interior degrees of freedom, which can either be expressed by physical degrees of freedom, $\mathbf{d}_{di}$, or generalised degrees of freedom, $\boldsymbol{\xi}_i$, are excluded. The displacements can then be expressed, using the fixed interface method, as

$$\left[\begin{array}{c} \mathbf{d}_{bS} \\ \mathbf{d}_{dS} \\ \mathbf{d}_{bs} \\ \mathbf{d}_{ds} \end{array} \right] = \left[\begin{array}{ccc} \boldsymbol{\psi}_{bS} & \boldsymbol{\phi}_S & \mathbf{0} \\ \boldsymbol{\psi}_{bs} & \mathbf{0} & \boldsymbol{\phi}_s \end{array} \right] \left[\begin{array}{c} \mathbf{d}_{bS} \\ \boldsymbol{\xi}_S \\ \boldsymbol{\xi}_s \end{array} \right] = \mathbf{T} \left[\begin{array}{c} \mathbf{d}_{bS} \\ \boldsymbol{\xi}_S \\ \boldsymbol{\xi}_s \end{array} \right] \tag{26}$$

Using this set of basis vectors to reduce the system would not be efficient due to the large number of degrees of freedom at the boundary $\mathbf{d}_{bS}$. Therefore, the interface modes are calculated by performing modal analysis of the system derived when only retaining the boundary degrees of freedom for the in vacuo structure, i.e. $\mathbf{T} = \left[\begin{array}{cc} \boldsymbol{\psi}_{bS} & \boldsymbol{\psi}_{bs} \end{array} \right]^T$, and the reduced system can be written

$$\begin{aligned} \left(-\omega^2 \mathbf{T}^T \left[\begin{array}{cc} \mathbf{M}_S & \mathbf{0} \\ \mathbf{0} & \mathbf{M}_{ss} \end{array} \right] \mathbf{T} + \mathbf{T}^T \left[\begin{array}{cc} \mathbf{K}_S & \mathbf{0} \\ \mathbf{0} & \mathbf{K}_{ss} \end{array} \right] \mathbf{T} \right) \mathbf{d}_{bS} = \\ = \mathbf{T}^T \left[\begin{array}{c} \mathbf{f}_{bS} \\ \mathbf{f}_{bs} \end{array} \right] + \mathbf{T}^T \mathbf{C}^T \tilde{\boldsymbol{\lambda}}_{lagr} \end{aligned} \tag{27}$$

Because $\mathbf{T}^T \mathbf{C}^T = \mathbf{0}$, and the system matrices in equation (27) denoted $\mathbf{M}_b$ and $\mathbf{K}_b$, the eigenvalue problem deriving the interface modes can be written

$$\lambda_s \mathbf{M}_b \boldsymbol{\phi}_b = \mathbf{K}_b \boldsymbol{\phi}_b \tag{28}$$

The derived eigenvectors, $\boldsymbol{\phi}_b$, are transformed back to original co-ordinates by

$$\left[\begin{array}{c} \boldsymbol{\Psi}_{bS} \\ \boldsymbol{\Psi}_{bs} \end{array} \right] = \left[\begin{array}{cc} \boldsymbol{\psi}_{bS} & 0 \\ 0 & \boldsymbol{\psi}_{bs} \end{array} \right] \mathbf{T} \boldsymbol{\phi}_b \tag{29}$$

These interface modes can also be used to fulfil the continuity of the displacements between the flexible structure and the fluid partition of the porous material by using the same interface vectors as were used for the structural partition. The displacements can be expressed in a reduced base by

$$\left[\begin{array}{c} \mathbf{d}_S \\ \mathbf{d}_s \\ \mathbf{d}_f \end{array} \right] = \left[\begin{array}{cccc} \boldsymbol{\Psi}_{bS} & \boldsymbol{\phi}_S & 0 & 0 \\ \boldsymbol{\Psi}_{bs} & 0 & \boldsymbol{\phi}_s & 0 \\ \boldsymbol{\Psi}_{bs} & 0 & 0 & \boldsymbol{\phi}_f \end{array} \right] \left[\begin{array}{c} \boldsymbol{\xi}_{bS} \\ \boldsymbol{\xi}_S \\ \boldsymbol{\xi}_s \\ \boldsymbol{\xi}_f \end{array} \right] \tag{30}$$

Only a few interface modes in the first column are now needed to fulfil the displacement continuity. This can be compared to using the constraint modes in equation (26), where all boundary degrees of freedom must be included.
To calculate the fixed interface normal modes for the partitions of the porous material, the structural and fluid partitions are uncoupled by assuming that the dilatational coupling coefficient, Q, is zero and by ignoring viscous and thermal damping effects. This assumption yields zero viscous forces and a constant bulk modulus, $K_f = P_0$, of the fluid domain [19]. The added density described by the tortuosity is included in the fluid mass matrix, and the effective density of the fluid partition thereby becomes $\alpha_\infty \rho_0$. The eigenvalue problem for the structural domain becomes

$$\lambda_s \mathbf{M}_{ss} \boldsymbol{\phi}_s = \mathbf{K}_{ss} \boldsymbol{\phi}_s \tag{31}$$

and for the fluid domain

$$\lambda_f \mathbf{M}_{ff} \boldsymbol{\phi}_f = \mathbf{K}_{ff} \boldsymbol{\phi}_f \tag{32}$$

where λ_i and $\boldsymbol{\phi}_i$ are the eigenvalue and eigenvector of domain $i = \{s, f\}$. Numerical problems are encountered for the fluid partition due to the lack of shear stiffness. Therefore, reduced integration and projection of the element mass matrix is used [17]. The zero energy modes for an 8-node hexahedral element can be found in, for example, [20]. The solution of the eigenvalue problem of the fluid partition yields a large number of rotational modes with no change in the volume of the elements and therefore with $\lambda_f = 0$ and a set of modes corresponding to dilatation with $\lambda_f > 0$. The straightforward way would now be to use a set of fluid eigenvectors with non-zero eigenvalues to reduce the system, i.e. using $\boldsymbol{\phi}_f = \boldsymbol{\phi}_f^{\lambda_f > 0}$ in equation (30). However, the zero energy fluid modes have to be included because they are needed to describe the motion due to inertial and viscous coupling between the fluid and structural domains. A large number of modes must be included, leading to an inefficient reduction procedure. Instead, a combined set of basis vectors is introduced to describe to the fluid domain, combining the structural and non-zero fluid normal modes

$$\boldsymbol{\phi}_f = \begin{bmatrix} \boldsymbol{\phi}_f^{\lambda_f > 0} & \boldsymbol{\phi}_s \end{bmatrix} \tag{33}$$

This set of basis vectors could, however, contain linearly dependent vectors, in which case the Gram-Schmidt method [21], for example, could be used to achieve an orthogonal set of basis vectors. Structural eigenvectors that are linearly dependent on the fluid eigenvectors are not included in equation (33). The combined set of basis vectors is used in equation (30) and ensures that rotations induced by the structural partition in the fluid partition are correctly described.

3 Numerical example

In the numerical example, the need to use the combined base for the fluid partition of the porous material is shown and a convergence study of the number of modes to be included is performed.
A porous material sample of 0.3 m in length (x direction), 0.02 m in width (y direction) and 0.10 m in depth (z direction) is bounded to a flexible aluminium panel at $z = 0$ m (see Figure 2). The panel is 0.003 m thick and is constrained in translation at $x = 0$ m

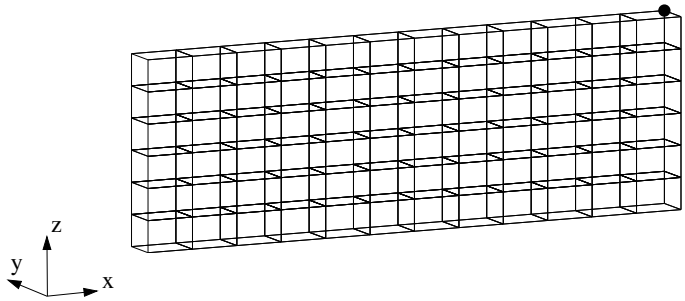

Figure 2: *Finite element model of the investigated problem. At $z = 0$ m, shell elements describe the aluminium panel. The marker shows where the velocity is studied.*

and $x = 0.30$ m. Boundary conditions are applied to achieve a two-dimensional behaviour, simulating the system having infinite extension in the y direction. The porous material is unbounded along the side walls, i.e. it can move parallel to the walls at $x = 0$ m and $x = 0.3$ m. In the finite element model, the porous material is described using an 8-node isoparametric element with six degrees of freedom in each node, while the flexible panel is described by a 4-node shell element with six degrees of freedom in each node. The shell element is an assembly of the thin plate element derived in [22] and the membrane element, with drilling degrees of freedom, derived in [23]. The material properties of the porous material and flexible panel are given in Table 1. The porous material properties can be found in [5]; the material was chosen to give a relatively high degree of stiffness in the structural frame.
To derive the subdomain modes, the eigenvalue problems of the two porous material partitions are solved, but with the interface degrees of freedom fixed. The shapes of the two fluid modes with the lowest natural frequencies are plotted in Figure 3, and the shapes of the structural modes are plotted in Figure 4. Also, the interface modes are derived for the in vacuo structural domains; Figure 5 displays the two modes with the lowest natural

Table 1: *Material data for air, the porous material and the flexible aluminium panel.*

Porous material:				Air (at 18°):			
E_s	=	845	kPa	ρ_0	=	1.21	kg/m^3
ν_s	=	0.3		P_0	=	$1.0132 \cdot 10^5$	Pa
η_s	=	0.1		γ	=	1.4	
ρ_s	=	30	kg/m^3	Pr	=	0.71	
ϕ	=	0.96		η	=	$1.84 \cdot 10^{-5}$	
σ	=	32000	Ns/m^4	Aluminium:			
α_∞	=	1.7		E	=	71	GPa
Λ	=	$90 \cdot 10^{-6}$	m	ν	=	0.3	
Λ'	=	$165 \cdot 10^{-6}$	m	ρ	=	2800	kg/m^3

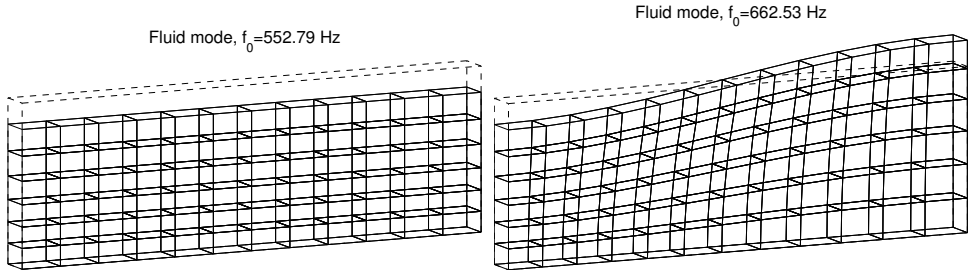

Figure 3: *Examples of mode shapes for the fluid partitions.*

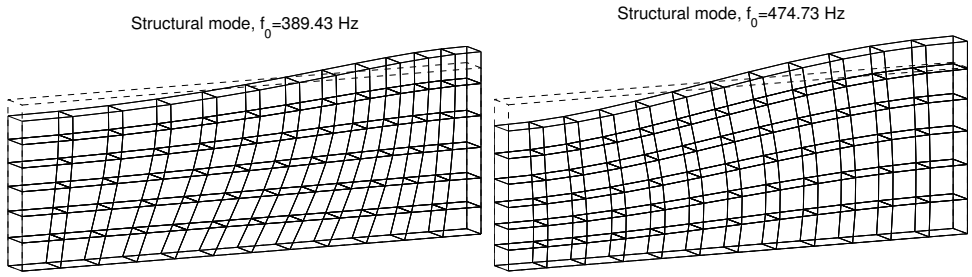

Figure 4: *Examples of mode shapes for the structural partitions with unbounded sides.*

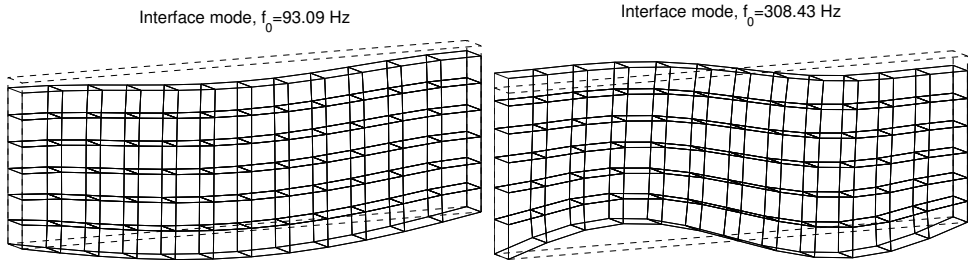

Figure 5: *Examples of interface modes.*

frequencies. To show the need to include a combined base using both structural and fluid modes to describe the fluid partition according to equation (33), the panel is assumed to be rigid and the system is excited by two load cases, first a uniform unit pressure and second a pressure distributed as a cosine function in the x direction, with a value of 1 at $x = 0$ m and of -1 at $x = 0.3$ m. The excitation is chosen to resemble two possible pressure distributions when the porous material is in contact with an acoustic fluid cavity. The velocity in the z direction at the corner node marked in Figure 2 is determined. The system is analysed using three different methods:

- Solving the total system having 1248 degrees of freedom

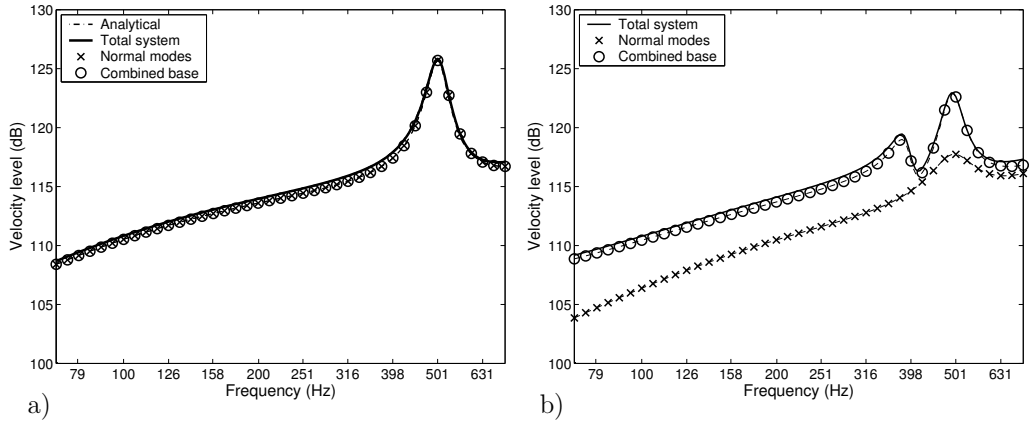

Figure 6: *Fluid velocity amplitude in the z direction when the porous material is excited by: a) a uniformly distributed pressure, and b) a cosine distribution of the pressure in the x direction*

- Reducing each partition with its non-zero eigenmodes using 40 modes for each domain
- Reducing the system using a combined base, equation (33), for the fluid domain derived from the 40 modes from each domain.

For the uniform pressure the results are also compared with the analytical solution. The velocity amplitude in the z direction for the fluid partition can be seen in Figure 6 for both the uniform and cosine distributions of the pressure.
A convergence study investigating the full system, including the flexible panel, is performed. The number of modes from the porous material partitions as well as the number of interface

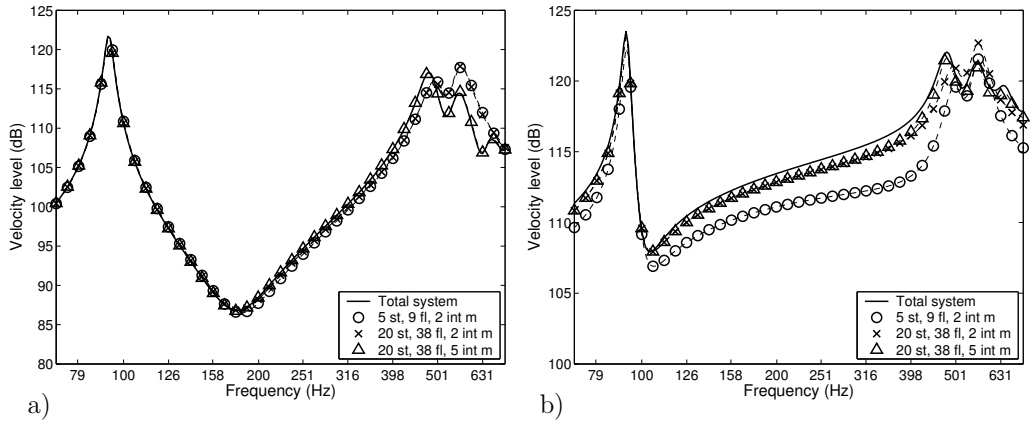

Figure 7: *Velocity amplitude in the z direction when the porous material is excited by a uniformly distributed pressure: a) shows the structural partition, and b) the fluid partition.*

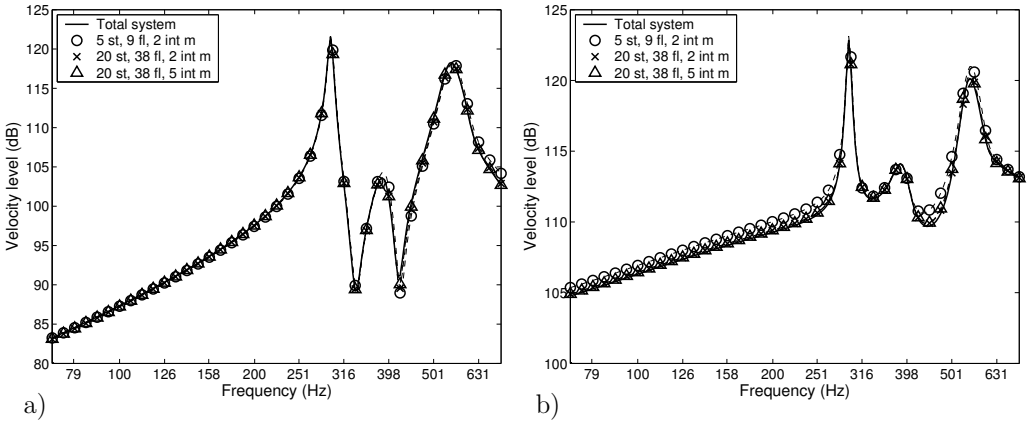

Figure 8: *Velocity amplitude in the z direction when the porous material is excited by a cosine distribution of the pressure in the x direction: a) shows the structural partition, and b) the fluid partition.*

modes included are varied. The velocity amplitude at the studied degree of freedom, when the system is excited by the previously defined pressure distributions, is displayed in Figures 7 and 8. The velocity level of both the structural and fluid partitions is displayed and the number of modes for the structural and fluid partitions and the number of interface modes are given in the legend.

4 Discussion and Conclusions

When the system is excited by a uniformly distributed pressure, the results from solving the total system agree with the analytical solution (see Figure 6 a). Both of the reduced set of basis vectors can also describe the motion of the porous material, i.e. the non-zero normal modes of the two domains are sufficient to describe the motion. However, for the case with non-uniform excitation (see Figure 6 b), the combined base is needed to reduce the system. The proposed combined base can describe the velocity distribution correctly, whereas the set of basis vectors with separate normal modes for each domain, removing the possibility of the fluid rotating, cannot describe the motion of the porous material.
In the convergence study, Figures 7 and 8, it is shown that the number of modes needed to describe the motion is limited compared to the total number of degrees of freedom. At the response peaks the corresponding modes dominate the behaviour, and the velocity is determined correctly if the excited mode is included in the reduced set of basis vectors. The proposed method enables an accurate description of the dynamic behaviour of the system, using a limited number of modes. It can be concluded from Figures 7 and 8 that, although the system matrices are frequency dependent, the same set of basis vectors can be used for different excitations across a wide frequency range.
However, the uncoupled modes are calculated with the surface, at which the pressure is applied, being unconstrained, i.e. the pressure is equal to zero. The convergence should therefore be considerably improved by using load-dependent basis vectors. This topic will

be studied in a subsequent paper.

5 Acknowledgements

The authors wish to thank their colleagues and friends at the Division of Structural Mechanics and Division of Engineering Acoustics, especially Dr. Jonas Brunskog. The Swedish Foundation for Strategic Research (project number IVS-98-501) is gratefully acknowledged for the financial support.

References

[1] M. A. Biot, Theory of propagation of elastic waves in fluid-saturated porous solid. i. low frequency range, The Journal of the Acoustical Society of America 28 (2) (1956) 168–178.

[2] J. F. Allard, Propagation of sound in porous media; modelling sound absorbing matarials, Elsevier Science Publishers Ltd, London, 1993.

[3] J. P. Coyette, The use of finite-element and boundary-element models for predicting the vibro-acoustic behaviour of layered structures, Adv. Eng. Soft. 30 (1) (1999) 133–139.

[4] Y. J. Kang, J. S. Bolton, Finite element modeling of isotropic elastic porous materials coupled with coustical finite elements, The Journal of the Acoustical Society of America 98 (1) (1995) 635–643.

[5] N. Dauchez, S. Sahraoui, N. Atalla, Convergence of poroelastic finite elements based on biot displacement formulation, The Journal of the Acoustical Society of America 109 (1) (2001) 33–40.

[6] N. Atalla, R. Panneton, P. Debergue, A mixed displacement pressure formulation for poroelastic materials, The Journal of the Acoustical Society of America 104 (3) (1998) 1444–1452.

[7] P. Göransson, A 3-d, symmetric, finite element formulation of the biot equations with application to acoustic wave propagation through an elastic porous medium, International Journal of Numerical Methods in Engineering 41 (1998) 167–192.

[8] N.-E. Hörlin, M. Nordström, P. Göransson, A 3-d hierarchical fe formulation of biot's equations for elasto-acoustic modelling of porous media, Journal of Sound and Vibration 245 (4) (2001) 633–652.

[9] P. Göransson, Acoustic finite element formulation of a flexible porous material– a correction for inertial effects, Journal of Sound and Vibration 185 (4) (1995) 559–580.

[10] F. Sgard, N. Atalla, R. Panneton, A modal reduction technique for the finite element formulation of the biot's poroelasticity equations in acoustics applied to multilayered structures, 135^{th} ASA Meeting (1998) 1183–1184.

[11] O. Dazel, F. Sgard, C.-H. Lamarque, N. Atalla, An extention of complex modes for the resolution of finite-element poroelastic problems, Journal of Sound and Vibration 253 (2) (2002) 421–445.

[12] P. Seshu, Substructuring and component mode synthesis, Shock and Vibration 4 (3) (1997) 199–210.

[13] R. R. Craig, Structural Dynamics; An introduction to computer methods, John Wiley & Sons Inc., New York, 1981.

[14] F. Bourquin, F. d'Hennezel, Numerical study of an intrinsic component mode synthesis method, Computer methods in applied mechanics and engineering 97 (1992) 49–76.

[15] F. Bourquin, F. d'Hennezel, Intrinsic component mode synthesis and plate vibrations, Computers & Structures 44 (1992) 315–324.

[16] N. Akkas, H. U. Akay, C. Yilmaz, Applicability of general-purpose finite element programs in solid-fluid interaction problems, Computers & Structures 10 (1979) 773–783.

[17] H. . C. Chen, R. L. Taylor, Vibration analysis of fluid-solid systems using a finite element displacement formulation, International Journal of Numerical Methods in Engineering 29 (1990) 683–698.

[18] N. Ottosen, H. Peterson, Introduction to the Finite Element Method, Prentice Hall, New York, 1992.

[19] M. Brennan, W. M. To, Acoustic properties of rigid-frame porous materials – an engineering perspective, Applied Acoustics 62 (2001) 793–811.

[20] T. Belytschko, J. S.-J. Ong, W. K. Liu, J. M. Kennedy, Hourglass control in linear and nonlinear problems, Computer methods in applied mechanics and engineering 42 (1984) 251–276.

[21] K.-J. Bathe, Finite Element Procedures, Prentice Hall, New York, 1996.

[22] J.-L. Batoz, M. B. Tahar, Evaluation of a new quadrilateral thin plate element, International Journal of Numerical Methods in Engineering 18 (1982) 1655–1677.

[23] R.-H. MacNeal, L. H. Harder, A refined four-noded membrane element with rotational degrees of freedom, Computers & Structures 28 (1) (1988) 75–84.

Paper 4

A reduction method for structure-acoustic and poroelastic-acoustic problems using interface-dependent Lanczos vectors

Peter Davidsson and Göran Sandberg
Division of Structural Mechanics,
Lund University

A reduction method for structure-acoustic and poroelastic-acoustic problems using interface-dependent Lanczos vectors

Peter Davidsson, Göran Sandberg
Division of Structural Mechanics, Lund University, Sweden

Abstract

A reduction method is proposed for analysing structure-acoustic and poroelastic-acoustic problems within a finite element framework. This includes systems consisting of an acoustic fluid domain coupled to a flexible structural domain and/or a porous sound absorbing material domain. The studied problem is reduced by dividing the system into a number of physical subdomains. A set of basis vectors is derived for each of these subdomains, including both normal modes and interface-dependent vectors that take account of the influence of connecting subdomains.
The method is verified in two numerical examples using the proposed method for both solving the structure-acoustic eigenvalue problem and performing a frequency response analysis in an acoustic cavity with one wall covered by porous material.

1 Introduction

This paper investigates the sound pressure distribution in enclosed acoustic cavities using finite element analysis. The studied system is typically a vehicle structure with an interior passenger compartment, illustrated in Figure 1. As vehicles develop towards being more fuel efficient and with a greater focus on stiffness in the interest of crashworthiness, lighter and stiffer construction can introduce the problem of interior noise. Therefore, the need to conduct detailed analysis of acoustic comfort is increasing.
In the finite element analysis of acoustic problems, the increase of the frequency limit of interest, the need to resolve the details of complex geometries in the finite element model and the inclusion of advanced material descriptions to model, for example, porous sound absorption material, lead to a rapid increase in the number of degrees of freedom in the model. Efficient techniques for solving such large equation systems are thus of great importance.
This structure-acoustic problem has been studied by several authors using the finite element method, and several different formulations have been proposed [1, 2, 3]. The difference between these formulations lies in the way the fluid domain is described. The fluid can be described by a displacement formulation which, due to the lack of shear stiffness, introduces spurious modes. Using reduced integration [4] and control of the hourglass modes [5], all

pure rotational modes have the eigenvalue zero. This procedure is adopted in this paper when studying the fluid partition of the porous material. The most straightforward and compact method for describing the fluid in structure-acoustic systems is to start with the acoustic wave equation using a potential description, for example, of pressure, with only one degree of freedom in each node [6]. The drawback is that the system matrices of this two-field formalisation become unsymmetric. If one instead uses both pressure and velocity potential to describe the fluid, symmetric system matrices are generated; however, this three-field formulation uses two degrees of freedom in each node, thereby increasing the total number of degrees of freedom of the system [7].
The dominant method for model reduction is the component mode synthesis method [8, 9]. The studied physical domain is divided into a number of components and a set of basis vectors is derived for each component to be included in the description of the entire system. This procedure is also adopted in the model reduction of structure-acoustic problems starting with the unsymmetric two-field formulation [3, 10, 11, 12, 13, 14]. The eigenvalue problems of the structural and fluid domains are first solved separately. The coupled system is then reduced by the calculated normal modes. The reduced unsymmetric system can, by using some matrix manipulations, be written as a symmetric standard eigenvalue problem [15]. A large number of eigenmodes must be included in the reduction to describe the coupled problem correctly, and only the most important of these modes can be chosen to be included in the reduction to decrease the problem size [16], paper 1.
The Lanczos procedure, described in, for example, [17], can be used when deriving the

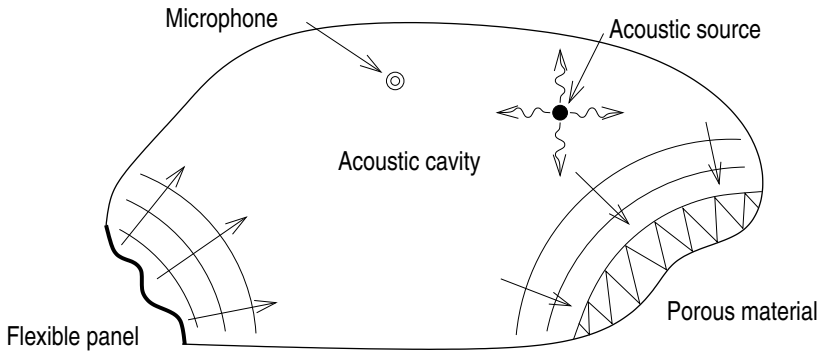

Figure 1: *Problem description: The vibrating panels generate noise inside the enclosed cavity where the noise can be reduced by the use of porous material. The noise, measured by a microphone at some point in the cavity, can also be generated by an acoustic source.*

normal modes for each component. It has also been used to derive load-dependent Lanczos vectors, achieving a very efficient basis for each excitation of the studied system, which has been applied to a symmetric three-field formulation of a structure-acoustic system in [2].
In modelling porous sound absorption material, Biot's theory can be adopted in order to include both the flexible frame material and the fluid in the open pores in the description [18, 19]. This is necessary when the flexibility of the frame material is important to the behaviour of the system. Both domains are then described by the equations of continuum mechanics. This theory has been implemented in the finite element environment using a $\langle \mathbf{u}_s, \mathbf{u}_f \rangle$ formulation [20, 21, 22], i.e. both the structural and fluid partitions are described by displacements, and using a $\langle \mathbf{u}_s, p_f \rangle$ formulation [23, 24, 25], i.e. the fluid partition is described by acoustic pressure. The problem with a porous material in contact with an acoustic cavity using a two-dimensional model is studied in [20]. The poroelastic problem has also been investigated using a reduced set of basis vectors starting from the $\langle \mathbf{u}_s, p_f \rangle$ formulation [26, 27].
The present paper examine two important properties in investigating sound pressure distribution in enclosed acoustic cavities: interaction with connecting flexible panels, and energy absorption in connecting porous sound absorption materials. A method is proposed for solving structure-acoustic and poroelastic-acoustic problems, based on substructuring and modal reduction. The system is divided into its physical domains and a set of basis vectors for each of the domains is derived based on the free motion of the studied domain and the normal mode characteristics of the connecting domains. The subdomain modes below the frequency limit of interest are first evaluated. This applies to both the structure-acoustic and poroelastic-acoustic analyses. The influence of the subdomain modes above the frequency limit is accounted for using the fact that the coupling between the subdomains is described by force terms. For example, the pressure distribution in the acoustic fluid domain results in forces that act on the structure or porous material. The spatial distribution of each calculated acoustic fluid mode at the boundary of the opposite domain, which is either the flexible structure or the porous material, is used in a Lanczos procedure to derive interface-dependent vectors for that domain. These vectors are then included in the set of basis vectors for the reduction of the coupled problem. The same procedure is employed in the opposite direction. This method derives an efficient reduced base for the studied problems. The structure-acoustic eigenvalue problem can be solved efficiently and a reduced set of basis vectors for the poroelastic-acoustic problem is derived, which can be used for response analysis over a wide frequency range. The method only involves well-known finite element tools and should be easily implemented in any standard finite element environment.
The paper is organised as follows: The proposed method is described after a short presentation of the involved theory. Two numerical examples are then presented and examined. The first, a coupled structure-acoustic eigenvalue problem consisting of a flexible panel and an enclosed acoustic cavity, is solved. The second is the evaluation of the pressure level in an acoustic cavity, one wall of which is covered by porous material, when the cavity is excited by a volume velocity source placed in a corner. The paper ends with a discussion and conclusions.

2 Method

2.1 Structural-acoustic analysis

The coupled system for the structure-acoustic problem is derived using the finite element method. The structural domain is described by the system of equations

$$\mathbf{M}_S\ddot{\mathbf{d}}_S + \mathbf{K}_S\mathbf{d}_S = \mathbf{f}_b + \mathbf{f}_F \tag{1}$$

where $\mathbf{d}_S$ contains the displacements, and $\mathbf{M}_S$ and $\mathbf{K}_S$ are the structural mass and stiffness matrices, respectively. The external forces are contained by $\mathbf{f}_b$, and $\mathbf{f}_F$ contains the forces acting on the structure from the fluid domain

$$\mathbf{f}_F = \mathbf{H}_{SF}\mathbf{p}_F \tag{2}$$

where $\mathbf{H}_{SF}$ describes the spatial coupling between the structural domain and the acoustic fluid domain. The governing system of equations of fluid domain can be written

$$\mathbf{M}_F\ddot{\mathbf{p}}_F + \mathbf{K}_F\mathbf{p}_F = \mathbf{f}_q + \mathbf{f}_S \tag{3}$$

where $\mathbf{p}_F$ contains the acoustic pressures, and $\mathbf{M}_F$ and $\mathbf{K}_F$ are the fluid mass and stiffness matrices, respectively. The external source terms are contained by $\mathbf{f}_q$, and $\mathbf{f}_S$ contains the forces acting on the fluid from the structural domain

$$\mathbf{f}_S = -\rho c^2\mathbf{H}_{SF}^T\ddot{\mathbf{d}}_S \tag{4}$$

The coupled problem can then be written

$$\begin{bmatrix} \mathbf{M}_S & \mathbf{0} \\ \rho c^2\mathbf{H}_{SF}^T & \mathbf{M}_F \end{bmatrix}\begin{bmatrix} \ddot{\mathbf{d}}_S \\ \ddot{\mathbf{p}}_F \end{bmatrix} + \begin{bmatrix} \mathbf{K}_S & -\mathbf{H}_{SF} \\ 0 & \mathbf{K}_F \end{bmatrix}\begin{bmatrix} \mathbf{d}_S \\ \mathbf{p}_F \end{bmatrix} = \begin{bmatrix} \mathbf{f}_b \\ \mathbf{f}_q \end{bmatrix} \tag{5}$$

The system is unsymmetric due to the coupling and therefore both the left and right eigenvectors, or normal modes, are needed to diagonalise the system. Further description of the system matrices is given in [28, 16]. The coupled system in equation (5) is reduced by the change of base

$$\begin{bmatrix} \mathbf{d}_S \\ \mathbf{p}_F \end{bmatrix} = \begin{bmatrix} \mathbf{\Phi}_S & \mathbf{0} \\ \mathbf{0} & \mathbf{\Phi}_F \end{bmatrix}\begin{bmatrix} \boldsymbol{\xi}_S \\ \boldsymbol{\xi}_F \end{bmatrix} \tag{6}$$

using the normal modes of the two subdomains: $\mathbf{\Phi}_S$ contains the structural normal modes, and $\mathbf{\Phi}_F$ the fluid normal modes.
The reduced coupled system is transformed into a symmetric system using a number of matrix manipulations

$$\begin{bmatrix} \ddot{\boldsymbol{\zeta}}_S \\ \ddot{\boldsymbol{\zeta}}_F \end{bmatrix} + \begin{bmatrix} \mathbf{\Lambda}_S & -\sqrt{\rho c^2}\sqrt{\mathbf{\Lambda}_S}\mathbf{\Phi}_S^T\mathbf{H}_{SF}\mathbf{\Phi}_F \\ -\sqrt{\rho c^2}\mathbf{\Phi}_F^T\mathbf{H}_{SF}^T\mathbf{\Phi}_S\sqrt{\mathbf{\Lambda}_S} & \mathbf{\Lambda}_F + \rho c^2\mathbf{\Phi}_F^T\mathbf{H}_{SF}^T\mathbf{\Phi}_S\mathbf{\Phi}_S^T\mathbf{H}_{SF}\mathbf{\Phi}_F \end{bmatrix}\begin{bmatrix} \boldsymbol{\zeta}_S \\ \boldsymbol{\zeta}_F \end{bmatrix} = \begin{bmatrix} \sqrt{\rho c^2}\sqrt{\mathbf{\Lambda}_S}\mathbf{\Phi}_S^T\mathbf{f}_b \\ \mathbf{\Phi}_F^T\mathbf{f}_q - \rho c^2\mathbf{\Phi}_F^T\mathbf{H}_{SF}^T\mathbf{\Phi}_S\mathbf{\Phi}_S^T\mathbf{f}_b \end{bmatrix} \tag{7}$$

where $\mathbf{\Lambda}_S$ and $\mathbf{\Lambda}_F$ contain the eigenvalues of the structural and fluid domains. This procedure is described in [15, 28]. Solving the eigenvalue problem of equation (7) gives the

eigenvalues and the right eigenvectors of the system. A large number of subdomain normal modes, i.e. large number of members of $\mathbf{\Phi}_S$ and $\mathbf{\Phi}_F$, must be included in the reduction in order to achieve a good description of the coupled system. A previous study, [16], Paper 1, proposed a method for determining the most important of these normal modes for describing the coupled system. In the present paper, the subdomain modes are calculated using information from the other domain, reducing the need to calculate most of the subdomain normal modes, further increasing the simulation speed-up compared to [16].
The Lanczos procedure, described in Table 1, is used to solve the eigenvalue problem [17]. In the procedure, also used in the proposed method and therefore described in detail, an arbitrary force vector, $\mathbf{r}$, is first generated. For this force vector a Lanczos stage is performed (Steps 3 to 6). A start vector, $\mathbf{x}_1$, is calculated (Step 3), which must be non-orthogonal to the desired normal modes. For this start vector, a set of Lanczos vectors is derived and the normal modes are calculated. A convergence check controls whether all eigenmodes below a frequency limit are derived. If not, either more Lanczos vectors are derived or the Lanczos stage is restarted with a new start vector. A new shift point, μ in Step 1, can be used in the restart to improve convergence.

2.2 Poroelastic-acoustic analysis

The system of equations describing the frequency response analysis of an acoustic fluid in contact with a porous sound absorption material, described by Biot's theory, can be written

$$\left(-\omega^2 \begin{bmatrix} \mathbf{M}_{ss} & \mathbf{M}_{sf} & 0 \\ \mathbf{M}_{fs} & \mathbf{M}_{ff} & 0 \\ (1-\phi)\rho_0 c^2 \mathbf{H}_{sF}^T & \phi\rho_0 c^2 \mathbf{H}_{fF}^T & \mathbf{M}_F \end{bmatrix} + \right.$$
$$\left. + \begin{bmatrix} \mathbf{K}_{ss} & \mathbf{K}_{sf} & -(1-\phi)\mathbf{H}_{sF} \\ \mathbf{K}_{fs} & \mathbf{K}_{ff} & -\phi\mathbf{H}_{fF} \\ 0 & 0 & \mathbf{K}_F \end{bmatrix} \right) \begin{bmatrix} \mathbf{d}_s \\ \mathbf{d}_f \\ \mathbf{p}_F \end{bmatrix} = \begin{bmatrix} \mathbf{f}_{bs} \\ \mathbf{f}_{bf} \\ \mathbf{f}_q \end{bmatrix} \tag{8}$$

where ω is the studied angular frequency. The porous material is modelled by two coupled partitions, the structural frame and the fluid in the open pores. Matrices $\mathbf{H}_{sF}$ and $\mathbf{H}_{fF}$ describe the spatial coupling between the partitions of the porous material and the acoustic fluid domain. The system matrices for the porous material are frequency dependent and are described in [29]. A detailed description of Biot's theory and the porous material properties is given in [18, 19].
A reduced modal base for the porous material is desired and the method in [29] has been adopted, where the structural and fluid modes are calculated in separate analyses. The dilatational, viscous and inertia coupling terms are ignored in deriving the normal modes of the two partitions. For the structural partition, the eigenvalue problem is written

$$\lambda_s \mathbf{M}_{ss} \mathbf{\Phi}_s = \mathbf{K}_{ss} \mathbf{\Phi}_s \tag{9}$$

and for the fluid partition

$$\lambda_f \mathbf{M}_{ff} \mathbf{\Phi}_f = \mathbf{K}_{ff} \mathbf{\Phi}_f \tag{10}$$

Because numerical problems can be encountered regarding the fluid partition due to the lack of shear stiffness, a procedure using reduced integration and projection of the element mass matrix has been adopted [5].

To avoid having to include a large number of zero energy fluid modes in describing the fluid motion due to the inertia and viscous coupling existing between the fluid partition and structural partition, a combined base is used [29]. This base includes both structural and fluid normal modes with $\lambda_f > 0$ describing the fluid partition, i.e.

$$\mathbf{\Phi}_f = \left[\begin{array}{cc} \mathbf{\Phi}_f^{\lambda_f > 0} & \mathbf{\Phi}_s \end{array} \right] \tag{11}$$

The reduced base for the porous material then becomes

$$\left[\begin{array}{c} \mathbf{d}_s \\ \mathbf{d}_f \end{array} \right] = \left[\begin{array}{cc} \mathbf{\Phi}_s & \mathbf{0} \\ \mathbf{0} & \mathbf{\Phi}_f \end{array} \right] \left[\begin{array}{c} \boldsymbol{\xi}_s \\ \boldsymbol{\xi}_f \end{array} \right] \tag{12}$$

The porous material is thereby described in a modal base which will be used in the following section to derive an efficient set of basis vectors for the poroelastic-acoustic problem.

2.3 Proposed method

The proposed method is based on the Lanczos procedure presented in Table 1 and takes advantage of the fact that the Lanczos vectors can be derived effectively using the spatial distribution of the dynamic forces. This is described for structure-acoustic systems in [2]. The external dynamic force acting on the system is written

$$\mathbf{f}_{ext} = \mathbf{r}_{ext} f(t) \tag{13}$$

where $\mathbf{r}_{ext}$ is the spatial distribution of the force and $f(t)$ is the time-varying force. In Step 2, $\mathbf{r}_{ext}$ is chosen as the force vector (see Table 1), and an efficient reduced base for the system can be derived for this specific force. The proposed method has adopted this methodology so as to achieve an efficient base in equations (6) and (12), in order to reduce the coupled systems.
For the structure-acoustic problem, the subdomain modes below the frequency limit of interest are first derived. Using these modes to describe the forces on the opposite domain, the fluid loading on the structure in the frequency domain becomes

$$\mathbf{f}_F = \mathbf{H}_{SF} \mathbf{\Phi}_F \boldsymbol{\xi}_F \tag{14}$$

and in the opposite direction

$$\mathbf{f}_S = -\rho c^2 \omega^2 \mathbf{H}_{SF}^T \mathbf{\Phi}_S \boldsymbol{\xi}_S \tag{15}$$

where ω is the frequency of interest. The spatial distributions of the above force terms, for the acoustic fluid modes that act on the structural domain

$$\mathbf{r}_F = \mathbf{H}_{SF} \mathbf{\Phi}_F \tag{16}$$

and for the structural modes that act on the fluid

$$\mathbf{r}_S = \mathbf{H}_{SF}^T \mathbf{\Phi}_S \tag{17}$$

which are used for deriving the starting vectors in the Lanczos procedure. The scheme described in Table 2 is used in generating a reduced base for the structure-acoustic system.

Table 1: *The Lanczos procedure.*

1. Choose a shift point, μ, and factorise the system matrix,
$$\mathbf{K} - \mu\mathbf{M} = \mathbf{LU} \qquad \text{or} \qquad \mathbf{K} - \mu\mathbf{M} = \mathbf{LDL}^T.$$
2. Generate p number of arbitrary force vectors $\mathbf{r}_1$ ... $\mathbf{r}_p$.

The Lanczos stage (Steps 3 to 6) is repeated p times.

3. Generate the first vector (start vector), $\mathbf{x}_1$.
   a) Solve for the first vector,
   $$(\mathbf{K} - \mu\mathbf{M})\hat{\mathbf{x}}_1 = \mathbf{r}_1.$$
   c) Mass-orthogonalise the vectors using the Gram-Schmidt method
   $$\hat{\mathbf{x}}_1 = \hat{\mathbf{x}}_1 - \sum_{j=1}^{n_c} (\hat{\mathbf{x}}_1 \mathbf{M} \mathbf{\Phi}_j) \mathbf{\Phi}_j$$
   b) Check for orthogonality,
   $$\gamma = \hat{\mathbf{x}}_1^T \mathbf{M} \hat{\mathbf{x}}_1.$$
   If $\gamma < \tau$ the new start vector is not orthogonal with previously generated eigenvectors and no new Lanczos vectors can be derived. τ is a selected tolerance controlling orthogonality.
   c) Compute
   $$\mathbf{x}_1 = \hat{\mathbf{x}}_1 / \gamma$$
4. Loop for achieving the additional vectors, $i = 1...m$;
   m is the maximum number of Lanczos vectors to be derived.
   a) Solve for vector $\hat{\mathbf{x}}_i$
   $$(\mathbf{K} - \mu\mathbf{M})\hat{\mathbf{x}}_i = \mathbf{M}\mathbf{x}_i$$
   b) Compute
   $$\alpha_i = \hat{\mathbf{x}}_i^T \mathbf{M} \hat{\mathbf{x}}_i$$
   c) Compute
   $$\tilde{\mathbf{x}}_i = \hat{\mathbf{x}}_i - \alpha_i \mathbf{x}_i - \beta_{i-1} \mathbf{x}_{i-1}$$
   d) Mass-orthogonalise the vector using the Gram-Schmidt method
   $$\tilde{\mathbf{x}}_i = \tilde{\mathbf{x}}_i - \sum_{k=1}^{i} (\tilde{\mathbf{x}}_i \mathbf{M} \mathbf{x_k}) \mathbf{x}_k - \sum_{j=1}^{n_c} (\tilde{\mathbf{x}}_i \mathbf{M} \mathbf{\Phi}_j) \mathbf{\Phi}_j$$
   e) Check for orthogonality
   $$\beta_i = \tilde{\mathbf{x}}_i^T \mathbf{M} \tilde{\mathbf{x}}_i.$$
   If $\beta_i < \tau$, end the Lanczos stage; a new start vector is needed.
   f) Compute
   $$\mathbf{x}_{i+1} = \tilde{\mathbf{x}}_i / \beta_i$$
5. Calculate the $n_c + 1$ to $n_c + r$ converged eigenvalues and eigenvectors of the transformed system by
   $$\mathbf{T}_i \hat{\mathbf{\Phi}} = \frac{1}{\hat{\lambda}} \hat{\mathbf{\Phi}}$$
   The convergence is controlled.
6. Calculate the real eigenvalues and eigenvectors by
   $$\lambda = \mu + \frac{1}{\hat{\lambda}} \qquad \text{and} \qquad \mathbf{\Phi} = \mathbf{X}\hat{\mathbf{\Phi}}$$
7. The convergence is controlled.

Table 2: *Algorithm to generate effective bases to use in the modal reduction of the structure-acoustic system.*

1.	a)	Set the frequency limit of interest for the analysis, f_{limit}.
	b)	Determine the normal modes of the structural domain, $\langle \hat{\mathbf{\Lambda}}_S, \hat{\mathbf{\Phi}}_S \rangle$, and the fluid domain, $\langle \hat{\mathbf{\Lambda}}_F, \hat{\mathbf{\Phi}}_f \rangle$, below this frequency limit.
2.		The forces acting on the opposite domain due to the geometrical distribution of the calculated eigenmodes are evaluated. For the structural domain $\mathbf{r}_F = \mathbf{H}_{SF}\hat{\mathbf{\Phi}}_F$ and for the acoustic fluid domain $\mathbf{r}_S = \mathbf{H}_{SF}^T\hat{\mathbf{\Phi}}_S$
3.		Use these vectors to calculate the Lanczos vectors in Table 1 for each domain. A Lanczos stage is performed for each mode of the opposite domain and m Lanczos vectors for each mode are calculated.
4.		Reduce the system with the new base and calculate the coupled eigenmodes.

The same scheme is adopted for the porous material; in this case the geometrical distribution of the force acting on the porous material from the acoustic fluid domain becomes, for the structural partition,

$$\mathbf{r}_{sF} = (1-\phi)\mathbf{H}_{sF}\mathbf{\Phi}_F \tag{18}$$

and for the fluid partition,

$$\mathbf{r}_{fF} = \phi\mathbf{H}_{fF}\mathbf{\Phi}_F \tag{19}$$

The geometrical distribution of the forces acting on the acoustic fluid domain due to the motion of the porous material becomes

$$\mathbf{r}_{Fb} = \left[\begin{array}{cc} (1-\phi)\mathbf{H}_{sF}^T\mathbf{\Phi}_s & \phi\mathbf{H}_{fF}^T\mathbf{\Phi}_f \end{array} \right] \tag{20}$$

The method introduces a new step between the analysis of each domain and the analysis of the coupled system. This is performed efficiently at the component level before the synthesis and with system matrices that are independent of frequency.

3 Numerical examples

3.1 Structure-acoustic analysis

An aluminium plate backed by an air cavity is studied, see Figure 2. The plate is 3 mm thick, the modulus of elasticity is 70 GPa, Poisson's ratio is 0.3 and the density is 2800 kg/m^3. For air, the density is 1.21 kg/m^3 and the speed of sound is 340 m/s. The frequency limit of interest is set to 300 Hz.
The number of Lanczos vectors, m, for each interface vector needed to achieve the correct eigenmodes of the coupled system is studied. The calculated eigenvalues are compared with those achieved by directly solving the eigenvalue problem for the unreduced system. The comparison of calculated mode shapes is evaluated by

$$\kappa = \frac{\mathbf{\Phi}_{reduced}^T \cdot \mathbf{\Phi}_{direct}}{|\mathbf{\Phi}_{reduced}| \cdot |\mathbf{\Phi}_{direct}|} \tag{21}$$

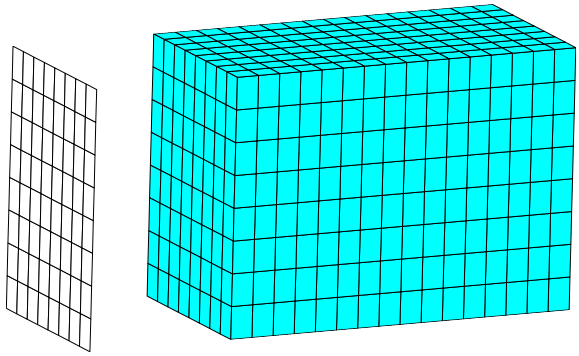

Figure 2: *The finite element model of the studied structure-acoustic problem.*

where κ is referred to as the mode shape similarity. For $\kappa = 1$ the compared vectors are identical, and here it is assumed that good agreement is achieved if $\kappa > 0.99$; κ is separately evaluated for the structural and fluid parts. For comparison, the coupled eigenvalue problem is solved using a standard procedure to include all the subdomain modes, say below twice the frequency limit of interest, in the reduction. The results of this analysis are here referred to by "$2f_{limit}$". Two simple examples are studied:
1) The plate is 0.55 m long and 0.35 m wide, the depth of the cavity being 2.1 m. This results in the natural frequencies of the first normal mode of the structural domain and of the fluid domain coinciding at 81 Hz. The computed coupled eigenvalues below 300 Hz, together with the number of subdomain modes included in the analysis, are shown in Table 3.
2) The plate is 0.9 m long and 0.65 m wide, the depth of the cavity being 1.25 m. The number of subdomain normal modes below the frequency limit is now larger. The error in natural frequency and mode shape is evaluated by $\varepsilon_\lambda = (\lambda_{red} - \lambda)/\lambda$, displayed in Figure

	"$2f_{limit}$"	Lanczos vectors, m			Direct
		0	1	2	
Mode	Natural frequencies (Hz)				
1	73.2197	73.3166	73.0821	73.0820	73.0820
2	89.2792	89.4187	89.0880	89.0879	89.0879
3	148.0841	148.9089	147.5391	147.5310	147.5306
4	163.9861	163.9952	163.9601	163.9600	163.9600
5	246.5600	246.5605	246.4992	246.4990	246.4990
6	252.0476	252.6919	251.1389	251.1246	251.1242
7	263.4865	263.6686	262.4484	262.4178	262.4121
Domain	Number of degrees of freedom				
Structural	4	4	5	6	243
Fluid	20	4	8	12	1377
Sum	24	8	13	18	1620

Table 3: *The calculated natural frequencies and the number of degrees of freedom used.*

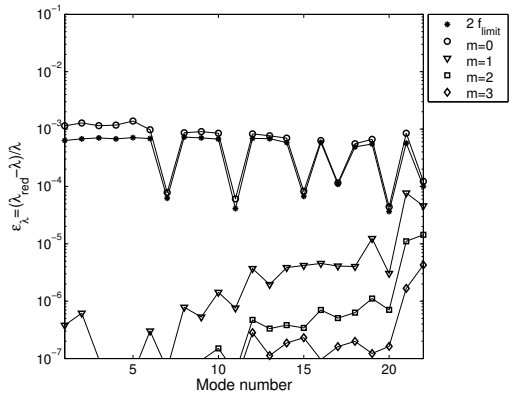

Figure 3: *Error in calculated eigenvalues.*

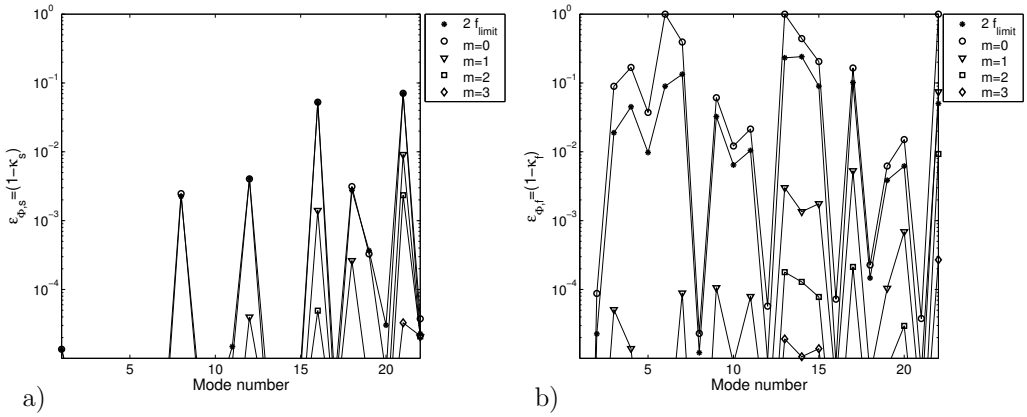

Figure 4: *Error in calculated eigenvectors, a) structural domain and b) fluid domain.*

3, and $\varepsilon_\phi = (1 - \kappa)$, displayed in Figure 4. The numbers of degrees of freedom (dofs) of the reduced systems are as follow: for all modes below "$2f_{limit}$", 46 dofs; for $m = 0$, 23 dofs; for $m = 1$, 42 dofs; for $m = 2$, 61 dofs; and for $m = 3$, 80 dofs.

3.2 Porous-acoustic analysis

A cavity, one wall of which is covered with porous material, is excited by means of a point source (see Figure 5). The length of the cavity parallel to the porous material is 0.6 m, the height is 0.4 m and the depth of the cavity is 0.75 m. The thickness of the porous material is 0.05 m. The properties of the porous material are given in Table 4. The point source produces a constant volume velocity, and the analysis is performed in the frequency range from 70 to 700 Hz.

For the studied poroelastic-acoustic problem the total number of degrees of freedom (dofs) is 5382, with 3510 dofs for the porous material and 1872 dofs for the acoustic cavity. Three

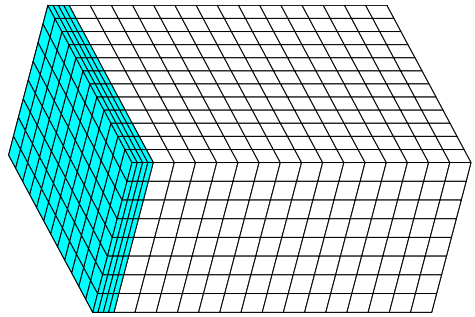

Figure 5: *Finite element model of the acoustic cavity in contact with a porous material. The shaded elements indicate the porous material domain.*

different approaches are used:

- Solving the total system
- Reducing the system using a number of normal modes for each subdomain with natural frequencies up to twice the maximum frequency of interest($f_0 < 2f_{limit}$)
- Using the proposed method with one interface vector for each subdomain normal mode from the opposite domain, i.e. $m = 1$. This will be shown to be sufficient to achieve a good description of the coupled system.

Including only normal modes, 120 modes are used for the structural partition, while the combined base for the fluid partition includes 138 modes. For the acoustic domain, 76 modes are included, the total number of modes being 334.
For the proposed method, 137 modes are used in total: the porous material is described using 43 modes for the structural partition, 51 modes for the combined base in the fluid partition and 43 modes for the acoustic domain.
The pressure distribution in the cavity is presented in Figure 6: the mean pressure level in the cavity is plotted in Figure 6 a), while the pressure level at the centre of the cavity

Table 4: *Material data for the porous material*

Porous material:			
E_s	=	845	kPa
ν_s	=	0.3	
η_s	=	0.1	
ρ_s	=	30	kg/m^3
ϕ	=	0.96	
σ	=	32000	Ns/m^4
α_∞	=	1.7	
Λ	=	$90 \cdot 10^{-6}$	m
Λ'	=	$165 \cdot 10^{-6}$	m

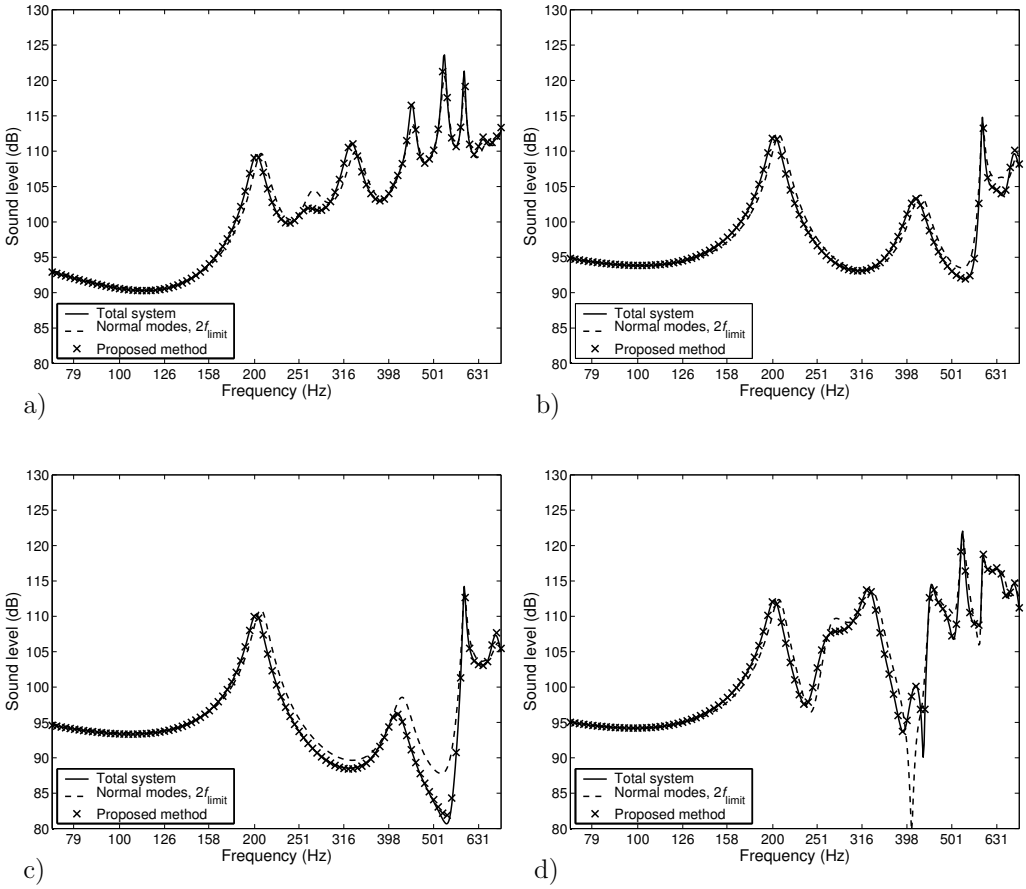

Figure 6: *The pressure level in the acoustic cavity as calculated using the proposed method is compared with the result obtained by solving the system directly and also with the result obtained by using a reduced base including the subdomain modes up to twice the frequency limit of interest: a) mean pressure, b) pressure at the centre of the cavity, c) pressure at the midpoint of the interface boundary, and d) pressure at a corner of the interface boundary.*

is plotted in Figure 6 b). Figures 6 c) and d) present the pressures at the mid and corner points of the boundary area between the acoustic cavity and porous material.

4 Discussion and conclusions

For the structure-acoustic eigenvalue problem, both the eigenvalues and eigenvectors – calculated using the proposed method – converge rapidly with the ones achieved by solving the system in the original coordinates. This is shown both in Table 3 and by the error norms given in Figures 3 and 4. The method especially improves the description of the acoustic field near the flexible structural domain which is of special interest when the sound

pressure level is to be determined close to a vibrating surface.
For the poroelastic-acoustic problem presented in Figure 6, the pressure distribution in the acoustic domain is described in detail using the proposed method when one Lanczos vector for each mode from the opposite domain is included. Solving the total system using a large number of normal modes produces results very similar to those obtained with the proposed method. However, the proposed method uses fewer than half of the modes when only normal modes are included.
The analysis step added to derive these reduced sets of basis vectors is performed at the substructure level and also with system matrices independent of frequency; it can therefore be conducted very efficiently. Only well-known finite element tools are used, and this method should be easy to implement in any standard finite element environment. The system matrices are frequency dependent, but it has been shown that the same reduced base can be used over a wide range of frequencies.

5 Acknowledgements

The Swedish Foundation for Strategic Research (project number IVS-98-501) is gratefully acknowledged for their financial support.

References

[1] G. Sandberg, Finite element modelling of fluid-structure interaction, TVSM 1002, Structural Mechanics, LTH, Lund University, Box 118, SE-221 00 Lund, Sweden (1986).

[2] H. Carlsson, Finite element analysis of structure-acoustic systems; formulations and solution strategies, TVSM 1005, Structural Mechanics, LTH, Lund University, Box 118, SE-221 00 Lund, Sweden (1992).

[3] H. Morand, R. Ohayon, Fluid structure interaction, John Wiley & sons, Chichester, 1995.

[4] N. Akkas, H. U. Akay, C. Yilmaz, Applicability of general-purpose finite element programs in solid-fluid interaction problems, Computers & Structures 10 (1979) 773–783.

[5] H. . C. Chen, R. L. Taylor, Vibration analysis of fluid-solid systems using a finite element displacement formulation, International Journal of Numerical Methods in Engineering 29 (1990) 683–698.

[6] A. Craggs, The transient response of a coupled plate-acoustic system using plate and acoustic finite elements, Journal of Sound and Vibration 15 (4) (1971) 509–528.

[7] G. Sandberg, P. Göransson, A symmetric finite element formulation for acosutic fluid-structure interaction analysis, Journal of Sound and Vibration 123 (3) (1988) 507–515.

[8] P. Seshu, Substructuring and component mode synthesis, Shock and Vibration 4 (3) (1997) 199–210.

[9] R. R. Craig, Structural Dynamics; An introduction to computer methods, John Wiley & Sons Inc., New York, 1981.

[10] H. Morand, R. Ohayon, Substructure variational analysis of the vibrations of coupled fluid-structure systems. finite elemtent results, International Journal of Numerical Methods in Engineering 14 (1979) 741–755.

[11] J. A. Wolf, Modal synthesis for combined structural-acoustic systems, AIAA Journal 15 (1977) 743–745.

[12] D. J. Nefske, J. A. Wolf, L. J. Howell, Structural-acoustic finite element analysis of the automobile compartment: A review of current practice, Journal of Sound and Vibration 80 (2) (1982) 247–266.

[13] W. J. T. Daniel, Modal methods in finite element fluid-structure eigenvalue problems, International Journal of Numerical Methods in Engineering 15 (1980) 1161–1175.

[14] J. Wandinger, A symmetric Craig-Bampton method of coupled fluid-structure systems, Engineering Computation 15 (4) (1998) 450–461.

[15] G. Sandberg, A new strategy for solving fluid-structure problems, International Journal of Numerical Methods in Engineering 38 (1995) 357–370.

[16] P. Davidsson, Finite element analysis of structure-acoustic systems – methods and applications, TVSM 3060, Structural Mechanics, LTH, Lund University, Box 118, SE-221 00 Lund, Sweden (2001).

[17] K.-J. Bathe, Finite Element Procedures, Prentice Hall, New York, 1996.

[18] M. A. Biot, Theory of propagation of elastic waves in fluid-saturated porous solid. i. low frequency range, The Journal of the Acoustical Society of America 28 (2) (1956) 168–178.

[19] J. F. Allard, Propagation of sound in porous media; modelling sound absorbing matarials, Elsevier Science Publishers Ltd, London, 1993.

[20] Y. J. Kang, J. S. Bolton, Finite element modeling of isotropic elastic porous materials coupled with coustical finite elements, The Journal of the Acoustical Society of America 98 (1) (1995) 635–643.

[21] J. P. Coyette, The use of finite-element and boundary-element models for predicting the vibro-acoustic behaviour of layered structures, Adv. Eng. Soft. 30 (1) (1999) 133–139.

[22] N. Dauchez, S. Sahraoui, N. Atalla, Convergence of poroelastic finite elements based on biot displacement formulation, The Journal of the Acoustical Society of America 109 (1) (2001) 33–40.

[23] N. Atalla, R. Panneton, P. Debergue, A mixed displacement pressure formulation for poroelastic materials, The Journal of the Acoustical Society of America 104 (3) (1998) 1444–1452.

[24] P. Göransson, A 3-d, symmetric, finite element formulation of the biot equations with application to acoustic wave propagation through an elastic porous medium, International Journal of Numerical Methods in Engineering 41 (1998) 167–192.

[25] N.-E. Hörlin, M. Nordström, P. Göransson, A 3-d hierarchical fe formulation of biot's equations for elasto-acoustic modelling of porous media, Journal of Sound and Vibration 245 (4) (2001) 633–652.

[26] F. Sgard, N. Atalla, R. Panneton, A modal reduction technique for the finite element formulation of the biot's poroelasticity equations in acoustics applied to multilayered structures, 135^{th} ASA Meeting (1998) 1183–1184.

[27] O. Dazel, F. Sgard, C.-H. Lamarque, N. Atalla, An extention of complex modes for the resolution of finite-element poroelastic problems, Journal of Sound and Vibration 253 (2) (2002) 421–445.

[28] G. Sandberg, Acoustic and interface elements for structure-acoustic analysis in calfem, TVSM 7113, Structural Mechanics, LTH, Lund University, Box 118, SE-221 00 Lund, Sweden (1996).

[29] P. Davidsson, Substructuring and modal reduction of finite element formulated poroelastic systems, Submitted to Computer methods in applied mechanics and engineering.

Paper 5

Structure-acoustic analysis in an integrated modelling environment

Peter Davidsson and Göran Sandberg
Division of Structural Mechanics,
Lund University

Gunnar Björkman and Johan Svenningstorp
Volvo Technological Development

WCCM V
Fifth World Congress on
Computational Mechanics
July 7–12, 2002, Vienna, Austria
Eds.: H.A. Mang, F.G. Rammerstorfer,
J. Eberhardsteiner

Structure-acoustic analysis in an integrated modelling environment

Peter Davidsson*, Göran Sandberg,

Division of Structural Mechanics, Lund Institute of Technology, Box 118, S-221 00 Lund, Sweden
e-mail: peter.davidsson@byggmek.lth.se

Gunnar Björkman, Johan Svenningstorp

Volvo Technological Development Corporation, Göteborg, Sweden

Key words: structure-acoustic, the finite element method, integrated modelling

Abstract
Structure-acoustic finite element analysis is implemented in an integrated modelling environment to demonstrate the possibilities such an environment provides. This allows research results to be used for analysing realistic vehicle structures, permitting research results and computational results to be readily displayed. Use of this environment aims at facilitating collaboration between different research projects and between researchers and industrial groups.

1 Introduction

The implementation of structure-acoustic finite element analysis in the Virtual Integral Vehicle Structure Laboratory (VIVS-lab) will be described. The VIVS-lab modelling environment aims at providing a common basis for communication between vehicle researchers and the vehicle industry, and at simplifying and facilitating cooperation and interaction between the two. In VIVS-lab, generic geometry models of different vehicle structures are created, allowing research results to be implemented and tested on realistic models. The present paper concerns the advantages of such an environment and the possibilities it opens up.

VIVS-lab is part of the Swedish national research programme IVS (Integral Vehicle Structure), which concerns future generations of vehicles. The programme aims at being multidisciplinary and at allowing different research projects to interact with each other. VIVS-lab is developed within the AML (Adaptive Modelling Language) modelling framework [6], aimed at facilitating the integration of the different parts of the product development cycle. AML is a modelling environment with an object-oriented architecture and with a graphical interface in which a parameterised model of the product of interest can be studied. Integration of the development cycle is accomplished with the help of interfaces to a variety of other programs. The program to be used depends on the task, which may involve design (CAD) or finite element analysis (FEA), for example. The design process is divided up by the modelling environment into different objects, each representing a part of the total process. A given object can consist of several different subobjects.

2 Structure-acoustic analysis

The finite element method can be used to study the interior noise level produced by structural vibrations. The structural domain and the fluid domain can be described by two separate equation systems of motion. For the structural domain

$$\mathbf{M}_s\ddot{\mathbf{d}} + \mathbf{K}_s\mathbf{d} = \mathbf{f}_b + \mathbf{H}\mathbf{p} \tag{1}$$

where **d** represent structural displacements and the dots indicate differentiation with respect to time. For the fluid domain

$$\mathbf{M}_f\ddot{\mathbf{p}} + \mathbf{K}_f\mathbf{p} = \mathbf{f}_q - \rho c^2\mathbf{H}^T\ddot{\mathbf{d}} \tag{2}$$

where **p** is the fluid pressure. For an account of the system matrices, see [1]. The coupling between the two domains is based on the force terms which include the coupling matrix **H** and allows the coupled system to be written as

$$\begin{bmatrix} \mathbf{M}_s & \mathbf{0} \\ \rho c^2\mathbf{H}^T & \mathbf{M}_f \end{bmatrix} \begin{bmatrix} \ddot{\mathbf{d}} \\ \ddot{\mathbf{p}} \end{bmatrix} + \begin{bmatrix} \mathbf{K}_s & -\mathbf{H} \\ 0 & \mathbf{K}_f \end{bmatrix} \begin{bmatrix} \mathbf{d} \\ \mathbf{p} \end{bmatrix} = \begin{bmatrix} \mathbf{f}_b \\ \mathbf{f}_q \end{bmatrix} \tag{3}$$

The strategy employed in the structure-acoustic analysis involves substructuring and modal reduction [1, 2]. First, the two eigenvalue problems, one for the structural domain and the other for the enclosed cavity domain, are solved separately. The uncoupled eigenmodes are then used to reduce the coupled problem by a change of base

$$\begin{bmatrix} \mathbf{d} \\ \mathbf{p} \end{bmatrix} = \begin{bmatrix} \Phi_s & \mathbf{0} \\ \mathbf{0} & \Phi_f \end{bmatrix} \boldsymbol{\xi} \tag{4}$$

Matrix transformation is used to derive two symmetric standard eigenvalue problems, providing the left and right eigenvectors needed to diagonalise the coupled equation system.

Determining the strength of the coupling between the modes of the two domains allows the most important uncoupled modes needed for describing the coupled system to be determined [4]. This is done by studying the modal coupling matrix

$$B_{ij} = \frac{\mathbf{\Phi}_{si}^T \mathbf{H} \mathbf{\Phi}_{fj}}{\omega_{si}^2 - \omega_{aj}^2} \tag{5}$$

where ω_{sj} and ω_{ai} are the structural and fluid eigenvalues with corresponding eigenvectors $\mathbf{\Phi}_{si}$ and $\mathbf{\Phi}_{fj}$. For each structural mode below a maximum frequency of interest a number of fluid modes with strong coupling to this structural mode, i.e. with large corresponding values in the modal coupling matrix, can be chosen to be included in the reduction of the coupled problem. The same procedure is used for each fluid mode below the maximum frequency of interest determining the structural modes with strong coupling. Thereby, only the most important uncoupled modes are included in the reduction.

Hysteretic damping of the two domains can be included in the reduction of the coupled problem [5]. The damping is introduced in the structural domain at a constitutive level, as a complex modulus of elasticity

$$\tilde{E}_s = (1 + i\eta_s) E_s \tag{6}$$

and in the fluid domain as a complex bulk modulus

$$\tilde{B}_f = (1 + i\eta_f) B_f \tag{7}$$

This gives the coupled system complex eigenvalues and eigenvectors. It can then be reduced to a system of uncoupled equations expressed in terms of modal coordinates, $\boldsymbol{\zeta}$. Frequency response analysis using a harmonic force $F = \hat{F} \sin \bar{\omega} t$ is then applied to obtain the equation system

$$(-\bar{\omega}^2 \mathbf{I} + \mathbf{\Lambda}) \boldsymbol{\zeta} = \mathbf{v}_L^T \begin{bmatrix} \hat{\mathbf{f}}_b \\ \hat{\mathbf{f}}_q \end{bmatrix} \tag{8}$$

where $\mathbf{\Lambda}$ is an (n×n) matrix having the system eigenvalues in the diagonal, the left eigenvectors being included in $\mathbf{v}_L$.

3 Implementation

VIVS-lab is created in an object oriented environment and the aim here is to create an analysis class that perform structure-acoustic analysis on a given geometry model. This could for example be an imported CAD model. Here a geometry object is created to serve as a simple model of a vehicle structure in which there is an interior cavity. The geometry object is displayed in the AML graphical interface in Fig. 1. This geometry should then be possible to replace with a more complex vehicle structure without having to perform changes in the analysis class. The analysis consists of two parts, first the finite element model is generated and then the finite element analysis is performed. This can be expressed in AML-code:

```
(define-class structure-acoustic-analysis-class
  :subobjects(
            (acoustic-mesh :class 'acoustic-mesh-class)
            (acoustic-analysis :class 'acoustic-analysis-class)
                )
 )
```

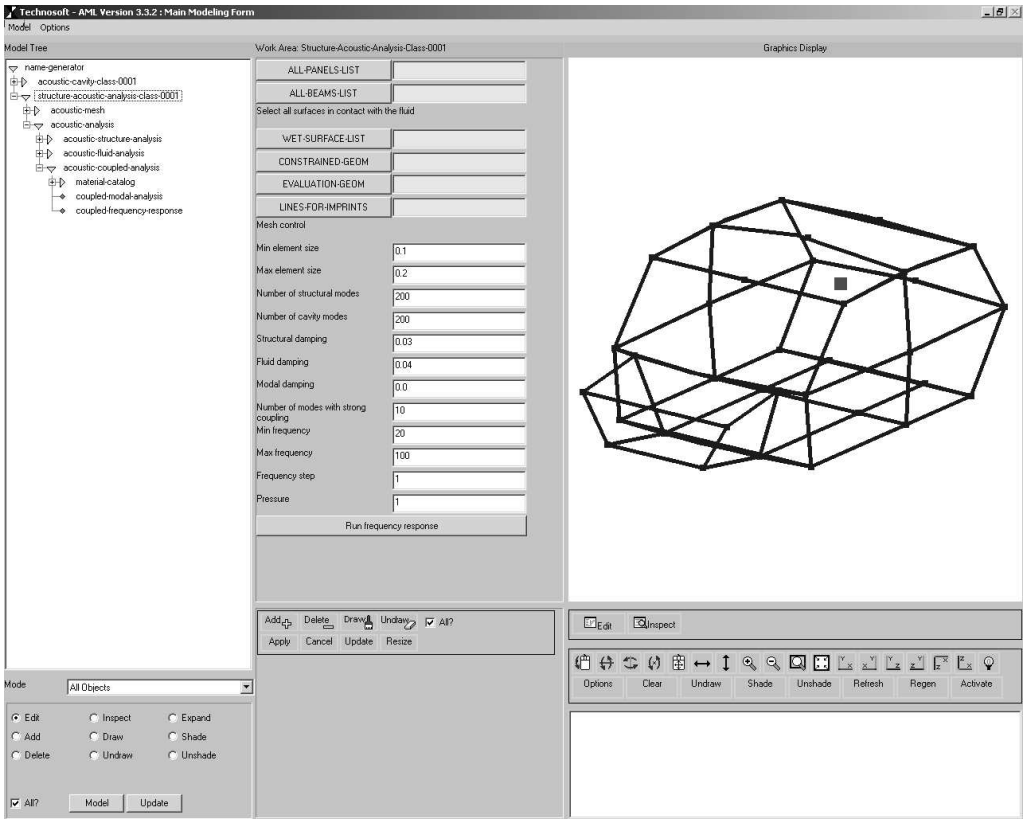

Figure 1: The AML graphical interface in which the geometry model has been plotted in the graphics display window. The object tree to the left shows the objects that have been instantiated. The acoustic-cavity-class contains the geometry and the structure-acoustic-analysis-class is instantiated to perform the analysis. In the center part of the interface the parameters controlling this analysis are displayed.

3.1 Meshing

In the analysis class the geometry is used to generate a finite element model. The geometry objects need to contain all the information necessary to perform the operations called for, such as the minimum element size, for example. This is accomplished by tagging the objects, giving them the attributes needed to generate the mesh by use of the AML-interface to MSC/Patran. The structural mesh and fluid mesh are plotted in Fig. 2. The coupling elements between the structural domain and the fluid domain used for determining the coupling matrix **H** contain information about which nodes from the two domains coincide. The mesh object generates a (coinciding) mesh of shared nodes from the two domains at the boundary between them. The shell elements in contact with the fluid can thus also be used as coupling elements, having all the information needed.

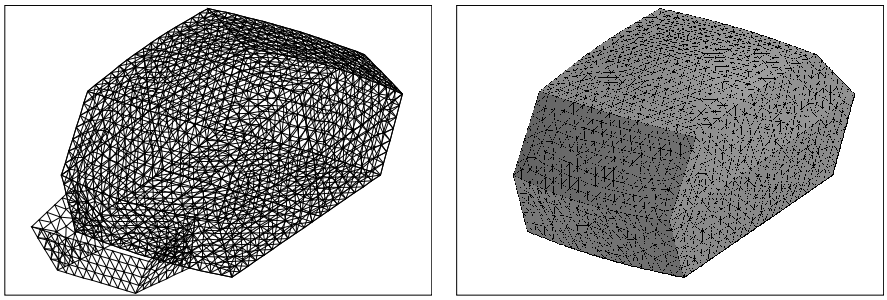

Figure 2: a) Finite element model of the structural domain. b) Finite element model of the acoustic fluid domain.

3.2 Analysis

The structure-acoustic analysis is performed following the above described scheme. The parameters controlling the analysis can be edited in the graphical interface, see Fig. 1, and each step of the analysis is carried out using interfaces to different programs. The modal analysis of the structural and fluid domain is carried out in MSC/Nastran [7]. The coupled analysis performed in Matlab [8] consists of two parts. Modal analysis is first used to determine the eigenvalues and the left and right eigenvectors. These results are used then, in the second step, for determining the frequency response to a given excitation. The object tree generated for the analysis can be seen in the left part of Fig. 1.

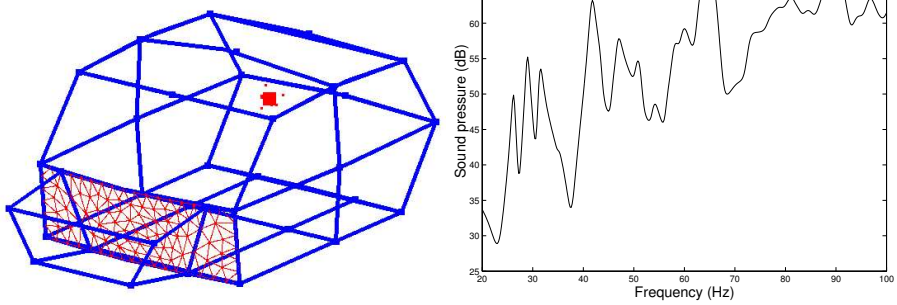

a) b)

Figure 3: a) The finite elements located where the pressure is applied and the evaluation nodes at the driver's ear. b) The sound pressure level at the drivers ear when a uniform pressure of 1 Pa is applied. The analysis parameters employed can be seen in Fig. 1.

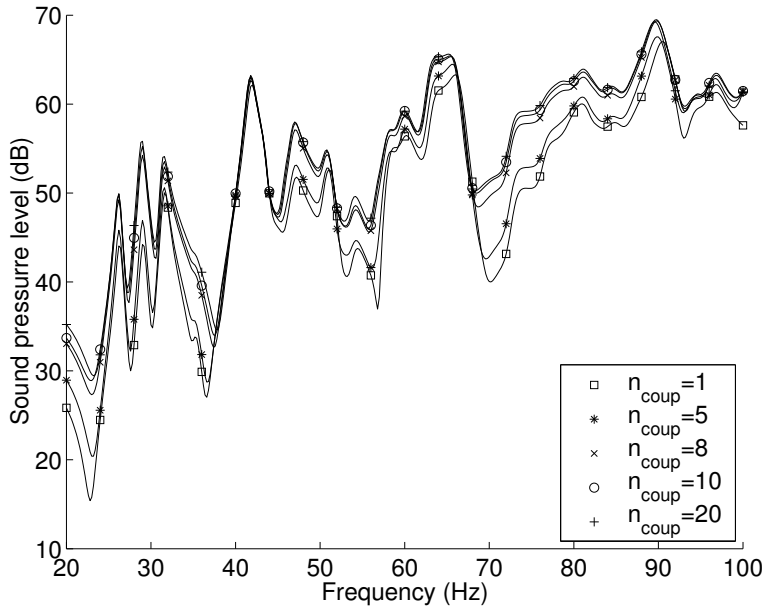

Figure 4: The number of uncoupled modes included in the reduction is varied.

3.3 Results

Structure-acoustic finite element analysis can be performed in an automated fashion for determining the sound level due to a force that is applied to the structure. As an example the sound pressure level at the driver's ear due to a uniform pressure in the frequency range from 20 to 100 Hz being applied to the outside of the front wall is calculated. The finite elements where the pressure is applied and the nodes where the sound level is evaluated are shown in Fig. 3 a). The frequency response curve is then displayed in Fig. 3 b). To show the advantage of the environment the influence on the result due to how many uncoupled modes are included in the coupled analysis is studied. This is done by varying the number of uncoupled modes with strong coupling, n_{coup}, by the method described above. The analysis parameters shown in Fig. 1 are kept constant except n_{coup} which is varied between 1 and 20. This gives the frequency response curves of Fig. 4.

4 Future work - Truck cabin

The next step is to apply the structure-acoustic analysis class to a more complex structure. This is to be done on a truck cabin generated in the VIVS-lab environment, see Fig. 5.

References

[1] G. Sandberg, A New Strategy for Solving Fluid-Structure Problems, International Journal for Numerical Methods in Engineering, vol 38, 357-370 (1995).

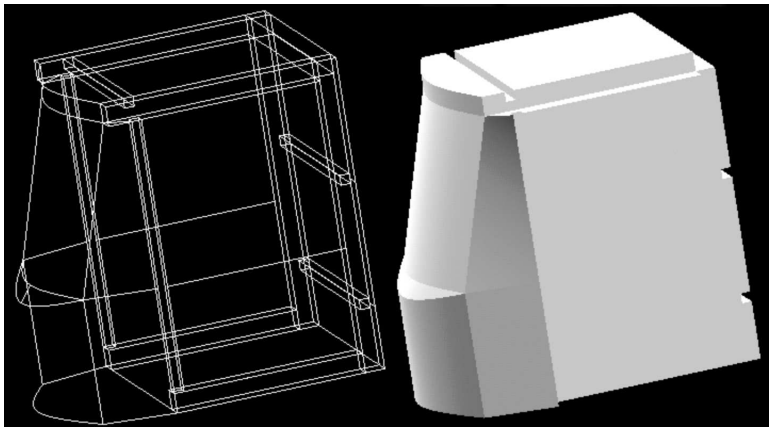

Figure 5: A truck cabin is generated in VIVS-lab. The geometry model of the structural and the cavity domain are displayed.

[2] G. Sandberg, Acoustic and Interface Elements for Structure-Acoustic Analysis in CALFEM, Report TVSM-7113, Lund Institute of Technology, Division of Structural Mechanics, Lund (1996).

[3] K.-G. Olsson, P.-E. Austrell, M. Ristinmaa, G. Sandberg, CALFEM — a finite element toolbox to Matlab, Version 3.2, Report TVSM–9001, Lund Institute of Technology, Division of Structural Mechanics and Department of Solid Mechanics, Lund, Sweden (1999).

[4] G. Sandberg, P. Davidsson, Choosing modes in the reduction of structure-acoustic systems, Submitted to Computer Methods in Applied Mechanics and Engineering (2001).

[5] P. Davidsson, G. Sandberg, Reduction of structure-acoustic systems that include hysteretic damping, Submitted to Computer Methods in Applied Mechanics and Engineering (2001).

[6] Technosoft Inc., AML Version 3.2.0, Reference manual, (2001).

[7] The MacNeal-Schwendler Corporation, MSC/NASTRAN ENCYCLOPEDIA - V70.5, (1998).

[8] The Mathworks Inc., Matlab Reference Guide, (2000).

Paper 6

Analysis of sound transmission loss of double-leaf walls in the low-frequency range using the finite element method

Peter Davidsson, Per-Anders Wernberg and Göran Sandberg
Division of Structural Mechanics,
Lund University

Jonas Brunskog and Per Hammer,
Division of Engineering Acoustics,
Lund University

Analysis of sound transmission loss of double-leaf walls in the low-frequency range using the finite element method

Peter Davidsson[†], Jonas Brunskog[‡], Per-Anders Wernberg[†], Göran Sandberg[†] and Per Hammer[‡]

[†]Division of Structural Mechanics, Lund University, Sweden

PO Box 118, SE-221 00 Lund, Sweden

Phone: + 46 46 222 33 71, E-mail: peter.davidsson@byggmek.lth.se

[‡]Engineering Acoustics, Lund University, Sweden

Abstract

The sound transmission loss of double walls in the low-frequency range is studied by means of structure-acoustic finite element analysis. The analysis simulates standard experiments to determine sound transmission loss in the walls. The model is a detailed description of the geometry of the system, including both the double wall and the rooms acoustically coupled to the wall. The frequency range studied is in the $\frac{1}{3}$-octave bands between 40 Hz and 200 Hz. A parametric study is performed to investigate the influence on the sound transmission loss of various material and geometric properties of the wall and the dimensions of the connecting rooms.

It is found that a very detailed description of the system is needed in order to describe sound transmission loss in the low-frequency range. The model confirms the importance of primary structural resonance and the size of the connecting rooms in determining the degree of sound transmission loss. The primary structural resonance is mainly determined by the distance between the wall studs and the properties of the sheeting material. Wall length is also important: if the length is such that the wall studs of last wall cavity are closer together than those of the other wall cavities, the primary structural resonance will be at a higher frequency, thereby decreasing sound transmission loss over a broader frequency range. Similar dimensions of the connecting rooms results in poor transmission loss, mainly at frequencies below 100 Hz (for the wall and room dimensions studied here).

1 Introduction

The ability to predict and measure sound transmission loss in the low-frequency range is needed. Road and air traffic noise as well as home cinema and stereo equipment have increased the demand for low-frequency sound transmission loss [1, 2]. When determining the sound transmission loss in the laboratory, a wall is placed in between two rooms, a

sending room with a loudspeaker and a receiving room. The spatial averages of the sound level in each of the two rooms are measured [3], and evaluated [4], indicating the sound transmission loss the wall provides.

It is well known that the sound transmission loss of a wall in the low-frequency range is limited by the resonances of the wall. In an investigation by Bradley et al. measurements were performed to evaluate the effects of various wall properties on sound transmission loss [5]. For double walls with mechanical coupling between the plates, sound transmission in the low-frequency range is governed by the primary structural resonance, not, as with a double wall without mechanical coupling between the plates, by a mass-air-mass resonance. A similar study was performed by Hammer et al. [6]. Maluski et al. [7] studied the sound transmission loss in single-leaf walls using the finite element method, including the connecting rooms in the model . The sound transmission loss of a wall in the low-frequency range was described as being mass controlled when the first wall resonance occurred below the first resonance in the connecting rooms, and as being stiffness controlled if the first room resonance was lower than the first wall resonance. In the transition between these regions the wall resonances control the sound transmission loss.

The dimensions of the sending and receiving rooms and thereby the room resonances also affect the measured sound transmission [7, 8, 9, 10, 11]. In an investigation by Kropp et al. [9], a large number of room configurations were examined. However, in the theoretical prediction model used, the wall was described as a locally reacting mass impedance. Therefore, the average sound transmission loss for these configurations was identical to the mass law.

To decrease room dependence in the measurements, thereby increasing the reliability of the predicted low-frequency sound transmission loss, absorbing elements, which reduce the sound level peaks in the rooms, can be inserted into the test rooms, as were done by Fuchs et al. [12]. However, Maluski et al. [13] showed that the damping and scattering provided by typical furnishing in a room have a small effect on the predicted sound pressure levels in the frequency range below 100 Hz compared to an empty room. The theoretical model presented by Papadopoulos [14] had the objective increase the reliability of numerical prediction of low frequency transmission loss. It presented a virtual laboratory, in which test rooms were optimised for improved mode distribution resulting in smaller sound pressure fluctuations in the low-frequency range. This virtual laboratory was used to study the sound transmission loss of single-leaf and double-leaf walls without mechanical coupling between the two leaves [15].

Brunskog et al. [16] analysed the sound transmission loss in a double wall using the finite element method; the rooms were described as semi-infinite tubes and were thereby included in the analysis as loading terms on the wall. A more compact description was achieved compared to including the modal bases of the rooms, and, thereby, the analysis can be extended to higher frequencies. The literature pertaining to predicting sound transmission loss in walls was also reviewed.

Osipov et al. predicted the sound transmission loss in single-leaf walls using three different theoretical models [11]. It was shown that the infinite plate model, i.e. the mass law, and the baffled plate model where a finite wall is placed within an infinitely extended rigid baffle cannot describe the low-frequency behaviour of the system. Although increasing the computational cost of the analysis, the full room-wall-room system must be studied when determining sound transmission loss in the low-frequency range.

This paper presents a parametric study of how properties of the sending-room–wall–receiving-room system influence sound transmission in double walls at low frequencies, based on a detailed geometric model. The analysis is performed by using the finite element method [17, 18, 19]. (Description of structure-acoustic analysis using the finite element method can be found in, for example, [20, 21, 22, 23].) The model used in the study mimics the measurement procedure for determining the sound transmission loss of a wall according to [3], and involves the following parameters:

- The material properties in the wall. The modulus of elasticity, E, and density, ρ, of the plasterboards and the flow resistivity, σ, and the density, ρ_s, of the porous material are studied.
- The geometric properties of the wall. The influence of wall stud spacing and the total length of the wall on the sound transmission loss is evaluated.
- The dimensions of the connecting rooms. The depth of the receiving room is varied. The effect of placing the wall within a baffle is also studied.

A low-frequency measure, which describes the sound transmission loss from 40 Hz to 200 Hz in a single value, is evaluated. This combined measure facilitates examination of the influence of the various parameters. This study gives a structured evaluation of the influence of various system properties on the sound transmission loss of double walls at low frequencies. Conclusions previously drawn from measurements and theoretical models can here be examined in detail. Also, the effect of varying both the material and geometric properties of the system can be evaluated and compared. For example, the importance of the primary structural resonance and the dimensions of the connecting rooms on the sound transmission loss and the sensitivity in the material properties describing the wall are displayed.

This paper is organised as follows: After the introduction the analysis procedure is described which is followed by the parametric study. The paper ends with the discussion of the results and some conclusions.

2 Analysis procedure

To determine the sound transmission loss, the studied wall is placed in between two rooms, a sending room with a loudspeaker and a receiving room, see Figure 1 (left). Here a computer model, based on the actual geometry used for the measurements, is derived for studying and simulating the same situation in order to determine the sound transmission loss in the low-frequency range.

Finite element procedure

The prediction model used is based on the finite element method. The structure is described by finite elements, and the two rooms and the enclosed wall cavities are described by analytical modal bases derived for a rectangular cavity with rigid wall boundary conditions. A modal base expressed in cosine modes is achieved for each cavity, see Fahy [24], page

163. Assuming harmonic motion, with the harmonic time dependency $e^{i\omega t}$ suppressed, the coupled structure-acoustic problem can be written

$$\left(-\omega^2 \begin{bmatrix} \mathbf{M}_s & \mathbf{0} \\ \rho c^2 \mathbf{\Phi}_f^T \mathbf{H}^T & \mathbf{I}_f \end{bmatrix} + \begin{bmatrix} \mathbf{K}_s & -\mathbf{H}\mathbf{\Phi}_f \\ 0 & \mathbf{\Lambda}_f \end{bmatrix}\right) \begin{bmatrix} \hat{\mathbf{d}} \\ \hat{\boldsymbol{\xi}}_p \end{bmatrix} = \begin{bmatrix} \mathbf{f}_b \\ \mathbf{\Phi}_f^T \mathbf{f}_q \end{bmatrix} \tag{1}$$

where ω is the angular frequency and

$$\hat{\boldsymbol{\xi}}_p = [\hat{\boldsymbol{\xi}}_p^1 \ldots \hat{\boldsymbol{\xi}}_p^M]^T; \quad \mathbf{\Lambda}_f = \mathrm{diag}([\mathbf{\Lambda}_f^1 \ldots \mathbf{\Lambda}_f^M]); \quad \mathbf{\Phi}_f = \mathrm{diag}([\mathbf{\Phi}_f^1 \ldots \mathbf{\Phi}_f^M]) \tag{2}$$

M is the number of fluid domains involved, one domain for each room and for each enclosed wall cavity. In the i'th fluid domain, the variable is the modal pressure, $\hat{\boldsymbol{\xi}}_p^i$, which is related to the actual pressure amplitude, $\hat{\mathbf{p}}^i$, by $\hat{\mathbf{p}}^i = \mathbf{\Phi}_f^i \hat{\boldsymbol{\xi}}_p^i$. $\mathbf{\Phi}_f^i$ contains the eigenvectors and $\mathbf{\Lambda}_f^i$ the eigenvalues. In the structural domain, $\mathbf{d}$ contains the displacements and $\mathbf{M}_s$ and $\mathbf{K}_s$ are the mass matrix and stiffness matrix, respectively. The geometric coupling between the structural and fluid domains is described by the coupling matrix $\mathbf{H}$. It couples the structural domain with each of the fluid domains, $\mathbf{H} = [\mathbf{H}^1 \ldots \mathbf{H}^i \ldots \mathbf{H}^M]$.

The sound levels in the two rooms are determined by means of frequency response analysis in the 35 Hz to 224 Hz interval, i.e. the lower and upper bounds of the $\frac{1}{3}$-octave bands studied. The system is reduced by first solving the eigenvalue problem for the structural domain using MSC/Nastran [25], and then performing a change of base in equation (1), given by

$$\begin{bmatrix} \hat{\mathbf{d}} \\ \hat{\boldsymbol{\xi}}_p \end{bmatrix} = \begin{bmatrix} \mathbf{\Phi}_s & \mathbf{0} \\ \mathbf{0} & \mathbf{I} \end{bmatrix} \begin{bmatrix} \hat{\boldsymbol{\xi}}_s \\ \hat{\boldsymbol{\xi}}_p \end{bmatrix} \tag{3}$$

where $\mathbf{\Phi}_s$ and $\hat{\boldsymbol{\xi}}_s$ contains the structural eigenvectors and structural modal co-ordinates, respectively. The coupled analysis is conducted in Matlab [26] using the finite element toolbox, CALFEM [27]. Further description of the structure-acoustic analysis of this type can be found in [21, 22].

The analysis model

The dimensions of the studied wall and the connecting rooms are given in Table 1. In the parametric study, the height and width of the wall and the connecting rooms are equal. However, the effect of placing the within a baffle is evaluated. In this case, the height and width of the rooms are increased, while keeping the dimensions of the studied wall fixed,

Table 1: *Geometric data.*

Wall length	4.2	m
Wall height	2.6	m
Sending room depth	4.91	m
Receiving room depth	5.2	m
Length of baffle	0	m
Measurement height	1.2	m
Measurement area	2×2	m^2

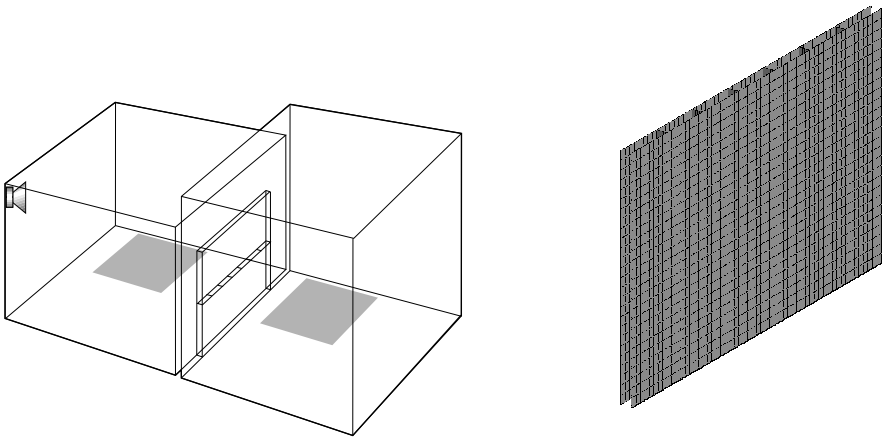

Figure 1: *Measurement setup (left) where the wall is placed in a baffle, and the finite element model of the wall (right).*

as can be seen in Figure 1 (left). The length of the baffle is the increased length and width of the rooms, on the sides and above the studied wall.

The finite element model of the structure can be seen in Figure 1 (right). The plasterboards, modelled by shell elements, are 12.5 mm thick. In the discretisation of the plasterboards, the length of each shell element is 0.075 m. To verify the finite element model, the eigenvalue problem of a simply supported beam with material properties of the plaster board and the length of 0.45 m, is solved. Six shell elements are used to describe the beam, i.e. using the same discretisation as for finite element model employed in the study. The second natural frequency (228 Hz) is calculated with an error of 4 % compared to the analytical solution, which shows that the model provides satisfactory accuracy. The sheet-metal wall studs, described by shell elements for the web and beam elements for the flanges, are 0.5 mm thick. The modulus of elasticity, E, Poisson's ratio, ν, and density, ρ, for the materials can be found in Table 2. The screws connecting the plasterboards to the wall studs are placed with 0.2 m between adjacent screws, modelled as springs connecting the nodes at the wall stud–plasterboard interface. The stiffness, K, of each screw for the in-plane deformation (parallel to the plasterboard) can be found in Table 2. The coupling in the normal direction and the rotational coupling in all three directions are assumed to be rigid. The loss factor, $\eta = 0.02$, is assumed independent of frequency and used in the analysis for both the wall and the connecting rooms. Damping is thereby included at a constitutive level in the structural domain as a complex modulus of elasticity

$$E \rightarrow (1 + \mathrm{i}\eta)E \tag{4}$$

and in the two rooms as a complex bulk modulus

$$B_0 \rightarrow (1 + \mathrm{i}\eta)B_0 \tag{5}$$

where $B_0 = \rho_0 c_0^2$, and where ρ_0 and c_0 are the density of and speed of sound in air. The sound absorbing material placed inside the wall cavities is described by an equivalent fluid

Table 2: *Material properties.*

Wall studs:			
E	=	210	GPa
ν	=	0.30	
ρ	=	7800	kg/m^3
Plasterboards:			
E	=	3	GPa
ν	=	0.10	
ρ	=	720	kg/m^3
Fasteners:			
K	=	500	kN/m
Air:			
ρ_0	=	1.21	kg/m^3
c_0	=	340	m/s
Porous material:			
c_p	=	280	m/s
ϕ	=	0.99	
σ	=	20000	Ns/m^4
k_s	=	1.7	
ρ_s	=	30	kg/m^3

introduced by Gransson [28], assuming the frame of the porous material to be limp and not in contact with the rest of the wall, i.e. no vibrations are induced in the porous material frame. The material parameters for air and the porous material are also given in Table 2: c_p is the speed of sound inside the porous material; ϕ is the porosity; σ is the flow resistivity; and k_s is the structure factor of the porous material. The equivalent fluid model introduces frequency-dependent density and bulk modulus. See [28] for a detailed description of the material model and parameters.

The walls studied are specified as, for example, R120 202 s600, where R120 denotes the wall thickness in mm, 202 denotes two plasterboards on each side of the wall, and s600 denotes the distance between the wall studs in mm.

Evaluation of sound transmission loss

The present study simulates the measurement standard set forth in [3]. Thus, the sound transmission loss, R, is determined by

$$R = L_s - L_r - 10\log\left(\frac{A}{S}\right) \tag{6}$$

where L_s and L_r are the spatial averages of the sound pressure level, filtered into $\frac{1}{3}$-octave bands, in the sending and receiving rooms, respectively. Pressure levels are evaluated in a rectangular partition in the centre of each room, the shaded are in Figure 1 (left), at the height and in the area given in Table 1. S is the area of the wall being studied and A is the absorption area in the receiving room, which can be expressed in terms of the

reverberation time, T, and the volume of the room, V:

$$A = 0.16\frac{V}{T} \tag{7}$$

The loss factor, $\eta = 0.02$, which is independent of frequency, is used in the analysis. The reverberation time then is

$$T = \frac{2.2}{f\eta} \tag{8}$$

where f is the frequency. The sound transmission loss can thereby be calculated in $\frac{1}{3}$-octave bands

$$R = L_s - L_r - 10\log\left(0.38 f\eta\right) \tag{9}$$

where the receiving room dimensions in Table 1 have been used. The same correction term for the room and wall dimensions and the reverberation time of the receiving room is used in all analyses.

Low-frequency measures

To derive a measure of the experienced difference in sound levels between the studied configurations, the pressure levels in the various frequency bands must be weighted together [4]. For this weighting, sound pressure levels in the 50–5000 Hz range are required, which are not available here. In the present study a linear weighted low-frequency measure is derived, determining the sound pressure level difference in the frequency range of interest. The low-frequency sound transmission loss, $\Delta L^{f_a-f_b}$, is calculated by integrating the pressure levels in the two rooms given in $\frac{1}{3}$-octave bands over the frequency range of f_a to f_b ($\frac{1}{3}$-octave band centre frequencies) indicated by the superscript, i.e.

$$\Delta L^{f_a-f_b} = L_s^{f_a-f_b} - L_r^{f_a-f_b} \tag{10}$$

where

$$L_i^{f_a-f_b} = 10\log\left(\sum_{f=f_a}^{f_b} 10^{L_i/10}\right) \tag{11}$$

where $i = \{s, r\}$. Note that $\Delta L^{f_a-f_b}$ only pertains to the pressure level difference, not including the last term in equation (9). Two different frequency intervals are used: ΔL^{40-200} is evaluated to investigate sound transmission loss in the low-frequency range for the $\frac{1}{3}$-octave bands with centre frequencies between 40 Hz and 200 Hz. (Thus, the actually studied frequency range is between 35 and 220 Hz.) To exclude the behaviour of the $\frac{1}{3}$-octave bands with centre frequencies from 100 Hz and below, $\Delta L^{126-200}$ is also evaluated. This second measure is derived to determine whether the studied properties only influence sound transmission loss at very low frequencies or also in frequencies above 100 Hz.

3 The parametric study

The influence of a number of system parameters on sound transmission loss is examined. When one of the parameters is varied the others are held constant and given in Tables 1 and 2. The sound transmission loss is evaluated by means of equation (9), using the

calculated sound pressure levels in the sending and receiving rooms. The results for each of the variables in the parametric study are displayed both by means of sound transmission loss (TL) curves and by the low-frequency measures, ΔL^{40-200} and $\Delta L^{126-200}$.

Material properties of the wall

The calculated TL when varying the modulus of elasticity, E, of the plasterboards is displayed in Figure 2 and the corresponding low-frequency measures in Figure 3. For the density, ρ, of the plasterboards, the calculated TL is given in Figure 4 and the low-frequency measures in Figure 5.

As the modulus of elasticity and density of the plasterboards affect the modal characteristics of the wall, the peaks in TL shift in frequency (see Figures 2 and 4). However, varying the modulus of elasticity of the plasterboard does not change the value of ΔL^{40-200}

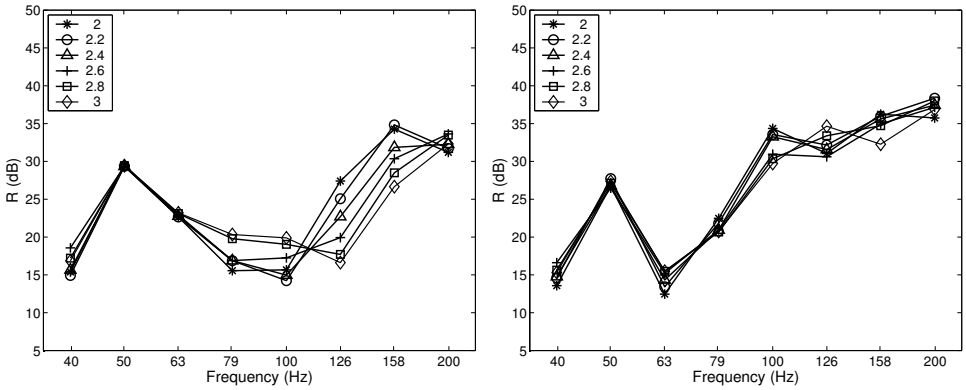

Figure 2: *Sound transmission loss when varying the plasterboard modulus of elasticity, E, for wall types* R120 202 c450 *(left) and* R120 202 s600 *(right).*

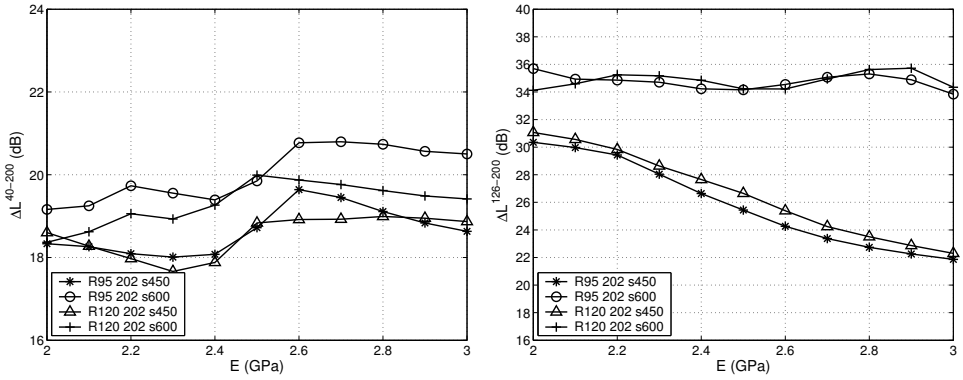

Figure 3: *The low-frequency pressure level difference when varying the plasterboard modulus of elasticity, E, ΔL^{40-200} (left) and $\Delta L^{126-200}$ (right).*

significantly (see Figure 3, left). Low-frequency sound transmission loss increases with increasing plasterboard density, as can be seen for the TL in Figure 4. For low-frequency measures the improvement roughly follows the mass law, which states that doubling the density of the plasterboards increases the TL by about 6 dB. This is shown in Figure 5 (left), where ΔL^{40-200} is displayed; the effect is even more evident in the case of $\Delta L^{126-200}$, displayed in Figure 5 (right).

For the porous material, the TL when varying the density, ρ_s, of the porous material frame and the flow resistivity, σ, is displayed in Figures 6 and 8 and the corresponding low-frequency measures in Figures 7 and 9.

Varying the porous material density and flow resistivity have little effect on the sound transmission in the low-frequency range, as displayed in Figures 6 and 8. The wall vibrations and thereby the sound transmission are mainly governed by the plates and wall studs. The description of the porous material in the present study is simplified, and measurements

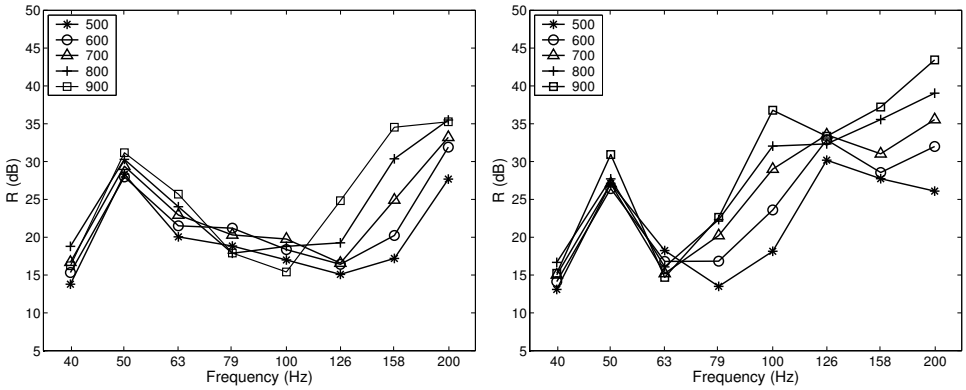

Figure 4: *Sound transmission loss when varying the plasterboard density, ρ, for wall types* R120 202 c450 *(left) and* R120 202 s600 *(right).*

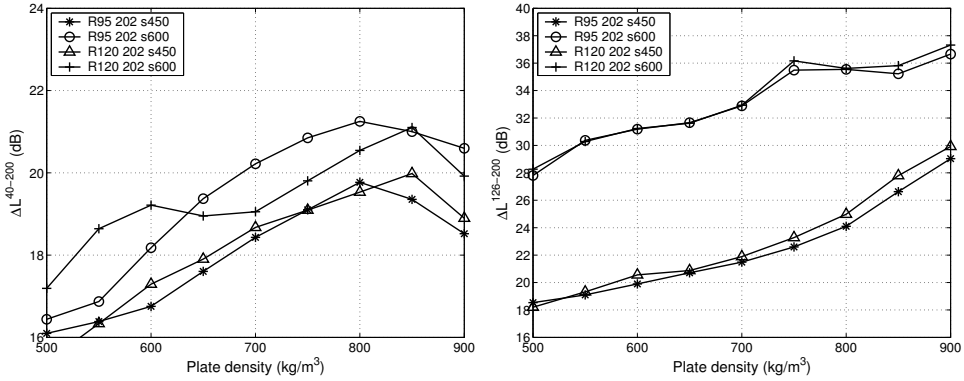

Figure 5: *The low-frequency pressure level difference when varying the plasterboard density, ρ, ΔL^{40-200} (left) and $\Delta L^{126-200}$ (right).*

indicate that the porous material strongly affects low-frequency sound transmission loss (as was found by, for example, Uris et al. [29]). Achieving reliable results regarding the influence of the porous material on sound transmission loss requires a more detailed material description of the porous material. This is provided in Biot's theory, which also includes the stiffness of the porous material frame. Allard [30] gives a detailed description of this theory, and a study of the sound transmission loss of a multilayered structure including porous material was performed by Panneton et al. [31].

Geometric properties of the wall

The TL calculated when varying the distance between the wall studs is displayed in Figure 10, and with the low-frequency measures given in Figure 11. The TL calculated when varying the wall length is displayed in Figure 13, and with the low-frequency measures

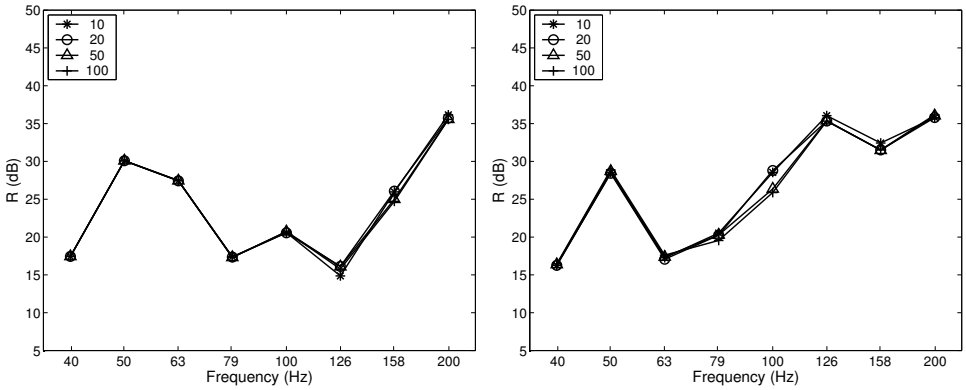

Figure 6: *Sound transmission loss when varying the porous material density, ρ_s, for wall types* R120 202 c450 *(left) and* R120 202 s600 *(right).*

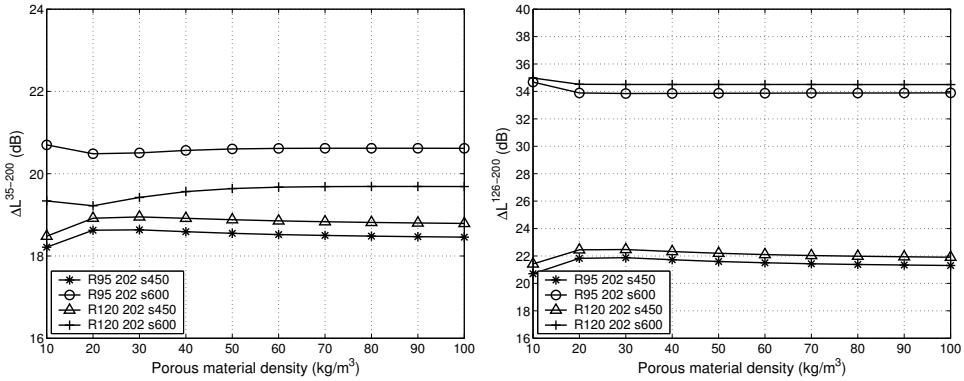

Figure 7: *The low-frequency pressure level difference when varying the porous material density, ρ_s, ΔL^{40-200} (left) and $\Delta L^{126-200}$ (right).*

given in Figure 14.

The sound transmission loss as affected by varying the wall stud spacing is displayed in Figure 10. The spacing affects the stiffness of the plasterboard by changing the distance between the supports, affecting the plate bending motion. The greater the distance between the wall studs, the weaker the wall becomes and the lower the frequency of the primary structural resonance. Above this resonance the wall has a mass-like behaviour and achieves good sound transmission loss. The change in stiffness is proportional to the distance between wall studs to the power of three, whereas the previously studied modulus of elasticity for the plate is linearly proportional to the stiffness, as found by Bradley et al. [5]. The low-frequency resonance of a double wall is, as stated in [5], not the mass-air-mass resonance but the primary structural resonance. This primary resonance is studied in detail for the particular wall type R95 202 s600. By repeating the analysis procedure, but only

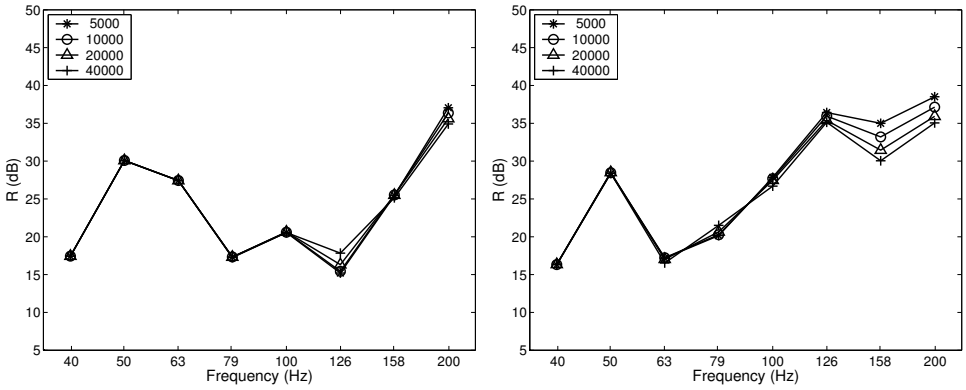

Figure 8: *Sound transmission loss when varying the porous material flow resistivity, σ, for wall types* R120 202 c450 *(left) and* R120 202 s600 *(right).*

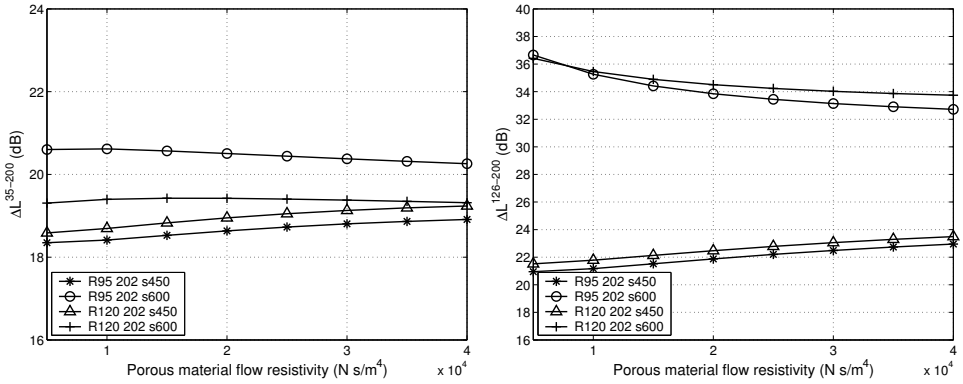

Figure 9: *The low-frequency pressure level difference when varying the porous material flow resistivity, σ, ΔL^{40-200} (left) and $\Delta L^{126-200}$ (right).*

including one in vacuo structural mode at a time in the description of the structure, it is found that the mode with a natural frequency of 70.7 Hz and the mode shape displayed in Figure 12 dominates sound transmission, this mode being the primary structural resonance. The natural frequency of this mode does not directly give the frequency where the sound transmission peaks, as this peak also depends on the porous material in the wall cavities and, to a great extent, on the room dimensions.

For the evaluated $\Delta L^{126-200}$, a wall stud spacing of 0.60 m generally produces 10–12 dB less sound transmission than does the 0.45 m spacing, this holding true for any parameter studied. This is also due to the primary structural resonance, which occurs below 100 Hz for the 0.6 m spacing but in the studied frequency range for the 0.45 m spacing.

Varying the length of the wall, and thereby also the dimensions of the rooms, the modal characteristics of the rooms is affected. This is evident in the $\frac{1}{3}$-octave band with centre frequency 80 Hz, where the calculated sound transmission loss varies greatly for the same

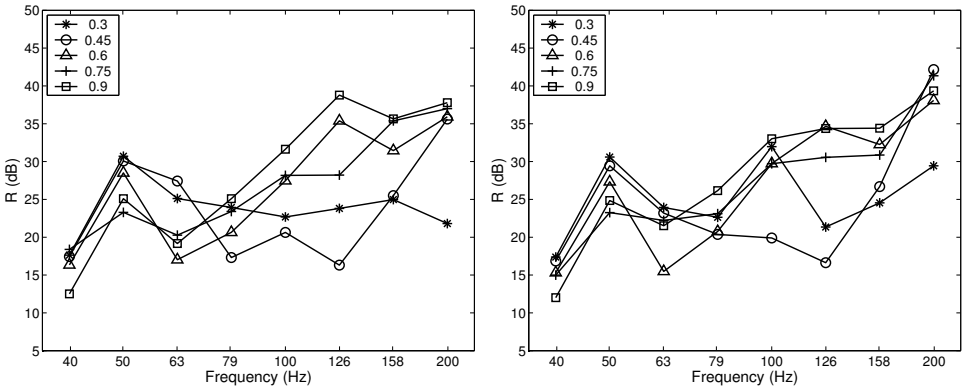

Figure 10: *Sound transmission loss when varying the wall stud spacing for wall types* R95 202 *(left) and* R120 202 *(right).*

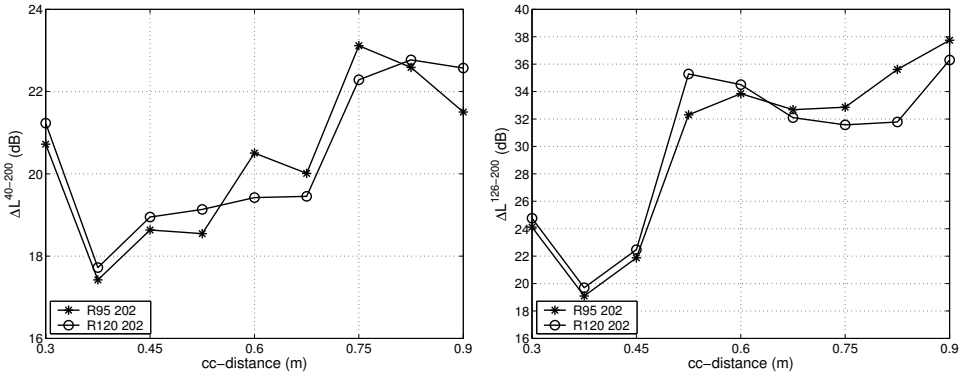

Figure 11: *The low-frequency pressure level difference when varying the wall stud spacing,* ΔL^{40-200} *(left) and* $\Delta L^{126-200}$ *(right).*

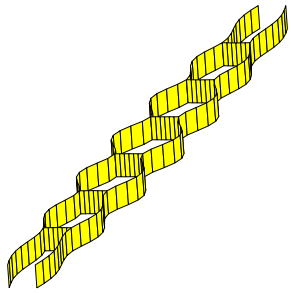

Figure 12: *The primary structural resonance for* R95 202 s600 *with the in vacuo natural frequency being 70.7 Hz. A slice along the length and at half the total height of the wall is displayed. The spacing of the wall studs, the plasterboard density, and the modulus of elasticity are important in determining the natural frequency of the mode.*

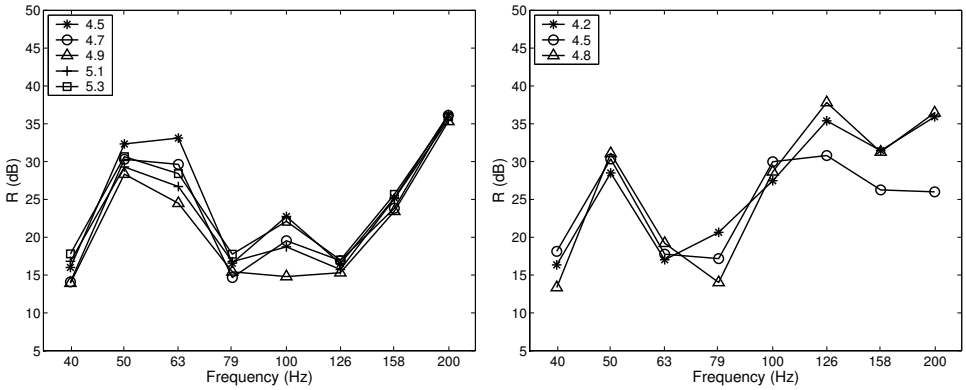

Figure 13: *Sound transmission loss when varying the wall length for wall types* R120 202 c450 *(left) and* R120 202 s600 *(right).*

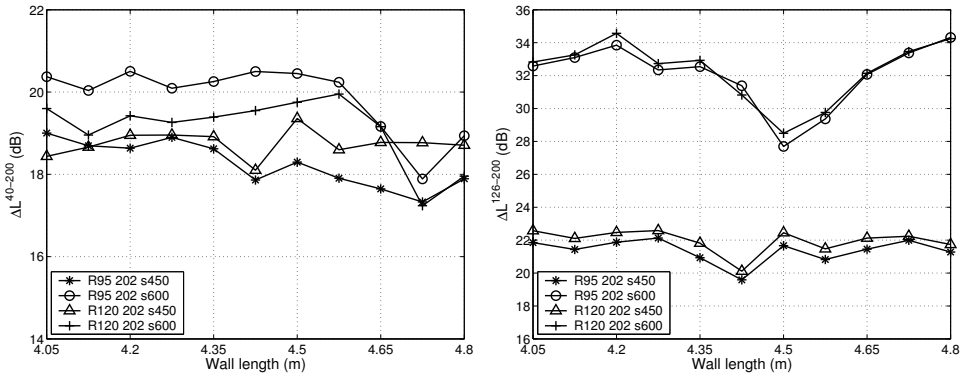

Figure 14: *The low-frequency pressure level difference when varying the wall length,* ΔL^{40-200} *(left) and* $\Delta L^{126-200}$ *(right).*

wall type (see Figure 13). Also, the smaller width of the last wall cavity means that the primary structural resonance is present in frequency bands higher up in the frequency range. This is evident in Figure 13 (right), where TL is displayed for a wall stud spacing of 600 mm. The same can be seen in the measure $\Delta L^{126-200}$, which varies 4 dB depending on the size of the last cavity (see Figure 14, right).

The sudden jump seen in the calculated $\Delta L^{126-200}$ in Figure 11 (right) can also be explained by the primary structural resonance. For wall stud spacings between 0.3 m and 0.45 m, this resonance occurs in the frequency range studied. The two configurations with stud spacings of 0.525 m and 0.60 m have their primary structural resonances at natural frequencies below the studied range (this also holds true for the last wall cavity, since the total wall length is a whole multiple of these wall stud spacings). The dynamic behaviour is governed by the mass of the system and the sound transmission loss is high.

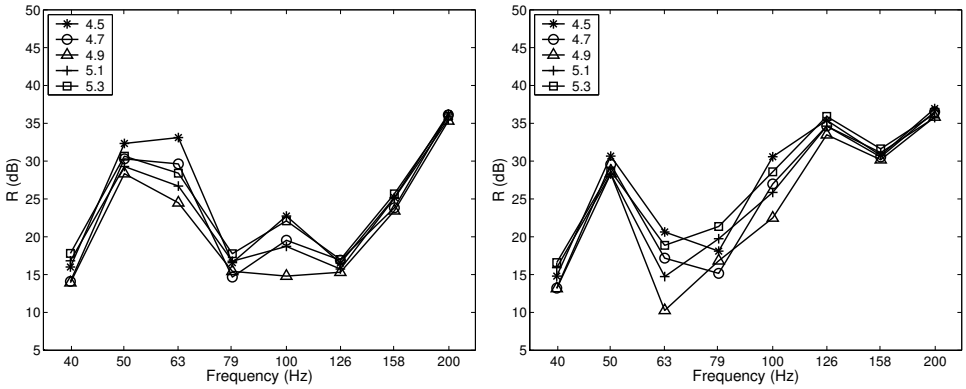

Figure 15: *Sound transmission loss when varying the receiving room depth for wall types* R120 202 c450 *(left) and* R120 202 s600 *(right).*

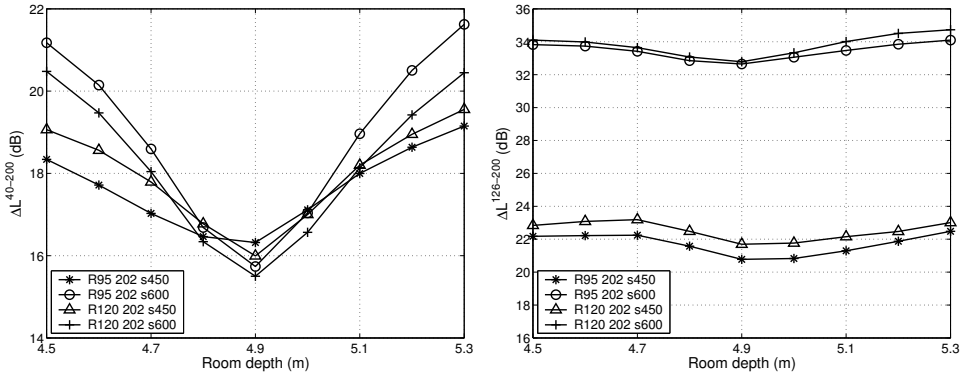

Figure 16: *The low-frequency pressure level difference when varying the receiving room depth,* ΔL^{40-200} *(left) and* $\Delta L^{126-200}$ *(right).*

Room dimensions

The effect on TL of varying the depth of the receiving room is evaluated in Figure 15, and with the low-frequency measures given in Figure 16. The effect on TL of placing the wall within a baffle is displayed in Figure 17, and the corresponding low-frequency measures are given in Figure 18.

The dimensions of the sending and receiving rooms strongly affect sound transmission (see Figure 15). These effects are well known, and similar results have been presented in, for example, [7, 9, 11]. The difference in sound transmission loss in the low-frequency range, ΔL^{40-200}, can be up to 6 dB depending on the receiving room length (see Figure 16, left). With equal room sizes, ΔL^{40-200} is almost equal for the different wall configurations due to the matching eigenmodes of the two rooms. Calculating $\Delta L^{126-200}$, the depth of the room has only a small effect, as indicated in Figure 16 (right). The influence of room

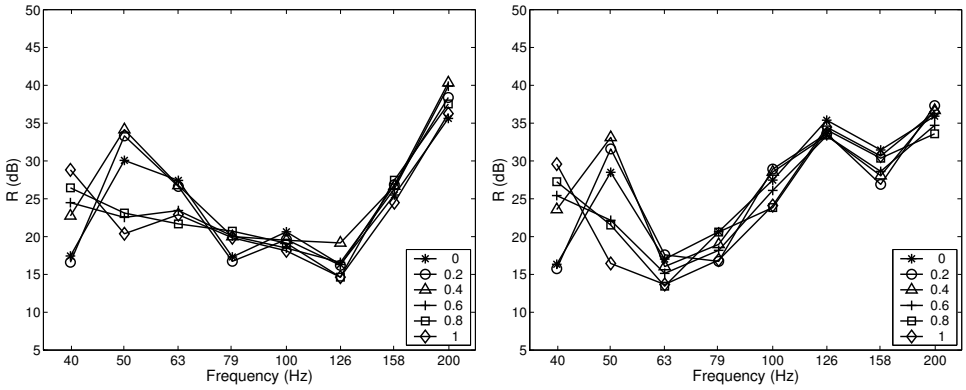

Figure 17: *Sound transmission loss when varying the length of the baffle for wall types* R120 202 c450 *(left) and* R120 202 s600 *(right).*

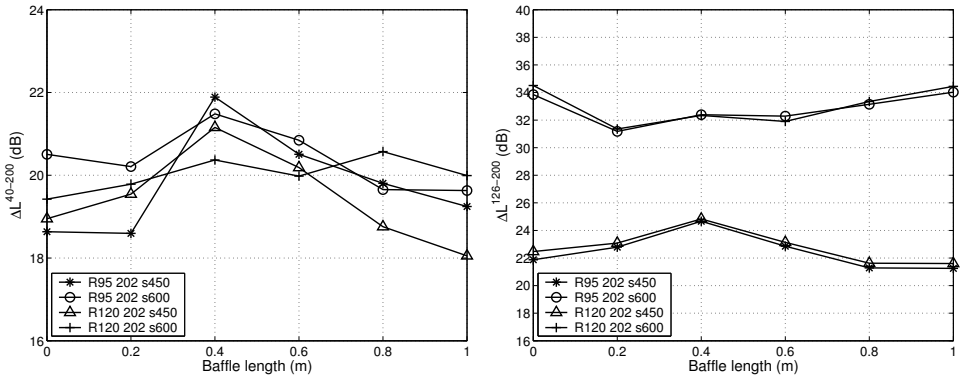

Figure 18: *The low-frequency pressure level difference when varying the length of the baffle,* ΔL^{40-200} *(left) and* $\Delta L^{126-200}$ *(right).*

dimensions is here limited to the 40-125 Hz range, this being dependent on the size of the studied rooms.

The calculated sound transmission loss when placing the wall within a baffle is displayed in Figure 17. Although, the low-frequency sound transmission loss in certain frequency bands fluctuates, ΔL^{40-200} is not significantly affected (see Figure 18, left). In [32], placing a single-leaf wall within a baffle was seen to improve the sound transmission loss. In that case, however, the wall size was decreased while keeping the room size fixed. In the present study, however, it is the room dimensions that are changed.

4 Conclusions

The need to perform a detailed analysis to be able to accurately predict sound transmission loss in the low-frequency range is demonstrated. This was done by examining a number of parameters that describe the sending-room-wall–receiving-room system.

The improved sound transmission loss when increasing the sheeting material density on average follows the mass law, whereas the modulus of elasticity only has a small effect on the modal characteristics of the wall. The distance between the wall studs, however, is important for low-frequency sound transmission loss. This distance affects the natural frequency of the primary structural resonance at which the sound transmission loss is low. The length of the studied double wall can affect the primary structural resonance, also leading to decreased sound transmission loss above 100 Hz. The room dimensions, both perpendicular and parallel to the wall, are of great importance, especially at frequencies below 100 Hz. Several of the studied effects have been presented in earlier work, both in terms of measurements and theoretical models for single-leaf walls. In this paper, however, the analysis, including the full geometric description of the double wall and connecting rooms, gives a structured presentation of the effects of various parameters on sound transmission loss in the low-frequency range and on the ability to compare different changes in the system.

5 Acknowledgements

The Swedish Foundation for Strategic Research (project number IVS-98-501), Formas (project number 24.2/2002-1601), and Lindab Profile AB, Sweden, are gratefully acknowledged for their financial support.

References

[1] J. Mathys. Low-frequency noise and acoustical standards. *Applied Acoustics*, 40:185–199, 1993.

[2] B. Berglund and P. Hassmen. Sources and effects of low frequency noise. *The Journal of the Acoustical Society of America*, 99(5):2985–3002, 1996.

[3] EN ISO 140-3:1995(E): Acoustics – measurement of sound insulation in buidings and of building elements– part 3: Laboratory measurements of airborne sound insulation of buiding elements. European standard, 1995.

[4] EN ISO 717-1:1996: Acoustics rating of sound insulation in buildings and building elements part 1: Airborne sound insulation. European standard, 1996.

[5] J. S. Bradley and J. A. Birta. On the sound insulation of wood stud exterior walls. *The Journal of the Acoustical Society of America*, 110(6):3086–3096, 2001.

[6] P. Hammer and E. Nilsson. Light weight partition walls and floors – The infludence of mineral wool on sound insulation. TVBA 3095, Engineering Acoustics, LTH, Lund University, Box 118, SE-221 00 Lund, Sweden, 1997.

[7] S. P. S. Maluski and B. M. Gibbs. Application of a finite-element model to low-frequency sound insulation in dwellings. *The Journal of the Acoustical Society of America*, 108(4):1741–1751, 2000.

[8] K. A. Mulholland and R. H. Lyon. Sound insulation at low frequencies. *The Journal of the Acoustical Society of America*, 54(4):867–878, 1973.

[9] W. Kropp, A. Pietrzyk, and T Kihlman. On the meaning of sound reduction index at low frequencies. *Acta Acustica*, 2(5):379–392, 1994.

[10] A. Pietrzyk. Sound insulation at low frequencies. Doctoral thesis, Chalmers Unsiversity of Technology, Department of Applied Acoustics, Göteborg, Sweden, 1997.

[11] A. Osipov, P. Mees, and G. Vermeir. Low-frequency airborne sound transmission through single partitions in buildings. *Applied Acoustics*, 52:273–288, 1997.

[12] H. V. Fuchs, X. Zha, and M. Pommerer. Qualifying freefield and reverberation rooms for frequencies below 100 hz. *Applied Acoustics*, 59:303–322, 2000.

[13] S. Maluski and B. M. Gibbs. The effect of construction material,contents and room geometry on the sound field in dwellings at low frequencies. *Applied Acoustics*, 65:31–44, 2004.

[14] C. I. Papadopoulos. Development of an optimised, standard-compliant procedure to calculate sound transmission loss: design of transmission rooms. *Applied Acoustics*, 63:1003–1029, 2002.

[15] C. I. Papadopoulos. Development of an optimised, standard-compliant procedure to calculate sound transmission loss: numerical experiments. *Applied Acoustics*, 64:1069–1085, 2003.

[16] J. Brunskog and P. Davidsson. Sound transmission of structures; a finite element approach with simplified room description. *Accepted for publication in Acta Acustica united with Acustica*, 2004.

[17] K.-J. Bathe. *Finite Element Procedures*. Prentice Hall, New York, 1996.

[18] O. C. Zienkiewicz and R. L.Taylor. *The Finite Element Method*, volume 1 and 2. MacGraw-Hill, London, 1994.

[19] N. Ottosen and H. Peterson. *Introduction to the Finite Element Method*. Prentice Hall, New York, 1992.

[20] H. Morand and R. Ohayon. *Fluid structure interaction*. John Wiley & sons, Chichester, 1995.

[21] G. Sandberg. A new strategy for solving fluid-structure problems. *International Journal of Numerical Methods in Engineering*, 38:357–370, 1995.

[22] G. Sandberg. Acoustic and interface elements for structure-acoustic analysis in calfem. TVSM 7113, Structural Mechanics, LTH, Lund University, Box 118, SE-221 00 Lund, Sweden, 1996.

[23] P. Davidsson. Finite element analysis of structure-acoustic systems – methods and applications. TVSM 3060, Structural Mechanics, LTH, Lund University, Box 118, SE-221 00 Lund, Sweden, 2001.

[24] F. Fahy. *Sound and structural vibration*. Academic Press, London, 1985.

[25] MSC/NASTRAN - V2001. The MacNeal-Schwendler Corporation, 2001.

[26] Matlab user's manual. Mathworks Inc., 2002.

[27] CALFEM – a finite element toolbox to matlab. Technical Report Report TVSM–9001, Lund University, 1996.

[28] P. Göransson. Acoustic finite element formulation of a flexible porous material– a correction for inertial effects. *Journal of Sound and Vibration*, 185(4):559–580, 1995.

[29] A. Uris, A. Llopis, and J. Llinares. Effect of the rockwool bulk density on the airborne sound insulation of lightweight double walls. *Applied Acoustics*, 58:327–331, 1999.

[30] J. F. Allard. *Propagation of sound in porous media; modelling sound absorbing matarials*. Elsevier Science Publishers Ltd, London, 1993.

[31] R. Panneton and N. Atalla. Numerical prediction of sound transmission through finite multilayer systems with poroelastic materials. *The Journal of the Acoustical Society of America*, 100(1):346–354, 1996.

[32] A. Nilsson. Reduction index for a panel in a baffle. Technical Report 73-02, Department of Building Acoustics, Chalmers University of Technology, 1973.

Paper 7

Sound transmission of structures; a finite element approach with simplified room description

Peter Davidsson
Division of Structural Mechanics,
Lund University

Jonas Brunskog,
Division of Engineering Acoustics,
Lund University

Sound transmission of structures; a finite element approach with simplified room description

Jonas Brunskog
Division of Engineering Acoustics, LTH, Lund University, P.O. Box 118, SE-221 00 Lund, Sweden. E-mail: jonas.brunskog@acoustics.lth.se

Peter Davidsson
Division of Structural Mechanics, LTH, Lund University, P.O. Box 118, SE-221 00 Lund, Sweden. E-mail: peter.davidsson@byggmek.lth.se

Summary
A theoretical prediction model for the sound insulation of a wall is an important tool when developing new wall structures. A full description of the entire room-wall-room system in a theoretical model for sound insulation is still today too computation-intensive, implying that the sound insulation at higher frequencies cannot be studied. Some simplifications must thus be introduced. The simplification proposed in this present paper is to describe the rooms with waveguides, i.e., infinity-long rooms. The model then reduces to the (more or less) two-dimensional wall. The question of how to apply the excitation then arises. The choice proposed here is to use a combination of diffuse field and Monte Carlo simulations. The incident and radiated power, expressed in waveguide modes, are used to calculate the transmission loss. A minor literature survey is also included, as well as numerical results and comparison with experimental results. The method presented is developed to study the sound insulation of lightweight double-leaf walls, and the numerical results of such walls are presented.

PACS no. 43.55.Rg, 43.55.Ti, 43.20.Mv

1. Introduction

The development of new building systems is intensive. These new systems are often related to lightweight constructions and developed for use in load-bearing structures and dwellings. When developing such new building structures, a theoretical prediction model for the sound insulation is an important tool.

When studying the airborne sound insulation of a building structure, various approaches have been used by researchers. The simplest approach is to describe the structure to be infinite in extent and coupled to semi-infinite sender and receiver rooms, as Cremer did for a homogenous wall in 1942 [1] (repeated in [2, pp. 544–547]), or as London did for a double wall some years later [3]. However, the vibration field in an actual structure can be divided into one part with wavenumbers that corresponds to the wavenumbers in the surrounding (excitating) medium, and one part with other wavenumbers – especially the wavenumbers of the free waves of the structure. The first part can be referred to as the *forced field* and the second part as the *reverberant field*. When studying infinite structures, only the forced field is present causing sound transmission (below the critical frequency). The finiteness of the structure introduces a continuous amount of wavenumbers, some of which are able to radiate sound; thus, the fact that the finiteness of the radiation region will cause extra radiation is not taken into account in the infinite model.

The approaches that include finiteness can schematically be divided into four groups, corresponding to the combinations of finite/infinite fluid field and finite/infinite structural field. The papers mentioned [1, 3] fall in the group of infinite fluid field and infinite structural field (i.e., no inclusion of finiteness). The finite-finite case has mostly been studied in the low frequency region using normal modes [4, 5, 6, 7, 8, 9, 10, 11, 12] or the finite element method (FEM) [13, 14, 15]. Kropp et. al. [16] made use of both FEM and normal modes, studying the meaning of the transmission loss at low frequencies (the FE-model was primarily used as a check of the simplifications in the normal mode model). Also the boundary element method (BEM) has been used, e.g., by Santos and Tadeu [17, 18] in a study of the insulation of a wall separating two contiguous "tunnels". Thus, they made the problem two-dimensional by means of infinite extensions of the rooms. However, in contrast to the present problem, they allowed one of the directions parallel to the wall to be infinite (as they were specially interested in the low frequency problems of the geometry of the room affecting the sound insulation). Other approaches are the use of the Green ray integral method [19] – an uncoupled approach where the structure is described by FEM and approximative Green's functions are used to describe the rooms – and the decoupled modal approach [20].

A common way to introduce finiteness is to let both the fluid and structural field be infinite, but to let the radiation area be finite, cf. Ljunggren [21], Villot et al. [22] and Cremer and Heckl [2, pp. 526–534], so that the phenomenon of finite radiating area is taken into account. However, in a later paper Ljunggren [23] states that the actual type of room boundary condition is important; the transmission of an ordinary homogenous wall due to resonant response increases by 6 dB at frequencies below the critical frequency if the rooms described by cosine-modes are compared with a wall mounted in a baffle (i.e., as in [21]). This

Received 1 January –,
accepted 1 January –.

effect was not seen by Kropp et. al. [16] in their analysis (as is more thoroughly discussed below); this fact can perhaps be explained by the fact that no boundary losses were present in [16], in contrast to [21]. The latter paper – even if it is not always easy to follow – provided one of the starting points for the present paper.

Many of the prediction models for sound insulation available today are restricted to very simplified structures: for example, many of them do not include the joists in a double-leaf structure [3, 24, 25]. However, there are prediction models that include the joists, e.g., [26, 27, 28, 29, 30]. Some of these deal with point excitation and some with airborne excitation (see also the literature survey [31]), but in these models the wall is assumed infinite in extent. One possibility then is to make use of the finite element method, so that all details of interest in the structure can be described and included in the model, and at the same time the finiteness of the real structure is included. A drawback using the finite element method directly is that it is computationally time consuming, meaning that normally only the low frequency range can be studied. Thus, the approach proposed here aims to reduce the computation time of the FE-approach.

It should be pointed out that the numerical results (presented in section 3) do not – at this stage – aim to yield further insight into the physics of sound insulation; the aim of the paper is merely to present an effective numerical prediction model for the transmission loss of a wall structure.

The present paper tries to predict the sound insulation of a wall structure by means of FEM, and thus, the low frequencies are of special interest (even if the goal is to stretch the limits to higher frequencies) as FEM is a deterministic low frequency range method. The prediction of sound insulation at low frequencies is a difficult task: the measured or calculated sound insulation is in principal only valid for the specific case under consideration. Parameters such as room dimensions, reverberation time, or geometry of the interface influence the sound insulation [16, 13, 14, 15]. For low frequencies there is a large dependence in the sound transmission loss of the size of the rooms. However, to include this dependency in a theoretical model studying the room-wall-room system the analysis will be limited to very low frequencies due to the size of the numerical model. As was found in e.g., [13, 14, 15], the dependence on the dimensions of the rooms to the sound reduction of the wall also makes it difficult to evaluate how changes in the wall properties affect the sound transmission in room configurations other than the one where the measurements (or calculations) are performed. Thus, it can be preferable to use the tube-like room, as it is well defined. Moreover, it is related to the ensemble average of every room (cf. SEA theory [32]).

The simplified room description – as reflected in the title of the present paper – is achieved by means of assuming the rooms as being infinite in extent in the direction perpendicular to the test wall (see Figure 1). Thus, the theory used is a waveguide theory. The walls normal to the transmitting wall are rigid, described by cosine-modes, but the walls parallel with the transmitting wall are not present (or are totally absorbing). Thus, the aim is to evaluate the sound transmission loss (TL) for walls without the influence of the depth dimensions of the connecting rooms. By using waveguide rooms, the problem can be reduced by including terms that are due to the loading of the rooms added to the dynamic stiffness of the wall. In other words, the problem is reduced from three dimensions to two. The calculation procedure presented here was first developed in [33]. The present paper states the calculation procedure in a more general way, develops it further, and uses notations and methods used in a FEM context.

When measuring the transmission loss, the two-room method is the laboratory technique most often used. A wall is built up between the sender and receiver rooms, the sound levels in both rooms are measured, and the transmission loss can be determined [34]. When measuring in a laboratory, the two rooms must fulfil the criteria for a diffuse sound field. Thus, the actual measurement situation that the prediction model is to be compared against is clearly finite in its character. However, there is also a measurement procedure where intensity measurements are applied [35]. This measurement procedure corresponds roughly to the calculation procedure proposed here.

There are some similarities between this paper and the paper by Kropp et. al. [16]: in the modal approach a wave formulation was used in the direction perpendicular to the test wall. The Kropp paper also has a "sketch" of a combined modal and finite element approach, where the wall is modelled by FEM and the sound field is described by the modal approach. The coupling is to be performed point-wise by means of a mobility matrix of the structure (determined in vacuum). However, the combined approach was not used in the paper. Kropp et. al. fulfilled the boundary conditions by means of point collocation: the modal amplitudes were adjusted so that the boundary conditions were fulfilled in a finite number of discreet points. The wall was described as a locally reacting mass impedance, and no boundary losses were introduced (as discussed above). Also Thomasson [11] formulated the problem with a wave formulation in the direction perpendicular to the test wall (and modes in the other directions). He also assumed the wall to be a locally reacting mass impedance, but avoided the use of point collocation. The back-side wall, parallel to the test wall, was absorbing. Other similar studies are Nilsson [9] and Gagliardini et al. [12], who were interested in baffle effect.

The problem setup can be seen in Figure 1, with the test wall in the x_1x_2-plane and the rooms and the perpendicular walls having infinite extension in the x_3 direction. The test wall has a total thickness d. The computational model is verified by comparison with measurement (see section 3.3) and by a theoretical comparison with simplified mass-law formulas (see the appendix section A2).

The paper is organised as follows: after the introduction in section 1 comes the theoretical section, starting with a general description in section 2.1, the structural displacement being primary described in FE-coordinates; the model used for the rooms is presented in section 2.2; the fluid-structure coupling is described in section 2.3, where

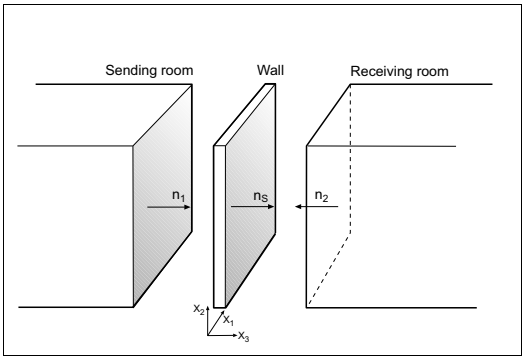

Figure 1. The model. The normal vectors of the fluid regions, n_1 and n_2, point outwards.

the structural displacement is expressed in terms of the fluid modes; in sections 2.4 and 2.5 the coupling expressions so found are rewritten in terms of the FE-coordinates primary used for the structure; the FE expressions are then solved in sections 2.6 and 2.7; the excitation is discussed in section 2.8; the power expressions used to calculate the transmission loss are presented in section 2.9; the numerical results are then presented in section 3, including a description of the numerical procedures and comparisons with measurements; then follows a short discussion of the findings in section 4; and the paper ends with some concluding remarks in section 5.

2. Theory

2.1. Problem description

The differential equation describing the structure in Figure 1 can be formulated as

$$\mathcal{L}_s \mathbf{w} = \mathbf{n}_1 \, p^e|_{x_3=0} + \mathbf{n}_1 p^r|_{x_3=0} + \mathbf{n}_2 p^t\big|_{x_3=d} \quad (1)$$

where

$$\begin{aligned} \mathbf{w} &= [w_1 \; w_2 \; w_3]^T, \\ \mathbf{n}_1 &= [0 \; 0 \; 1]^T, \; \mathbf{n}_2 = [0 \; 0 \; -1]^T, \end{aligned}$$

and where $\mathcal{L}_s$ is the differential operator acting on the structural displacement $\mathbf{w}$. Moreover, p^e is the excitation pressure and p^r the reflected pressure at the wall in the source room and p^t is the transmitted pressure in the receiving room. The normal vectors $\mathbf{n}_1$ and $\mathbf{n}_2$ are defined in Figure 1. The pressures and displacements are assumed to be in the linear range. A time dependency $\mathrm{e}^{\mathrm{i}\omega t}$ is assumed and omitted ($\mathrm{i} = \sqrt{-1}$), $\omega = 2\pi f$ being the angular frequency. A finite element formulation of the structure, as described in (1), results in a system with n equations of motion (n is the number of degrees of freedom)

$$(-\omega^2 \mathbf{M}_s + \mathbf{K}_s)\mathbf{u} = \mathbf{f}^e + \mathbf{f}^r + \mathbf{f}^t, \quad (2)$$

where $\mathbf{M}_s$ and $\mathbf{K}_s$ are the mass and stiffness matrices for the structure (which are not to be discussed in the present paper; we refer to standard FE-literature such as [36, 37], for coupling between internal cavity and wall structure, see [38]). The structural displacement $\mathbf{w}$ is related to the FE nodal displacement vector $\mathbf{u}$ as

$$\mathbf{w} = \mathbf{N}_s \mathbf{u},$$

where $\mathbf{N}_s$ is the structural shape functions. Moreover, the pressures are transformed to force vectors

$$\mathbf{f}^i = \int_{\partial\Omega_j} \mathbf{N}_s^T \mathbf{n}_j p^i \mathrm{d}S, \quad (3)$$

where $i = \{e, r, t\}$ and $j = \{1, 1, 2\}$. The integration is performed on each side of the structure; i.e. $\partial\Omega_1$ is the surface between the structure and the sending room and $\partial\Omega_2$ is the surface between the structure and the receiving room (see Figure 1).

2.2. The rooms

The infinitely long walls perpendicular to the test wall structure are assumed to be rigid. Hence, the boundary condition

$$\begin{aligned} \frac{\partial p^i}{\partial x_1}\bigg|_{x_1=0} &= \frac{\partial p^i}{\partial x_1}\bigg|_{x_1=L_1} \\ &= \frac{\partial p^i}{\partial x_2}\bigg|_{x_2=0} = \frac{\partial p^i}{\partial x_2}\bigg|_{x_2=L_2} = 0 \end{aligned} \quad (4)$$

must be fulfilled. To meet this condition, the pressure field is expanded by means of cosine modes. Thus, the pressure field in the rooms is described by (letting $\hat{\cdot}$ denote amplitudes in the fluid mode coordinates)

$$p^i(x_1, x_2, x_3) = \sum_{m,n=0}^{\infty} \hat{p}^i_{mn} \psi^i_{mn}(x_1, x_2, x_3) \quad (5)$$

with the shape functions

$$\psi^e_{mn}(x_1, x_2, x_3) = \psi_{nm}(x_1, x_2)\mathrm{e}^{-\kappa_{mn} x_3} \quad (6a)$$
$$\psi^r_{mn}(x_1, x_2, x_3) = \psi_{nm}(x_1, x_2)\mathrm{e}^{+\kappa_{mn} x_3} \quad (6b)$$
$$\psi^t_{mn}(x_1, x_2, x_3) = \psi_{nm}(x_1, x_2)\mathrm{e}^{-\kappa_{mn}(x_3-d)} \quad (6c)$$

where equations (6–b) are valid for $x_3 \leq 0$ and equation (6c) is valid for $x_3 \geq d$, where d is the thickness of the wall. The remaining common modal function are cosines

$$\psi_{nm}(x_1, x_2) = \gamma_m \gamma_n \cos(\alpha_m x_1) \cos(\beta_n x_2) \quad (7)$$

where $\alpha_m = \pi m / L_1$, $\beta_n = \pi n / L_2$ and

$$\kappa_{mn} = \sqrt{\alpha_m^2 + \beta_n^2 - k^2}.$$

The modes in equation (7) fulfil the boundary condition in equation (4), and thereby the boundary condition is also fulfilled for the total pressure field. The wavenumber in the air in the rooms is $k = \omega / c_f$, where ω is the angular

frequency and c_f the speed of sound in air. γ_m and γ_n normalise the shape functions

$$\gamma_m = \begin{cases} 1/\sqrt{2} \text{ if } m = 0 \\ 1 \quad \text{if } m \neq 0 \end{cases}. \tag{8}$$

(See also the appendix, section A1). The pressure distribution at $x_3 = 0$ or $x_3 = d$ is truncated and rewritten in matrix notation

$$p^i(x_1, x_2) \approx \sum_{m,n=0}^{M,N} \hat{p}^i_{mn} \psi_{mn}(x_1, x_2) = \boldsymbol{\psi} \hat{\mathbf{p}}^i, \tag{9}$$

where the following vector notations are introduced in the last equality:

$$\boldsymbol{\psi} = [\psi_{11} \ \cdots \ \psi_{mn} \ \cdots \ \psi_{MN}], \tag{10a}$$
$$\hat{\mathbf{p}}^i = [p^i_{11} \ \cdots \ p^i_{mn} \ \cdots \ p^i_{MN}]^T, \tag{10b}$$

and where M and N are the number of terms used in x_1- and x_2-directions in the truncated series expansions of the pressures.

Note that the boundary conditions for the rooms can be other than the rigid boundary conditions now used; other duct modes applies as long as an orthogonality condition can be found. However, the rigid boundary conditions are of most practical interest and are easy to apply.

2.3. Fluid-structure coupling

The boundary conditions at $x_3 = 0$ and $x_3 = d$, connecting the fluid fields with the structural field, are still to be fulfilled. These boundary conditions are, for the sending room

$$\left.\frac{\partial (p^e + p^r)}{\partial x_3}\right|_{x_3=0} = \omega^2 \rho w_3 \big|_{x_3=0} \tag{11}$$

and for the receiving room

$$\left.\frac{\partial p^t}{\partial x_3}\right|_{x_3=d} = \omega^2 \rho w_3 \big|_{x_3=d} \tag{12}$$

where w_3 is the structural displacement normal to the wall in positive x_3-direction. The pressure derivatives at $x_3 = 0$ and $x_3 = d$ are

$$\frac{\partial p^e}{\partial x_3} = -\sum_{m,n=0}^{\infty} \kappa_{mn} \hat{p}^e_{mn} \psi^e_{mn}(x_1, x_2), \tag{13a}$$
$$\frac{\partial p^r}{\partial x_3} = \sum_{m,n=0}^{\infty} \kappa_{mn} \hat{p}^r_{mn} \psi^r_{mn}(x_1, x_2), \tag{13b}$$
$$\frac{\partial p^t}{\partial x_3} = -\sum_{m,n=0}^{\infty} \kappa_{mn} \hat{p}^t_{mn} \psi^t_{mn}(x_1, x_2). \tag{13c}$$

These derivatives are to be used in equations (11) and (12). The structural vibrations is now expressed in terms of the fluid modes,

$$w_3|_{x_3=0} = \sum_{m,n=0}^{\infty} \hat{u}_{1,mn} \psi_{mn}(x_1, x_2), \tag{14a}$$
$$w_3|_{x_3=d} = \sum_{m,n=0}^{\infty} \hat{u}_{2,mn} \psi_{mn}(x_1, x_2). \tag{14b}$$

Note here that the structure is primary described in terms of the FE-coordinates, see equations (2), (16–b) and the solution in section 2.6 – equation (14–b) is used just for the fluid-structure coupling. Using equation (14–b), together with the derivatives in equation (13–c), inserted in the boundary conditions equations (11–b), yields (if letting the boundary condition be fulfilled for every term in the infinite sums)

$$\hat{p}^r_{mn} = \omega^2 \rho \hat{u}_{1,mn} / \kappa_{mn} + \hat{p}^e_{mn}, \tag{15a}$$
$$\hat{p}^t_{mn} = -\omega^2 \rho \hat{u}_{2,mn} / \kappa_{mn}. \tag{15b}$$

A relation is thus found between the structural displacements and the pressures. This relation must now be expressed in the FE-coordinates.

2.4. Description in terms of FE-coordinates

The relation between the structural vibrations expressed in fluid modal coordinates and the finite element coordinates may now to be derived. The structural displacements in the x_3-direction at the two sides of the wall can be written, using the FE-coordinates $\mathbf{u}$

$$w_3|_{x_3=0} = \mathbf{n}_1^T \mathbf{w}\big|_{x_3=0} = \mathbf{n}_1^T (\mathbf{N}_s \mathbf{u})\big|_{x_3=0}, \tag{16a}$$
$$w_3|_{x_3=d} = -\mathbf{n}_2^T \mathbf{w}\big|_{x_3=d} = -\mathbf{n}_2^T (\mathbf{N}_s \mathbf{u})\big|_{x_3=d}. \tag{16b}$$

(The sign in equation (16b) is due to the orientation of $\mathbf{n}_2$.)The same displacements can also be expressed in terms of the fluid modal coordinates,

$$w_3|_{x_3=0} = \sum_{m,n=0}^{M,N} \hat{u}_{1,mn} \psi_{mn} = \boldsymbol{\psi} \hat{\mathbf{u}}_1, \tag{17a}$$
$$w_3|_{x_3=d} = \sum_{m,n=0}^{M,N} \hat{u}_{2,mn} \psi_{mn} = \boldsymbol{\psi} \hat{\mathbf{u}}_2. \tag{17b}$$

Set equations (16-b) equal to equations (17-b), respectively. Multiplying with $\boldsymbol{\psi}^T$ from left in these equations and integrating over the surface $\partial\Omega_j$ of the structure

$$\int_{\partial\Omega_1} \boldsymbol{\psi}^T \mathbf{n}_1^T \mathbf{N}_s \mathrm{d}S \mathbf{u} = \int_{\partial\Omega_1} \boldsymbol{\psi}^T \boldsymbol{\psi} \mathrm{d}S \hat{\mathbf{u}}_1 \tag{18a}$$
$$-\int_{\partial\Omega_2} \boldsymbol{\psi}^T \mathbf{n}_2^T \mathbf{N}_s \mathrm{d}S \mathbf{u} = \int_{\partial\Omega_2} \boldsymbol{\psi}^T \boldsymbol{\psi} \mathrm{d}S \hat{\mathbf{u}}_2 \tag{18b}$$

The analytical fluid modes can be expressed as

$$\boldsymbol{\psi} = \mathbf{N}_f \tilde{\boldsymbol{\psi}}, \tag{19}$$

where $\tilde{\boldsymbol{\psi}}$ is the discretisation of the analytical fluid modes $\boldsymbol{\psi}$, and $\mathbf{N}_f$ is the finite element shape functions used for

the fluid. Using equation (19), the left part of equations (18–b) can be written as coupling matrices $\mathbf{H}_1$ and $\mathbf{H}_2$,

$$\mathbf{H}_1 = \int_{\partial\Omega_1} \mathbf{N}_s^T \mathbf{n}_1 \mathbf{N}_f \mathrm{d}S, \;\; \mathbf{H}_2 = \int_{\partial\Omega_2} \mathbf{N}_s^T \mathbf{n}_2 \mathbf{N}_f \mathrm{d}S, \quad (20)$$

which now are introduced. For the right part of equations (18–b), making use of the orthogonality of $\psi_{nm}(x_1, x_2)$ yields

$$\int_{\partial\Omega_j} \boldsymbol{\psi}^T \boldsymbol{\psi} \mathrm{d}S = \frac{L_1 L_2}{4} \mathbf{I} \quad (21)$$

with $\mathbf{I}$ being the identity matrix (the orthogonality is more elaborately treated in the appendix, section A1). Using (19–21) the structural modal displacements can now be written

$$\hat{\mathbf{u}}_1 = \frac{4}{L_1 L_2} \tilde{\boldsymbol{\psi}}^T \mathbf{H}_1^T \mathbf{u}, \quad (22a)$$

$$\hat{\mathbf{u}}_2 = -\frac{4}{L_1 L_2} \tilde{\boldsymbol{\psi}}^T \mathbf{H}_2^T \mathbf{u}. \quad (22b)$$

Thus, the structural displacement described in terms of the fluid modal coordinates, $\hat{\mathbf{u}}$, is now related to the structural FE-coordinates, $\mathbf{u}$. The negative sign depends on the direction of $\mathbf{n}_2$.

With the notation

$$\boldsymbol{\Lambda} = \mathrm{diag}([1/\kappa_{11} \; \cdots \; 1/\kappa_{mn} \; \cdots \; 1/\kappa_{MN}]) \quad (23)$$

where M and N are the number of terms used in x_1- and x_2-directions in the series expansions of the pressures, the reacting pressures, as described in equation (15–b), can be written

$$\hat{\mathbf{p}}^r = \omega^2 \rho \frac{4}{L_1 L_2} \boldsymbol{\Lambda} \tilde{\boldsymbol{\psi}}^T \mathbf{H}_1^T \mathbf{u} + \hat{\mathbf{p}}^e, \quad (24a)$$

$$\hat{\mathbf{p}}^t = \omega^2 \rho \frac{4}{L_1 L_2} \boldsymbol{\Lambda} \tilde{\boldsymbol{\psi}}^T \mathbf{H}_2^T \mathbf{u}. \quad (24b)$$

2.5. The force terms

The force terms in equation (2) was rewritten in the pressures in matrix notation in equation (3). Making use of equations (9) and (19–20), equation (3) can be rewritten

$$\mathbf{f}^i = \mathbf{H}_j \tilde{\boldsymbol{\psi}} \hat{\mathbf{p}}^i \quad (25)$$

Using (24–b) in equation (25) gives the force terms expressed in exciting pressure and structural displacements

$$\mathbf{f}^e = \mathbf{H}_1 \tilde{\boldsymbol{\psi}} \hat{\mathbf{p}}^e \quad (26a)$$

$$\mathbf{f}^r = \omega^2 \rho \frac{4}{L_1 L_2} \mathbf{H}_1 \tilde{\boldsymbol{\psi}} \boldsymbol{\Lambda} \tilde{\boldsymbol{\psi}}^T \mathbf{H}_1^T \mathbf{u} + \mathbf{H}_1 \tilde{\boldsymbol{\psi}} \hat{\mathbf{p}}^e \quad (26b)$$

$$\mathbf{f}^t = \omega^2 \rho \frac{4}{L_1 L_2} \mathbf{H}_2 \tilde{\boldsymbol{\psi}} \boldsymbol{\Lambda} \tilde{\boldsymbol{\psi}}^T \mathbf{H}_2^T \mathbf{u} \quad (26c)$$

The first term in equation (26b) is due to the elastic scattered field, and the second term is due to the geometrical reflection of the incident field.

2.6. Solving for the displacement field

The equation of motion for the structure including the exciting pressure and the fluid loading, equations (1–2) can now be written in FE matrix notations, if discreticising the fluid load according to equations (26–c). Introducing the notations

$$\mathbf{D} \equiv \mathbf{D}_s + \mathbf{D}_f \quad (27)$$

which are dynamic stiffness matrixes: $\mathbf{D}_s$ is the structural dynamic stiffness matrix and $\mathbf{D}_f$ is the fluid load dynamic stiffness matrix, and they are

$$\mathbf{D}_s = -\omega^2 \mathbf{M}_s + \mathbf{K}_s$$

$$\mathbf{D}_f = -\omega^2 \rho \frac{4}{L_1 L_2} \left(\mathbf{H}_1 \tilde{\boldsymbol{\psi}} \boldsymbol{\Lambda} \tilde{\boldsymbol{\psi}}^T \mathbf{H}_1^T + \mathbf{H}_2 \tilde{\boldsymbol{\psi}} \boldsymbol{\Lambda} \tilde{\boldsymbol{\psi}}^T \mathbf{H}_2^T \right).$$

Note that the dynamic stiffness matrix $\mathbf{D}_s$ in case of a double wall structure also contains the description of the wall cavities, where the acoustic pressure is used as the primary variable. These cavities do not couple to the pressure fields in the rooms and are left out of the description for clarity. A detailed description of the finite element model of the double wall can be found in [15]. The excitation vector can in a similar way be denoted

$$\mathbf{f} = 2 \mathbf{H}_1 \tilde{\boldsymbol{\psi}} \hat{\mathbf{p}}^e. \quad (28)$$

The FE displacement vector of the structure can then be found as

$$\mathbf{u} = \mathbf{D}^{-1} \mathbf{f}. \quad (29)$$

2.7. Expressing solution in normal modes

In order to reduce computation time, the displacements can be expressed in the m number of structural normal modes $\boldsymbol{\Phi}_s$, found by eigenvalue analysis of the unloaded structure, with $m \ll n$,

$$\mathbf{u} = \boldsymbol{\Phi}_s \boldsymbol{\xi} \quad (30)$$

were $\boldsymbol{\xi}$ is the yet unknown modal coordinates. The reduced set of basis vectors for the coupled system, being the wall structure and the interior wall cavities, is, for readability, only described as structural modes. The basis vectors consists, in reality, of both the in vacuo structural modes and the analytical cosine modes describing the interior wall cavities. The mode superposition is based on two assumptions. First, that the fluid pressure only excites the structural modes included in the reduction. And second, that the finite element model has an upper frequency limit where it ceases to be valid, the modes above this frequency being non-physical [39]. Equation (30) inserted in (2) and (26b–c) gives the reduced equations to solve, making use of the notations

$$\tilde{\mathbf{D}} \equiv \tilde{\mathbf{D}}_s + \tilde{\mathbf{D}}_f \quad (31)$$

where

$$\tilde{\mathbf{D}}_s = -\omega^2 \boldsymbol{\phi}_s^T \mathbf{M}_s \boldsymbol{\phi}_s + \boldsymbol{\phi}_s^T \mathbf{K}_s \boldsymbol{\phi}_s$$
$$\tilde{\mathbf{D}}_f = -\omega^2 \rho \frac{4}{L_1 L_2} \boldsymbol{\Phi}_s^T \left(\mathbf{H}_1 \tilde{\boldsymbol{\psi}} \boldsymbol{\Lambda} \tilde{\boldsymbol{\psi}}^T \mathbf{H}_1^T + \mathbf{H}_2 \tilde{\boldsymbol{\psi}} \boldsymbol{\Lambda} \tilde{\boldsymbol{\psi}}^T \mathbf{H}_2^T \right) \boldsymbol{\Phi}_s$$

and further

$$\tilde{\mathbf{f}} = \boldsymbol{\Phi}_s^T \mathbf{f}. \tag{32}$$

The displacement is now found as

$$\mathbf{u} = \boldsymbol{\Phi}_s (\tilde{\mathbf{D}}^{-1} \tilde{\mathbf{f}}). \tag{33}$$

2.8. Excitation pressure

In an actual measurement situation, the excitation is realised by means of a loudspeaker in a certain position. However, it can be argued that in a theoretical analysis it is a better idea to use a diffuse sound field; e.g., the basic requirement of the sound transmission loss theory is then met (a diffuse field is assumed in the power balance), and the solution is not dependent on the position of the loudspeaker, cf. [40].

In idealisation, a diffuse sound field is a field that consists of an infinite number of uncorrelated plane progressive waves, with their intensity uniformly distributed with respect to direction. The diffuse field is statistically homogeneous and isotropic. For a single frequency analysis (as the present), the idealised diffuse field consists of an infinite number of uncorrelated single-frequency plane waves, all with the same infinitesimal amplitude but with the phase randomly distributed, and the waves arrive from all directions with equal probability [41]. However, in the present case, the exciting pressure must also fulfil the boundary conditions in the room, equation (4). There are thus two conditions to be fulfilled: the diffuseness and the boundary conditions at the rigid walls. To meet these conditions, the diffuseness condition must be released: not all angles of incidence can be present. Thus, the excitation pressure is described as in equation (5). However, only plane progressive waves must be included. The condition for the exciting wave to be a travelling wave in the x_3-direction is that $k^2 > \alpha_m^2 + \beta_n^2$, so that κ_{mn} is imaginary.

Summing up all these conditions, the exciting pressure coefficients then are found as

$$\hat{p}^e_{mn} = \begin{cases} \mathrm{e}^{\mathrm{i}2\pi\theta_{mn}} & \text{if } k^2 > \alpha_m^2 + \beta_n^2 \\ 0 & \text{if } k^2 < \alpha_m^2 + \beta_n^2 \end{cases} \tag{34}$$

where θ_{mn} is a uniformly distributed stochastic variable $\in [0, 1]$. Thus, we will have a finite number of travelling waves with random phase and at the same time fulfilling the boundary conditions. For each calculation one representation according to (34) is chosen. A Monte Carlo procedure is then used to yield an average response (or the variance).

Alternatively, if only the average value is of interest, one can then express equation (34) as

$$\hat{p}^e_{mn} = \begin{cases} \frac{1}{N_{mc}} \sum_{\nu=1}^{N_{mc}} \mathrm{e}^{\mathrm{i}2\pi\theta^{(\nu)}_{mn}} & \text{if } k^2 > \alpha_m^2 + \beta_n^2 \\ 0 & \text{if } k^2 < \alpha_m^2 + \beta_n^2 \end{cases} \tag{35}$$

where N_{mc} is the number of Monte Carlo simulations.

2.9. Transmission loss

The sound transmission loss (or sound reduction index) of a wall is defined as

$$R = \log_{10} \left(\frac{1}{\tau} \right). \tag{36}$$

The transmission coefficient, τ, is the quotient of real power radiated from the plate to the receiver room over real incident power, exciting the plate from the source room,

$$\tau = \frac{\Re\{\Pi_t\}}{\Re\{\Pi_e\}}. \tag{37}$$

The incident power can be written

$$\Pi_e = \frac{1}{2} \int_{\partial\Omega} p^e (\mathrm{i}\omega w_3^e)^* \mathrm{d}S \tag{38}$$

where $\mathrm{i}\omega w_3^e$ is the acoustic velocity in x_3-direction due to the excitation pressure p^e, and $\cdot^*$ denotes complex conjugate. The velocity can be written as

$$\mathrm{i}\omega w_3^e = \mathrm{i}\omega \boldsymbol{\psi} \hat{\mathbf{w}}_3^e \tag{39}$$

where

$$\hat{\mathbf{w}}_3^e = -\frac{1}{\omega^2 \rho} \boldsymbol{\Lambda} \hat{\mathbf{p}}^e. \tag{40}$$

Expressing these quantities in finite element coordinates $p^e = \mathbf{N}_f \mathbf{p}^e$, the incident power can be written

$$\begin{aligned} \Pi_e &= \frac{1}{2} \left(\frac{-\mathrm{i}}{\omega\rho} \boldsymbol{\Lambda} \hat{\mathbf{p}}^e \right)^* \int_{\partial\omega} \boldsymbol{\psi}^T \boldsymbol{\psi} \mathrm{d}S \hat{\mathbf{p}}^e \\ &= \mathrm{i} \frac{L_1 L_2}{8\omega\rho} (\hat{\mathbf{p}}^e)^* (\boldsymbol{\Lambda}^{-1})^* \hat{\mathbf{p}}^e \end{aligned} \tag{41}$$

where for matrixes $\cdot^*$ denotes both transposed and complex conjugate. The displacement on the receiving room side in the x_3-direction can be written $w_3^e = -\mathbf{n}_2 \mathbf{N}_s \mathbf{u}_s$ The transmitted pressure $\mathbf{p}^t$ can be calculated from equation (24–b) and the transmitted power becomes

$$\begin{aligned} \Pi_t &= -\frac{2}{L_1 L_2} (\mathrm{i}\omega \mathbf{u})^* \omega^2 \rho \mathbf{H}_2^T \tilde{\boldsymbol{\psi}} \boldsymbol{\Lambda} \tilde{\boldsymbol{\psi}}^T \mathbf{H}_2^T \mathbf{u} \\ &= \frac{\mathrm{i}2\omega^3 \rho}{L_1 L_2} (\mathbf{u})^* \mathbf{H}_2^T \tilde{\boldsymbol{\psi}} \boldsymbol{\Lambda} \tilde{\boldsymbol{\psi}}^T \mathbf{H}_2^T \mathbf{u}. \end{aligned} \tag{42}$$

The Transmission loss R in equation (36) is then easily calculated using equations (37), (41) and (42). The result can then be integrated to third octave band values in order to compare with measurements (see section 3.3).

Table I. Material data. For the different notations, see [2, 42].

Wall studs:		
E	15	GPa
μ	0.10	
ρ	500	kg/m^3
Plaster boards:		
E	3	GPa
μ	0.10	
ρ	720	kg/m^3
Screw connection:		
K	500	kN/m
Air:		
ρ_0	1.21	kg/m^3
c_0	340	m/s
P_0	$1.01 \cdot 10^5$	Pa
γ	1.4	
η	$1.84 \cdot 10^{-5}$	
Porous material:		
ϕ	0.99	
σ	1000	Ns/m^4
α_∞	1	
B^2	0.71	
Λ	$1.92 \cdot 10^{-4}$	m
Λ'	$3.84 \cdot 10^{-4}$	m

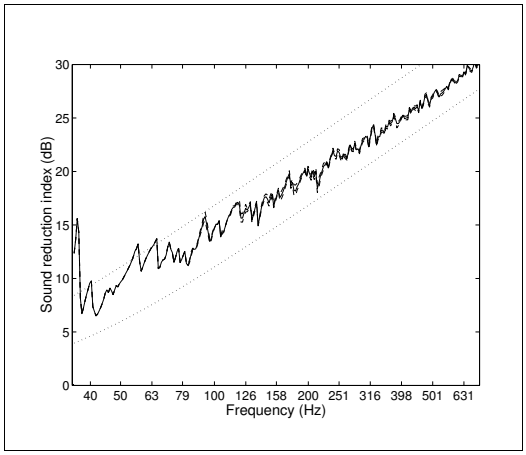

Figure 2. Sound transmission loss of a single plaster board, solid line calculated and the two dotted lines are the mass law, equation (43), with the wave incidence angle of 90° (top line) and 45° (bottom line). The dashed lines (close to the solid line) is the mean $\pm$ the standard deviation.

3. Numerical results

The proposed prediction approach is used to evaluate the sound transmission loss, first, of a single plasterboard and, second, of two different double walls, where also comparison with measurements found in the literature is performed.

3.1. Numerical implementation and data

The material properties used for both the single and the double walls can be found in Table I.

The double walls studied are constructed using wooden wall studs covered with plasterboards and with absorbtion material in the wall cavities (see Figure 3). The length of the wall in the numerical model is 4.05 m and the height is 2.5 m. The plasterboard plates have a thickness of 12.5 mm, using two together on each side of the wall (no shear or viscous connection is present between the plates). Wooden wall studs are used, with a width of 45 mm and a thickness of 45 or 95 mm. The distance between the studs are 0.6 m. The absorption material inside the wall – in the real structure mineral wool with the same thickness as the studs (i.e., the cavity is full of mineral wool) – is modelled as an equivalent fluid as described by Allard [42, p. 92]. The screw connection between the plasterboard and wall stud is modelled as flexible, using spring elements for the in-plane (of the plate) deformation for each screw connection. The stiffness used is given in Table I, and the other deformation directions in the connection are assumed to be rigid. A loss factor $\eta = 0.02$ is introduced for the structural domain. The boundary conditions of the structure were simply supported (for each sub-plate).

The analysis is performed in the frequency range from 45 Hz to 700 Hz. The finite element model of the wall is shown in Figure 4. The plasterboards and wall studs are modelled using 4 node shell elements and a modal (cosine) description is used for the cavities between the wall studs inside the wall. All cavity modes below 1000 Hz are included in the analysis. The finite element model of the wall consists of 22 000 degrees of freedom and the 800 lowest structural eigenmodes are included in the reduction of the system in equation (31). The analysis is conducted in MATLAB [43]. However, in order to speed up the calculations, the structural eigenvalue problem is solved using MSC.Nastran [44] (not including the cavity of the wall). The FE-model is shown in Figure 4.

3.2. Single-leaf wall

The transmission loss (TL) for a wall consisting of a single plasterboard is studied, see Figure 2. The standard deviation of the TL due to stochastic excitation (the random phase angles in equation (34), evaluated with Monte Carlo simulations) is plotted. The results are compared to the mass law with the wave incidence angle of 90° and 45°. The mass law used is

$$R = 10 \log_{10} \left(1 + \frac{\omega^2 m''^2 \cos^2 \theta}{4 \rho_0^2 c_0^2} \right), \qquad (43)$$

where m'' is the mass per unit area of the wall and θ is the incidence angle , see e.g. [2, p. 546].

3.3. Double-leaf wall – comparison with measurement

The transmission loss of two double walls with different wall stud thickness, and therefore also total thickness, is evaluated and compared with measurements, see also Figures 3 and 4. The measurements, found in [45], were performed in an ordinary transmission loss laboratory accord-

ACUSTICA · acta acustica
Vol. – (–)

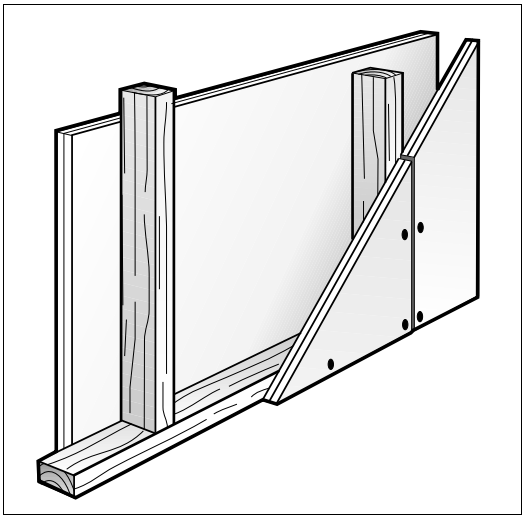

Figure 3. Sketch of the double walls with wooden joists studied in Figures 5 and 6.

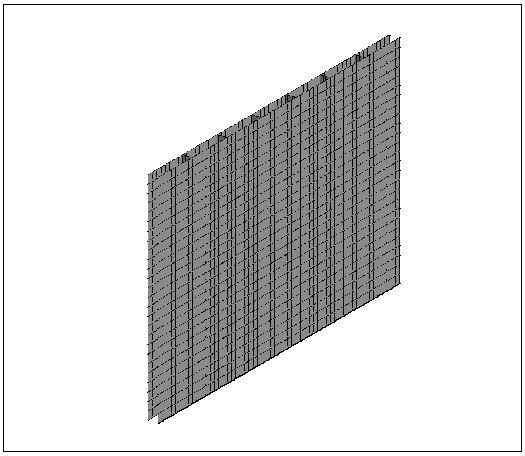

Figure 4. FE model of the double walls studied in Figures 5 and 6.

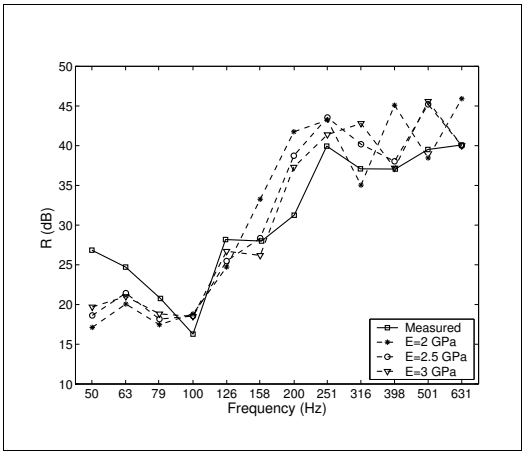

Figure 5. The transmission loss for a double wall with thickness 45 mm, comparing calculations and measurements.

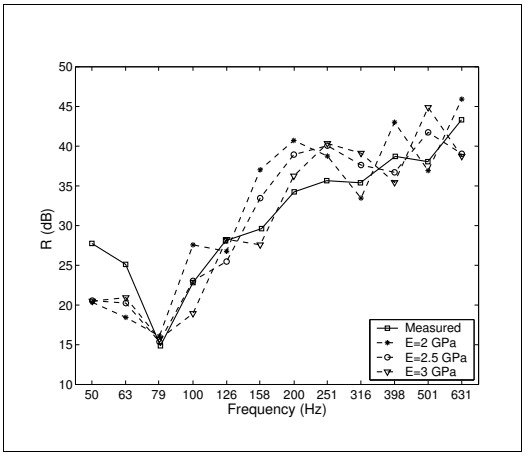

Figure 6. The transmission loss for a double wall with thickness 95 mm, comparing calculations and measurements.

ing [34] (the measurement opening is 4×2.5 m^2 whereas the room dimensions are $6 \times 3.5 \times 6.3$ m^3).

In the analysis, the modulus of elasticity of the plasterboards is varied, being 2, 2.5 or 3 GPa. The transmission loss for the wall stud thickness 45 mm is plotted in Figure 5 and for the wall stud thickness 95 mm in Figure 6.

3.4. Computational efficiency

The main aim of the present prediction model approach is to be more time-efficient than ordinary FE-models. Thus, the approach proposed in the present paper is compared to a FE-analysis including full modal descriptions of the sending and receiving rooms. In this analysis the rooms have the height and width equal to the studied wall and the length perpendicular to the wall is 4.91 m for the sending room and 5.2 m for the receiving room. All walls of the rooms are assumed rigid. The number of degrees of freedom – i.e., the size of the equation system – needed for the two types of analysis are plotted against the maximum frequency of interest in Figure 7. The number of degrees of freedom increases rapidly when including the modal description of the rooms. For the tube-like description of the rooms, the number of degrees of freedom are only determined by the the eigenmodes of the wall. In Figure 8, the computational time for one frequency step of the analysis is plotted against the maximum frequency of interest of the solution. The solid lines are the total time for each step, and the dotted lines are the time for actually solving the derived system of equations. The proposed approach

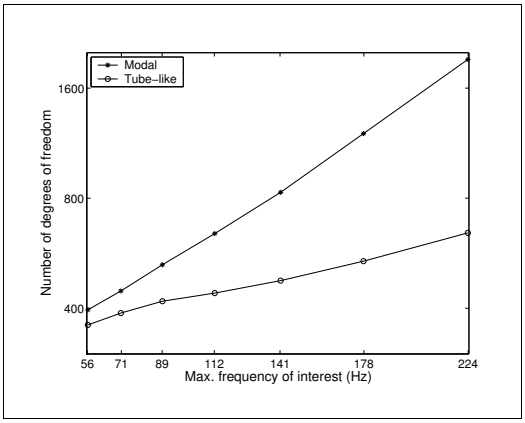

Figure 7. The number of degrees of freedom needed in the analysis: the present tube-like description of the sending and receiving room compared to a full modal analysis.

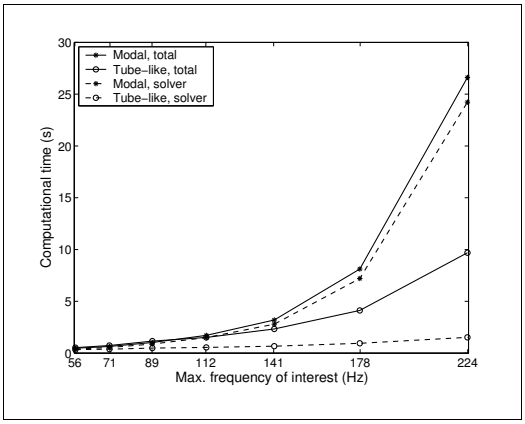

Figure 8. The computational time: the present tube-like description of the sending and receiving room compared to a full modal analysis. The solid lines are the total time for each step and the dotted lines show the time for solving the derived equation system.

has a larger part of matrix manipulations in each step, but the solution time (the dotted line with circular markers) is much smaller. The total computational time to calculate the transmission loss for a double wall in the studied frequency range is a matter of hours – not days. The analyses are performed in MATLAB [43] on a computer with an 1.4 GHz AMD Athlon processor and 1 GB RAM.

4. Discussion

Figure 2 shows both the transmission loss and the standard deviation of the transmission loss are plotted: only a minor variation around the average value can be seen. Thus, the influence of the random phase angle is very small. The roughness in the curve is due to the resonances in the structure and rooms; the calculation is performed for the single frequencies.

In Figures 5 and 6, the uncertainties involved in choosing material parameters – the Young's modulus E is varied between 2 and 3 GPa – are seen to have a large influence on the predicted transmission loss. However, the agreement between calculations and measurements is reasonably good if the uncertainties in the input data and the difference in measurement and analysis situation are taken into account. Note that no tuning or measurement of the input data has been done.

With use of the present prediction model the transmission loss can be evaluated efficiently, compared to the full FE-model including the modal description of the sending room and receiving room, cf. [13, 14, 15]. With increasing frequency of interest, as can be seen in Figure 7, the full modal description leads to a much faster increase of the number of degrees of freedom needed to describe the system. Using the full FE-model also means that a specific room-wall-room system must be chosen and studied. Thus, the calculated transmission loss is dependent on the geometrical properties of the rooms. One drawback with the present approach is that the sparsity of the structural system matrix $\mathbf{D}$ is lost due to the fact that all degrees of freedom describing out-of-plane motion at respective sides of the wall become coupled (i.e. the coupling matrix, $\mathbf{D}_f$, is fully populated at all these degrees of freedom). Thus, the bandwidth thereby becomes equal to the number of the degrees of freedom describing the out of plane motion at each side of the wall, compared for the uncoupled structural problem where the bandwidth is limited to the number of connecting degrees of freedom in each element and the node numbering.

5. Concluding remarks

The present approach is a combination of the normal mode methods, as [4, 5, 6, 7, 8, 9, 10, 11, 12] and the finite element method (FEM), as [13, 14, 15]. The sender and receiver rooms are applied to the structure as a load expressed in cosine-modes.

It can be concluded that the proposed procedure is computation-effective compared with the traditional alternative of including the entire fluid fields in the FE-model; a reasonable frequency range is achieved with a modest computational time. However, this positive effect is gained along with a loss of sparsity of the structural system matrix – i.e., the bandwidth of the matrix is increased – due to coupling between the degrees of freedom on each side of the wall.

The detailed description of the wall that can be accomplished due to the finite element formulation enables the prediction of the transmission loss for changes in wall properties. For example, the effects of varying the wall stud dimensions or stiffness of the fasteners between the plasterboards and the wall studs can be studied, as well as the effects of the wall area in combination with baffling. Also, the procedure can be used in predicting the change

in transmission loss due to uncertainties in the material, geometrical, and boundary properties.

Regarding computational efficiency, large benefits could be achieved in implementing the procedure in an efficient finite element environment (e.g. MSC.Nastran).

Acknowledgement

The authors wish to thank their colleagues and friends at the Division of Engineering Acoustics, especially Professor Per Hammer, and the Division of Structural Mechanics, especially Professor Göran Sandberg. Formas (project number 24.2/2002-1601) and the Swedish Foundation for Strategic Research (project number IVS-98-501) are also gratefully acknowledged for their financial support. The two authors share equal responsibility for the paper and have equally shared the research work involved in its development.

Appendix

A1. Orthogonality

The orthogonality relations for the fluid modes ψ_{nm} are examined. In connection to the fluid structure coupling in section 2.4, the following integral matrix appears:

$$\int_{\partial\Omega_j} \boldsymbol{\psi}^T \boldsymbol{\psi} \mathrm{d}S. \tag{A1}$$

One element of this matrix is

$$\begin{aligned} &\int_{\partial\Omega} \psi_{nm}(x_1,x_2)\,\psi_{pq}(x_1,x_2)\,\mathrm{d}S \\ &= \gamma_n\gamma_m\gamma_p\gamma_q \int_0^{L_1} \cos(\alpha_m x_1)\cos(\alpha_p x_1)\,\mathrm{d}x_1 \\ &\times \int_0^{L_2} \cos(\beta_n x_2)\cos(\beta_q x_2)\,\mathrm{d}x_2. \end{aligned} \tag{A2}$$

Using $\alpha_m = \pi m/L_1$ and $beta_n = \pi n/L_2$, the first integrals in (A2) can be written

$$\begin{aligned} &\int_0^{L_1} \cos\left(\frac{\pi m}{L_1}x_1\right)\cos\left(\frac{\pi p}{L_1}x_1\right)\mathrm{d}x_1 \\ &= \begin{cases} 0 & \text{if} \quad n \neq p \\ L_1/2 & \text{if } n = p \neq 0 \\ L_1 & \text{if } n = p = 0 \end{cases} \end{aligned} \tag{A3}$$

and a corresponding equation can be written for the second integral. Thus, if $n \neq p$ or $m \neq q$ the matrix element is zero, and if else, that is $n = p$ and $m = q$, we have

$$\begin{aligned} &\int_{\partial\Omega} \psi_{mn}^2(x_1,x_2)\,\mathrm{d}S \\ &= \gamma_n^2\gamma_m^2 L_1 L_2 \begin{cases} 1/4 \text{ if } n \neq 0 \text{ and } m \neq 0 \\ 1/2 \text{ if } \quad n = 0 \text{ or } m = 0 \\ 1 \quad \text{if } n = 0 \text{ and } m = 0 \end{cases} \end{aligned} \tag{A4}$$

and thus is the definition of γ_m in equation (8) correct in connection to the orthogonality relations used in equation (21).

A2. A special case – normal incident wave

To verify the model a simple test problem is constructed. The wall is assumed to be a SDOF system, a rigid plate with an area of 1 m^2 and mass of m kg/m^2 connected to a spring with the stiffness $k(1+\mathrm{i}\eta_s)$ kN/m^3 where η is the loss factor of the system. The natural frequency of the wall becomes $f_0 = \sqrt{\lambda_s}/(2\pi) = \sqrt{k/m}/(2\pi)$ with the structural eigenmode $\boldsymbol{\Phi} = [100100...100]^T$. The normal incident wave is the first wave in the series expansion, with the pressure distribution at the wall, i.e. $x_3 = 0$, written in matrix notation $\boldsymbol{\psi} = [0.5\ 0.5\ ...\ 0.5]^T$. The amplitude of the excitation wave is $\hat{p}^e$. Reducing the system using the eigenmodes and noting that $\tilde{\boldsymbol{\psi}}^T \mathbf{H}_1^T \boldsymbol{\Phi} = L_x L_y/2 = 1/2$ and $\boldsymbol{\Lambda} = 1/\kappa_{00} = -\mathrm{i}(c_f/\omega)$. The system can now be written

$$(-\omega^2 m + k + 2\mathrm{i}\omega\rho c_f)\hat{u} = \hat{p}^e$$

and therefore

$$\hat{u} = \frac{\hat{p}^e}{(-\omega^2 m + k + 2\mathrm{i}\omega\rho c_f)} \tag{A5}$$

The complex exciting and transmitted powers become

$$\Pi_e = \frac{|\hat{p}^e|^2}{8\rho_f c_f} \tag{A6}$$

and

$$\Pi_t = \frac{\omega^2\rho c_f}{2}\frac{|\hat{p}^e|^2}{|(-\omega^2 m + k + 2i\omega\rho c_f)|^2} \tag{A7}$$

and the transmission coefficient can therefore be written

$$\begin{aligned} \tau &= \frac{\Re\{\Pi_t\}}{\Re\{\Pi_e\}} \\ &= \frac{4\omega^2\rho^2 c_f^2}{(-\omega^2 m + k)^2 + (2\omega\rho c_f)^2} \end{aligned} \tag{A8}$$

Choosing the natural frequency of the structure close to zero, the transmission corresponds to the mass law for normal incident waves

$$R = \log_{10}\left(1 + \frac{\omega^2 m^2}{4\rho^2 c^2}\right) \tag{A9}$$

References

[1] L. Cremer: Theorie der Schalldämmung dünner Wände bei schrägem Einfall. Akust. Z. **7** (1942) 81–104.
[2] L. Cremer, M. Heckl, E. E. Ungar: Structure-borne sound. Springer-Verlag, Berlin, 1988.
[3] A. London: Transmission of reverberant sound through double walls. J. Acoust. Soc. Am. **22** (1950) 270–279.
[4] T. Kihlman: Sound radiation into a rectangular room. Applications to airborne sound transmission in buildings. Acustica **18** (1967) 11–20.
[5] M. C. Bhattachrya, M. J. Crocker: Forced vibration of a panel and radiation of sound into a room. Acustica **22** (1969/70) 275–294.
[6] A. C. Nilsson: Reduction index and boundary condition for a wall between two rectangular rooms, Part I: Theoretical results. Acustica **26** (1972) 1–18.
[7] K. A. Mulholland, R. H. Lyon: Sound insulation at low frequencies. J. Acoust. Soc. Am. **54** (1973) 867–878.
[8] M. C. Bhattachrya, R. W. Guy: The transmission of sound through a cavity-backed finite plate. J. Sound Vib. **27** (1973) 207–223.
[9] A. C. Nilsson: Reduction index for a panel in a baffle. Report 73–02, Dep. Building Acoustics, Chalmers University of Technology, Göteborg, Sweden, 1973.
[10] R. W. Guy: The steady state transmission of sound at normal and oblique incidence through a thin panel backed by rectangular room – a multi-modal analysis. Acustica **43** (1979) 295–304.
[11] S.-I. Thomasson: Ljudtransmission mellan rektangulära rum försedda med absorbenter av lokalt reagerande typ (in swedish). TVBA 3003, (Avd. byggnadsakustik) Engineering Acoustics, LTH, Lund University, Box 118, SE-221 00 Lund, Sweden, 1980.
[12] L. Gagliardini, J. Roland, J. L. Guyader: The use of a functional basis to calculate acoustic transmission between rooms. J. Sound Vib. **145** (1991) 457–478.
[13] A. Pietrzyk: Sound insulation at low frequencies. PhD thesis. F 97–01 3060, Chalmers University of Technology, Sweden, 1997.
[14] S. P. S. Maluski, B. M. Gibbs: Application of a finite-element model to low-frequency sound insulation in dwellings. J. Acoust. Soc. Am. **108** (2000) 1741–1751.
[15] P. Davidsson, G. Sandberg: Sound reduction in double walls at low frequencies – a parametric study. Proceedings of Tenth International Congress on Sound and Vibration, Stockholm, Sweden, 2003. (8 pages).
[16] W. Kropp, A. Pietrzyk, T. Kihlman: On the meaning of the sound reduction index at low frequencies. Acta Acustica **2** (1994) 379–392.
[17] P. Santos, A. Tadeu: Acoustic insulation provided by a single wall separating two contiguous tunnels via BEM. J. Sound Vib. **257** (2002) 945–965.
[18] P. Santos, A. Tadeu: A note on the acoustic insulation between two-dimensional acoustic spaces at low frequencies. J. Sound Vib. **257** (2003) 185–191.
[19] P. Jean, J. Roland: Application of the Green ray integral method (GRIM) to sound transmission problems. J. Building Acoustics **8** (2001) 139–156.
[20] P. Jean, J. F. Rondeau: A simple decoupled modal calculation of sound transmission between volumes. Acta Acustica united with Acustica **88** (2002) 924–933.
[21] S. Ljunggren: Airborne sound insulation of thin walls. J. Acoust. Soc. Am. **89** (1991) 2324–2337.
[22] M. Villot, C. Guigou, L. Gagliardini: Predicting the acoustical radiation of finite size multi-layered structures by applying spatial windowing on infinite structures. J. Sound Vib. **245** (2001) 433–455.
[23] S. Ljunggren: Air-borne sound insulation of single walls at low frequencies: A discussion on the influence of boundary and mounting conditions. J. Building Acoustics **8** (2001) 257–267.
[24] B. H. Sharp: Prediction methods for the sound transmission of building elements. Noise Control Engineering **11** (1978) 53–63.
[25] W. Kropp, E. Rebillard: On the air-borne sound insulation of double wall constructions. Acta Acustica united with Acustica **85** (1999) 707–720.
[26] G. F. Lin, J. M. Garrelick: Sound transmission through periodically framed parallel plates. J. Acoust. Soc. Am. **61** (1977) 1014–1018.
[27] D. Takahashi: Sound radiated from periodically connected double-plate structures. J. Sound Vib. **90** (1983) 541–557.
[28] E. A. Skelton: Acoustic scattering by parallel plates with periodic connectors. Proc. R. Soc. Lond. A **427** (1990) 419–444.
[29] J. Brunskog, P. Hammer: Prediction model for the impact sound level of lightweight floors. Acta Acustica united with Acustica **89** (2003) 309–322.
[30] J. Brunskog: Including the influence of finite cavities on the sound insulation of double-plate structures. TVBA 3119, Engineering Acoustics, LTH, Lund University, Box 118, SE-221 00 Lund, Sweden, 2002.
[31] J. Brunskog, P. Hammer: Prediction models of impact sound insulation on timber floor structures; A literature survey. J. Building Acoustics **7** (2000) 89–112.
[32] R. H. Lyon, R. G. DeJong: Theory and application of statistical energy analysis. Butterworth-Heinemann, Boston, 1995.
[33] J. Brunskog: Flanking transmission of continuous ground plates. Proceeding of Inter–Noise 2002, Dearborn, MI, USA, 2002. (8 pages).
[34] EN ISO 717-1:1996: Acoustics – Rating of sound insulation in buildings and building elements – Part 1: Airborne sound insulation. European standard, 1996.
[35] ISO 15186-1:2000: Acoustics – Measurement of sound insulation in buildings and of building elements using sound intensity – Part 1: Laboratory measurements. International standard, 2000.
[36] K.-J. Bathe: Finite element procedures. Prentice Hall, Upper Saddle River, New Jersey, 1996.
[37] N. Ottosen, H. Petersson: Introduction to the finite element method. Prentice Hall, 1992.
[38] G. Sandberg: Acoustic and interface elements for structure-acoustic analysis in CALFEM. TVSM 7113, Structural Mechanics, LTH, Lund University, Box 118, SE-221 00 Lund, Sweden, 1996.
[39] R. Clough, J. Penzien: Dynamics of structures. McGraw-Hill, London, 1993.
[40] A. C. Nilsson: Reduction index and boundary condition for a wall between two rectangular rooms, Part II: Experimental results. Acustica **26** (1972) 19–23.
[41] C. L. Morfey: Dictionary of acoustics. Academic Press, London, 2001.
[42] J. F. Allard: Propagation of sound in porous media: Modeling sound absorbing materials. Elsevier Applied Science, London, 1993.
[43] MATLAB User's Manual. Mathworks Inc., 2002.
[44] MSC.Nastran encyclopedia. The McNeal-Schwendler Corporation, 2001.
[45] P. Hammer, E. Nilsson: Light weight partition walls and floors – the influence of mineral wool on sound insulation. TVBA 3095, Engineering Acoustics, LTH, Lund University, Box 118, SE-221 00 Lund, Sweden, 1997.